EFFECT OF INDUCED DRAG DAMPING ON THE NEAR RESONANT RESPONSE OF A DEEPWATER PLATFORM

N. SRINIVASAN, B.Sc., B.Tech., M.Tech.

EFFECT OF INDUCED DRAG DAMPING ON THE NEAR RESONANT RESPONSE OF A DEEPWATER PLATFORM

by

© N. SRINIVASAN, B. Sc., B. Tech., M. Tech.

A thesis submitted to the School of Graduate
Studies in partial fulfillment of the
requirements for the degree of
Doctor of Philosophy

Faculty of Engineering and Applied Science
Memorial University of Newfoundland
July 1991

St. John's Newfoundland Canada

To:

Swami Thayumanavar,

Chirapalli, India

Abstract

Occurrence of resonance in the design of deepwater structures is unavoidable under all operating conditions. When the wave forces on the structure are dominated by the inertial component of loading, the hydrodynamic damping in the system is low. It is also known that the structural response can be reduced if energy can be dissipated through the fluid-media via the mechanism of flow-separation since it increases the fluid component of the total damping. Thus the resonant response could be suitably reduced by the generation of increased flow-separation. In view of certain new types of structures which possess one or more large diameter circular cylinders crossing the free surface, this dissertation describes an innovative technique to control the response at frequencies near resonance to moderate waves.

When the Keulegan-Carpenter (KC) number for the flow is less than 4, the time available for the development of vortices behind a circular cylinder is less than adequate to form a stable wake. Consequently the drag forces on the structure are small. The first objective of this study was to increase the drag forces on a 0.3 m diameter circular vertical cylinder at low KC numbers (KC $\leq$ 2) for regular and irregular waves. The dissertation proposes a physical device to induce flow-separation that will increase the drag forces experienced by the circular cylinder.

An experimental set-up was made to measure the wave forces on a simple vertical cylinder. The measured wave elevations and the wave forces were used to fit the Morison wave force formula, in the least squares sense, and the values of the inertial (C_m) and drag (C_d) force coefficients were determined. To study the effect of the physical device on the circular cylinder, the experiment was repeated by attaching the device to the cylinder. The experimental results revealed that, at low KC numbers, the value of C_d for the circular cylinder with the device increased by a factor of 4, irrespective of the wave height and wave period. The device did not significantly increase the value of the inertial coefficient of the main cylinder.

The significant increase in the drag forces due to the attachment of the device could be successfully used to control the resonant response of certain deepwater

structures. To investigate this, the dynamic response of an offshore platform model was tested in a wave tank, both with and without the device. The three-dimensional platform model was a 1/50th scale structure possessing the key features of a typical deep water tripod tower platform. The scaling considerations required for a hydroelastic model study in a wave tank were utilized to fabricate the 8.6 m tall hydroelastic model. The vibration properties of the model structure were determined both in air and water. To reliably estimate the modal parameters, modal testing and analysis were used. Parallel studies were conducted to analytically determine the natural frequencies and mode shapes, using a finite element method. The natural frequencies obtained by the two methods were in good agreement.

The response of the physical model to resonant wave excitation was investigated for both regular and random waves and the experimental results were complemented by analytical results. Excellent correlation was obtained over the entire range of test conditions. In the analytical study concerning the effect of the device on the dynamic response of the structure to waves, a relative velocity formulation was used in the Morison forcing term and the nonlinear equations of motion were solved in the time domain. The experimental values of the C_m and C_d coefficients, with and without the device, were utilized in the analytical study.

Both experimental and analytical results support the potential application of the device in controlling the resonant response of large diameter structures. Measured experimental results demonstrate that with the device the longitudinal acceleration response was reduced by a maximum of 32% for resonant wave conditions. Findings show that, as the wave height increases under resonant excitation, the percentage reduction due the induced drag damping also increases.

Key words: Dynamics of offshore structures, Deepwater structures, Induced drag damping, Hydrodynamic damping, Hydroelastic model, Hydroelastic response

Acknowledgements

This research was sponsored by the Association of Universities and Colleges of Canada under the Canadian Commonwealth Scholarship and Fellowship plan. First and foremost, I gratefully acknowledge the source of support that made the study possible.

I express my deep sense of gratitude to my thesis advisor Professor A. S. J. Swamidas for his long and patient help. His excellent guidance, support, encouragement and willingness to allow me to pursue my own ideas helped me to contribute to the field of my study. I will always be indebted to him.

My co-supervisor, Dr. J. S. Pawlowski, offered many valuable suggestions. His participation, insight, and standard of excellence have been a very positive influence on my education at Memorial University. It has been a pleasure working with such a truly kind and cordial person.

My special thanks to Professor D. B. Muggeridge, the Ocean Engineering Chairman and to Dr. H. Marzouk, for their support and encouragement, and also for serving on the supervisory committee. Professor Muggeridge helped for the first experiment by providing the faculty wave tank facility and Dr. Marzouk provided material for constructing the supporting steel base. I once again thank them for these assistance.

My understanding on experimental model study came from Professor J. J. Sharp, Civil Engineering Chairman, for which I am ever grateful. Dr. K. Munaswamy helped me during the proposal stage of this study and my sincere thanks to him. Technical discussions with Dr. Munaswamy were especially informative.

I also wish to thank Mr. N. E. Jeffrey, the Director General of Institute for Marine Dynamics, National Research Council Canada, for providing the clear water

towing/wave tank facility for conducting the second experiment. Grateful acknowledgement is due to Dr. C. Williams, for his help during the second experiment. Dr. Williams also spent long hours in reviewing the entire thesis. I am thankful to him for the criticisms and the helpful suggestions.

I am deeply in debt to professor T. R. Chari, the Associate Dean of the faculty, for his interest and encouragement. Help in all matters was readily and freely given. His continued support has been both an inspiring and indispensable element in my success. Gratitude is extended to Dr. G. R. Peters, the Dean of the faculty, for providing the opportunity to do research in Memorial University.

I also owe to Professor F. A. Aldrich, the former Dean of Graduate Studies, to Professor J. Malpas, the Dean of Graduate Studies, and to Dr. C. Sharpe, the Associate Dean of Graduate Studies, for their valuable assistance. Mrs. J. Fairley in the office of graduate studies helped me on nontechnical matters. My thanks to her.

I express my warm appreciation to the members of the technical services, structures laboratory, and the wave tank group. My sincere thanks to Mr. S. Foster, for his invaluable assistance in preparing the experimental models. The generous support from the Centre for Computer Aided Engineering of this faculty on computing services is very much appreciated.

I am grateful to the fellow graduate students for their encouragement and company. The East-Indian community of this city (St. John's) helped me in various ways during my stay in this country. My sincere thanks to them.

Finally, I appreciate the continuous moral support of my father.

Contents

List of Tables

List of Figures

List of Symbols

Symbol	Description
$a, a_1, \cdots, a_5$	- parameters used in Stokes' fifth order theory
$[c]$	- generalized damping matrix
d	- water depth
df	- frequency resolution
dt	- time increment
f	- force per unit length or frequency
$f(t)$	- hydrodynamic load intensity vector
f_d	- damped natural frequency
f_{max}	- maximum frequency
f_n	- natural frequency of structure
f_u	- cut-off frequency
f_0	- peak frequency in random wave elevations
f_1	- lower half-power band width point in FRF
f_2	- upper half power band width point in FRF
g	- acceleration due to gravity
$h(t, y)$	- impulse response function for depth y
k	- wave number
$[k]$	- generalized stiffness matrix
$[m]$	- generalized mass matrix
$p(t)$	- time history of input force

Symbol	Description
q	- generalized displacement vector
rms	- root mean square
$r(t)$	- time history of output response
$r(y)$	- a factor defining variation of particle velocity with depth y
r_0	- output response at time equal to zero
t	- time
u	- horizontal fluid particle velocity
$u(t,y)$	- horizontal fluid particle velocity time series at depth y
$\|u\|$	- modulus of u
$< \|u\| >$	- time average of modulus of u
u_R	- relative velocity between fluid particle and structure
$\dot{u}$	- horizontal fluid particle acceleration
$\{u\}$	- horizontal fluid particle velocity vector
$\{\dot{u}\}$	- horizontal fluid particle acceleration vector
u_N	- fluid velocity vector normal to cylinder axis
$\dot{u}_N$	- fluid acceleration vector normal to cylinder axis
x	- horizontal structural displacement
$\dot{x}$	- horizontal structural velocity
$\{x\}$	- structural displacement vector
$\{\dot{x}\}$	- structural velocity vector
$\{\ddot{x}\}$	- structural acceleration vector
$\dot{x}_N$	- member velocity vector normal to the axis
$\ddot{x}_N$	- member acceleration vector normal to the axis
y	- vertical coordinate
y_i	- vertical coordinate of the i^{th} node
A_I	- sectional volume for inertia force calculation

Symbol	Description
A_D	- sectional area for drag force calculation
$A_1, A_2, \cdots, A_i$	- concentrated joint areas
$[A]$	- diagonal matrix indicating area projected in the direction of flow
$A_n(\omega, \theta)$	- amplitude of waves approaching structure at an angle θ
$A_{11}, A_{13}, A_{15},$	- velocity parameters defined in Stokes' wave theory
$A_{22}, A_{24}, A_{33},$	- velocity parameters defined in Stokes' wave theory
A_{35}, A_{44}, A_{55}	- velocity parameters defined in Stokes' wave theory
$B_{nn}(\omega, \theta)$	- radiation damping coefficient for n^{th} mode of structure
$[B(\Omega)]$	- modal radiation damping coefficient
$B_1, B_2, \cdots, B_i$	- concentrated joint volume
$[B]$	- diagonal matrix indicating volume displaced by structure
B_{22}, B_{24}, B_{33}	- wave profile parameters defined in Stokes' wave theory
B_{35}, B_{44}, B_{55}	- wave profile parameters defined in Stokes' wave theory
C	- wave celerity from Stokes' theory
C_a	- added mass coefficient
C_{as}	- added mass coefficient for a section
C_d	- drag coefficient in Morison's formula
C_{ds}	- drag coefficient for a section
C_g	- wave group velocity
C_m	- inertia coefficient in Morison's formula
C_{ms}	- inertia coefficient for a section
$[C]$	- global damping matrix
$[C_{rad}]$	- radiation damping matrix
$[C_{str}]$	- structural damping matrix
C_0	- wave celerity from linear theory
C_1 and C_2	- frequency parameters defined in Stokes' wave theory

Symbol	Description
D	- member diameter
E	- error between predicted and measured values of forces
F	- total horizontal force on cylinder
F_d	- drag force on cylinder for $C_d = 1$
FEM	- Finite Element Methods
FFT	- Fast Fourier Transform
FRF	- Frequency Response Function
$[F_D]$	- coefficient matrix for generalized drag forces
$[F_M]$	- coefficient matrix for generalized inertia forces
$\{F\}$	- nodal force vector
Fi	- nodal force vector at ith joint
F_i	- inertial force on a cylinder for $C_m = 1$
F_m	- measured wave force on cylinder
$F_n(\omega, \theta)$	- modal wave exciting force for n^{th} mode
$G_{PP}(f)$	- power spectral density of $p(t)$
$G_{PR}(f)$	- cross spectral density of $p(t)$ and $r(t)$
$G_{RR}(f)$	- power spectral density of $r(t)$
$G_1, \cdots, G_5$	- parameters used in Stokes' fifth order theory
H	- wave height for regular waves
$H(f)$	- frequency response function
$\|H(f)\|$	- magnitude of frequency response function
$H_1(f)$	- H_1 estimator for frequency response function
$H_2(f)$	- H_2 estimator for frequency response function
$H_3(f)$	- H_3 estimator for frequency response function
H_p	- wave height for regular waves for prototype situations
H_s	- significant wave height

Symbol	Description
H_{sp}	- significant wave height in prototype situations
KC	- Keulegan-Carpenter number
K_E	- elastic moduli ratio
K_I	- scale factor for moment of inertia
K_L	- length ratio in Froude scale
K_M	- submerged density ratio
K_t	- wall thickness ratio
K_T	- time ratio in Froude scale
$[K]$	- global stiffness matrix
$[K_D]$	- matrix to obtain drag force
$[K_M]$	- matrix to obtain inertial force
L	- wave length and also length unit in Froude scale
$[M]$	- global mass matrix
M	- filter length
$[M_A]$	- added mass matrix
M_{ai}	- added mass at i^{th} joint
$[M_T]$	- total mass matrix including added mass matrix
N	- number of frequency points in spectrum
$P(f)$	- Fourier integral transform of input $p(t)$
Q	- magnitude of FRF at resonance
$R(f)$	- Fourier integral transform of output $r(t)$
$\|R\|^2$	- mean square value of $R_n(\omega, \theta)$, for unidirectional waves
$< \|R\|^2 >_\theta$	- mean square value of $R_n(\omega, \theta)$
R_e	- Reynold's number
$RAOD$	- response amplitude operator for drag force spectrum
$RAOI$	- response amplitude operator for inertia force spectrum

Symbol	Description
$[S_f(\omega)]$	- modal wave force spectral matrix
$S_F(\omega)$	- spectrum of total wave force on cylinder
$S_F(\omega)_{ii}$	- diagonal element of wave force spectral matrix
$S_F(\omega)_{ij}$	- non-diagonal element of wave force spectral matrix
$S_{Fd}(\omega)$	- spectrum of total drag force on cylinder
$S_{FI}(\omega)$	- spectrum of total inertia force on cylinder
$S_{Fp}(\omega)$	- predicted wave force spectrum
$S_{Fm}(\omega)$	- measured wave force spectrum
$S_{nf}(\omega)$	- modal wave force spectrum for nth mode
$S_u(\omega)$	- water-particle velocity spectrum
$S_{\dot{u}}(\omega)$	- water-particle acceleration spectrum
$[S_f(\omega)]$	- modal wave force spectral matrix
$[S_F(\omega)]$	- wave excitation spectral matrix
$S_u(\omega)$	- horizontal particle velocity spectrum
$S_{\dot{u}}(\omega)_i$	- horizontal particle acceleration spectrum at node i
$S_\eta(\omega)$	- wave elevation spectrum
T	- wave period for regular waves
T_c	- record length
T_P	- wave period for regular waves for prototype situation
T_z	- zero up-crossing period
$T_{z_{up}}$	- zero up-crossing period for prototype situations
T_0	- peak period
U_m	- maximum horizontal particle velocity
α and β	- factors defined in the proportional damping model
ϵ	- standard error in the prediction of wave forces
ζ	- structural damping coefficient in terms of critical damping

Symbol	Description
η	- free surface water elevation
θ	- direction of wave propagation
γ	- peakedness parameter used in JONSWAP wave elevation
ν	- kinematic viscosity of fluid
$\nu(f)$	- coherence function
ρ	- density of water
ρ_s	- density of material
σ	- standard deviation
$\sigma_s^2(u)$	- fluid particle velocity variance
σ_{u_R}	- rms value of U_R
ω	- wave circular frequency
$\bar{\omega}$	- mean wave circular frequency
ω_0	- peak wave circular frequency
Ω	- natural frequency of structure
$[\Phi]$	- modal matrix
2D	- two-dimensional
3D	- three-dimensional

On principle, it is wrong to try founding a theory on observable magnitudes alone. It is the theory which decides what we can observe.

—Einstein

Chapter 1

Introduction

Deep seas and the Arctic zones are the areas of prime concern for offshore technologies of the future. In many parts of the world oil prospecting is moving into deep waters and frontier areas, encountering significant environmental challenges. Presently, the world's most spectacular deepwater drilling and developmental accomplishments are taking place in the Gulf of Mexico, Offshore California, the North Sea and in Brazil's Campos Basin. In 1983, a guyed tower platform was installed in a 300 m water depth in the Gulf of Mexico. In 1984, a tension leg platform was installed in a 150 m water depth in the North Sea. In 1989, a tension leg well platform was installed in 563 m deep waters in the Gulf of Mexico. Presently, Brazil is planning to install developmental systems in water depths up to 1500 m in the Campos Basin. The term 'deepwater', hence, has no exact definition of its own. Strictly speaking, it means different water depths to different people at different times. Deepwater, in the context of offshore platforms, may be defined as water depths which have not been commonly and widely experienced by offshore industry at present.

The offshore activities in deepwater are carried out with a variety of floating and fixed structures. Many economical structural concepts have been proposed to produce oil from beneath the deep ocean. Presently, the offshore oil industry is actively involved with the development of new structural concepts for deepwater

applications. Heerema Engineering Service in the Netherlands, has developed a steel tripod tower concept, an applicable system for the North Sea environment for water depths around 300 to 400 m. ETPM (Paris) has proposed the Roseau (reed) tower for water depths in the range of 300 m to 1000 m. C. G. Doris in France has developed a new concept, called the gamma tower, for drilling and production in water depths ranging from 350 to 750 m. Semisubmersible floating production systems are efficient and proven for depths up to 1000 m. Petrobras (Brazil) and Exxon (Houston, Texas) are studying alternatives, such as tension leg platforms and compliant piled towers, for depths beyond 1000 m.

As the search for hydrocarbons continues to increase in deep water, it becomes essential and imperative to study the functional behaviour of these deepwater applicable systems to environmental forces.

1.1 Practical Significance

Deepwater structures are designed against fatigue failure and dynamic analysis is required when the fundamental structural frequencies are sufficiently low as to fall within the band of moderate wave frequencies. Since the moderate waves significantly contribute to the fatigue damage of the structure, resonant vibration of the structure, due to these waves, has to be avoided in the design. Obviously the natural tendency in design is either to increase or decrease the structural stiffness and thus to shift the natural frequencies to either the uppermost or the lowermost range of the frequencies of the wave spectrum. For instance, if structural stiffness is increased, the cost also increases and beyond a certain depth the structure becomes uneconomical. On the other hand, if the structural stiffness is decreased, the structure becomes more compliant to waves and undesirable large structural motions take place. In the latter case, second order wave forces could excite these structures at their low natural frequencies and cause resonant oscillations in the structures.

At this stage, two questions need to be answered: Is it feasible and economical to avoid resonance? If not, could additional fluid-dynamic damping, which has proved to be an effective response reduction mechanism in the resonant regime, be used to reduce the structural motions? If the motion of a resonating structure to moderate waves, and consequently the fatigue stress levels, are reduced substantially, the structure could be used for greater water depths than is normally applicable; hence many marginal fields may become economical for production. If one decides not to select compliant structures because of their disadvantages, it is always desirable to control the resonant response by increasing the damping in the system. Furthermore, it should be pointed out here that the damping present in most of the deepwater structures is small and even a small increase in damping by any means can significantly reduce the response. In this thesis, effort is made to increase the hydrodynamic damping of a deepwater structure to reduce its resonant response to moderate waves.

1.2 Objectives

The need to avoid the occurrence of resonance, to everyday waves, and the consequent susceptibility to fatigue damage are compelling reasons for directing research efforts to the problem of controlling the dynamic response of deepwater structures. When the flow field around a structure is such that the drag forces on the structure are an order of magnitude greater than inertial forces, the response of the structure is said to be 'drag force dominated'. When such a structure is subjected to resonant excitation to waves, the separated-flow drag damping plays an important role in limiting the response and stress levels. Nevertheless, questions remain regarding the behaviour of inertial force dominated structures. Are the drag forces significant in these type of structures? What is the mechanism that causes the oscillatory flow not to generate vortices, if the cylinder diameter is relatively large? How does a

large diameter circular cylinder behave in an oscillatory wave flow? Is this response fundamentally different from the drag force dominated situation? How is the flow characterized and which parameters are important? Is it feasible to increase the drag forces? If so, by how much? Is it feasible to control the dynamic structural responses by the use of these increased drag forces?

This work differs, in several aspects, from the previous studies where attention was primarily focused on the jacket type of structures and studies generally centered on the mathematical modelling of existing phenomena. The main purpose of this research is to control the resonant response of an inertial force dominated deepwater structure, to moderate waves, by generating additional hydrodynamic damping in the system. A hydroelastic model was designed so that it possessed the key features and properties of a typical steel tripod tower platform. The steps required to reach the research goal are listed as follows:

1. A clear understanding of the mechanics of the wave flow, around a large diameter circular cylinder, must be realized before attempting to increase the drag forces on the model structure. It is desirable first to concentrate on the wave forces rather than on the structural responses. A test is required to measure the wave forces on a simple circular cylinder and to provide information on the drag and inertial components of the wave forces.

2. If a device is designed to generate increased hydrodynamic damping, based on the oscillatory flow phenomena, its workability has to be demonstrated. The effect of the device on the values of the hydrodynamic coefficients should be determined both in regular and random waves.

3. Hydroelastic physical modelling of a three dimensional structure, at a reduced scale for a wave tank study, is highly complex and difficult to achieve. The design should prove that the physics of the loading and the elastic behaviour

are adequately represented in the physical model.

4. Damping is generally more difficult to estimate than frequency. Selection of appropriate pre-test and data analysis procedures is necessary to estimate the dynamic properties of the structure. The value of the fundamental natural frequency is required to plan the wave excitation tests since it is intended to vibrate the structure at resonance. The value of damping ratio is important to accurately predict the resonant response.

5. Once the physical model is ready for a wave excitation study, the structural response to resonant vibration should be investigated. The test procedure must investigate the resonant response of the structure to regular and random waves and correlate them with the analytical results. The effect of the flow-separation device, on the resonant response of the structure, should also be investigated.

1.3 Method and Scope

A steel tripod tower platform (TTP), designed for application in 345 m waters of the North Sea Troll field was chosen. The portion above the mud-level was selected as the prototype of the test structure. Two wave tank experimental studies were planned: one for investigating the mechanics of wave forces on the structure and the second for investigating its hydroelastic behaviour to waves. For both the experimental studies, the Froude scale criterion was used. These experiments were aimed to simulate moderate sea conditions, which govern the fatigue life of the selected prototype structure. In fact the wave parameters were selected according to a typical North Sea environment.

For the first experiment, a prominent portion of the center column of the prototype was scaled down to 1/50th geometric scale; this resulted in a 0.3 m diameter

vertical circular cylinder. A technique was developed to measure the wave forces on the vertical cylinder. In-line forces on the cylinder were measured, in the Memorial University Hydraulic Laboratory wave tank, for the generated regular and random waves. A physical device was designed and fabricated to induce flow-separation on the 0.3 m diameter circular cylinder. Wave force measuring tests were performed again, with the device attached to the cylinder. The measured wave elevations and the wave forces were used to fit the Morison wave force formula, and the values of the C_m and C_d coefficients computed. To compute the particle kinematics, for regular waves, Stokes' fifth order theory was used; in the case of random waves, linear wave theory was used.

For the second experiment, a three dimensional hydroelastic model, based on the prototype design, was constructed. The model was constructed in three pieces, viz., the top deck, the middle tower and the bottom supporting steel base. Hydroelastic model laws were used in the design of the model. For the fabrication of the tower and the deck portions, acrylic plastic material was used and an 8.6 m tall structure was constructed. For the test, the 200 m long Clear Water Towing Tank facility, situated at the National Research Council of Canada Institute for Marine Dynamics, was utilized.

The water depth in the tank was set to 7.0 m. The tower was fixed rigidly at the bottom over the steel base. First the vibration properties of the model were estimated in air and water. In air, both pluck tests and modal testing were performed, while in water only pluck tests were carried out.

A finite element model was used to mathematically model the structure. The mass and stiffness properties of the mathematical model reflected the key features of the physical model; the submergence effect also was included. The mode shapes and frequencies were determined numerically.

An analytical model was also formulated to study the response of the model

structure to regular and random waves. The relative velocity Morison's wave force formula was used to mathematically model the structural response to waves. The resulting set of second order differential equations was nonlinear in terms of the response of the structure. A time-domain methodology was formulated to retain this nonlinearity while obtaining the solution.

Both experimental and analytical models were used to obtain the resonant response of the structure to wave exciting forces. Comparisons were made between the experimentally measured and analytically calculated acceleration responses. Both regular and random waves were considered. Finally the effect of the induced drag damping, due to the flow-separation device, on the structural response at and near resonance was investigated. Experimental results were compared with the analytical results using the experimentally obtained hydrodynamic coefficients.

1.3.1 Summary of Chapters

This thesis consists of nine chapters and two appendices. While Chapter 1 gives the general introduction, in Chapter 2 we critically assess the state-of-the-art of dynamics of deepwater structures. Emphasis is placed on the importance of the separated-flow drag damping around the resonant regime. Also the thesis problem is identified by reviewing the literature on the behaviour of vertical cylinders at low KC numbers. A method to increase the drag force on a 0.3 m diameter circular cylinder, at low KC numbers, is presented in Chapter 3, by the addition of a physical device. The Morison wave force coefficients were determined for the cylinder with and without the device through a wave force measuring experiment. The study ascertains the effectiveness of the device in inducing additional drag forces on the circular cylinder. The feasibility of designing and fabricating a hydroelastic model, for a laboratory wave tank study to correctly represent the physics of the loading and the elastic structural behaviour is investigated in Chapter 4. The fabrication,

transportation and installation of one of the tallest models, ever built in a university environment, are also described here.

In Chapter 5, the vibration properties of the model structure are estimated. In order to measure these vibration properties which technique is the best choice, a signal analysis or a system analysis? Comparative results are given in this chapter. The finite element modelling and eigenproblem solution of this chapter describes the higher modes of vibration of the structure. In Chapter 6 we develop a response prediction analytical model for regular and random waves. Inclusion of the relative velocity between fluid and structure, together with the development of a time-domain algorithm utilizing the normal mode superposition technique are reported herein.

In Chapter 7 we study the physical response of the model structure to resonant wave excitation. Analytical results are also presented to complement the experimental results. Comparison of the analytical predictions with the measurements for random waves in the time-domain is one of the highlights of this thesis. Chapter 8 is devoted to explaining the practical significance of the developed concept. The effect of the induced drag damping on the resonant response of the model structure is investigated herein using both experimental and analytical methods. Chapter 9 highlights the conclusion of this study, and presents recommendations for future investigations.

In Appendix A, the computer code for the determination of the hydrodynamic coefficients for regular wave data is given. A similar coding for random wave data can be found in Appendix B.

Chapter 2

A Review of Literature on Related Areas

The present level of understanding on the problems associated with deepwater structures is much more superior and advanced than what it was two decades ago. Many structural concepts discussed in the literature are now being fabricated and used for applications in deepwater offshore. The fields which were felt uneconomical once in the past are now being exploited and made feasible for oil production. In fact designing structures for water depths of 300 to 400 m has become a very common activity in the present offshore oil industry. These achievements are made possible by the constant and dedicated work of a large number of researchers in the field of offshore structures.

The development of structural concepts for deepwater has posed many new problems to the investigators. The principle, the geometrical configuration and the behaviour of the new generation concepts are unique in nature and entirely different from the conventional jacket structures. These developments, in deep offshore technology, dictate special methods for analysis, design approach, fabrication technique, and transportation and installation procedures. Consequently new design codes have been prepared for each type of concept. (For example the American Petroleum Institute has prepared API RP-2T for designing Tension Leg Platforms.)

Due to the importance of the technological development in the deep offshore, a number of researchers have investigated the various unique problems associated with these newly developed deepwater concepts. The areas of their interest include problems relating to fluid-structure interaction, the determination of structural response properties, damping and modal shapes, the ability to predict the dynamic response of the structures to wind, waves and currents, and improving the life and reliability of the structure by reducing the static/dynamic responses.

This thesis focuses on one such topic which centers on reducing the resonant response of a deepwater structure to everyday wave environment. Particular emphasis is given to a class of structures which consist of a few large diameter circular members. However the term large diameter used here is relative. In the present context a diameter around 15 m is considered to be large compared to the smaller member diameters of the conventional jacket type platforms. The family of structures, with this characteristics, includes the mono tower platform (MTP), the tripod tower platform (TTP) and tension leg platform (TLP). These structures are subjected to various kinds of dynamic loads that produce resonant oscillations under the operational environmental loads. Limiting the resonant response of the structure to waves would involve the utilization of various principles available from the diverse areas of offshore technology. In order to summarize the current knowledge available on topics pertinent to this research, the present chapter is divided into five major sections: (i) deepwater structures, (ii) responses to waves, (iii) fluid-structure interaction, (iv) flow-separation at low KC numbers and (v) summary.

2.1 Deepwater Structures

2.1.1 Conventional Jacket Platform

The offshore oil industry has a long history of experience with conventional fixed jacket structures. The design, fabrication, transportation and installation proce-

dures are well known and the technology is highly advanced and also reliable. For this reason some of the big offshore oil companies are still interested in the jacket structures for deepwater applications. (The world's tallest four-pile offshore platform, *Crystal*, is being built in McDermott's Louisiana fabrication yard and its installation is scheduled during the summer of 1991, in 189 m deep waters.) In the literature, Will (1983)[1], has made an interesting study on the feasible tallest jacket structure for the Gulf of Mexico type environment.

The rigid jacket structures resist the wave forces as a stiff cantilever beam. As the water depth increases, the structure becomes more flexible changing its natural period to be closer to the period of dominant waves. Under this condition the structure becomes dynamically sensitive and the amplification of response is significant for both the extreme and the every day waves. This makes the jacket structure increasingly inefficient with increased water depth. The principal means of improving the jacket design for deepwater applications is only by increasing the base dimension of the platform. However increasing the base dimension makes the structure uneconomical for use in deeper water.

Fig. 2.1 (Langewis, 1987a) compares the sway periods of different offshore structures designed for different water depths relative to the sea-state energy. (The comparison has been made for the conventional jacket structure, the guyed tower and the tension leg platform.) The jacket structures designed for water depths over 300 m have their first natural period above 5 s, which is within the wave periods corresponding to high energy content. Also the jacket structure experiences a very low hydrodynamic damping; consequently, the motions and stresses tend to be amplified by the resonant vibrations, resulting in an unacceptable fatigue life. Hence it is clear that occurrences of resonance is a critical problem which has restricted the use of jacket structures for deep waters, offshore.

[1] Name and/or year included in the parentheses refer to the publications listed under 'References and Bibliography' at the end of the text

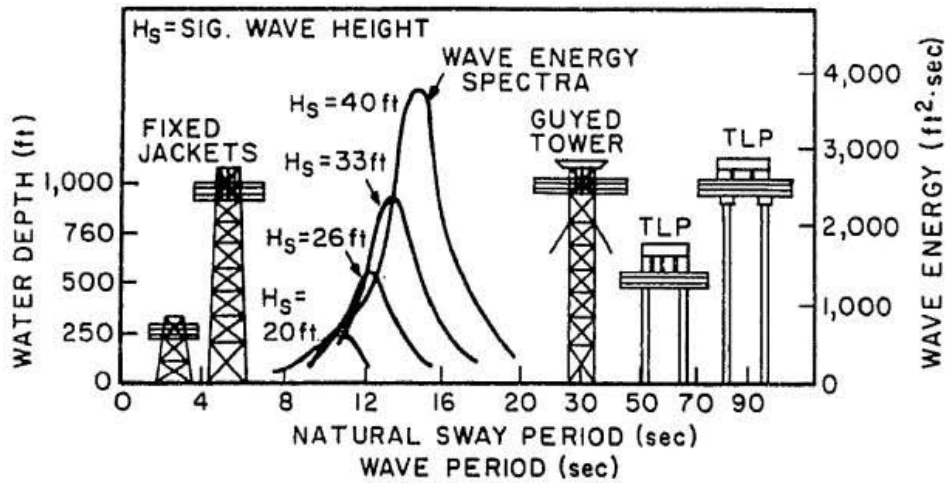

Figure 2.1: Sway periods of platforms relative to sea-state energy (Langewis, 1987a)

2.1.2 Deepwater Concepts

Compliant Structures

The structures with less lateral stiffness, evolved during 1980-86, are called compliant structures (Example: gamma tower, guyed tower, tension leg platform and reed tower). The motivation for these designs was to avoid the occurrences of resonance for all operating and storm conditions. This point is clearly illustrated in the comparison study shown in Fig. 2.1. If the natural period was set to a large value (on the order of 30 to 100 s), one may, therefore, think that the dominant sea state energy should not excite the compliant structures laterally. However, it should be pointed out here, that the second-order slowly varying drift forces can easily reach this natural period. (The second order forces, despite being much less in magnitude than the first order forces, introduce large horizontal movements for the tension leg platforms.)

Hence resonant oscillation of response to environmental wave forces is unavoidable even in the case of the compliant structures.

Tension Leg Platform

A brief review of some of the background of the tension leg platform is given in Mercier (1982). The world's first tension leg platform was deployed by Conoco at the Hutton field in the U. K. This platform has received significant attention from engineering and scientific communities throughout the world. The recent installation of a tension leg well platform, in 563 m deep waters, in the Jolliet field of the Gulf of Mexico (Hunter et al., 1990), has proved that the tension leg platform is a technically feasible and economically viable structure for deepwater applications.

The tension leg platform experiences two kinds of resonance to wave forces called the slow drift and springing oscillations (Marthinsen, 1989). The cause for the slow drift resonance has already been explained before. The springing resonance occurs in the heave mode of the structure. The natural periods for the TLP in the vertical direction is in the range 2-4 s. The sum of different wave frequencies can easily excite the vertical mode of the tension leg platform.

This shows that even for TLP structures, with large diameter members, occurrences of resonance cannot be avoided for all operating conditions.

Fixed Deepwater Platforms

The other interesting type of structures designed for deepwater applications are the fixed deepwater platforms (Earl and Silva, 1986). They are designed to carry much larger and heavier topside facilities than a floating system, thus enabling a single platform to be used for the central processing of many production wells. The wells can be drilled in the conventional manner. The disadvantages faced in the compliant structures are avoided in the case of the fixed deepwater structures. (For example

the large deck accelerations and the large stresses in the risers, which are critical in the design of tension leg platform, are eliminated here.) These structures are suitable for large production facilities which at the same time need to withstand severe environments (like the North Sea). A summary of 27 fixed type deepwater concepts are presented by Buslow (1986).

As the water depth increases the total wave forces remain constant and the overturning moments at the base increase drastically. For this reason most of the fixed deepwater concepts have been designed with a large base. These structures are generally designed for water depths of 300 to 400 m. The first fundamental natural period (sway mode) is in the range 5-7 s. Hence these storm resistant structures are very sensitive to every day fatigue loading. In order to avoid fatigue failures some of the structures are designed with a few members and joints. This class of structures which include monotower platform, and concrete/steel tripod tower platforms are characterized by a slender large diameter vertical cylinder piercing the free surface. The main advantage in these structures is that all the piping systems can be accommodated inside the centre column and thus be protected from the environmental loads. These structures are also suitable for ice covered waters.

Tripod Tower Platform

The steel tripod tower platform (TTP) is a fixed deepwater platform, specifically designed for the hostile environment of the northern North Sea (Michelsen and Meek, 1982). The structure is suitable for water depths up to 375 m. The tripod concept was originally conceived as a possibility for the Troll field, where it would have supported a 60,000 tonnes topside weight in 340 meters of water. In fact the first concept was designed for 300 meters water depth (see Fig. 2.2), with a 30,000 tonnes of deck weight.

The wave forces experienced by the platform are minimized due to a reduced area

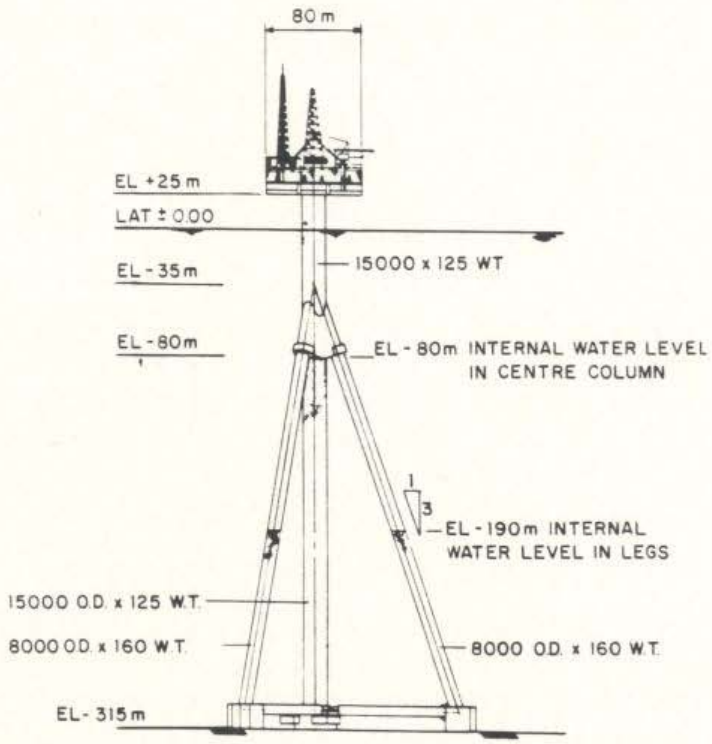

Figure 2.2: Steel tripod tower design developed by Heerema Engineering Service, the Netherlands (Michelsen and Meek, 1982)

near the water surface. The concept aimed at maximum simplicity, maximum use of unstiffened tubular elements and minimum number of nodes. Large diameter (15 m), heavy wall thickness (125 mm) tubular members are used for the main column. A main central concentric vertical column is supported by three inclined legs, at a batter of 3:1, to transmit the vertical and horizontal loads of the structure to the sea bed.

The TTP concept can also be designed for shallow waters. The world's first tripod tower platform was installed in July 1986 by Heerema Engineering Service B.V. in the Unocal's Helder field, 55 km off the Dutch Coast (Duncan and Vander, 1987).

The fundamental natural period of the deepwater TTP structure is in the range of 5-7 s. The structure experiences similar problems as discussed for the case of the fixed deepwater platforms. Fig. 2.3 shows the classical single degree-of-freedom

dynamic amplification factor relative to wave periods. The figure compares the dynamic characteristics of the TTP concept with a compliant tower (Roseau). In the case of the TTP, high frequency resonance excitation occurs due to moderate waves while resonance also occurs in the case of the compliant towers due to the second and third superharmonic of the fundamental frequency which is closer to the peak spectral power of the storm sea state.

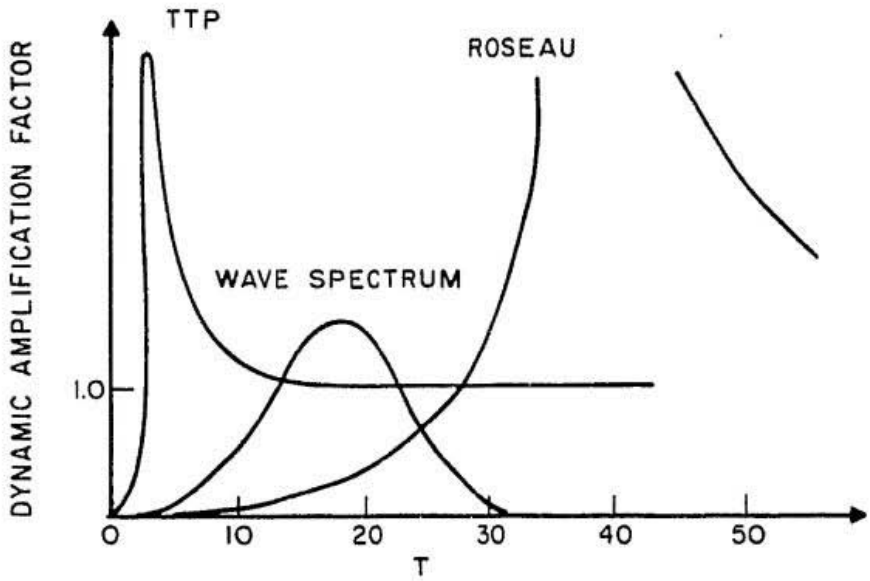

Figure 2.3: Dynamic amplification of response in tripod tower platform and in platform Roseau

2.2 Response to Waves

It has been emphasized in the foregoing section that complete avoidance of the occurrence of resonance for all operating and extremal conditions is practically impossible in the design of deepwater concepts. These structures are dynamically sensitive to wave forces. Hence dynamic analysis has become an integral part of the design process. Such analysis is required not only for estimating structural response to ex-

treme (design) storms but also for estimating response to less severe but frequently occurring sea states.

2.2.1 Theoretical Studies

The dynamic analysis of offshore structures has received increasing attention over the past two decades (Malhotra and Penzien, 1970 and Kint and Morrison, 1990). Investigation of the resonant behaviour of a deepwater structure subjected to regular waves was first carried out by Selna and Cho (1969). Finite element and lumped mass models were widely used in assessing the dynamic behaviour of the structure to wave forces (Gray et al., 1975; Vandiver, 1977). Both time and frequency domain solution techniques are followed depending on the analysis requirements (Basu and Singh, 1981). The main advantage of the time domain approach is the possibility of taking into account any kind of non-linearities. But unfortunately this method requires a lot of computer time. The frequency domain analysis requires, usually, the linearization of any type of nonlinear forces, in order to determine the set of transfer functions needed to compute the dynamic response of the structure. The method of stochastic analysis of offshore structures has been reported by Berge and Penzien (1974). In general the frequency domain approach is used in the stochastic response analyses.

In some cases the time domain approach has been followed even for the stochastic response analysis (Shinozuka et al., 1977). The method uses a simulation technique which generate random wave loads. The environmental conditions are described by a wave spectrum. A linear filtering method makes it possible to compute a time history of the wave elevation, and then, the time history of the water particle kinematics. With Morison's definition of the wave loading, the dynamic equations of motion are solved numerically in a Monte-Carlo sense.

In general the industry prefers to use a frequency domain model during the

preliminary design stage. However the time domain analysis is inevitable during the detailed engineering phase.

Simulation of Wave Profile

Performing a dynamic analysis in the time domain for random waves involves modelling the random fluid field. Several numerical formulations are available in the literature for establishing the time series of water particle kinematics in random seas. A review of the most relevant formulation was presented by Chakrabarti (1987). The conventional method computes the water particle kinematics by summing a finite number of sinusoidal time histories with different frequencies and random phase angles. The principle of this method is given by Borgman (1969). Although this method gained general acceptance, it has been shown later that summing the sinusoidal components is somewhat a numerically inefficient technique to use for time domain analyses. To replace this numerical inefficiency, Sami and Vandiver (1984) proposed a model which uses an auto-regressive moving average (ARMA) filter to simulate random water particle kinematics.

Estimation of Damping Parameters

Accurate determination of the response of an offshore structure is not only dependent on the method used for the analysis but also on the dynamic parameters which are described in the analytical model.

Stiffness and mass properties of an offshore structure can be adequately reproduced in the finite element model. However it is not the case with the damping matrix. To date there exists no exact formulation for the description of the damping mechanism in the analytical model. In the analysis of large offshore structures it is customary to assume a proportional damping model (Rayleigh damping), where the damping matrix is assumed to be proportional to mass and (or) stiffness matrix

of the structure. The calculation of the Rayleigh damping is presented in Bathe and Wilson (1976). Vugts and Hayes (1979) present the various sources of damping and their characteristics for a fixed offshore structure. The important sources of damping are: (a) material damping, (b) structural damping (c) wave making damping (d) flow-separation damping, (e) skin friction damping, and (f) foundation damping.

The damping factor has a large influence on the response amplitude in the region of resonance. In fact the damping serves to limit the motions to a finite value at and close to resonance. For this reason most of the investigations carried out during the last decade concentrated on the damping of offshore structures.

Vandiver (1980) developed an elegant method for predicting the dynamic response of an offshore structure to random waves at a known natural frequency. The method is very useful when the dynamically amplified response of a structure at a natural frequency is of prime concern. Since the wave exciting forces can be defined in terms of radiation damping [according to the reciprocity relations of Newman (1962)], Vandiver expressed the response of an inertial dominated structure in terms of the damping parameters. The method shows that the response is not inversely proportional to the total damping, but is proportional to the ratio of radiation damping to the total damping. The application of the Vandiver method to an existing single pile platform has been shown by Cook and Vandiver (1982).

Even though there are several physical possibilities for the dissipation of energy by damping, the total damping is only around 2 to 5 percent of critical damping in a deepwater structure (Spidsoe and Langen, 1985).

The magnitude of damping used in the analytical model plays an important part in deciding the fatigue life of the structure (Vandiver, 1982). Hence a good estimate of the value of the damping ratio is very important for the design of a deepwater structure. In view of the importance of the actual magnitude of damping and the lack of knowledge regarding this matter, it is essential that field studies on

the existing structures be made to measure the damping coefficients.

Campbell and Vandiver (1980) developed an accurate technique to estimate the damping ratios of an offshore structure. The power spectral densities of the structural responses were estimated using Burg's Maximum Entropy Method and the damping coefficient determined. The method is more reliable than the case of using a conventional non-parametric estimation of power spectral densities.

More recently, research has been concerned with the estimation of dynamic parameters using modal testing and analysis (Ewins, 1986). Modal damping parameters can be estimated more accurately using modal testing and analysis techniques. Though the technique as such is not new, the most powerful methods have only recently been developed. The structure is excited by a known input force and the response output is measured at the points of interest. The relationship between the input force and the output response is defined as a transfer function. The transfer function can be estimated using a conventional nonparametric method (in the frequency domain) or using Auto-Regressive Moving Average models (in the time domain). The modal damping parameters can be estimated directly from the computed transfer function. Gundy and Scharton (1980) conducted modal testing for a steel template platform in the North Sea. The estimated damping ratios were in the range of 1 to 3 percent of critical damping.

2.2.2 Experimental Techniques

The response of an offshore structure to waves may also be assessed by using reduced scale models in the laboratory wave tank. In such investigations a hydroelastic design is adopted in the preparation of the physical models. Initially model studies were used only to verify the results obtained by analytical approaches. Later on it has become mandatory to use a physical model study in a wave tank to assess the viability of a newly developed deep water structural concept. For an example a 1:50

scale model of Lena Guyed Tower (water depth 350 m and pay load 19,500 metric tonnes) was tested in a large wave tank (50x80x10 m) to prove the feasibility of using this concept for the North Sea environment (Rajabi and Mangiavacchi, 1988). The model was fabricated with aluminium tubes and Froude similarity was followed to obtain the model properties.

More recently, it has been recognized that model studies in the wave tank are of paramount importance to the final design. This is very evident from the recommendation given by API RP-2T, 1987 (see Section 1.2.2, under the title *Planning and Construction*) to include a model study in the design of a tension leg platform.

Freire et al. (1987) designed a hydroelastic reduced scale model for a tension leg platform and studied the wave-structure interaction phenomena. A geometrically similar flexible model which behaves, in terms of its elastic deformations, in a manner corresponding to its prototype structure is called a hydroelastic model. The wave forces are also reproduced at the model scale. Hence the model is very useful in studying problems related to fluid-structure interaction phenomena.

Roitman et al. (1985) fabricated a hydroelastic model for a jacket type platform and studied the dynamic response of the structure to laboratory generated wave forces. A 1:70 geometric scale was used and the model was constructed with ABS plastic tubes.

In wave tank experiments, since the gravity waves are the prime source of loading, a Froude number similarity criterion is inevitably applied to the model design. However the observed Reynolds number discrepancy in the Froude model similarity largely affects the nature of the forces and the flow-separation behaviour (Holmes, 1981). For this reason a drag-dominated structure cannot be modelled successfully in a wave tank study.

However in the case of large diameter structures, a successful reduced scale hydroelastic model can be fabricated for the wave tank experiments (Srinivasan and

Swamidas, 1987). This is due to the fact that at low KC numbers the wave forces are predominantly controlled by the KC numbers in which case the effect of the Reynolds number can be neglected.

2.3 Fluid-Structure Interaction

It has been emphasized in the literature that the dynamics of offshore structures is of paramount importance in the design of deepwater structures. The significant role of damping in the vicinity of resonance has also been pointed out in the previous section. However, it is very important to review certain literature pertaining to the source and nature of damping in offshore structures. Whether it is a fixed structure or a floating platform, the total damping in the system is seldom more than 2% of critical damping which is considered to be a very small value. Out of this 2%, the hydrodynamic damping contributes 75% of the total damping. For this reason, the major attention in the literature is given to damping that arises from hydrodynamic sources.

2.3.1 Hydrodynamic Damping

Hydrodynamic damping is due to the interaction effect between the structure and the fluid surrounding the structure. When a structure oscillates in an oscillatory wave flow, energy is dissipated through the infinite fluid media by various mechanisms. Considerable effort has been made in the mathematical modelling of these damping mechanisms during the past two decades.

In general hydrodynamic damping has three physical sources: the generation of surface waves which radiate energy to infinity, the skin friction (viscous) effect and the flow-separation effect. Mathematical modelling of the wave radiation damping was first described by Newman (1962). It has been proved using the Haskind-Newman reciprocity relations that the radiation damping can be explicitly defined in

terms of modal wave exciting forces (Vandiver, 1980). In fact the radiation damping is frequency dependent and hence is non-proportional by nature. McCormick (1989) proposed a method of analysis for a fixed offshore structure which considered the radiation damping as a non-proportional damping.

Unlike the floating structure, the radiation damping in fixed offshore structures is very low. The wave radiation damping is also neglected from the analysis if the frequency of response is very low (as in the case of the TLP, in surge motion).

Skin friction damping at very high Reynold's number is very small. Thus in prototype structures the damping contribution from the skin friction effects may not significantly affect the responses. However this may not be true in the case of a laboratory model study where the wave flow is in the subcritical region (ie., low Reynold's number).

To date the importance of damping, arising from the flow-separation phenomena, is best understood through the large volume of work available on this topic. Attempts have also been made to numerically model the separated flow behind bluff bodies in an oscillatory flow (Lian, 1986). However due to the complexity of the physical problem, such as interaction between vortices which cannot yet be modelled mathematically, such methods are not commonly used in the literature. However, it is customary to use empirical relations to incorporate the damping that arises from the flow-separation phenomena.

2.3.2 Separated-Flow Drag Damping

The separated-flow drag damping may be represented in terms of the relative velocity between the velocity of the water-particle and the velocity of the structure in the underwater portion of the offshore structures. The Morison wave force formula is accordingly modified and the equations of motion are then solved either in the frequency domain or in the time domain. In this formulation the separated flow

damping is inherently incorporated in the analysis. The serious problem associated with this type of modelling is that due to the square term in the drag forces. The result is that the governing differential equation becomes nonlinear in terms of the response of the structure.

When considering a stochastic analysis, the square term in the modified Morison formula is linearized and the analysis is carried out in the frequency domain. The earliest successful work on stochastic response analysis, with an equivalent linearization technique for the non-linear fluid-structure interaction problem, was carried out by Malhotra and Penzien (1970). The advantage of such a linearization is that the normal mode superposition technique may be used and the response of the structure, in the frequency domain, may be obtained through simple numerical means. The procedure is computationally very efficient.

Several approximations for the nonlinear damping term are proposed in the literature. The coupled drag term may be decoupled under this assumption as follows (see Penzien, 1976):

$$|u - \dot{x}|(u - \dot{x}) = |u|u - 2(< |u| >)\dot{x} \tag{2.1}$$

where $< |u| >$ represents time average of $|u|$, u is water particle velocity and $\dot{x}$ is the structural velocity. In the above equation the higher order time-dependent damping terms (in powers of $\dot{x}$) are neglected.

The error involved in the linearization of the nonlinear drag term is explained by Blevins (1977). In a drag force dominated structure, when the structural velocities are comparable with the water-particle velocity, the linearization significantly affects the response calculations. However in the case of inertial force dominated structures or in the case of responses away from resonance, linearization of the nonlinear drag term is permitted in the analysis.

The latest studies also indicate that during low frequency oscillations (especially for the large diameter structures like the TLP), the drag damping is no longer

nonlinear and a linear damping model is adequate for the analysis (see Chakrabarti, 1990a, and Verley and Moe, 1979).

On the other hand, the measured damping of fixed gravity and jacket platforms is found to be highly nonlinear in a full scale experiment conducted on existing structures in North Sea by Spidsoe and Langen (1985). They also showed that the commonly applied linear damping models are non-conservative.

From the above discussions it can be stated that, in the case of low frequency motions, a linear damping model may be adequate for the analysis. However for the high frequency responses the nonlinear damping model is essential for realistic response calculations.

Another interesting work, by Dunwoody and Vandiver (1981), on the modelling of the drag damping, applied a sophisticated technique in which the nonlinear damping is approximated by a cubic polynomial in terms of the relative velocity between the fluid and structure:

$$|u_R|u_R = C_1\,\sigma_{u_R}\,u_R + C_3\,\frac{u_R^3}{\sigma_{u_R}} \tag{2.2}$$

where $|u_R|$ is the magnitude of the relative velocity between the water particle and the structure; $C_1 = \frac{\sqrt{2}}{\pi}$ and $C_3 = \frac{\sqrt{2}}{9\,\pi}$ and σ_{u_R} is the rms value of u_R.

The comparison between the nonlinear term and the approximation in the Dunwoody and Vandiver equation has been quite good over a large range of the rms value of u_R.

Effect of Drag Damping

In spite of the various sophisticated developments which have been achieved in the linearization technique, a group of researchers are still interested on the time-domain approach in which the drag nonlinearity is retained. The time-domain stochastic analysis uses the Monte-Carlo simulation technique and generates the

random flow field for a given wave elevation spectrum. The two important earliest works published on the dynamic analysis of fixed deepwater offshore structures are by Burke and Tighe (1972) and by Shinozuka et al. (1977). Both these approaches are similar; however Shinozuka et al. used the Fast Fourier Transform technique to simulate the water particle kinematics.

Before concluding this section it is worthwhile to study the effect of the separated flow damping on the dynamic response of deepwater structures through the reviewed literature.

Malhotra and Penzien (1970) observed that the fluid-structure interaction, included in their stochastic analysis, reduced the rms response of a drag dominated fixed offshore structure. Burke and Tighe (1972) showed that when this interaction was included, the magnitude of the spectral peak at the fundamental frequency is reduced markedly; the amplitude of the peak corresponds to an internal structural damping of about 6% of critical damping.

Shinozuka et al. (1977) found that an equivalent linearization technique at high wind velocities (ie., at extreme sea state) might underestimate the magnitude of the nonlinear drag forces. At low to moderate wind velocities the response was observed to be a narrow band random process with the apparent frequency near the first natural frequency of the structure. Under this condition the inclusion of the nonlinear drag term reduces the response at the resonant peak.

2.4 Flow-Separation at Low KC Numbers

Ever since Morison, et al., in 1950 introduced an empirical formula to describe the wave forces on a vertical pile, understanding the mechanics of oscillatory flow around a cylinder and predicting the forces acting of the cylinder has been of prime interest to researchers in the area of hydrodynamics. Predicting wave induced forces on cylinders is a complex problem and it alone is treated as a broad subject (Shaw,

1979). Much of the present level of understanding on this complex behaviour is made possible by a great deal of experimental effort which has been devoted in the past two decades by a large number of investigators. Numerous references on this topic may be found (see Chakrabarti, 1990b) and the complete coverage of them is practically not possible.

The present interest of this section is to understand the characteristics of the shedding mechanism in an oscillatory flow past a vertical cylinder. It is obvious that the drag damping due to fluid-structure interaction phenomena discussed in the previous section is also associated with the mechanics of flow-separation. If flow-separation occurs then the structural motion alone cannot have the independent capacity to dissipate energy in the fluid media (in the form of flow-separation).

Oscillatory flow is a special case in the subject of fluid dynamics. Unlike a unidirectional flow the flow-separation characteristics are not completely dependent on the Reynolds number (R_e)[2]. The Keulegan-Carpenter number (KC) also plays an important role in deciding the location of the separation point and in the formation of the wake behind the cylinder.

The dependency of wave forces on R_e and KC numbers may be derived through dimensional analysis (Srinivasan and Swamidas, 1987). In fact Stokes (1851) was the first to show that the force acting on a cylinder, oscillating sinusoidally in a viscous fluid, is dependent on both KC and R_e numbers. Various researchers have shown that the Morison coefficients C_m and C_d (also called the hydrodynamic coefficients), are continuous functions of Keulegan-Carpenter numbers (see Fig. 2.4).

2.4.1 Wave Force Measuring Experiments

Laboratory wave tank and U-tube apparatus tests are the two general methods which are used to determine these two hydrodynamic coefficients. The fundamental

[2]The nondimensional numbers, Reynolds number and Keulegan-Carpenter number, are defined in Eqns. 3.2 and 3.3, respectively

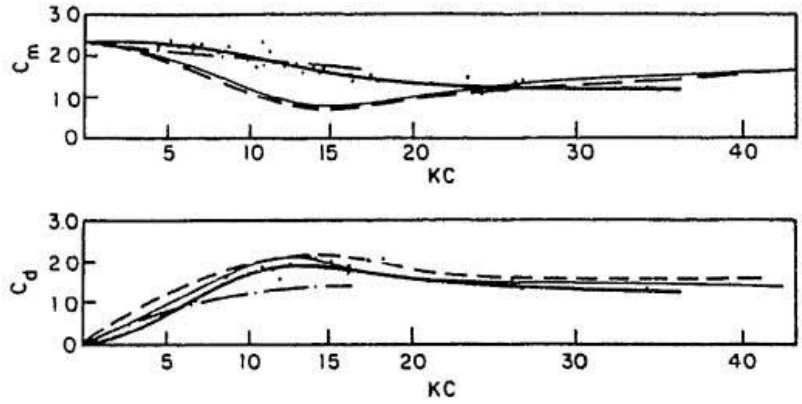

SOURCE OF RESULTS	RANGE OF KC	RANGE OF R_e	RANGE OF DIA.	TYPE OF EXPERIMENT
DAVIES, 1976	0 to 35	$\geq 15 \times 10^3$	½", ¾", 1"	VERTICAL & INCLINED CYLINDERS IN WAVES
CHAKRABARTI ET AL, 1976	0 to 16	$\geq 28 \times 10^3$	3"	VERTICAL CYLINDERS IN WAVES
SARPKAYA, 1976	0 to 200	$\geq 7 \times 10^3$	2" to 3"	HORIZONTAL CYLINDERS IN ONE-DIMENSIONAL OSCILLATING FLOW
KEULEGAN & CARPENTER, 1958	0 to 200	$\geq 23 \times 10^3$	½", ¾", 1", 3"	HORIZONTAL CYLINDERS IN ONE-DIMENSIONAL OSCILLATING FLOW

Figure 2.4: Hydrodynamic coefficients vs. KC number for vertical cylinders

difference between these two methods are that in the U-tube apparatus the motions are strictly one-dimensional while in the wave tank the particle motions are orbital. Although the wave tank testing is more realistic with respect to the actual ocean, the basic advantage of the U-tube apparatus is the greater controllability which allows the researchers to obtain higher Reynolds numbers. Sarpkaya has reported numerous studies on the variation of hydrodynamic coefficients as functions of Keulegan-Carpenter number, Reynolds number and roughness parameter (see Sarpkaya and Isaacson, 1981).

It is interesting to begin this review with one of the earliest work reported by Sarpkaya et al. in 1977. In this study a U-tube apparatus was used and the hydrodynamic coefficients were obtained as smooth functions of R_e numbers for different KC's. In general, it has been observed that the increase in C_m with R_e (or KC) results in a corresponding decrease in the C_d value. Parallel studies and the determination of hydrodynamic coefficients using wave force measurements in the

laboratory have also been published in the literature (Chakrabarti, 1980). Unlike the U-tube apparatus, in the wave tank experiments the relation between the C_m and C_d values, with respect to R_e, may not be easily obtained. This is due to the limited range of R_e numbers possible in the wave tank experiments. For this reason in most of the literature C_m and C_d values are presented as a function of KC number only. With the availability of data from two different types of experiments it is natural for a designer to wonder which data may be more appropriate to use in his analysis. To solve this problem Chakrabarti (1990b) compares his wave tank results with Sarpkaya's U-tube results. In general a good agreement between these two sources of results has been observed except at a localized region where KC ranges between 10-15. In this region a one-dimensional oscillatory flow shows a larger flow-separation than the case of the orbital particle motion. Thus the C_d values in the wave tank experiments are found to be lower and the C_m values to be higher than the corresponding values in the U-tube experiments.

2.4.2 C_m and C_d coefficients

Some investigators have indicated, through flow-visualization studies, that the vortex shedding characteristics for a circular cylinder are controlled by the KC numbers (Stansby and Isaacson,1986). For KC < 4, vortices are shed symmetrically, for 4 < KC < 8 stronger vortices are shed on one side of the cylinder which produce a time-varying asymmetric wake; for 8 < KC < 15 there is a transverse wake; for 15 < KC < 22 the wake is diagonal; for 22 < KC < 30 a third vortex is shed per half cycle and for KC > 30 the wake is quasi-steady (see Fig. 2.5).

Practically all the laboratory experiments (until very recently) have been conducted for KC larger than about 4, keeping in mind the jacket type platforms. The member diameters for jacket type structures are relatively small and the total wave forces are dominated by the drag effect. In most of the operating conditions the

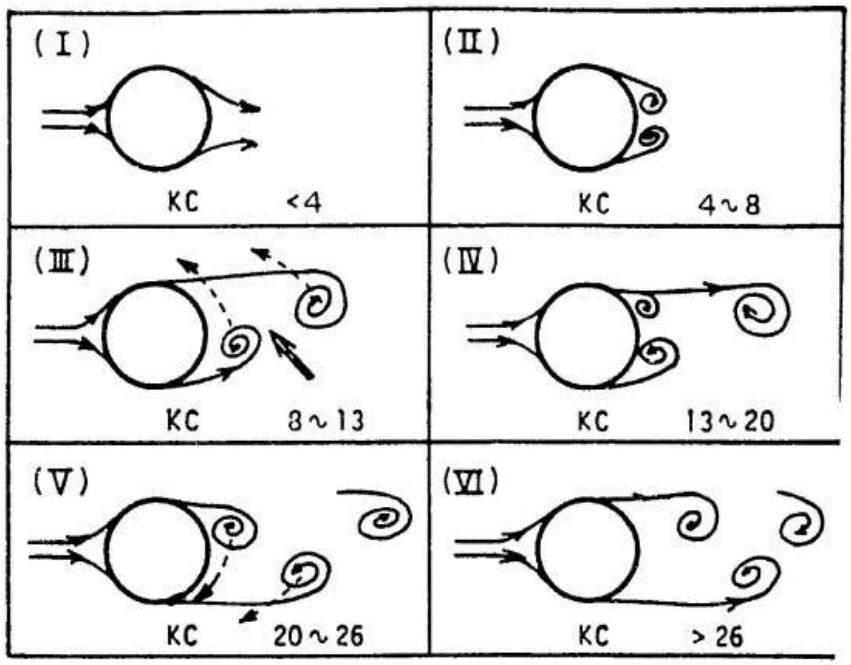

Figure 2.5: Vortex shedding patterns around a vertical cylinder in an oscillatory flow as functions of KC

range of KC numbers is very large. Hence, the experiments were conducted using small diameter cylinders (1.27 cms - 7.62 cms; ref. Fig. 2.4).

Many recent studies have reported using large diameter vertical cylinders for the C_m and C_d analysis (see Bearman, 1988; Klopman and Kostense, 1989; and Srinivasan et al., 1990a). In these studies 30 to 50 cm diameter vertical cylinders were tested in large wave flumes with regular and random waves. One of the main advantages of using large diameter cylinders is that higher Reynolds numbers (up to 5.5×10^5) may be achieved in the experiment.

The hydrodynamic coefficients obtained as a function of KC numbers by Klopman and Kostense (1989) for a 0.5 m diameter vertical cylinder, in 5 m water depth, are shown in Fig. 2.6.

Although Figs. 2.4 and 2.6 fundamentally define the same thing, noticeable differences may be observed in Fig. 2.6 due to the increase in diameter from 7.62 cms

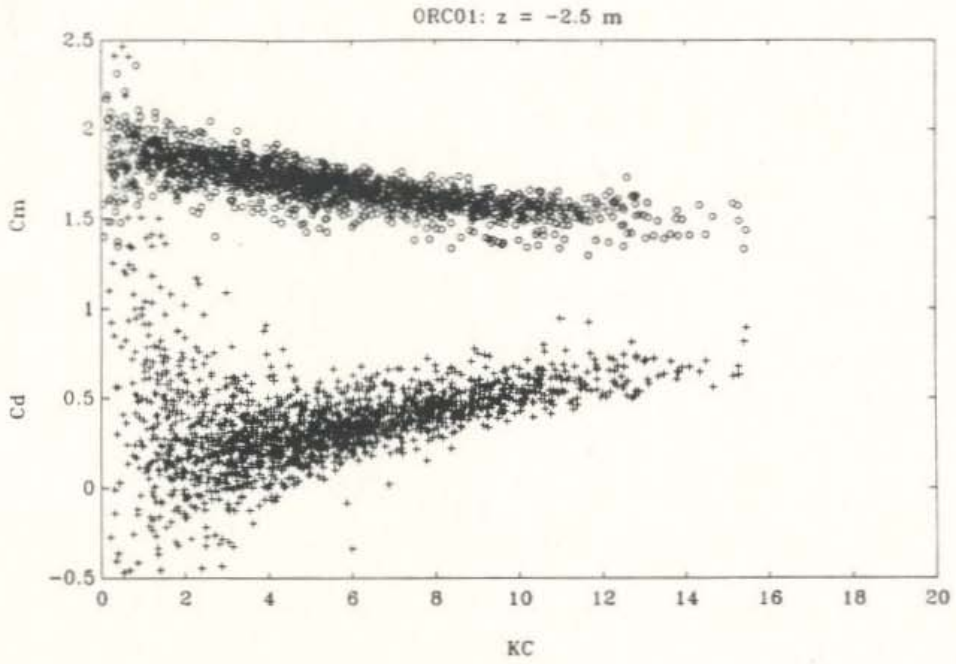

Figure 2.6: C_m and C_d versus KC number for a 0.5 m diameter vertical cylinder (Klopman and Kostense, 1989)

to 50 cms. In the case of large diameter members the value of the drag coefficient at KC < 2 is greater than in the case of small diameter members. In Fig. 2.4, the value of C_d approaches zero as the KC number tends to zero. Therefore at low KC numbers the C_d value for a large diameter cylinder can be much higher than what is commonly expected based on the measurements with small diameter cylinders.

The dependency of hydrodynamic coefficients on Reynolds number at low KC numbers is also very important. Justensen (1989) presented C_m and C_d values as functions of low KC numbers for two different R_e numbers, viz., 2.5×10^5 and 1.0×10^6. He observed that at KC number above 5 the C_d value for $R_e = 1.0 \times 10^6$ is much higher than the C_d value for $R_e = 2.5 \times 10^5$. However, at low KC numbers (KC < 5), the two curves merge with one another and show that there is no dependency of Reynolds number on the hydrodynamic coefficients.

Therefore the dependency of C_m and C_d coefficients on Re numbers is not evident

at very low KC numbers.

2.4.3 Investigations at Low KC numbers

Investigation of the separated flow damping phenomena at low KC numbers is a relatively new area, but progress in this area over the last few years has been rapid and steady. In the literature many interesting flow phenomena have been observed at low KC numbers.

Bearman et al. (1985) reported experimental data and analysis for a number of cylinders of different cross-section including circular cylinders and sharp-edged sections in planar oscillatory flows (also see Graham, 1978 and Graham, 1980). The emphasis has been on flow-separation due to sharp edges. The hydrodynamic coefficients at low KC numbers for circular, square, and diamond cylinders and a flat plate are compared in Fig. 2.7. At a KC number equal to 1 the C_d for a circular cylinder was 0.8, for a square cylinder 3, for a diamond cylinder 4.5 and for a flat plate it was 7.5. Similarly the C_m for a circular cylinder was 2.05, for a square cylinder 3, for a diamond cylinder 1.8 and for the flat plate it was 1.2.

More recently, Hamel-Derouich (1991) studied the wave forces on rectangular cylinders at very low KC numbers. The experiment was conducted in a wave tank for KC numbers less than 1 and the obtained C_m and C_d values were plotted as a function of KC numbers (see Fig. 2.8). It can be seen from the figure that the drag coefficient exhibits very large values (up to 400) as KC number approaches zero, then falls very sharply as KC number increases within a small range.

From these reported studies it can be concluded that the cylinders with sharp edged corners behave contrary to the circular cylinder at low KC numbers ($KC < 2$). In this range, large values for the drag coefficient and a drop in the value of inertial coefficient are noticed.

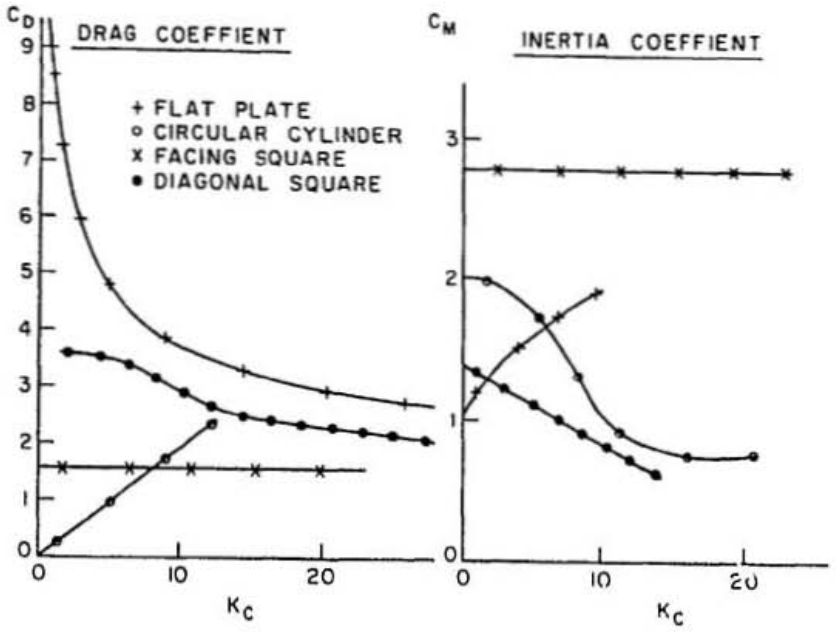

Figure 2.7: C_m and C_d versus KC number for various sections (Graham, 1978)

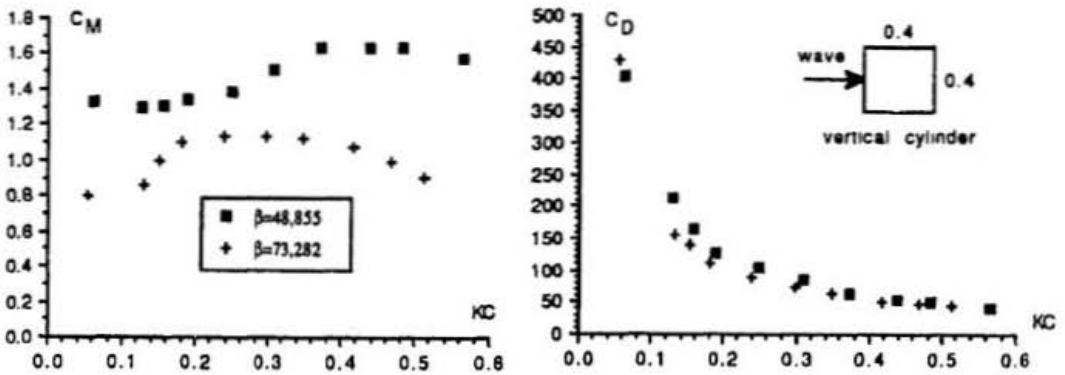

Figure 2.8: C_m and C_d versus KC number for rectangular cylinder (Hamel-Derouich, 1990)

Application of Low KC number C_d

Graham (1988) discusses the practical application of the flow-separation from sharp edges to the problem of roll damping of barges. Damping is caused by vortex shedding and its magnitude depends on whether the corners are rounded, sharp or with bilge keels. A significant increase in damping has been found in the computation.

Drag damping due to sharp edge cylinders (at low KC numbers) has also been applied to other deepwater structures. Qi et al. (1984) tested a TLP model at a scale of 1:64 and reported the value of hydrodynamic damping factor in surge (low frequency) motion. Two different pontoon geometries were used, viz., a circular and a rectangular shape. The damping factor increased from 0.06 to 0.09 due to the sharp edged pontoon. For the case of semi-submersible platforms, the square corners were found to increase the heave damping to a maximum of five times that of rounded ones (Marchand et al., 1988).

It has been mentioned earlier that springing is an unwanted resonant behaviour which has been observed in the heave motion of tension leg platforms (Huse, 1990 and Chakrabarti, 1990a). The hydrodynamic damping in the heave oscillation is very low. In order to increase the drag damping in the heave mode Chakrabarti (1989) proposed a new technique which uses a device consisting of a circular ring. The device is attached to the TLP leg at a lower elevation in the water. When the structure oscillates in the heave motion the device induces flow-separation and thus dampens the heave oscillations. The experiment was carried out for the Conoco TLP structure at a reduced scale.

2.5 Summary

The following important points are summarized from the literature review. Structures specially designed for deepwater applications offer superior performance over the conventional jacket type platforms. In the deepwater concepts, whether it is

a fixed or a floating structure, occurrence of resonance at all operating and extremal conditions cannot be avoided. The theoretical and experimental investigations showed that large dynamic amplification of response occurs for moderate and extreme wave conditions. In the vicinity of resonance separated-flow damping plays an important role in determining the structural response to wave excitations.

Separated flow-damping is included in the analytical model by using the relative velocity formulation in Morison's wave force formula. This empirical model has been the most widely used as the accepted method to explicitly include the damping associated with flow-separation phenomena. The drag term in the model is nonlinear in terms of the velocities of the fluid particles and that of the structure. At and close to resonance the nonlinearity influences the response significantly. Hence a time domain analysis which retains this nonlinearity is recommended for the response calculations.

In the final section the characteristics of vortex shedding are discussed. Emphasis has been placed on the behaviour of the flow at low KC numbers. Interestingly the drag forces for the sharp edged cylinders are found to be much larger than that for circular cylinders. This shows the feasibility of introducing flow-separation at low KC numbers for a circular cylinder. Many recent studies have included the drag force due to sharp edges for the application of damping in deepwater structures.

Chapter 3

Effect of Induced Flow-Separation on the In-Line Forces for a Vertical Cylinder at Low KC Numbers

Investigation of the mechanics of flow-separation at low Keulegan-Carpenter (KC) numbers has become increasingly important due to its wide application in the damping of many offshore structures. Until recently it was generally assumed that the drag forces at low KC numbers were not important from the research point of view. Observations as well as numerical experiments carried out by Graham (1978), for some simple geometries at relatively low KC numbers (0 to 5), indicated large drag forces. Consequently, recognizing the engineering applications of these findings has also become an important part in many recent studies.

The principal goal of this investigation is to induce drag forces on a circular cylinder at low KC numbers. The underlying principles are based on the mechanics of flow-separation at low KC numbers. Therefore, this chapter first briefly explains the phenomenon of the flow-separation for bluff bodies at low KC numbers and then introduces a conceptual design (a physical device) to induce flow-separation for a large diameter vertical circular cylinder. In the rest of this chapter, the effect of the device on the hydrodynamic coefficients of the cylinder, established through a wave

force measuring experiment, is discussed. Prior to that the experimental program used for this study is also explained.

3.1 Mechanics of Flow-Separation

Flow-separation occurs when real fluids interact with bluff bodies and viscosity is the key factor which plays an indirect role in the mechanics of flow-separation. The effect of flow-separation on problems related to fluid-structure interactions is best understood in terms of its consequences.

In a unidirectional steady 2D flow, separation of the flow from the surface of the body can be characterized by a single nondimensional parameter called the Reynolds (R_e) number. However, in an oscillatory 2D flow, vortex shedding characteristics have been found to depend on one more nondimensional parameter called the Keulegan-Carpenter number (KC). The oscillatory flow is fundamentally different from the unidirectional flow in many aspects. Consider a 2D circular cylinder which is subjected to a harmonic flow where the direction of the flow is normal to the axis of the cylinder. In the case of the oscillatory flow the flow, does not only accelerate from and decelerate to zero, but, also changes the direction during each cycle. As a result of this flow-reversal, wakes form on both the downstream and upstream sides of the cylinder. During this process some vortices are convected and some are newly formed in each cycle of the flow. This complex behaviour is predominantly controlled by the KC number. For this reason it can be stated that in a harmonic oscillatory motion the KC number controls the formation of the wake to a far greater extent than the R_e number. The KC number takes into account the time, necessary for a wake to form, and compares it with the time available before flow-reversal occurs every half cycle of the oscillation.

The behaviour of the oscillatory flow past a 2D circular cylinder at low KC numbers is a unique problem. For KC numbers less than 4, there is insufficient time

available for the flow-separation to initiate and develop behind a circular cylinder. Even before the flow-separation is initiated, the occurrences of the flow-reversal diminishes the chances of the formation of vortices behind the cylinder. As a result of this behaviour, the drag forces on a circular cylinder reduce progressively towards zero as the KC number decreases to zero. This physical behaviour has already been illustrated, schematically, in Fig. 2.5.

However a sharp edged cylinder behaves in an entirely different manner from the circular cylinder. Flow-separation is bound to occur in spite of the frequent flow-reversals occurring at low KC numbers. This is due the fact that the sharp edges automatically produce flow-separation and, unlike the circular cylinder, there is no time factor involved for the adverse pressure to develop and the separation to initiate. The vortices which are produced at the rear of the cylinder convected from the rear to the front side of the cylinder during each cycle of the flow-reversal. This further develops the wakes behind the cylinder. The flow-reversal, which prevents the possibility of wake generation behind a circular cylinder, creates the possibility for a wider wake in the case of a sharp edged cylinder. Under this condition the generation of the wakes (at low KC numbers) gives rise, not only to a form drag, but, also to significant changes in the inertial forces. Hence the added mass coefficient for the separated-flow past sharp edged cylinders is not necessarily equal to that given by the potential flow theory for the unseparated flow (in which case, the Morison equation approach would be preferable).

It is not the purpose of this thesis to examine the mechanics of flow-separation for sharp edged cylinders at low KC numbers. Rather it is our interest to understand the mechanics of flow-separation and use it for the application of damping in an offshore structure. The previous study carried out by Graham (1978) perhaps will help us to further understand the behaviour of the oscillatory-flow at low KC numbers. For the purpose of this discussion, the illustration shown in Fig. 2.7 may be recalled

here. The figure presents C_d values of the planar oscillatory flow past 2D cylinder of different geometries, viz., a flat plate, a circular cylinder, a normal-facing square and a diagonal-facing square (hereafter called as a diamond section or cylinder). The hydrodynamic coefficients for these geometries are presented as a function of the KC number in this figure.

In Fig. 2.4 it can be observed that the value of the drag coefficient (C_d) for circular cylinders decreases towards zero as the KC number tends toward zero. On the other hand, it is interesting to see that, sharp edged cylinders behave in a contrary fashion to circular cylinders. For these cylinders, the drag coefficient increases to a large value as KC $\rightarrow$ 0 and consequently the value of C_m decreases.

For example consider the case of a diamond-shaped cylinder; the value of C_d increases and the value of C_m decreases as KC $\rightarrow$ 0. The value of C_d for the circular cylinder at KC = 1 is 0.2 and for the diamond cylinder it is 3.2. Similarly the value of C_m for the circular cylinder at KC = 1 is 2.0 and for the diamond cylinder it is 1.4. The large increase in the value of C_d by a factor of 16, as well as the significant decrease in the value of C_m (in the comparison made between the diamond and circular cylinders), indicates that the flow around sharp edged cylinders behaves fundamentally differently from that around circular cylinders.

With the insight gained from the above discussions, on the mechanics of flow-separation, a conceptual design (a configuration), which would induce the flow around a circular cylinder to separate at low KC numbers, is introduced. The objective is to increase the drag forces on a large diameter vertical cylinder without significantly changing the inertial forces.

3.2 The Flow-Separation Device

For the purpose of this study, a 0.3 m diameter circular cylinder is considered, which in fact is the reduced size (1:50 scale) of the center column of the prototype

structure. Although previous studies have indicated the feasibility of introducing flow-separation at low KC numbers, the procedure to design a device which would satisfy the above objectives is somewhat cumbersome. Based on the principles of flow-separation, many configurations were designed and then tested for their effectiveness in a wave tank.

Numerical investigation can also be used to investigate the effectiveness of the designed configurations for a planar oscillatory flow. However the technique generally followed in the literature (see Lian, 1986), using arbitrary assumptions, is not completely relevant to the physical situation where the behaviour is highly complex due to the effect of interaction between vortices. In this case it is important to use an experimental method to identify a suitable device for the present purpose.

In order to assess the effectiveness of the designed devices, the devices were individually attached to the test cylinder (a major portion of the prototype structure) and the in-line forces were measured in the wave tank. Although the experimental set-up, the measuring technique, and the data analyses will be discussed in detail in the subsequent sections, it is instructive at this point to present the global behaviour of each of the fabricated devices. This will indicate the reason for selecting a particular device for the subsequent part of this chapter. It should be mentioned here that the scope of this thesis is not to present the results of all the designed devices; only the device which performed well in the wave tank will be discussed in detail.

Three different devices were designed and fabricated to induce flow-separation about the test cylinder. They were a hexagonal cylinder, a bundle of circular tubes and a bundle of diamond tubes. The hexagonal arrangement was used with an expectation that it would behave in a combined form of a facing square and a diagonal square (as reported in the Graham's study). The circular tubular bundle and the diamond tubular bundle had identical configurations. The concept of induc-

ing flow-separation was based on the observed interference effect between multiple cylinders in a bundle (see Chakrabarti, 1982). The details of this configuration will be discussed in the next subsection.

The results of the series of tests conducted by generating regular and random waves in the wave tank, without and with the attachment of the devices to the cylinder, can be summarized as follows. In the case of the hexagonal arrangement, a significant increase in the C_m value was noticed and the increase in C_d was also appreciable. When the circular tube bundle was attached to the test cylinder no significant changes in the value of C_m were observed, however the observed increase in the value of C_d was not sufficient to warrant a serious consideration. A significant increase in the value of C_d was found when the diamond tube bundle was used; at the same time very little change in the C_m values was noticed.

In this thesis the diamond tube bundle, which showed a much better performance than the other two devices, was selected for further analysis and experimentations.

3.2.1 Design of the Device

In this subsection the design aspects, of the diamond tube device, are outlined. The device consists of six small diamond cylinders (tubes) of size 2.3x2.3cm placed around the 0.3 m diameter test cylinder. The configuration of the device is shown schematically in Fig. 3.1. The principal objective of this configuration was to induce flow-separation around the main cylinder without contributing to the inertial forces on the main cylinder. The position and orientation of the diamond tubes were selected so as to give maximum flow-separation at low KC numbers. The interference effect, between the main cylinder and the tubes, introduces flow-separation from the circular cylinder and consequently enhances the vortices behind this cylinder. However, to avoid occurrences of a solidification inside the bundle, a minimum distance of six times the effective diameter of the diamond tube was provided as the

clear spacing between the main cylinder and the small tubes. The design principles can be further explained with the help of a previous study, conducted by Chakrabarti (1982), on the interference effects between closely placed cylinders, in a tubular bundle. For the purpose of explaining the principles involved, in the design of the device, the conclusions of his study are briefly listed below:

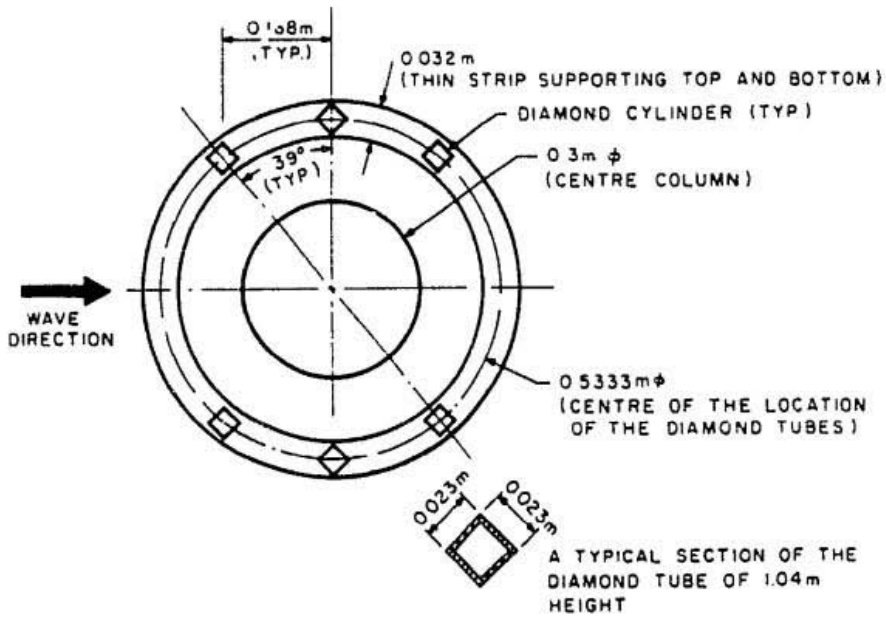

Figure 3.1: Configuration of the device to separate oscillatory flow

- For a relative spacing of more than 2 times the diameter of a cylinder in a bundle, there are no significant changes in C_m and C_d values for the cylinder.
- For the relative spacing exceeding 5 diameters, there is absolutely no interference effect occurring in the bundle.

Hence the present design, with more than six times the relative spacing between cylinders, obviously has adequate transparency for flow around the main cylinder.

3.2.2 The Working Principle of the Device

Related investigations, based on a flow visualization study, show that for KC numbers around 14, complete vortices develop behind the circular cylinder. Consider a flow regime in which the KC number for the main cylinder is equal to 1.5. For the same wave condition, the KC number for the small diamond tube is 14. Under this condition complete vortices can be generated behind the small diamond tubes. The presence of fully developed small vortices, around the diamond tubes, initiates a major flow-separation on the main cylinder. Thus the device induces immediate flow-separation similar to the case of sharp edged cylinders. When flow-separation is initiated the flow-reversal phenomenon, at low KC numbers, develops major vortices behind the main cylinder. This occurs due to the interaction between the vortices shed, during one half-cycle and those shed in the next half cycle of reversed flow.

The generation of vortices, by the device, may be explained further by considering the interference effect between the main cylinder and the diamond tubes in the bundle. Consider a diamond tube in the device attached to the test cylinder. As far as the diamond tube is concerned, the main cylinder and the rest of the diamond tubes are kept at distances more than six times the diameter of the diamond tube. Hence the diamond tube can be assumed to be an independent element which is free of the interference effect from the rest of the elements in the bundle. It is possible that independent vortices can be generated around the diamond tube. Under this condition, one can expect a clear flow-transparency around the main cylinder and, the possibility for the solidification of fluid mass inside the bundle is very small. However, the small diamond tubes are within the effective zone of interaction with the main cylinder. Though there is a flow transparency, the main cylinder is very sensitive to changes in the flow which occur around the diamond cylinders. Thus major flow-separation, and consequently large vortices, can be generated on the main cylinder.

3.3 Experimental Program

The major objective of this experimental program was to investigate the effect of the device on the hydrodynamic coefficients of the test cylinder as it interacts with waves of moderate amplitude and high frequency. The device was fabricated, attached to the test cylinder and then the behaviour of the cylinder was investigated for regular and random waves. These experiments were performed in a $57 \times 4.5 \times 3$ m wave tank, situated in the hydraulics laboratory, Faculty of Engineering, Memorial University of Newfoundland, Canada. The wave tank consists of a hydraulic piston type wave maker, situated at one end, and a parabolic beach, situated at the other extreme end. The tank is also provided with a towing carriage. During the experiment the wave elevations and the corresponding total wave forces on the test cylinder were measured.

In this section the experimental set-up and the measuring technique used are presented.

3.3.1 Experimental Set-Up

A significant portion of the main column of the candidate structure was reduced to a 1:50 geometric scale and used for this wave force measurement study. The test cylinder is made of acrylic material tubes of 0.3 m diameter, 3mm wall thickness, and 1.5 m height. The water depth was set at 1.44 m. The submerged length was 1.2 m measured to the still water level. The cylinder was installed at a distance of 16m in front of the wave maker.

Measuring System

A very accurate technique was used to measure the in-line wave forces on the cylinder. The special arrangement, which used an instrumented frictionless table, measured the wave forces directly and furnished the readings independent of the mo-

ments due to the horizontal forces at the base of the cylinder. The measuring technique is described below:

The cylinder was glued to a thick circular acrylic plate, which was attached rigidly to a circular steel plate. The whole set-up was fixed over a frictionless table as shown in Fig. 3.2. The frictionless table consisted of two parallel bars over which the circular steel plate was placed and supported at four equi-distant points. With that arrangement, the cylinder and its supporting system were guided by the parallel bars for free and smooth back and forth movements in the longitudinal direction. However the remaining degrees of freedom, including the rotational motions, were restrained automatically. In order to measure the in-line forces on the cylinder, a 50 pound capacity S-type load cell (manufactured by Transducers Inc.) was used. One end of the load cell was attached to the rigid and stationary frictionless table while the other end was attached to the freely moving cylinder (see Fig. 3.2).

For an applied horizontal force in the longitudinal direction at any point along the height of the cylinder, the moment at the base of the cylinder was resisted by the vertical reactions at the four supporting points over the parallel bars. And the horizontal force was independently resisted by the reaction absorbed by the load cell. Thus the measured readings from the load cell were independent of the moment due to the horizontal forces acting on the cylinder.

The results of the measuring system was verified by a separate calibration test as shown in Fig. 3.3. Known concentrated horizontal loads (static) were applied at a height above the supporting base of the cylinder. The load cell readings were noted down. A linear variation between the output voltage and applied force which was independent of the range of the applied load and the point of application of the load on the cylinder was observed. The calibration showed that the measuring technique was very accurate and reliable for the in-line wave force measurements.

It should be mentioned here that the method developed for this experimental

investigation is superior to the technique generally followed in the literature in which case the cylinder is usually supported by a flexible plate (or cylinder). Two strain gauges are fixed on the supporting plate. From the readings of the two strain gauges, the moments and consequently the horizontal forces can be calculated. The major disadvantage of the conventional method is that the cylinder movements may significantly affect the measured wave forces and secondly the wave forces have to be obtained indirectly from the moment calculations.

The frictionless table was placed, upside down, on the towing carriage and then fixed rigidly as shown in Fig. 3.4. The carriage was positioned at the test location in the tank. The cylinder was placed along the longitudinal center line of the tank and then the tank was filled with water. Three capacitance type wave probes were placed in the water, to measure the wave elevations at different locations. Two of them were kept, on either side of the cylinder, in line with the transverse center line of the cylinder. The purpose of such a set-up was to measure the wave elevations which were in phase with the measured wave forces. The third probe was placed in front of the cylinder at a distance of 4.1 m from the cylinder. The experimental set-up after filling water in the tank is shown in Fig. 3.5.

The analog voltages from the three wave probes and the load cell were digitized using a KEITHLEY SYSTEM 570 data acquisition instrument. Real time recording was used with 43.52 Hz sampling frequency. It should be mentioned here that, in the case of the random waves, the sampling frequency was changed to 36.4 Hz. The experimental variables were recorded with a desk-top computer and then subsequently transferred to a VAX 8530 computer for further analyses.

The Flow-Separation Device

The device was made out of six acrylic square tubes, placed diagonal to the wave direction. The dimensions and the positions of these tubes have already been given

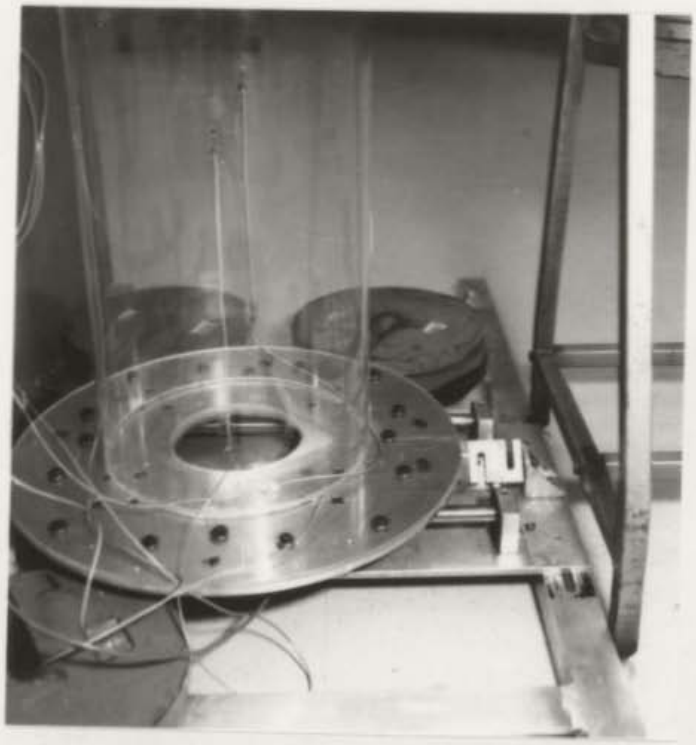

Figure 3.2: Fixing arrangement of the test cylinder on the frictionless table

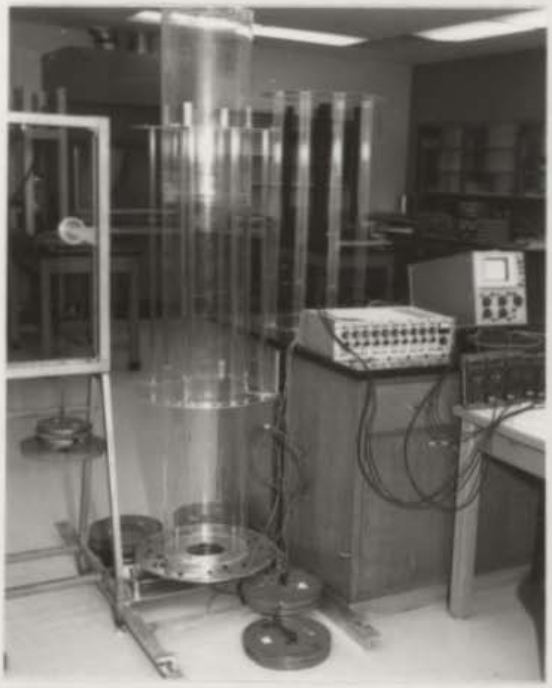

Figure 3.3: A calibration test in progress

Figure 3.4: The experimental set-up inside the wave tank before filling water in the tank

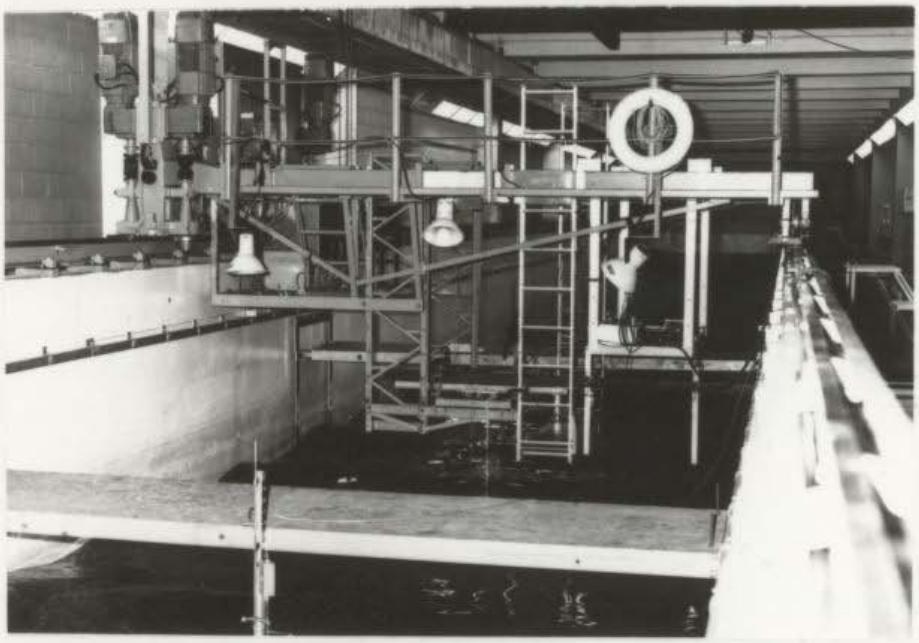

Figure 3.5: The experimental set-up after filling water in the tank

in Fig. 3.1. The fabricated device is shown in Fig. 3.6. Proper stiffening and supports were provided to hold the device in place. The device was designed for easy mounting on the test cylinder, so that it can be removed easily from the test cylinder and then be fixed again rigidly to the cylinder in the water. Fig. 3.7 shows the device, in place, with the cylinder in still water.

3.3.2 Preprocessing of Wave Data

The response of the cylinder was studied by generating regular and random waves in the tank. The device was attached to the test cylinder and the experiments were repeated with similar wave conditions. Sufficient interval of time was given between tests to allow the water to settle down in the tank. Prior to the wave force testing, calibration tests for the wave probes were performed and the calibration constants were taken.

Two special computer programs were developed to process this experimental data, one for regular waves and the other for random waves. Given the wave elevation and the wave force time series these programs compute the hydrodynamic coefficients using a least-squares technique. The programs are highly interactive and user friendly. The listing for these programs are presented, in appendices A and B, for the regular and random wave cases, respectively.

The procedure used in the preprocessing of the wave data is briefly outlined herein. The calibration constants obtained form the calibration tests were entered into the programs and the recorded data were converted to physical units. Then the preprocessor filtered out the high frequency noises and removed the linear trend from the recorded data. The computer program estimated the wave parameters by tracing the wave elevations in the time-domain. However in the case of the regular waves the trend removal from the data was not required.

In the experimental program, no analog filters were used to filter-out the high

Figure 3.6: The fabricated diamond tube bundle, the device

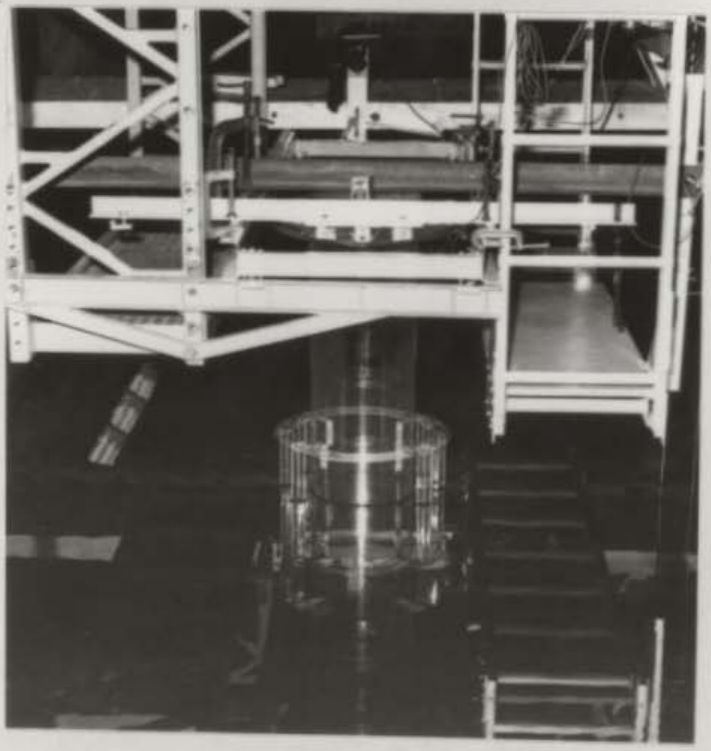

Figure 3.7: The device in place with the test cylinder in still water

frequency noise. Hence a digital filter was designed in the preprocessor and used to filter out noise above 6.0 Hz. Care was taken in the selection of the suitable filter required for this data analyses. In Fig. 3.8, the frequency response function of three popular digital filters (Yule Walk, Butterworth and Chebyshev) are compared. The performance of these filters were studied by inputting the measured wave elevations to the filter. Butterworth and Chebyshev were found to distort the input signal. However the Yule Walk filter (order 16) showed an excellent performance. Hence the Yule Walk filter was selected for the preprocessing of data. Typical wave elevation data, before and after applying the digital filtering, are shown in Fig. 3.9. In order to introduce the same time delay for all the measured channels, the measured wave force data were also passed through the designed filter.

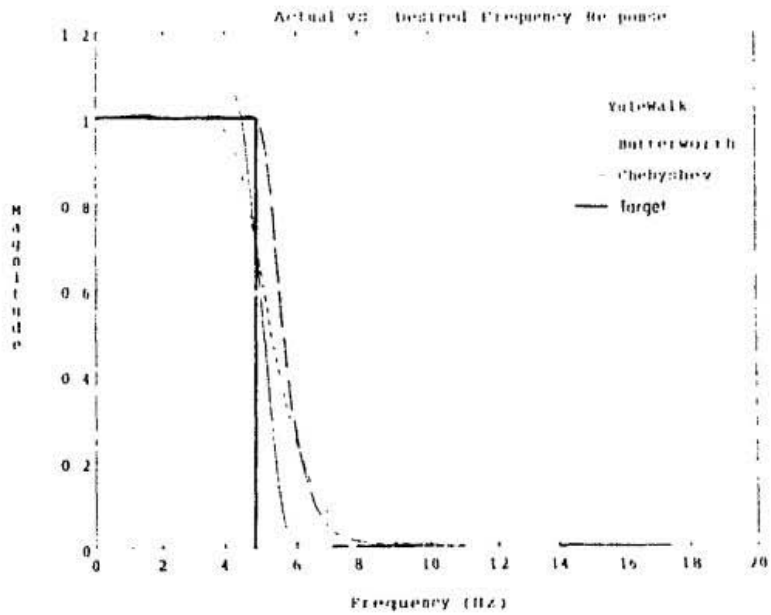

Figure 3.8: Comparison of the frequency response function for different digital filters

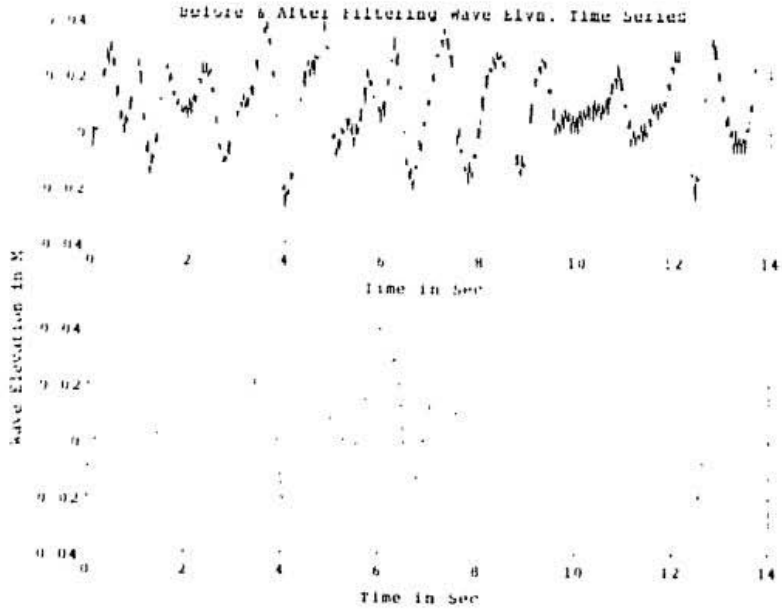

Figure 3.9: A typical wave elevation time series before and after filtering out the noise

3.4 C_m and C_d Analysis for Regular Waves

3.4.1 Morison's Formula

Morison's formula is generally applied to evaluate the hydrodynamic forces, both in the deterministic and stochastic approaches. The in-line wave forces on a unit section of a vertical cylinder are calculated by Morison's formula (Morison et al. 1950):

$$f = C_{ms} A_I \dot{u} + C_{ds} A_D |u| u \tag{3.1}$$

in which

f = force per unit length of the vertical cylinder

u = instantaneous horizontal water-particle velocity

$\dot{u}$ = instantaneous horizontal water-particle acceleration

C_{ms} = inertia coefficient for the cylinder per unit length

C_{ds} = drag coefficient for the cylinder per unit length

$A_I = \rho \frac{\pi}{4} D^2$

$A_D = \frac{1}{2} \rho D$

D = diameter of the cylinder

ρ = mass density of water

The empirical coefficients, C_{ms} and C_{ds}, are at least functions of the Keulegan Carpenter number (KC) and the Reynolds number (R_e). The definition of the KC and R_e numbers used in this study are:

$$R_e = \frac{U_m D}{\nu} \tag{3.2}$$

$$KC = \frac{U_m T}{D} \tag{3.3}$$

in which ν is the kinematic viscosity, U_m is the maximum horizontal water-particle velocity and T is the wave period.

3.4.2 Stokes Fifth Order Wave Theory

The particle kinematics defined in Eqn. 3.1 can be evaluated,for regular waves, using Stokes' fifth order wave theory. Although the details of theory can be found in Skjelbreia and Hendricksen (1961), the essential equations are presented here. The free surface water elevation η (see Fig. 3.10) from the still water level for a given wave height H, wave number k and frequency ω is defined by the equation:

$$\eta = \frac{1}{k} \sum_{n=1}^{5} a_n cosn(kx - \omega t) \tag{3.4}$$

in which

$a_1 = a$

$a_2 = a^2 B_{22} + a^4 B_{24}$

$a_3 = a^3 B_{33} + a^5 B_{35}$

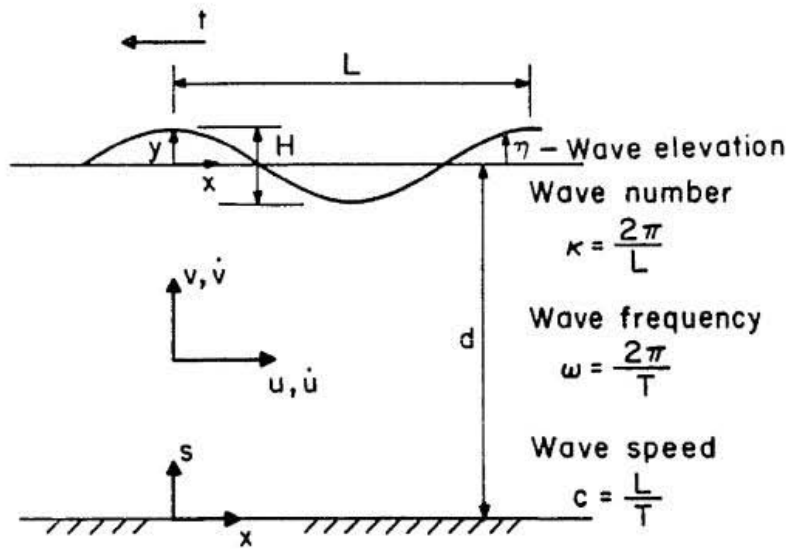

Figure 3.10: Definition sketch for a progressive wave train

$$a_4 = a^4 B_{44}$$

$$a_5 = a^5 B_{55}$$

and B_{22}, B_{24} etc are called wave-profile parameters. The wave height is given by

$$H = \frac{2}{k}[a + a^3 B_{33} + a^5(B_{35} + B_{55})] \tag{3.5}$$

The wave profile parameters and the wave height are calculated iteratively until the frequency relation defined below is satisfied to its best accuracy.

$$\omega^2 = gk(1 + a^2 C_1 + a^4 C_2)\ tanh\ kd \tag{3.6}$$

where C_1 and C_2 are frequency parameters.

The wave celerity for this theory is defined in terms of the wave celerity given by linear wave theory $C_0^2 = \frac{g}{k}\ tanh\ kd$:

$$C^2 = C_0^2(1 + a^2 C_1 + a^4 C_2) \tag{3.7}$$

Once the accurate value of 'a' (the wave amplitude parameter) in Eqns. 3.6 and 3.7 is obtained the horizontal water-particle velocities can be computed by the following equation:

$$u = \frac{\omega}{k} \sum_{n=1}^{5} G_n \cosh n(ky) \cos n(\omega t) \tag{3.8}$$

in which

$$\begin{aligned} G_1 &= aA_{11} + a^3A_{13} + a^5A_{15} \\ G_2 &= 2(a^2A_{22} + a^4A_{24}) \\ G_3 &= 3(a^3A_{33} + a^5A_{35}) \\ G_4 &= 4a^4A_{44} \\ G_5 &= 5a^5A_{55} \end{aligned}$$

and A_{11}, A_{13} etc are called velocity parameters. The water-particle accelerations can simply be obtained from Eqn. 3.8 by differentiation with respect to time t:

$$\dot{u} = \frac{\omega^2}{k} \sum_{n=1}^{5} G_n \cosh n(ky) \sin n(\omega t) \tag{3.9}$$

3.4.3 Least-Squares Technique

The total horizontal force F exerted by the wave on the cylinder can be obtained by integrating Eqn. 3.1 over the height of the cylinder

$$F = \int_{y_1}^{y} f(y)dy = \int_{y_1}^{y} C_{ms}A_I\dot{u}dy + \int_{y_1}^{y} C_{ds}A_D|u|udy \tag{3.10}$$

in which y_1, is the draft of the cylinder below the still water level and y is the instantaneous wave elevation from the still water level.

The total inertial (F_i) and drag (F_d) component of wave forces for a particular regular wave train and for unit hydrodynamic coefficients (ie., by assuming C_{ms} = C_{ds} =1) can be obtained by integrating the corresponding term of Eqn. 3.10 over the immersed portion of the cylinder at each time step. In fact in the developed

computer program, given in appendix A. these integrations were performed analytically using the software MAXIMA available in the VAX unix system. With this method the measured wave elevation can be input to the program and the forces F_i and F_d can be computed as a function of time t.

For simplicity, Eqn. 3.10 can be defined in a form:

$$F = C_m F_i + C_d F_d \tag{3.11}$$

in which the inertial (C_m) and drag (C_d) coefficients are defined for the complete cylinder. If we replace F by Fm, the measured wave force time series, then all the quantities except C_m and C_d are known in Eqn. 3.11.

Once F_i and F_d are computed for the input wave elevation time series, the hydrodynamic coefficients can be evaluated by a best fit to the measured wave force time series (F_m) in the least squares sense. The sum of the squares of the differences between the measured and the theoretical forces are given as:

$$E^2 = \sum_{i}^{N} [F_m(i) - C_m F_i(i) - C_d F_d(i)]^2 \tag{3.12}$$

in which N is the total number of points in the time series. The force coefficients C_m and C_d which minimize E^2 are given by

$$C_m = \frac{\sum(F_m F_i) \sum(F_d^2) - \sum(F_m F_d) \sum(F_d F_i)}{\sum(F_i^2) \sum(F_d^2) - (\sum F_d F_i)^2} \tag{3.13}$$

$$C_d = \frac{\sum(F_m F_d) \sum(F_i^2) - \sum(F_m F_i) \sum(F_d F_i)}{\sum(F_i^2) \sum(F_d^2) - (\sum F_d F_i)^2} \tag{3.14}$$

in which the summation is understood to run from 1 to N in each case.

The estimated coefficients obtained from the above least squares method were substituted into Eqn. 3.11 and the total wave forces on the structure predicted and then compared with the measured wave forces (F_m). The standard error in this prediction of wave forces is defined as:

$$\epsilon = [\frac{1}{(N-1)} \sum_{1}^{N} (F_m - F)^2]^{\frac{1}{2}} \tag{3.15}$$

3.5 Experimental Results for Regular Waves

The procedure described in the foregoing section was used and the C_m and C_f coefficients, for cases without and with the device fixed to the test cylinder, were determined. The experimental results and the wave force prediction are presented and discussed herein.

The experiment was carried out for frequencies in the range from 0.65 Hz to 0.8 Hz, in steps of 0.05 Hz. For each frequency the wave height also was varied between 0.2 m to 0.09 m. This gave a range of KC from 0.9 to 1.6. These tests were first performed for the test cylinder without the device (for convenience, hereafter referred to as the *simple cylinder*). The wave elevations and the cylinder response were recorded for an adequate duration of time, that is for at least 10 wave periods. During that time it was ensured that the system behaved in its steady state. When the sequence of experiments was completed, the device was attached to the cylinder and the whole process repeated for essentially the same wave conditions. (For convenience hereafter referred to as the *cylinder with device*.)

The particle kinematics were obtained by inputting the measured wave elevation time series to the developed computer program. The program used the Stokes' fifth order wave theory. Some of the typical results of the program obtained in the intermediate steps are first presented herein.

In order to check if the evaluated wave parameters obtained from the preprocessor were compatible with the Stokes' fifth order theory, the measured wave elevations were compared with the Stokes' fifth order wave profile. A typical comparison made between the measured wave profile and the theoretical wave profile, for H = 0.1067 m and T = 1.24 s, is shown in Fig. 3.11. (The solid line shows the predicted wave profile whereas the dashed line indicates the measured wave elevation.) In all cases excellent agreement was obtained in the comparison made between the theoretical

and the measured wave profiles. Once this was established, the inertial and drag forces for $C_m = C_d = 1$ (ie. F_i and F_d defined in Eqn. 3.11) were computed for the instantaneous wave elevation. The computed F_i and F_d are shown in Fig. 3.12 for wave conditions H = 0.1146 m and T = 1.413 s. (The solid line shows the inertial force, the dashed line shows the drag force and the dashed and dotted line indicates the wave profile.) Note that F_i and F_d are for unit hydrodynamic coefficients and are different from the total inertial and drag forces on the cylinder.

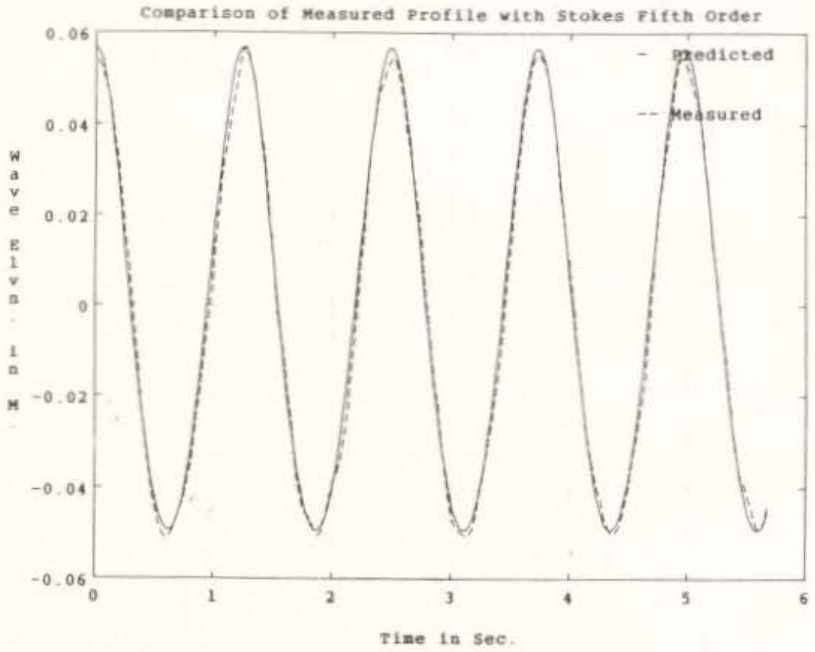

Figure 3.11: Comparison of measured wave elevation with Stokes' fifth order profile for H = 0.1067 m and T = 1.24 s

The drag forces for the simple cylinder are much smaller than the inertial forces. Figs. 3.13 and 3.14 show that the maximum inertial force is over 7 times the maximum drag force. The study also computed these forces using linear wave theory and then compared them with the predictions from the Stokes' theory. Fig. 3.13 presents the drag force (F_d), represented by the solid line, and the drag force obtained from the linear wave theory, shown by the dashed line. (These figures are presented for

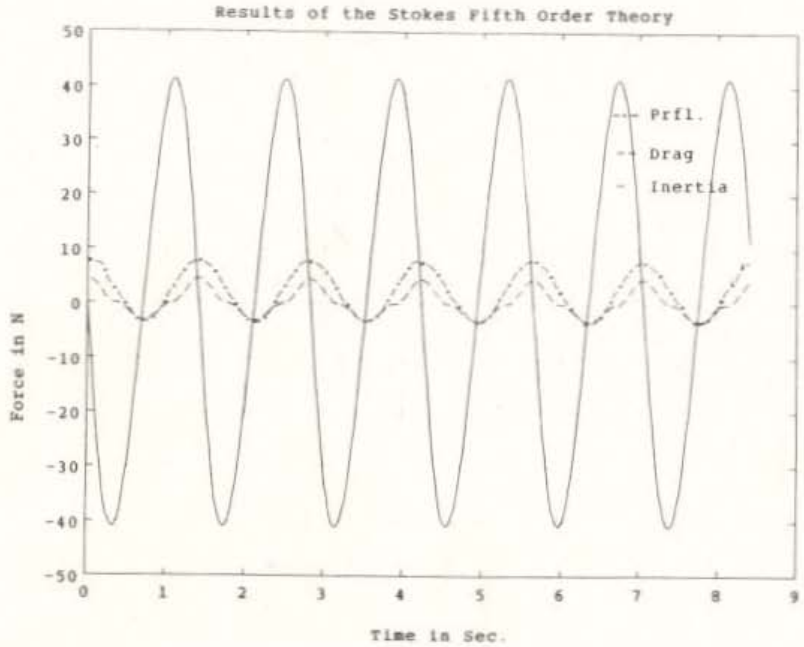

Figure 3.12: Results of the Stokes' fifth order theory for H = 0.1146 m and T = 1.413 s

a wave height of H = 0.132 m and a wave period 1.413 s) Significant differences between the predictions of the two theories is seen in this figure. The drag forces obtained from the fifth order theory are greater than the linear theory forces. As the wave period increases the difference between the results of these theories also increases. However no significant difference in the results is observed in the case of the inertial forces, F_i (see Fig. 3.14).

Once F_i and F_d are computed for a given wave profile, the values of C_m and C_d can be evaluated from Eqn. 3.13 and Eqn. 3.14. The total wave forces on the simple cylinder were predicted by using Eqn. 3.11 and then compared with the measured wave forces. These comparisons are presented in Figs. 3.15 to 3.23. (The dashed line in these figures shows the measured responses while the solid line indicates the predicted responses.) In all the cases the predicted results showed excellent agreement with the measured wave forces. The standard errors in the wave force

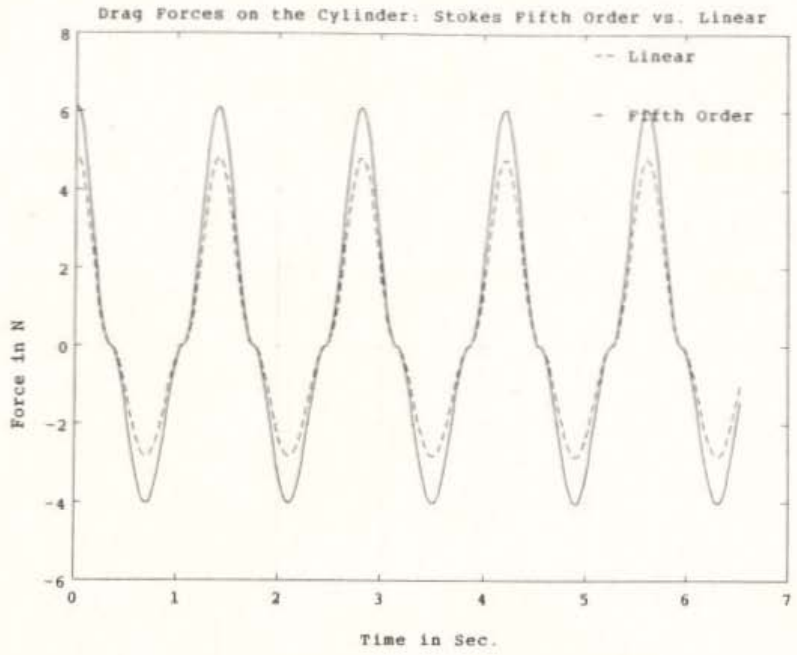

Figure 3.13: Comparison of the results of the Stokes' fifth order theory with the linear theory for H = 0.1325 m and T = 1.413 s, for the simple cylinder

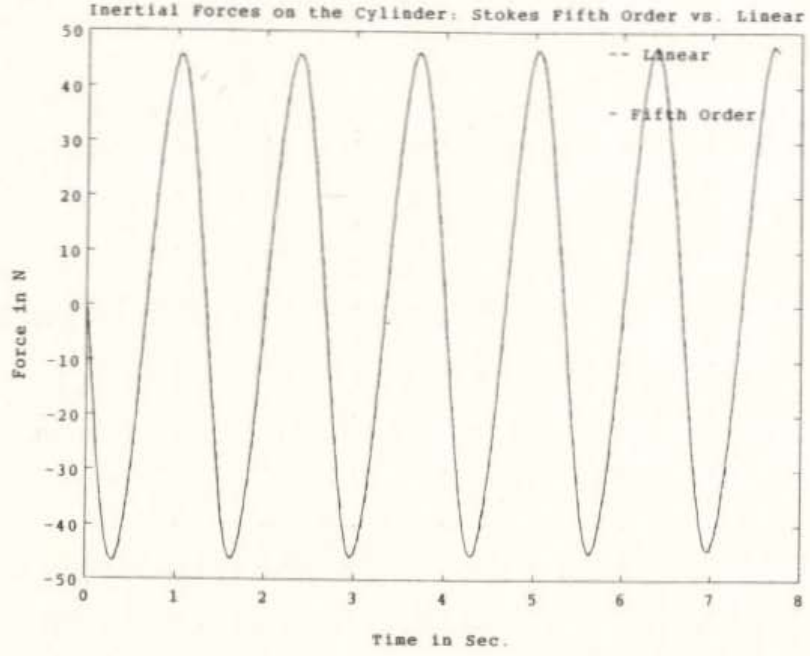

Figure 3.14: Comparison of the results of the Stokes' fifth order theory with the linear theory for H = 0.1325 m and T = 1.33 s, for the simple cylinder

predictions, computed from Eqn. 3.15, varied from 0.86 to 3.92 N which is about 3% of the maximum measured wave force. (Note that the standard error defined in Eqn. 3.15 is for the prediction of total forces on the cylinder and not for the C_m and C_d coefficients.) The summary of these results are given in Table 3.1.

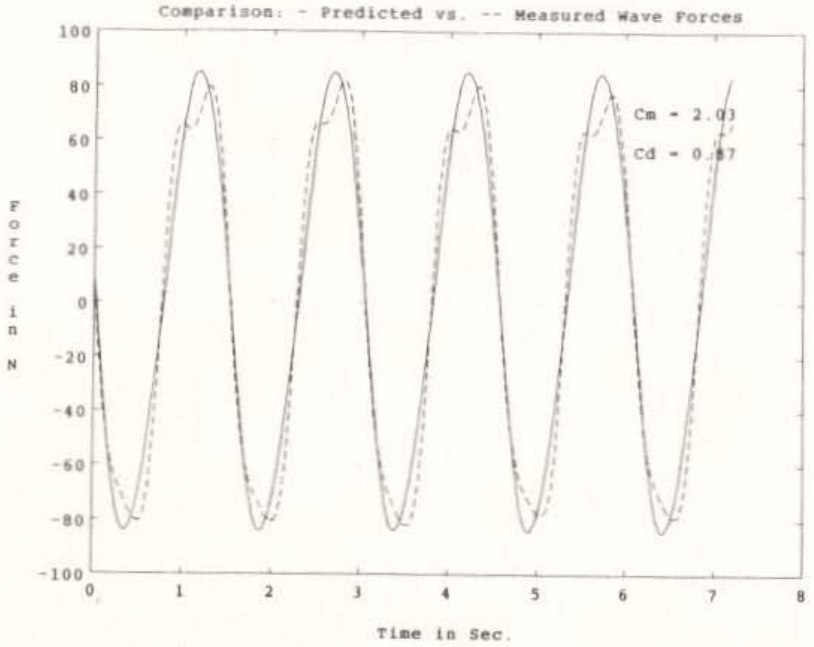

Figure 3.15: Comparison of the predicted wave forces with the measured wave forces for H = 0.124 m and T = 1.517 s, for the simple cylinder

The KC number for these test conditions varied from 0.95 to 1.6 and the R_e number varied from 0.69×10^5 to 1.14×10^5. The flow was virtually in the subcritical region and the KC numbers for the flow are very small. The results presented in Table 3.1 for wave frequencies 0.67, 0.707, 0.75 and 0.81 Hz, show that the drag coefficient exhibits large values as KC number decreases. The value of C_d falls sharply as KC number increases within a small range. For example when the KC number was equal to 1.5, the value of C_d was 1.25 while the KC number reduced to 0.96, the value of C_d became 4.07. The value of C_m was more or less constant in the series of tests. No relationship was found between the hydrodynamic coefficients

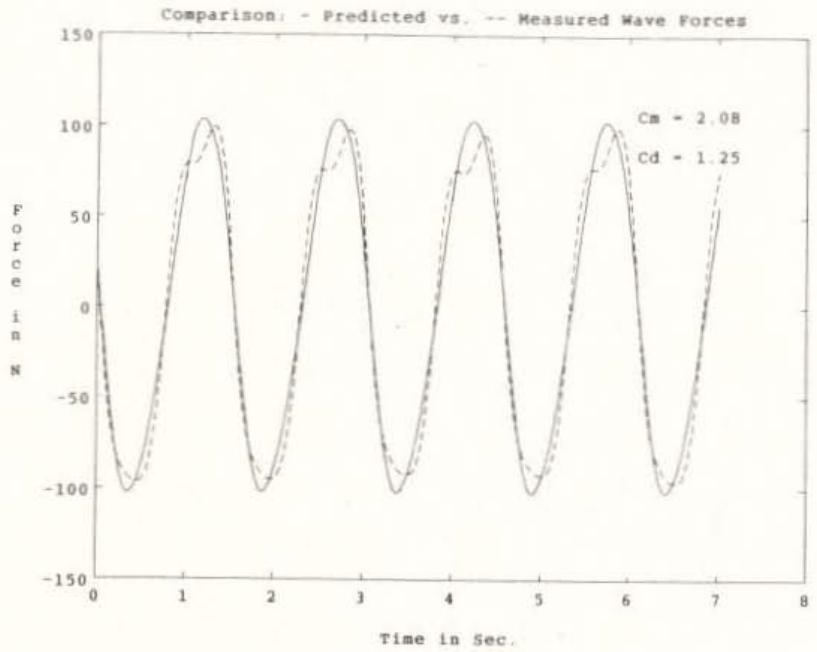

Figure 3.16: Comparison of the predicted wave forces with the measured wave forces for H = 0.147 m and T = 1.517 s, for the simple cylinder

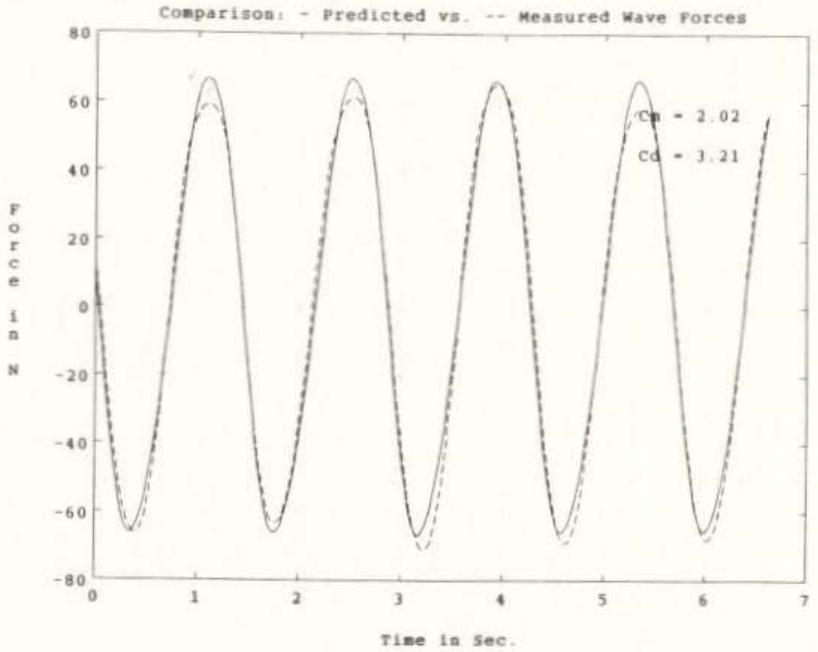

Figure 3.17: Comparison of the predicted wave forces with the measured wave forces for H = 0.093 m and T = 1.424 s, for the simple cylinder

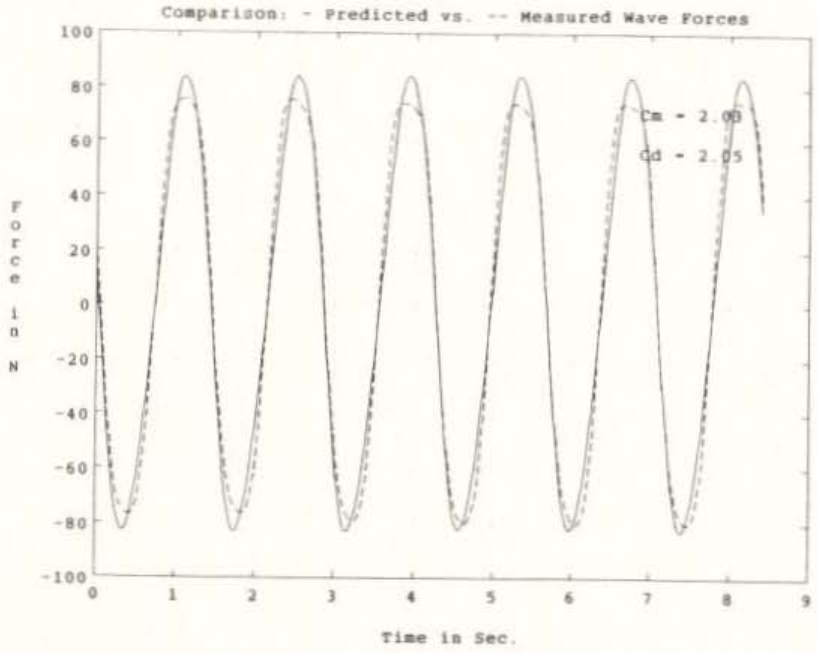

Figure 3.18: Comparison of the predicted wave forces with the measured wave forces for H = 0.115 m and T = 1.413 s, for the simple cylinder

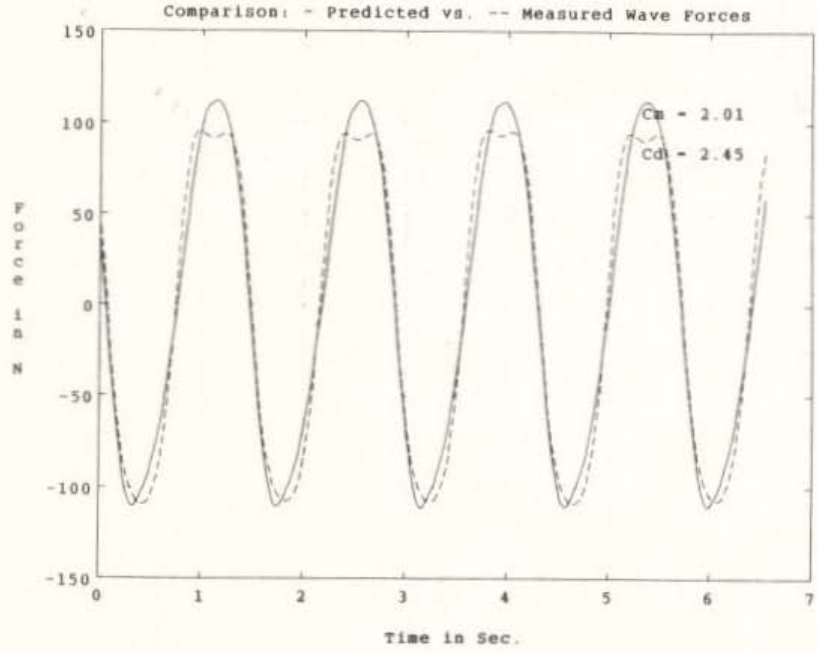

Figure 3.19: Comparison of the predicted wave forces with the measured wave forces for H = 0.155 m and T = 1.413 s, for the simple cylinder

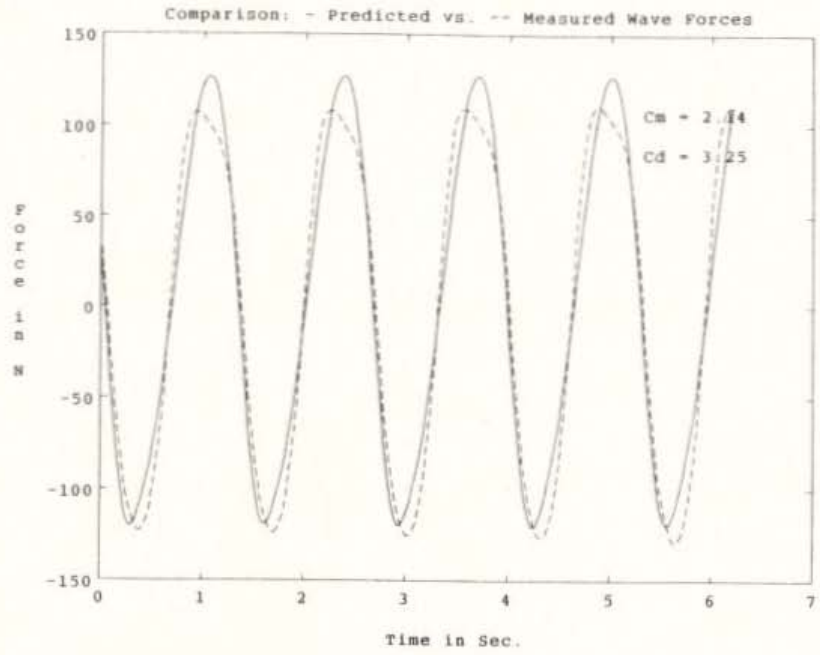

Figure 3.20: Comparison of the predicted wave forces with the measured wave forces for H = 0.159 m and T = 1.333 s, for the simple cylinder

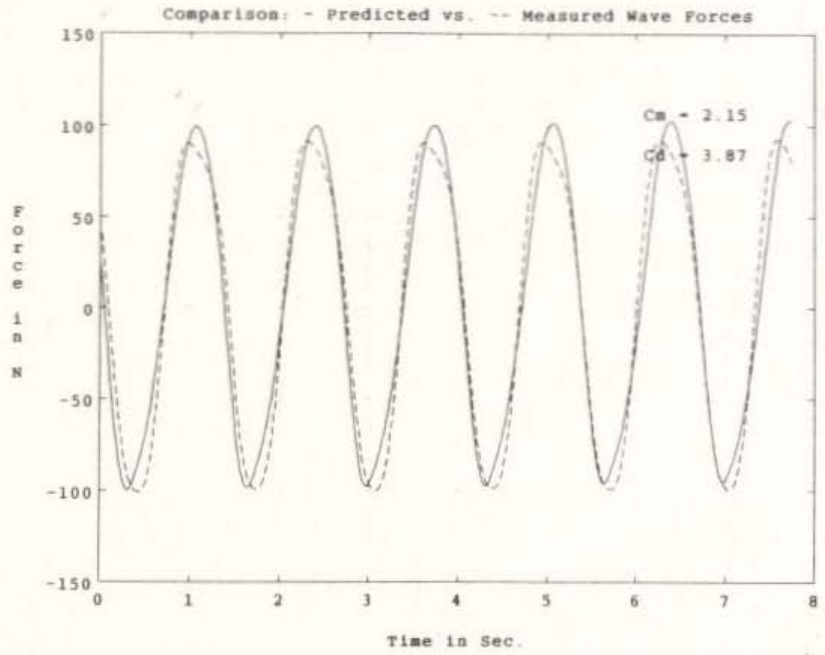

Figure 3.21: Comparison of the predicted wave forces with the measured wave forces for H = 0.132 m and T = 1.333 s, for the simple cylinder

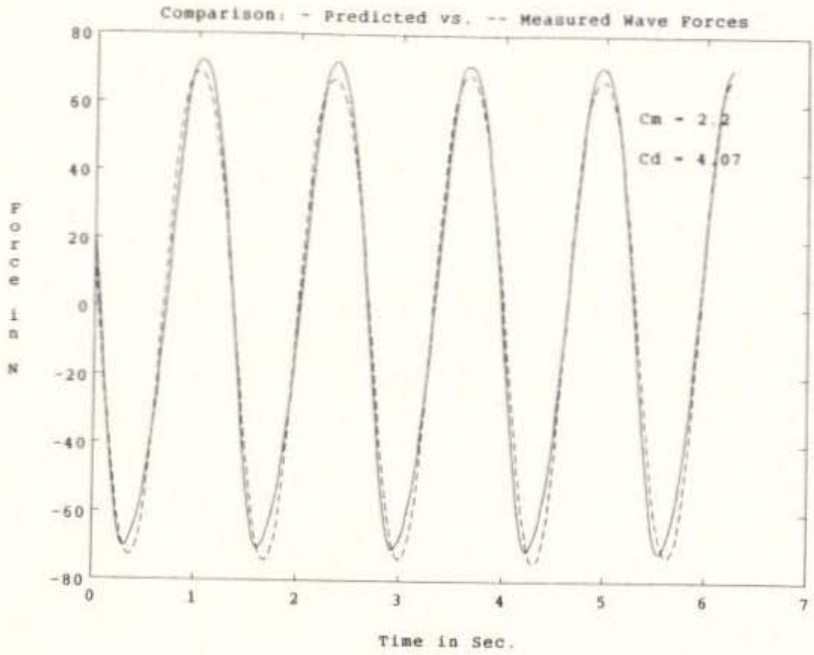

Figure 3.22: Comparison of the predicted wave forces with the measured wave forces for H = 0.094 m and T = 1.320 s, for the simple cylinder

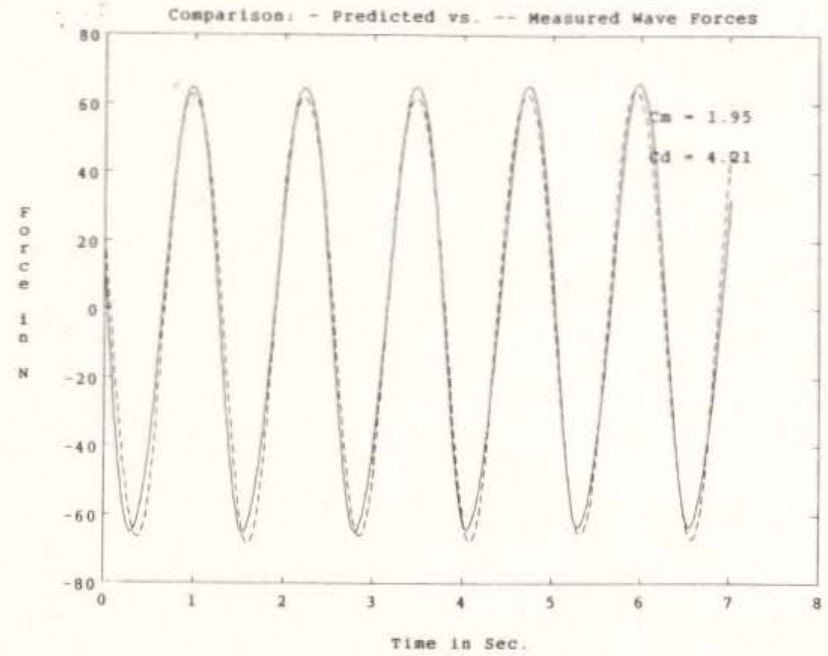

Figure 3.23: Comparison of the predicted wave forces with the measured wave forces for H = 0.093 m and T = 1.241 s, for the simple cylinder

and the R_e number within the test range. However the C_d value was observed to be very sensitive to the changes to the KC number at low KC numbers.

The C_d values found in this experiment are larger than what would be anticipated for such a low range of KC numbers (KC < 2). It should be pointed out here that the C_d values obtained are for the simple 3D cylinder which cannot be compared with previous results presented for a 2D section. Secondly, some of the recent studies (see Sarpkaya, 1986) have also indicated larger C_d values for circular cylinders at very low KC numbers. Little data is available in the literature to provide some more information onto this unique behaviour. However it is clear that the behaviour of a circular cylinder in waves at low KC is a very special case in the general problem. Although the C_d values obtained appear large, the total drag forces on the simple

Table 3.1: Summary of the results of the C_m and C_d analysis for the simple cylinder; diameter 0.3 m and submerged length 1.2 m

Sl. No	H m	T s	f Hz	C_m	C_d	KC	R_e $\times 10^5$	Standard error
1	0.124	1.517	0.670	2.03	0.87	1.281	0.801	2.35
2	0.147	1.517	0.670	2.08	1.25	1.506	0.941	2.81
3	0.115	1.413	0.707	2.03	2.05	1.173	0.787	1.73
4	0.155	1.413	0.707	2.01	2.45	1.574	1.056	3.01
5	0.159	1.333	0.750	2.14	3.25	1.600	1.139	3.92
6	0.132	1.333	0.750	2.15	3.87	1.339	0.952	3.04
7	0.094	1.320	0.758	2.20	4.07	0.957	0.688	1.18
8	0.093	1.241	0.806	1.95	4.21	0.947	0.724	0.87

cylinder compared to the inertial forces in all these cases are small. The value of

maximum drag forces is 10 to 16% of the value of the maximum inertial forces. For illustration purposes, the drag forces on the simple cylinder (dashed and dotted line) are compared with the inertial (dashed line) and the total forces (solid line) for H = 0.094 m and T = 1.32 s in Fig. 3.24. In this figure the drag forces are very small and the maximum value (9.5 N) is only 14% of the maximum inertial force (70.9 N). It can be noticed that the inertial forces almost coincide with the total wave forces. Hence the wave forces on the cylinder for this case are dominated by the inertial forces and the drag forces are small and in this case can be ignored.

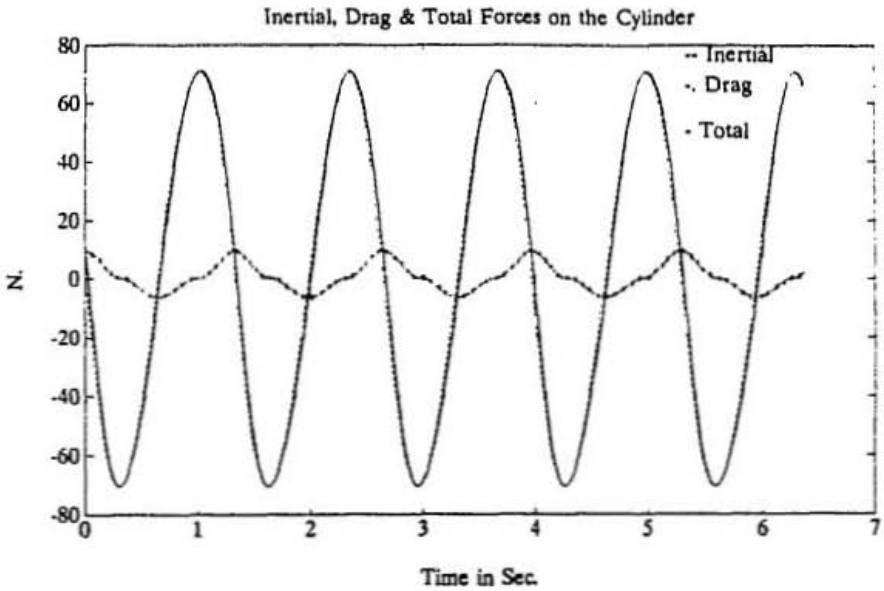

Figure 3.24: Comparison of the drag forces with the inertial and total wave forces for H = 0.094 m and T = 1.32 s, for the simple cylinder

3.5.1 Effect of the Device on C_m and C_d Values

The second stage of the experiments investigated the effect of the device on the hydrodynamic coefficients. As mentioned earlier, the device was attached to the circular cylinder, and the series of tests repeated. A significant change in the flow around the cylinder was observed when the device was placed. The behaviours of the

cylinder before and after attaching the device is illustrated presented in Figs. 3.25 and 3.26. (The flow-patterns around the cylinder are compared.) For the cylinder without the device, the flow around the cylinder was laminar ($R_e = 10^5$). No vortices were found to develop behind the simple cylinder. The moment the device was installed, both local and global vortices were produced. The development of a local vortex behind the middle diamond tube can be seen in Fig. 3.26. The fully developed vortex detaches from the diamond cylinder and independently moves towards the downstream end of the flow field and then merges with the vortices developed globally on the circular cylinder. As a result of these two localized and global effects the width of the wake behind the circular cylinder has also increased.

The other important point which should be noted here is that in the case of the simple cylinder (in Fig. 3.25), the upstream flow is clear and undisturbed whereas with the device (in Fig. 3.26) the upstream flow is turbulent. The vortices generated in the previous half cycle are not completely washed out and are convected downstream. On the other hand, in the case of the simple cylinder, no vortices were developed behind the circular cylinder. Even if anything is generated, the produced vortices are washed away and further generation of vortices is prevented. Although the visualized flow patterns explain the functioning of the device to some extent, the quantitative assessment which can be made with the C_m and C_d analysis for the cylinder, with and without the device in place, will give us a clear picture of the complete behaviour. The C_m and C_d analysis, discussed earlier, was repeated for the experimental data obtained for the cylinder with the device. The comparisons made between the predicted and the measured wave forces are shown in Figs. 3.27 to 3.35. Excellent agreement between the predictions and measurements is seen in all the cases. The standard error in these predictions varied from 1.02 to 3.11. The measured wave parameters and the computed hydrodynamic coefficients obtained in this set of experiments are summarized in Table 3.2.

Figure 3.25: The flow pattern around the cylinder before attaching the device

Figure 3.26: The flow pattern around the cylinder after attaching the device

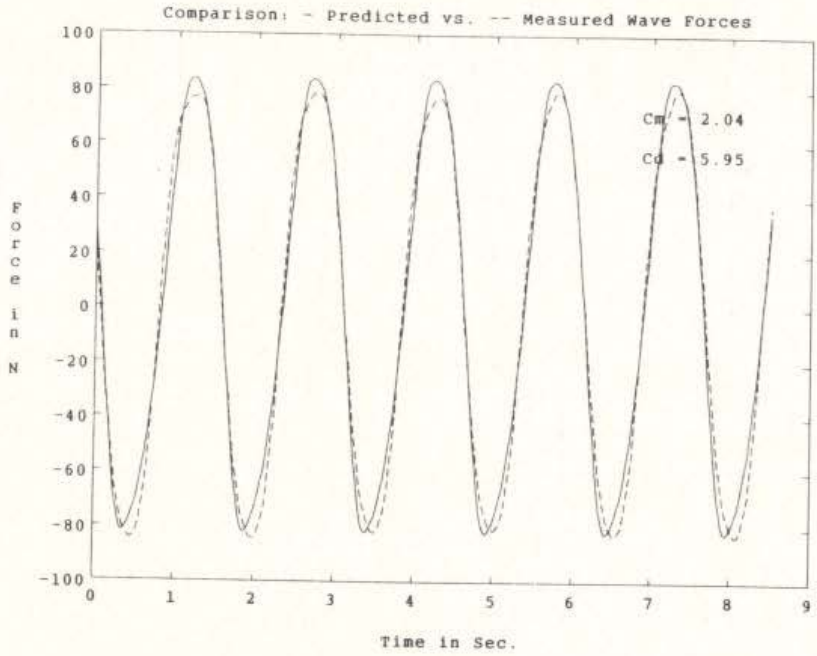

Figure 3.27: Comparison of the predicted wave forces with the measured wave forces for H = 0.117 m and T = 1.52 s, for the cylinder with device

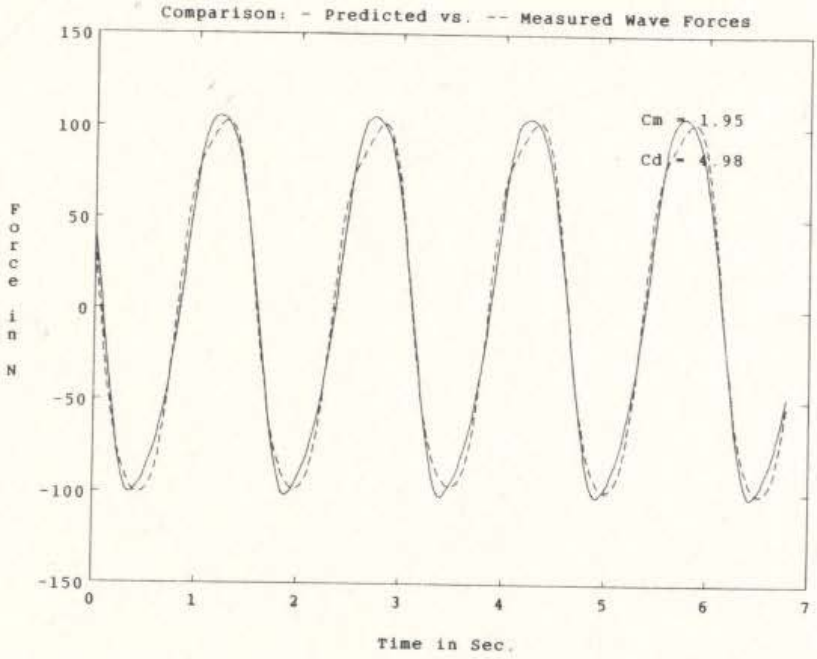

Figure 3.28: Comparison of the predicted wave forces with the measured wave forces for H = 0.152 m and T = 1.516 s, for the cylinder with device

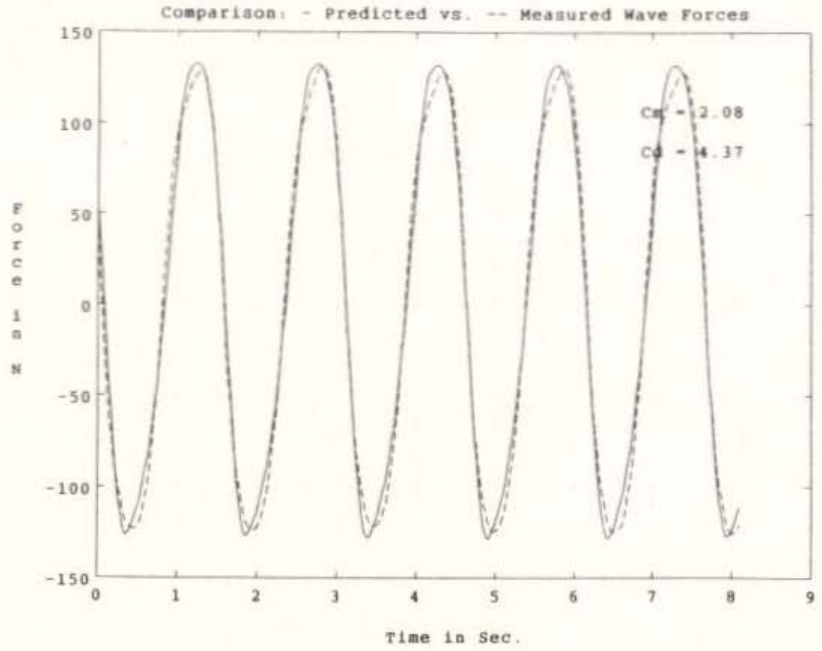

Figure 3.29: Comparison of the predicted wave forces with the measured wave forces for H = 0.178 m and T = 1.516 s, for the cylinder with device

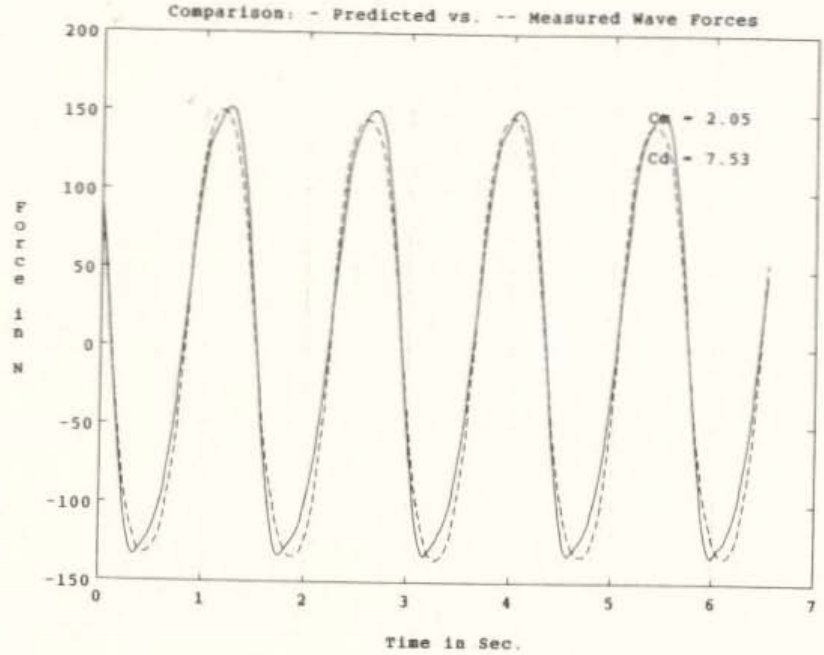

Figure 3.30: Comparison of the predicted wave forces with the measured wave forces for H = 0.182 m and T = 1.415 s, for the cylinder with device

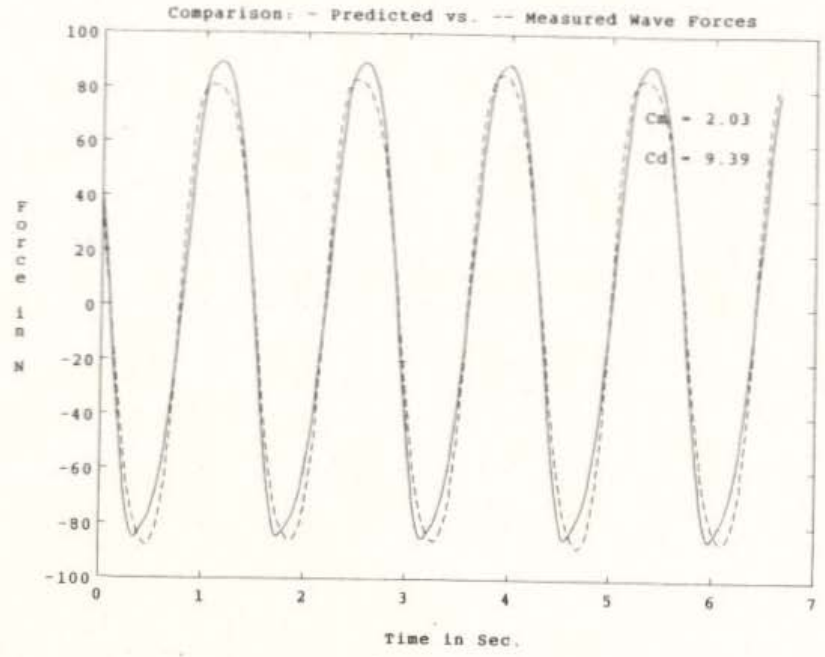

Figure 3.31: Comparison of the predicted wave forces with the measured wave forces for H = 0.125 m and T = 1.41 s, for the cylinder with device

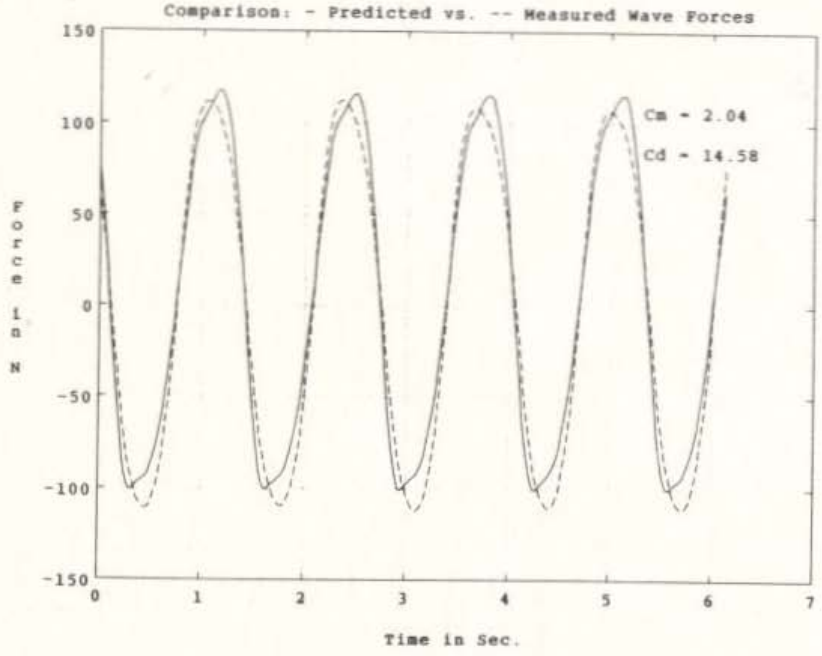

Figure 3.32: Comparison of the predicted wave forces with the measured wave forces for H = 0.140 m and T = 1.325 s, for the cylinder with device

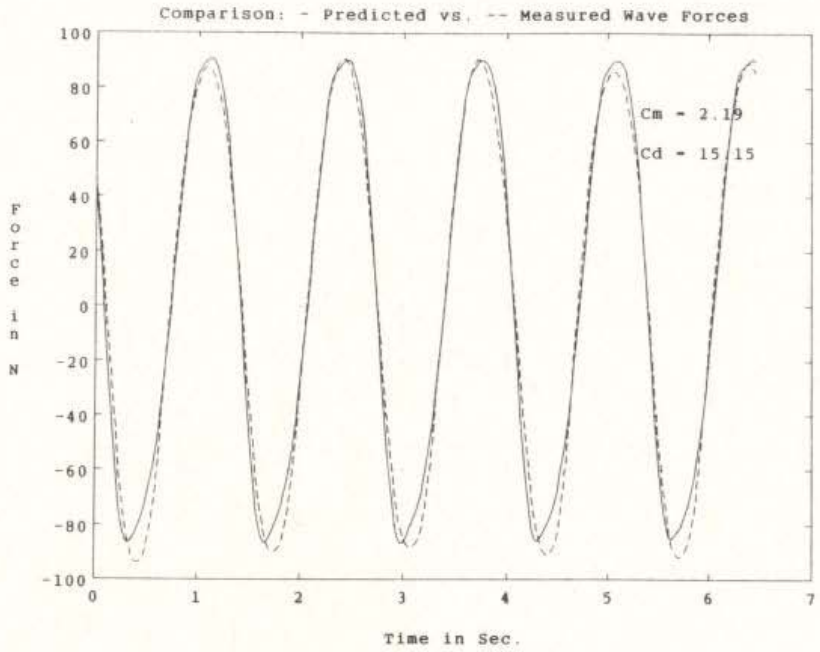

Figure 3.33: Comparison of the predicted wave forces with the measured wave forces for H = 0.112 m and T = 1.325 s, for the cylinder with device

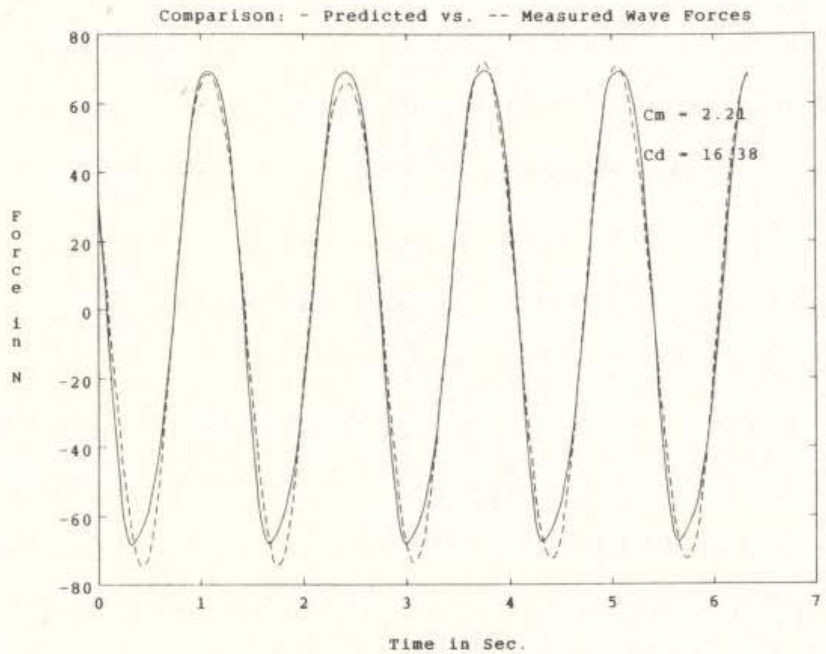

Figure 3.34: Comparison of the predicted wave forces with the measured wave forces for H = 0.089 m and T = 1.325 s, for the cylinder with device

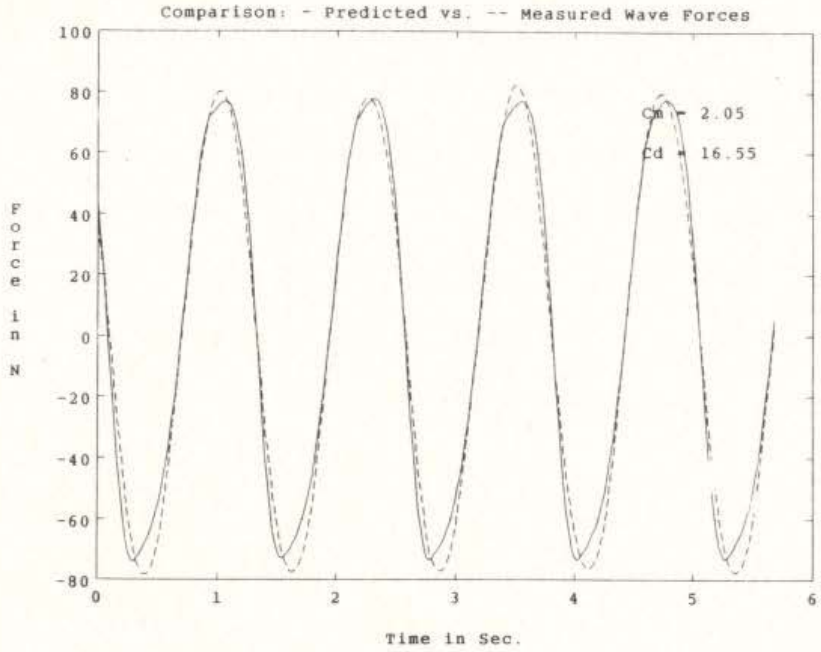

Figure 3.35: Comparison of the predicted wave forces with the measured wave forces for H = 0.107 m and T = 1.241 s, for the cylinder with device

Trends similar to the case of the simple cylinder, wherein the drag coefficients increased with the small decrease in the KC number at low KC numbers, are observed. Since the wave conditions were kept more or less the same, as in the case of the cylinder without the device, the range of KC and R_e numbers in this experiment also remains the same. Insignificant changes in the value of C_m were observed due the attachment of the device to the cylinder. However the value of C_d has increased by a factor of 4. Table 3.3 compares the hydrodynamic coefficients obtained for the cylinder with and without the device in place. Note that the wave conditions generated may not be exactly the same for both cases, but are very close to each other. **With the device in place, the cylinder drag coefficients have increased by a factor of four (irrespective of the wave height and frequency).** Hence a significant increase in the drag forces is observed while the inertial forces are shown to be insensitive to the device.

To get a clear picture of the effect of the device, the drag forces were compared with the inertial and total forces. A typical comparison for the wave conditions H = 0.112 m and T = 1.325 s is shown in Fig. 3.36. Significant increase in the drag force can be seen in this figure compared to the similar study shown in Figs. 3.22 and 3.24. The magnitude of the maximum drag force (52.5 N) is 59% of the maximum wave force (90 N) on the cylinder whereas without the device (in Fig. 3.24) it is only 14%. The foregoing study clearly indicates that the device increases the drag

Table 3.2: Summary of the results of the C_m and C_d analysis for the circular cylinder with device

Sl. No	H m	T s	f Hz	C_m	C_d	KC	R_e $\times 10^5$	Standard error
1	0.117	1.520	0.658	2.04	5.95	1.206	0.752	1.81
2	0.152	1.516	0.670	1.95	4.98	1.565	0.978	2.00
3	0.178	1.516	0.670	2.08	4.37	1.818	1.137	2.31
4	0.182	1.415	0.707	2.05	7.53	1.838	1.231	2.89
5	0.125	1.409	0.709	2.03	9.39	1.276	0.860	2.37
6	0.140	1.325	0.754	2.04	14.6	1.416	1.013	3.11
7	0.112	1.325	0.754	2.19	15.2	1.141	0.816	3.36
8	0.089	1.325	0.754	2.21	16.4	0.907	0.649	1.02
9	0.107	1.241	0.806	2.05	16.6	1.083	0.827	1.43

forces on the cylinder without significantly affecting the inertial forces. However it is still not clear whether the increase in the drag forces is due to the forces exerted by the attached device itself or due to the effect of the device inducing the drag forces on the main cylinder. Since the device was attached to the main cylinder,

Table 3.3: Comparison of the hydrodynamic coefficients for the circular cylinder with and without the device in place

Sl. No	Results of C_m & C_d Analysis for the Cylinder								Increase of C_d by a Factor
	without the Device				with the Device				
	H m	f Hz	C_m	C_d	H m	f Hz	C_m	C_d	
1	0.147	0.670	2.08	1.25	0.152	0.670	1.95	4.98	3.98
2	0.115	0.707	2.03	2.05	0.125	0.709	2.03	9.39	4.58
3	0.132	0.750	2.15	3.87	0.140	0.754	2.04	14.6	3.77
4	0.094	0.758	2.20	4.07	0.089	0.754	2.21	16.4	4.03
5	0.093	0.806	1.95	4.21	0.107	0.806	2.05	16.6	3.94

it is necessary to quantify the drag forces contributed by the induced effect of the device. In Fig. 3.37, a comparison was made between the total drag forces on the cylinder before and after attaching the device for the wave conditions H = 0.115 m and T = 1.413 s. The maximum drag force for the case with the device is 39.0 N whereas for the simple cylinder it is 8.5 N. The maximum wave force on the device alone obtained by separate calculation for the same wave conditions is 5.6 N. Hence the surplus increase of 24.9 N in the maximum drag force is obviously contributed by the inducing effect of the device. Thus 81% of the increased drag forces were contributed by the induced separation effect on the cylinder. In view of these results, it can be concluded that the device is very effective in inducing large drag forces on a circular cylinder at low KC numbers.

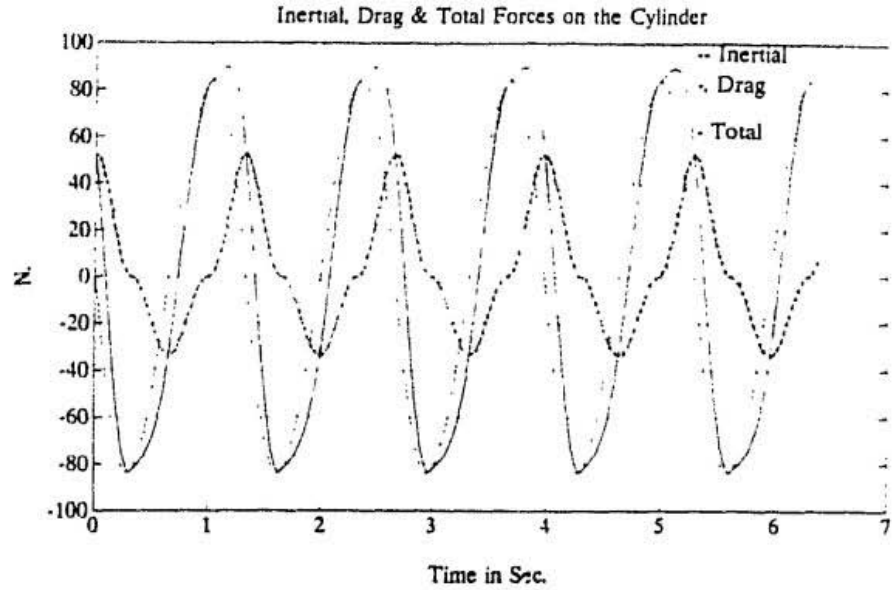

Figure 3.36: Comparison of the drag forces with the inertial and total wave forces for H = 0.089 m and T = 1.325 s (with device)

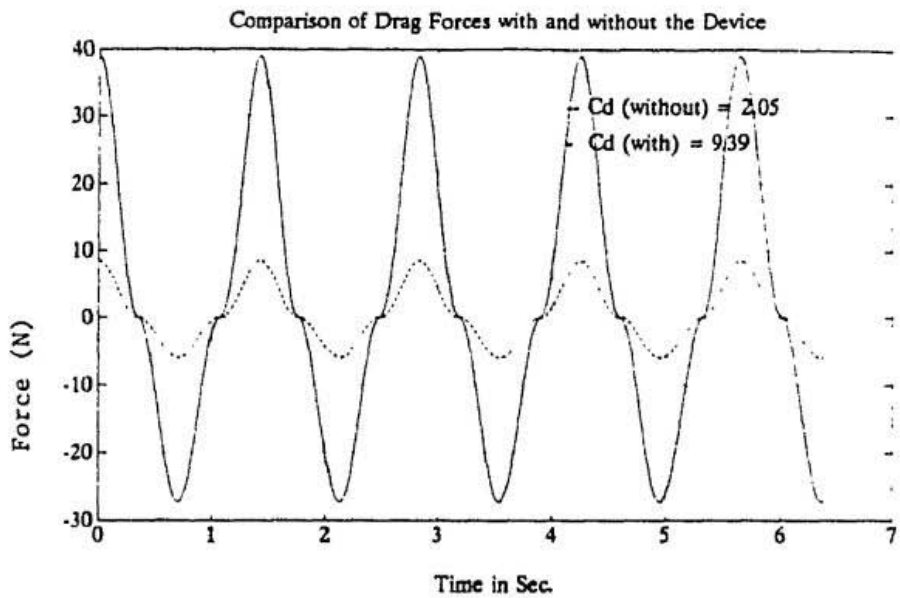

Figure 3.37: Comparison of the total drag forces on the cylinder with and without the device for H = 0.115 m and T = 1.413 s

3.6 C_m and C_d Analysis for Random Waves

The effectiveness of the device in increasing the drag forces on the cylinder was also investigated for the random wave environment. Random waves were produced in the wave tank and the wave forces were measured. For the generation of random sea states ISSC and JONSWAP spectra were used. The formula for the ISSC spectrum is:

$$S_\eta(\omega) = 0.1107 H_s^2 (\bar{\omega}^4/\omega^5) e^{-B} \tag{3.16}$$

in which $B = 0.4427(\bar{\omega}^4/\omega^4)$. The mean frequency, $\bar{\omega}$, and the peak frequency, ω_0, are related by $\bar{\omega} = 1.296\omega_0$. The formula for the JONSWAP spectrum is:

$$S_\eta(\omega) = (A/\omega^5) e^{[-B(\omega_0/\omega)^4]} [\gamma^a] \tag{3.17}$$

in which

$$\begin{aligned}
a &= e^{[-(\omega-\omega_0)^2/(2\sigma^2\omega_0^2)]} \\
\sigma &= 0.07 \rightarrow \omega \leq \omega_0 \\
\sigma &= 0.09 \rightarrow \omega \geq \omega_0 \\
B &= 1.25 \\
\gamma &= \text{peakedness parameter} \\
A &= 5H_s^2\omega_0^4/(1/(16\gamma^3)) \rightarrow \text{for } 1 \leq \gamma \leq 4 \\
H_s &= \text{significant wave height} \\
\omega_0 &= \text{peak frequency}
\end{aligned}$$

Further the peak period, T_0, and the zero-crossing period, T_z, are related by

$$T_0 = (1.49 - 0.102\,\gamma + 0.0142\,\gamma^2 - 0.00079\,\gamma^3)\,T_z \tag{3.18}$$

3.6.1 Simulation of Random Waves

Several numerical formulations are available for establishing time series of the random fluid field. A review of the most relevant formulations are given by Chakrabarti

(1987). For the purpose of this study a model with random phase angle was chosen. This formulation has been proven to be computationally very efficient, mainly due the fact that the Fast Fourier Transform, (FFT-technique), can be used for the calculation of the harmonic functions.

The surface elevation, for a statistically stationary random sea, measured relative to mean water level is given by [Borgman, 1969]:

$$\eta(x,t) = \sum_i a_i \cos[k_i x - \omega_i t + \alpha_i] \tag{3.19}$$

The wave frequency, ω_i, and wave number, k_i, are related by

$$\omega_i^2 = g k_i \tanh k_i d \tag{3.20}$$

in a water depth, d. The amplitudes, a_i, of each linear wave component are defined in terms of the one-sided spectrum, $S_\eta(\omega)$, by

$$a_i = [2S_\eta(\omega_i)(\delta\omega)]^{\frac{1}{2}} \tag{3.21}$$

The random phase angle, α_i, are assumed to be statistically independent and are drawn from a uniform probability distribution over $0 \leq \alpha_i \leq 2\pi$.

The numerical simulation procedure requires certain parameters to be optimized for its best operation. The maximum frequency by which the wave board in the tank can be operated is 9.1 Hz. In practice this was selected as the maximum frequency (f_{max}) in the FFT analysis. Thus the time increment is automatically fixed by the relation $dt = 1/(2f_{max}) = 0.055$ s.

Having selected the time step, the number of time points (N), in the FFT based simulation procedure (which must be a power of two), fixes the record length given by the relation $T_L = N \times dt$. In order to study the response of the cylinder for all the simulated frequencies, it is necessary to keep the record length the same while collecting data in the experiment. A larger record length increases the frequency resolution which may be good for the frequency domain analyses. However

a shorter record length is preferred to prevent the data from being contaminated by the disturbances of the reflected waves from the beach.

In order to optimize the record length between these two criteria a small calculation was made. Let us assume that the generated waves are within the small band width of frequency whose significant wave period is 1.67 s. Using linear wave theory, the wave celerity (C) for that period was computed which is 2.58 m/s. The reflected waves from the beach generally travel with the group velocity (C_g) which is given by C_g = C/2 = 1.29 m/s. Knowing the distance between the test section and the beach location (Y = 38 m), the time required (T_r) for the waves to travel back to the test section can be computed approximately by $T_r = 2 \times Y \times C_g = 59$s. It is essential to keep the record length $T_L \leq T_r$. Hence the number of time point that need to be used in the FFT simulation is given by $N = T_r/dt = 1073$ points. Since the FFT demands N in terms of a power of two, N was set to 1024 and the data were recorded for $T_L = N \times dt = 56.264$s.

Having selected the record length, the frequency resolution df is given by $df = 1/T_L = 0.01777$Hz. In the laboratory wave generation, for frequencies above 2.3 Hz, the wave energy is low and the proper physical spectra shape is very uncertain. So even if the theoretical wave spectra are defined for frequencies above 2.3 Hz an upper cut-off frequency should be introduced to the wave spectrum applied in the FFT-algorithm. The number of frequency points (M) used in the simulation introduces a cut-off frequency to the wave elevation power spectrum. For the simulation, M was set to 128 points and the theoretical wave spectrum was truncated at an upper-cut-off frequency $f_u = 2.2743$ Hz.

3.6.2 Spectral Description of Loading

The Morison formula defined in Eqn. 3.1 was first extended to random waves by Borgman (1967). Using a stochastic approach, Borgman derived an appropriate

form for the spectrum of the wave force by expressing the non-linear drag term in a series form. Retaining only the first linear term of the drag force series, the basic Morison's formula for the spectrum of wave force on a unit section of the cylinder reads as

$$S_f(\omega, z) = K_m^2 \, S_{\dot{u}}(\omega, z) + \frac{8}{\pi} \, K_d^2 \, \sigma_u^2 \, S_u(\omega, z) \tag{3.22}$$

in which $K_m = \frac{1}{4} \rho \pi D^2 C_m$, $K_d = \frac{1}{2} \rho D C_d$, $S_u(\omega, z)$ and $S_{\dot{u}}(\omega, z)$ are the particle velocity and acceleration power spectra and they can be defined in terms of the wave elevation power spectrum $S_\eta(\omega)$ using linear wave theory as

$$S_u(\omega, z) = \omega^2 \, r^2(z) \, S_\eta(\omega) \tag{3.23}$$

$$S_{\dot{u}}(\omega, z) = \omega^4 \, r^2(z) \, S_\eta(\omega) \tag{3.24}$$

where $r(z)$ defines the variation of wave amplitude with depth, z

$$r(z) = \frac{cosh \; k(z+d)}{sinh \; kd} \text{ with } -d < z < 0 \tag{3.25}$$

The wave frequency, ω, and wave number, k, are related by

$$\omega^2 = gk \; tanh \; kd \tag{3.26}$$

For random wave conditions the R_e and KC numbers should also be defined in terms of stochastic parameters. These parameters may be defined with the significant velocity amplitude $2\sigma_u$ and the average zero-crossing period T_z, as (Isaacson and Nwogu, 1988):

$$R_e = 2 \, \frac{\sigma_u \, D}{\nu} \tag{3.27}$$

$$KC = 2 \, \frac{\sigma_u \, T_z}{D} \tag{3.28}$$

Eqn. 3.22 was integrated over the immersed position of the cylinder to get the total force spectrum in terms of the wave elevation spectrum.

$$S_F(\omega) = \int_{s_1}^{s_2} S_f(\omega, s) ds \tag{3.29}$$

where 's' is the vertical coordinate and s_1 = -1.44 m and s_2 = 0.24 m. The integration was carried out individually for the inertial and drag components of wave loading and the resulting equation is defined as

$$S_F(\omega) = S_{FI}(\omega) + S_{FD}(\omega) \tag{3.30}$$

where

$$S_{FI}(\omega) = [RAOI]^2 \; S_\eta(\omega) \tag{3.31}$$

$$S_{FD}(\omega) = [RAOD]^2 \; S_\eta(\omega) \tag{3.32}$$

In which RAOI and RAOD are called, respectively, the Response Amplitude Operator for Inertia and Drag force spectra. They can be defined individually as:

$$RAOI(\omega) = \frac{K_m \, \omega^2}{sinh \; kd} \int_{s1}^{s2} cosh \; ks \; ds \tag{3.33}$$

and

$$RAOD(\omega) = \sqrt{\frac{8}{\pi}} \; \frac{K_d \, \omega}{sinh \; kd} \int_{s1}^{s2} \sigma_u(s) \; cosh \; ks \; ds \tag{3.34}$$

Eqn. 3.33 can be integrated analytically and is given as

$$RAOI(\omega) = \frac{K_m \, \omega^2}{k \; sinh \; kd} \left(sinh \; k(s2) - sinh \; k(s1)\right) \tag{3.35}$$

It should be noted that in the above equation k and ω are related by the linear dispersion relation defined earlier in Eqn. 3.26.

However Eqn. 3.34 cannot be integrated analytically over the immersed height of the cylinder. Since $\sigma_u(s)$ varies with the parameter s, Eqn. 3.34 dictates a numerical integration procedure. The velocity variance for each depth can be evaluated as:

$$\sigma(u)^2(z) = \int_0^\infty S_u(\omega) \; d\omega \tag{3.36}$$

The above integration has to be carried out numerically for 1 to 128 frequency components with $d\omega = df \times 2 \times \pi = 0.1167$ rad/s.

In practice, the immersed portion of the cylinder was divided into 64 equal parts and at each depth 'z' the value of $\sigma_u^2(z)$ was assumed to be constant. For the known value of $\sigma_u^2(z)$ at each section, Eqn. 3.32 was integrated numerically and then summed for all the sections over the immersed height of the cylinder. Thus the RAOD for the cylinder was evaluated. The typical plots of RAOI and RAOD for the wave conditions, significant wave height (Hs) equal to 0.076 m and peak frequency (ω_0) equal to 5.7 rad/s, are shown in Figs. 3.38 and 3.39 respectively.

Once the two operators (RAOI and RAOD) are obtained, the total inertial and drag force spectra for the cylinder can be evaluated using Eqns. 3.31 and 3.32.

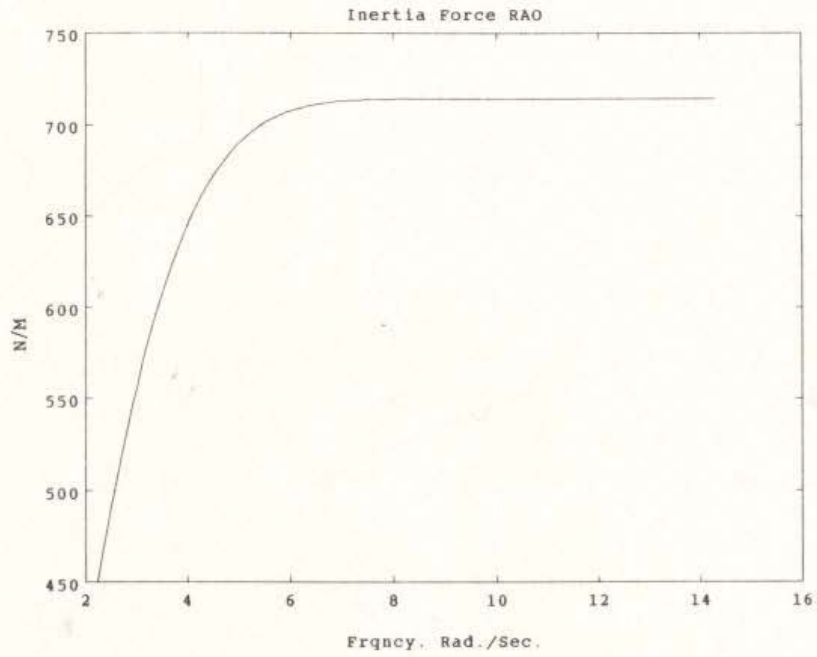

Figure 3.38: Inertia force RAO for the test cylinder (same for all wave conditions)

3.6.3 Least-Squares Technique

The task of finding the hydrodynamic coefficients for the random waves is some what similar to the regular wave analysis. Only two time series are available, ie., the measured wave elevation and the corresponding measured wave force. The C_m

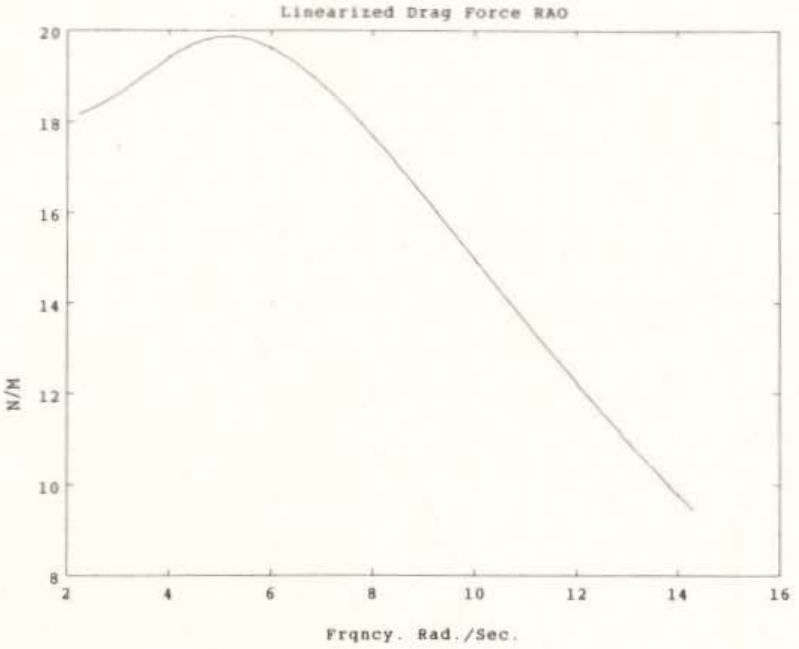

Figure 3.39: Linearized drag force RAO for the test cylinder for wave conditions H_s = 0.076 m, ω_0 = 5.7 rad/s

and C_d coefficients were computed for the random wave environment using a least-squares technique. Unlike the case of the regular waves, the computations were performed in the frequency domain using power spectral densities of the measured data. The method developed for this study is described herein. Eqn. 3.30 can now be written as

$$S_{Fp}(\omega) = [RAOI]^2 \, S_\eta(\omega) + [RAOD]^2 \, S_\eta(\omega) \tag{3.37}$$

in which $S_{Fp}(\omega)$ is the predicted wave force spectrum for the measured wave profile spectrum $S_\eta(\omega)$. The force coefficients can be estimated from a measured force spectrum ($S_{Fm}(\omega)$), by minimizing the square of the error (E) between the measured and the predicted wave force spectra. The error is given as

$$E^2 = \sum_{i}^{M} [S_{Fm}(\omega_i) - S_{Fp}(\omega_i)]^2 \tag{3.38}$$

where M is the number of frequency components of the spectrum.

The force coefficients C_m and C_d which minimize E^2 are given by

$$C_m = \frac{4}{\rho\pi D^2}\left[\frac{F_1 F_5 - F_2 F_4}{F_3 F_5 - F_2 F_6}\right]^{1/2} \tag{3.39}$$

$$C_d = \frac{2}{\rho D}\left[\frac{F_3 F_4 - F_1 F_6}{F_3 F_5 - F_2 F_6}\right]^{1/2} \tag{3.40}$$

in which F_1, F_2, F_3, F_4, F_5 and F_6 are computed using the following formulae by assuming unit force coefficients:

$$\begin{aligned}
F_1 &= \sum_{i}^{M} S_{Fm}(\omega_i)\, S_U(\omega_i) \\
F_2 &= \sum_{i}^{M} S_{FD}(\omega_i)\, S_U(\omega_i) \\
F_3 &= \sum_{i}^{M} S_{FI}(\omega_i)\, S_U(\omega_i) \\
F_4 &= \sum_{i}^{M} S_{Fm}(\omega_i)\, S_{FI}(\omega_i) \\
F_5 &= \sum_{i}^{M} S_{FD}(\omega_i)\, S_{FI}(\omega_i) \\
F_6 &= \sum_{i}^{M} S_{FI}(\omega_i)\, S_{FI}(\omega_i)
\end{aligned}$$

where

$$S_U(\omega) = S_{FI}(\omega)/(\omega) \tag{3.41}$$

3.7 Experimental Results for Random Waves

The numerically simulated random waves were generated in the tank and the wave elevation and wave force data were recorded. In the data analysis first the high frequency noise above 6.0 Hz was removed and then the linear trend in the data was eliminated. Most of the spectral parameters like the zero-up-crossing wave period and significant wave height were computed in the time domain from the wave elevation data. The power spectral densities of the recorded data were computed

using the FFT method. The computed spectra were smoothed using a centered 4-point moving average procedure.

Fig. 3.40 presents the measured wave elevation spectrum which is compared with the theoretical JONSWAP spectrum. (The solid line indicates the measured wave spectrum and the dashed line represents the theoretical spectrum for the significant wave height $H_s = 0.0911$ m and peak frequency $\omega_0 = 4.914$ rad/s.) In most cases excellent agreement between the measured spectrum and the theoretical spectrum was observed. After obtaining the wave elevation and force spectra, the two operators RAOI and RAOD were computed using Eqns. 3.34 and 3.35. Assuming initially $C_m = C_d = 1$ (for the purpose of computation), Eqns. 3.31 and 3.32 can be evaluated. Consequently the remaining equations defined to evaluate C_m and C_d can also be solved. The computed C_m and C_d values were entered into Eqn. 3.37 and the wave force spectrum predicted and compared with the measured wave force spectrum.

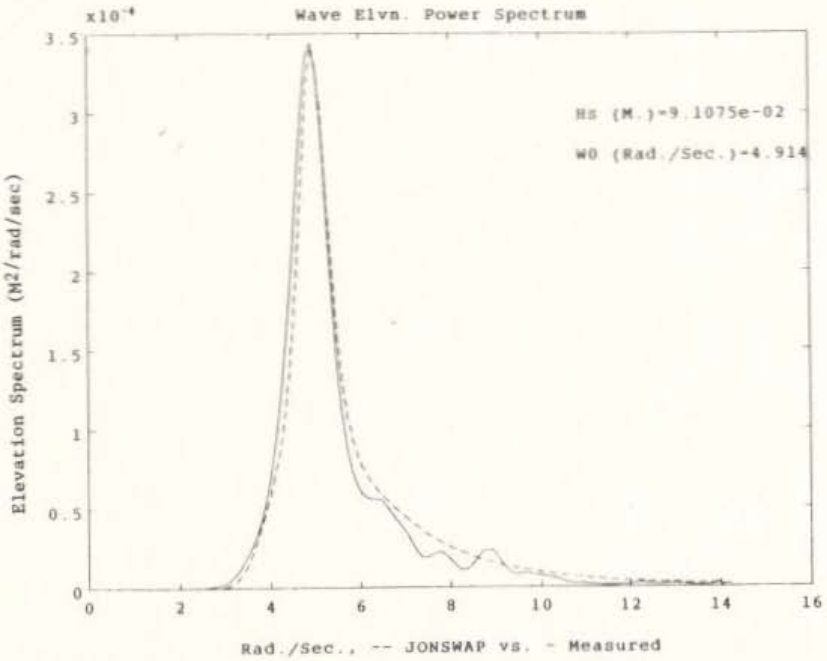

Figure 3.40: Comparison of the measured wave elevation and the theoretical JONSWAP spectra

In Figs. 3.41 to 3.45, the predicted wave spectra are compared with the measured wave spectra. (The dotted line shows the predicted force spectra and the solid line indicates the measured force spectra.) In general the predicted force spectra are in very good agreement with the measured force spectra. At frequencies above 1.0 Hz some discrepancies are noticed. The prediction is better in the case of the narrow band JONSWAP spectra compared to the case of the broad band ISSC spectra. When the peakedness factor γ was set to a large value (say above 2.7), excellent agreement between measurements and predictions were obtained, see Figs. 3.44 and 3.45. The computed hydrodynamic coefficients are then of the same order as in the regular wave tests. The KC number for these tests varied from 0.82 to 1.56. The results obtained in the data analysis are summarized in Table 3.4, where 'fo' is the frequency calculated from the peak period 'To'. Again the value of drag coefficients is sensitive to the change in the KC numbers. However no systematic change is identified in the case of the inertial coefficients.

Table 3.4: Summary of the results of the C_m and C_d analysis for the cylinder without the device - random waves

Sl. No	H_s m	T_z s	fo Hz	γ	C_m	C_d	KC
1	0.127	1.47	0.533	1.5	2.09	2.86	1.27
2	0.151	1.47	0.533	1.0	2.11	1.21	1.53
3	0.110	1.32	0.587	2.1	2.13	3.19	1.06
4	0.086	1.28	0.781	2.7	2.10	4.80	0.82
5	0.090	1.22	0.783	3.4	2.05	4.61	0.95

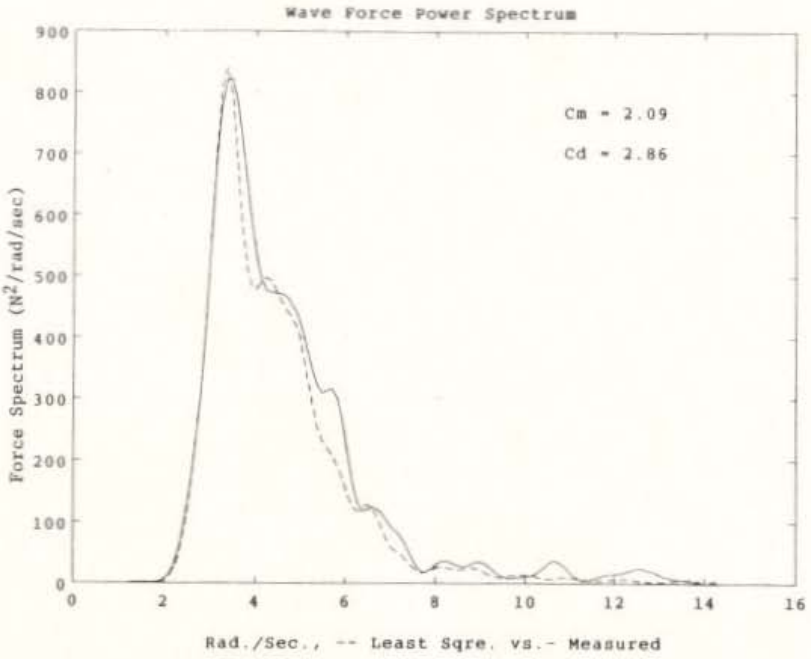

Figure 3.41: Comparison of the measured and the predicted wave force spectra for $H_s = 0.127$ m, fo = 0.533 Hz. and $\gamma = 1.5$, for the simple cylinder

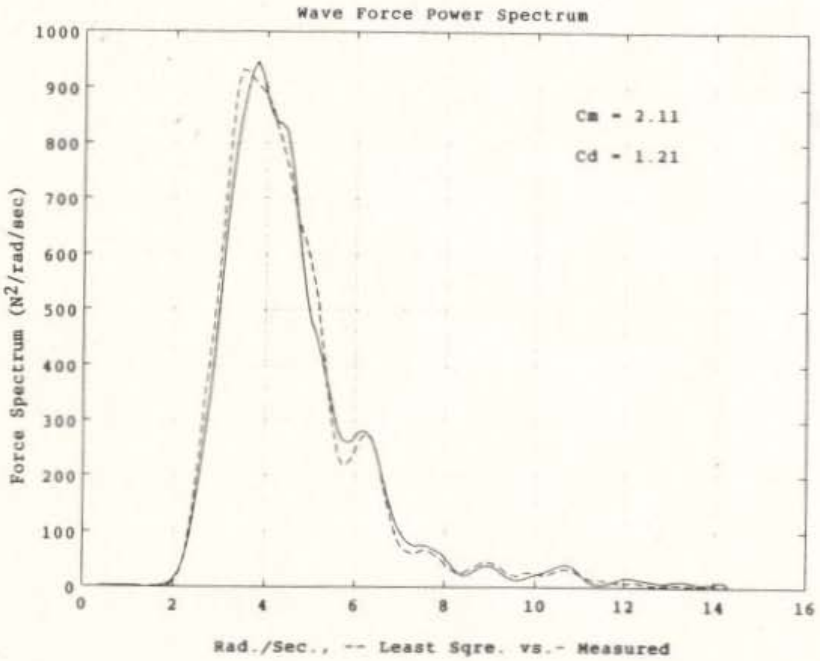

Figure 3.42: Comparison of the measured and the predicted wave force spectra for $H_s = 0.151$ m, fo = 0.533 Hz. and $\gamma = 1.0$, for the simple cylinder

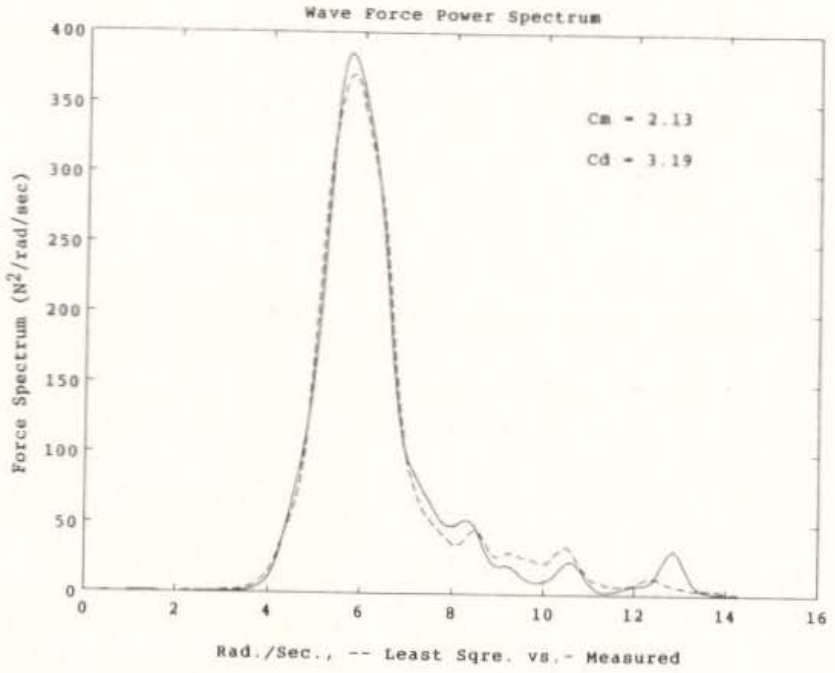

Figure 3.43: Comparison of the measured and the predicted wave force spectra for $H_s = 0.110$ m, fo = 0.587 Hz. and $\gamma = 2.1$, for the simple cylinder

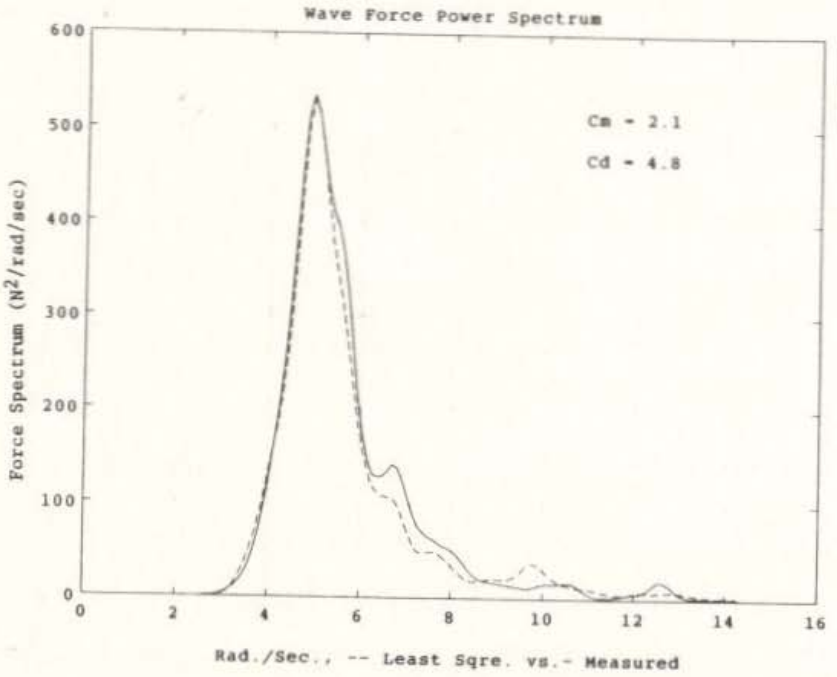

Figure 3.44: Comparison of the measured and the predicted wave force spectra for $H_s = 0.086$ m, fo = 0.781 Hz. and $\gamma = 2.7$, for the simple cylinder

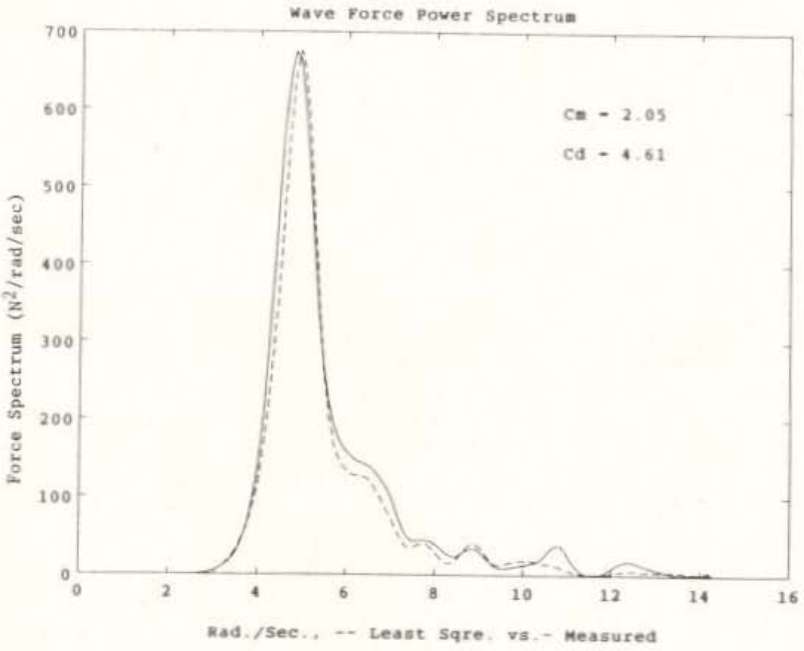

Figure 3.45: Comparison of the measured and the predicted wave force spectra for $H_s = 0.09$ m, fo = 0.783 Hz. and $\gamma = 3.4$, for the simple cylinder

3.7.1 Effect of the Device on C_m and C_d Values

A similar analysis was carried out for the case with the cylinder plus device, in random wave tests; this analysis has shown large increases in drag forces. The measured wave force spectra were compared with the predicted wave force spectra and are presented in Figs. 3.46 to 3.50. Good agreement in the comparisons can be seen in all these figures. The computed C_m and C_d coefficients are summarized in Table 3.5. The KC number for these cases varied from 0.81 to 1.26 which is of the same order as in the previous experiments without the device. It can be seen that the wave conditions were also kept the same as in the without device tests except for Serial Nos. 2 & 4, in which cases the γ factor is smaller. However, the comparisons between C_m and C_d coefficients obtained from these two set of experiments (with and without the device) are presented for all the five tests in Table 3.6. The increase in the drag coefficient due to the attachment of the device is larger than in the case

of the regular waves. However the inertial coefficient is again found to be insensitive to the presence of the device. In Table 3.6, it is seen that the values of the drag coefficients for the cylinder with device in random waves are 5 times larger than the corresponding values in regular waves. It should be noticed that in all the tests, conducted with random waves, both with and without the device, a good spectral shape for the measured wave force spectra is seen; and the measured force spectra are in good agreement with the predicted force spectra.

Table 3.5: Summary of the results of the C_m and C_d analysis for the cylinder with the device - random waves

Sl. No	H_s m	T_z s	fo Hz	γ	C_m	C_d	KC
1	0.128	1.45	0.533	1.5	2.05	11.55	1.26
2	0.147	1.57	0.533	1.5	2.07	7.41	1.55
3	0.108	1.18	0.604	1.5	2.09	19.82	0.94
4	0.084	1.26	0.764	1.0	2.15	24.73	0.81
5	0.091	1.12	0.782	3.4	2.12	22.77	0.90

3.8 Summary of Wave Tank Test Results

A wave force measuring experiment was carried out in the wave tank with the objective of examining a device that would increase the drag forces on a vertical circular cylinder, without significantly affecting the inertial forces. Both regular and random waves were produced in the wave tank. This study was performed on a 0.3 m diameter vertical cylinder, with the need for inducing flow-separation at low KC numbers. The sequence of tests was designed to select a physical device, which effectively in-

Table 3.6: Comparison of the hydrodynamic coefficients for the cylinder with and without the device in place - random waves

Sl. No	Results of C_m & C_d Analysis for Random Waves								Increase of C_d by a Factor
	without the Device				with the Device				
	H_s m	fo Hz	C_m	C_d	H_s m	fo Hz	C_m	C_d	
1	0.127	0.533	2.09	2.86	0.128	0.533	2.05	11.55	4.03
2	0.151	0.533	2.11	1.21	0.147	0.533	2.07	7.41	6.12
3	0.110	0.587	2.13	3.19	0.108	0.604	2.09	19.82	6.21
4	0.086	0.781	2.10	4.80	0.084	0.764	2.15	24.73	5.15
5	0.090	0.783	2.05	4.61	0.091	0.782	2.12	22.8	4.95

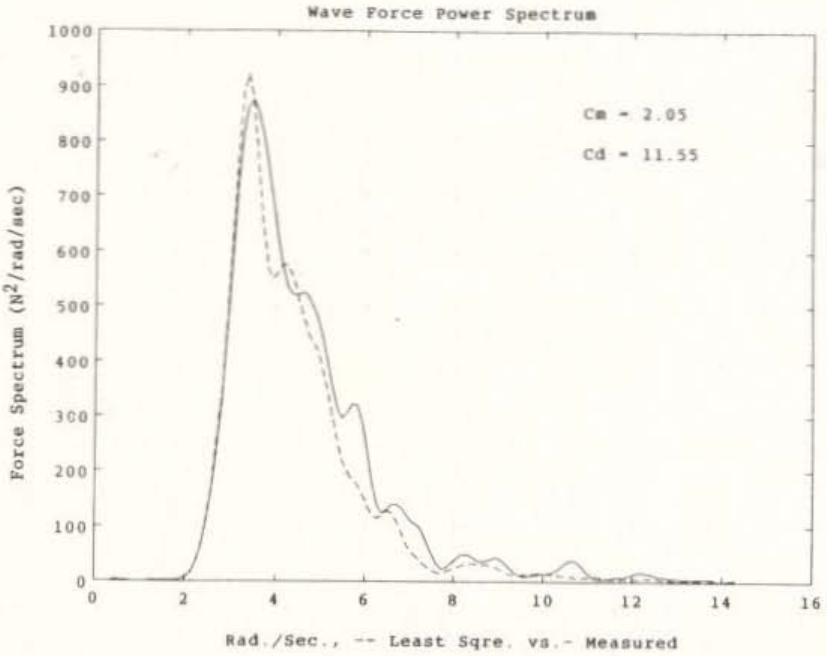

Figure 3.46: Comparison of the measured and the predicted wave force spectra for $H_s = 0.128$ m, fo = 0.533 Hz. and $\gamma = 1.5$, for the cylinder with device

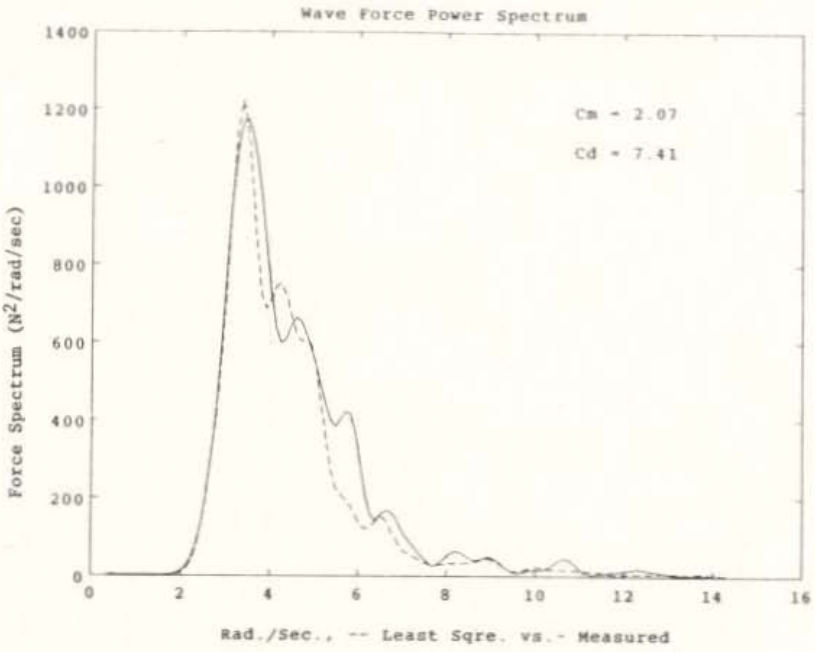

Figure 3.47: Comparison of the measured and the predicted wave force spectra for $H_s = 0.147$ m, fo = 0.533 Hz. and $\gamma = 1.5$, for the cylinder with device

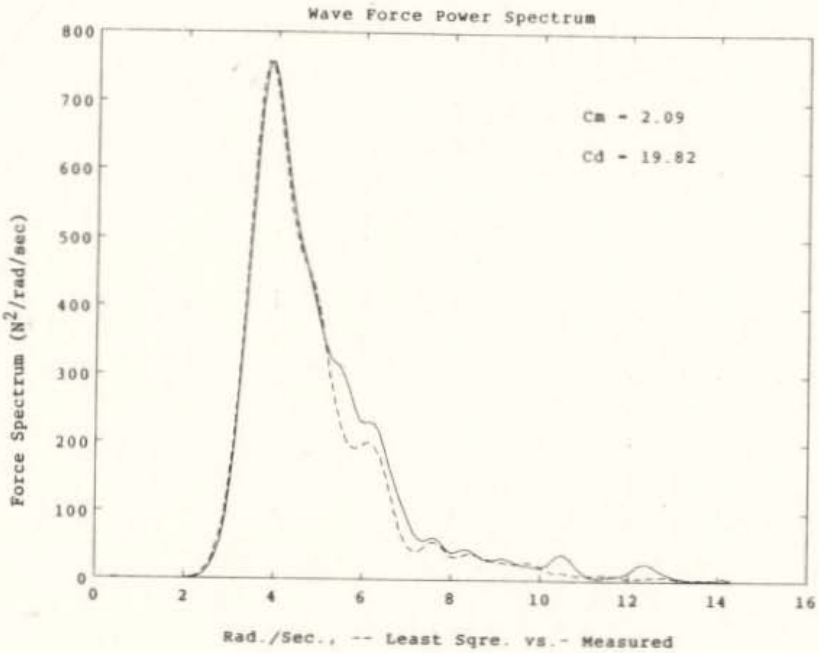

Figure 3.48: Comparison of the measured and the predicted wave force spectra for $H_s = 0.108$ m, fo = 0.604 Hz. and $\gamma = 1.5$, for the cylinder with device

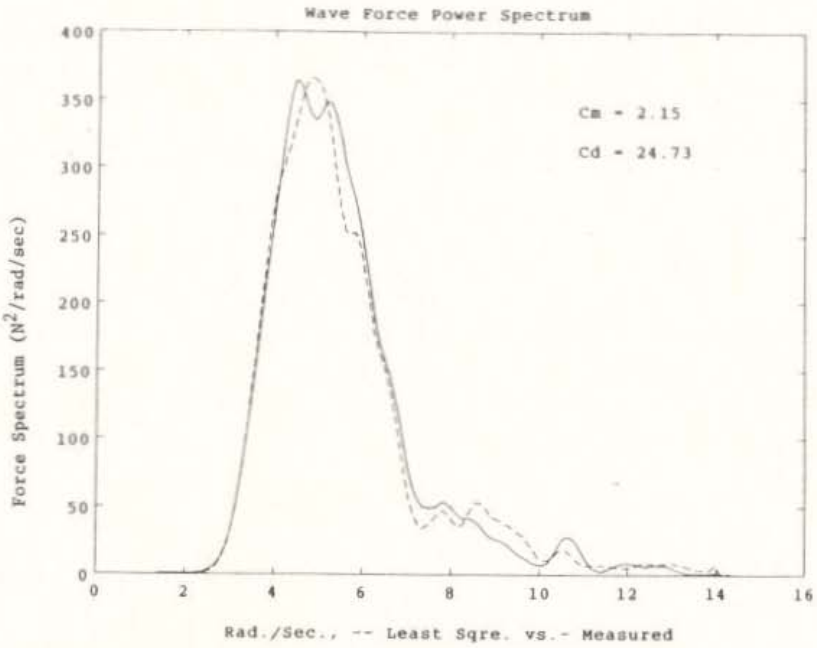

Figure 3.49: Comparison of the measured and the predicted wave force spectra for $H_s = 0.084$ m, fo = 0.764 Hz. and $\gamma = 1.0$, for the cylinder with device

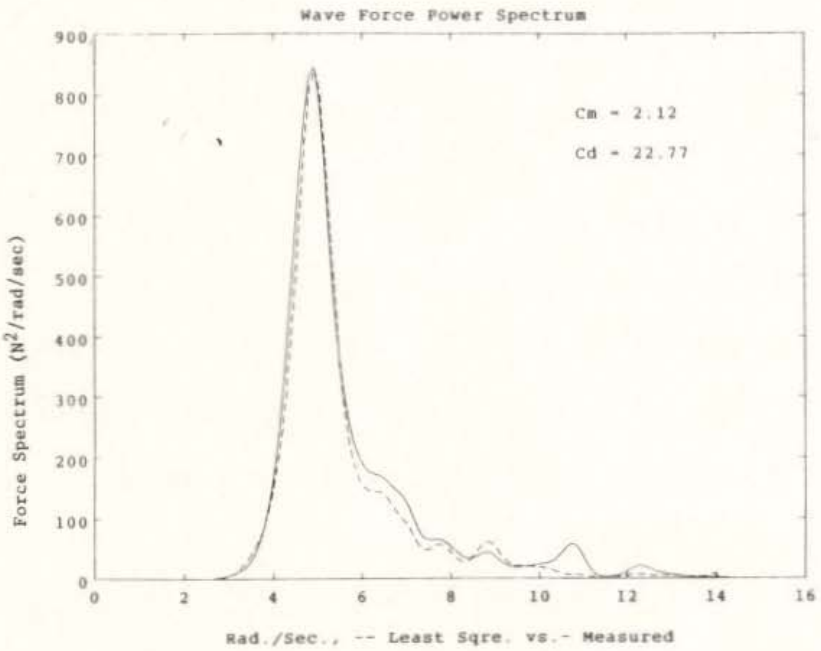

Figure 3.50: Comparison of the measured and the predicted wave force spectra for $H_s = 0.091$ m, fo = 0.782 Hz. and $\gamma = 3.4$, for the cylinder with device

creased the drag forces on the cylinder. While three devices were tested the results are presented only for the selected device. The experimental program is outlined. For the measurement of wave forces a new measuring technique was developed which used a friction less table and single-component load cell. The wave forces and the wave elevations were recorded and the conventional least squares technique was used to compute the Morison coefficients for the test cylinder. Experimental results were presented for the cylinder, with and without the device in place.

The computed C_m and C_d coefficients are higher than what is normally expected at such low KC numbers. This is due to the fact that the computed C_m and C_d are for the full height of the 3-dimensional cylinder and they cannot be compared with the values obtained for a 2-dimensional section in the literature. It also should be noted that the recent studies carried out by various investigators for low KC numbers have also indicated larger C_d values than what was anticipated. In the present experimental study, it was found that the value of drag coefficients is sensitive to the changes in the KC number at low KC numbers. It increases sharply as KC number decreases within a small range. Same behaviour is noticed also in the case of random waves. However no abrupt change in the value of C_m was noticed. Thus it can be concluded that the behaviour of the cylinder at low KC numbers is a special problem in which the C_m and C_d estimations and further experiments should concentrate on a localized value of the KC numbers. Experiments conducted for small diameter cylinders with large KC numbers cannot clearly interpret the behaviour at low KC numbers. Although the computed C_d values look larger, the total drag forces on the cylinder are small and negligible compared to the total wave forces. The wave force on the structure is clearly dominated by the inertial component of loading.

Investigations were carried out to find the influence of the diamond tube bundle device on the circular cylinder. It was found that the regular wave drag coefficients increased by a factor of 4, due to the attachment of the device to the cylinder.

Also the inertial forces were found to be insensitive to the device. In the case of the random waves the drag forces increased by a factor greater than 5, which was higher than the regular wave results. It was found that about 81% of the total increase in the drag force was due the indirect effect of the device which induced the shedding of large vortices behind the main cylinder.

Physical arguments suggest that the device, which is very effective at low KC numbers, may become less effective as the wave height and wave period increases. For extreme storm conditions the cylinder tends to become drag dominated. For large KC numbers ($KC \geq 5$), detached vortices can develop behind the simple circular cylinder. Under these conditions the device may become inactive. However there are no experimental results available to support this point. In this thesis the attention was restricted to the behaviour of the cylinder for $KC \leq 2$.

For the simple cylinder (without the device) the maximum value of the drag force component is typically 14% of the maximum wave force on the cylinder. With the device in place the maximum drag force increases to 59% of the maximum total force. Thus a significant increase in the magnitude of the drag force is observed due to the attachment of the diamond tube bundle device to the test cylinder.

Chapter 4

The Hydroelastic Model: Design and Fabrication

The main aim of the research is to verify the principle of inducing drag damping, for the purpose of reducing the resonant response of an inertial force dominated structure. To meet this purpose a steel tripod tower platform was selected as the prototype but the scaling requirements were used only as a general guide in designing the model. Hence, the model was designed not to simulate the behaviour of the particular steel tower selected but only to behave similar to a typical steel tripod structure.

In this chapter, basic concepts related to scaling are summarized, and the necessary similitude requirements for a hydroelastic model structure are presented. The important guidelines followed in designing the experimental model are also described.

4.1 The Model Scale

The investigation of the use of the induced drag forces for damping purposes of the structure demands a wave response study for an offshore structure. For this purpose a reduced scale physical model was fabricated and tested in a wave tank. However the concept of introducing fluid-induced resonance in a laboratory requires

a hydroelastic model in which the elastic deformation and the wave loading are modelled to a reduced scale. Before proceeding to the model design, the different criteria involved in the selection of the model scale are described herein.

The principal requirement of the model is to induce flow-separation at low KC numbers which would require a large diameter cylindrical tube. The larger the diameter of the cylinder, the better the possibility of verifying the viability of the concept.

Secondly, the modelled wave frequencies in the wave tank should have their significant energy frequency in the same range as the modelled structural frequency. In our laboratory, the wave tank high quality waves can be generated only at frequencies lower than 0.75 Hz. Since the study was interested in the response at and close to resonance, it is preferable to choose the model scale such that the natural frequency of the model structure is lower than 0.75 Hz.

Thirdly, the available material properties and the tubing sizes that could be used to construct the model, are also important for the model scale.

Fourthly, the model scale is also governed by the size of the available testing facility. The water depth in the tank and the base dimension of the structure which needs to be accommodated in the tank are important considerations which decide the model scale.

And fifthly, the problems related to the transportation of the model, from the fabrication place to the wave tank location, need a detailed consideration.

After considering all the above requirements, a 1:50 scale was selected for the model study in a wave tank of size 200 m long, 12 m wide and 7 m deep.

4.2 The Hydroelastic Model

Design of a hydroelastic model involves the modelling of waves, wave forces and the elastic structure. By definition a reduced scale hydroelastic model can be defined

as a flexible model in which the geometrically similar model behaves, in terms of its elastic deformations, in a manner corresponding to its target prototype structure. Every physical value (like the wave force and structural response) is related by the physical relationship that exists between the prototype and model. The model laws, which formulate the relationship, are obtained by a dimensional analysis of all the independent pertinent variables. (The model laws derived from such dimensional analysis yield the scale factors which are used to predict the prototype behaviour from the model response.)

These scale factors are simply the ratios of the variables in the model to their corresponding prototype variables. Modelling of wave motions in the laboratory demands two inevitable conditions: (1) water is used in the model fluid; and (2) Froude similarity is retained (ref. Srinivasan and Swamidas, 1987).

4.2.1 Modelling of Waves and Wave Forces

The validity of the hydroelastic model is first based on how adequately the physics of loading is represented in the laboratory model scale. This problem is discussed here using similitude theory. For the sake of simplicity, consider the force exerted on a vertical surface-piercing circular cylinder by progressive gravity waves. The force on the cylinder can be defined as:

$$F = \mathcal{F}(\rho, \nu, H, T, d, D, g) \tag{4.1}$$

in which F is the wave force, D the cylinder diameter, H the wave height, T the wave period, d the water depth, ρ the density of water, g the gravitational acceleration and ν the kinematic viscosity of fluid. These are all called pertinent variables. From Eqn. 4.1, the dimensional analysis returns a possible solution with a set of non-dimensional parameters defined in terms of the pertinent variables (Sharp, 1981):

$$\frac{F}{\rho g H D^2} = \mathcal{F}\left(\frac{d}{gT^2}, \frac{H}{gT^2}, \frac{D}{gT^2}, \frac{HD}{T\nu}\right) \tag{4.2}$$

In the case of deepwater (for d $\geq$ L/2 where L is the wave length), 'd' is no longer a relevant variable so it can be excluded from Eqn. 4.2. The parameter $\frac{HD}{\nu}$ accounts for fluid viscosity and is replaced by the Reynolds number, Re which is defined as $R_e = \frac{U_m D}{\nu}$ where ν is the kinematic viscosity, U_m is the maximum horizontal water-particle velocity and T is the wave period. Also by assuming a small amplitude wave theory, the term gT^2 in Eqn. 4.2 can be replaced by the parameter L, the wave length. These changes lead to an alternate form of Eqn. 4.2.

$$\frac{F}{\rho g H D^2} = \mathcal{F}(\frac{H}{L}, \frac{D}{L}, R_e) \tag{4.3}$$

The first non-dimensional parameter, $\frac{H}{L}$, ensures that the wave train is scaled geometrically to have the same ratio of wave height to wave length in the model and prototype situations. The second non-dimensional parameter, $\frac{D}{L}$, ensures that the waves are scaled geometrically to the size of the cylinder, and is also used in the definition of the Keulegan-Carpenter number, 'KC' (Sarpkaya and Isaacson, 1981) which is $KC = \frac{U_m T}{D}$. Therefore, Eqn. 4.3 can be expressed by:

$$\frac{F}{\rho g H D^2} = \mathcal{F}(\frac{H}{L}, KC, R_e) \tag{4.4}$$

In the foregoing, the experimental problem of a cylinder subjected to the action of progressive gravity waves has been approached through dimensional analysis. However in Chapter 3, the same problem was handled using the empirical formula developed by Morison et al., 1950. Therefore, it would be interesting to compare these two approaches and see the appropriateness of Morison's formula through this dimensional analysis. On such comparison it is very clear that to reconcile the two forms, it is necessary that the coefficients of inertia (C_m) and drag (C_d) must, in general, be of the form:

$$C_m = \mathcal{F}(KC, R_e) \tag{4.5}$$

$$C_d = \mathcal{F}(KC, R_e) \tag{4.6}$$

It must be mentioned here that the Keulegan-Carpenter number automatically remains invariant in a Froude scale similarity. Therefore Eqn. 4.4 suggests that in order to reproduce the physics of wave loading in the laboratory wave tank, the criteria for the model design should take into account both the Froude and Reynolds number similarities, simultaneously. However it is well known that fulfilling these two similarities, simultaneously, is practically impossible in any model design.

In a unidirectional steady flow, the influence of the Reynolds number on the flow behind a circular cylinder is well documented. The Reynolds number characterizes the flow as subcritical, critical, supercritical and postcritical regime. However in an oscillatory flow the KC number also plays a very important role. It characterizes the flow in terms of vortex shedding which we have seen already in Fig. 2.5.

The Froude scale similarity retains the ratio of the inertia forces to the gravitational forces, between the model and prototype. Since the gravity waves are the prime source of loading, a Froude model similarity criterion is inevitably applied in a wave tank model study.

In terms of the Reynolds number of the flow, the laboratory model of an offshore structure generally operates in the subcritical regime whereas its prototype is either in the supercritical or in the post-supercritical regime. This Reynolds number discrepancy largely affects the nature of the viscous flow and the flow-separation behaviour. For this reason a drag dominated structure cannot usually be modelled successfully in a wave tank study.

However in the case of inertial force dominated structures, if the structure has large diameter members for which the drag forces are very small compared to the inertial forces, the physics of the loading can be reproduced at the laboratory scale by following the Froude scale similarity. Not only that, but in addition, the mechanism of flow-separation and the formation of vortices behind the cylinder are controlled predominantly by the KC number when the structure operates at low KC numbers.

This is due to the fact that at very low KC numbers, the KC number controls the flow around the vertical cylinder to a greater extent than the R_e number. Considering the structures at very low KC numbers, it can be stated that Froude scale modelling can adequately reproduce the physics of loading in the laboratory wave tank. However the error due the R_e number discrepancy is generally accepted as a scale error.

The dimensional analysis discussed in this section can readily be extended to the case of random wave generation in the wave tank. The significant wave height H_s and zero crossing period T_z may be used as pertinent variables in place of the wave height and period of regular waves.

4.2.2 Modelling the Fluid-Structure Interaction

The preceding discussions dealt with the adequacy of physical modelling of wave loading at an reduced model scale. However a true fluid-structure interaction problem should also include the elastic behaviour of the structure in the dimensionless analysis. The similarity conditions are so restrictive that reduced scale models for the study of the dynamic behaviour of offshore structures would be practically impossible unless a geometrically distorted model is proposed. For problems involving fluid-structure interaction in a wave tank study, we normally encounter the following conditions:

1. The model is generally built using plastic material whose modulus of elasticity and density are much lower than that of the prototype structure.

2. The internal dimensions of the tubular members of the structure are distorted relative to the geometric scale, but the external dimensions of these members are kept according to the general geometric scale, since it is the external surface of a member that is exposed to the waves.

3. Extra masses have to be distributed throughout the model structure without affecting the stiffness properties of the model.

The necessity for the above three conditions can be explained mathematically by again repeating the dimensional analysis in which case the mass, elastic and damping properties of the structure are included. The additional variables involved are the modulus of elasticity (E), the density of material (ρ_s) and the structural damping ratio (ζ). Note that the damping ratio ζ is non-dimensional which will reappear in the same form after the dimensional analysis. After the dimensional analysis, the non-dimensional form can be derived as (similar to Eqn. 4.2):

$$\frac{F}{\rho g H D^2} = \mathcal{F}(\frac{H}{L}, KC, R_e, \frac{\rho_s}{\rho}, \frac{T}{H}\sqrt{\frac{E}{\rho}}, \zeta) \tag{4.7}$$

We have already seen the physical meaning for the first three non-dimensional parameters which are concerned with the adequacy of the wave load modelling at small scale. The new term $\frac{\rho_s}{\rho}$ represents the ratio of the structural inertial force to the fluid inertia force which needs to be retained the same in the model and prototype situations. The term $\frac{T}{H}\sqrt{\frac{E}{\rho}}$ can be identified as the Cauchy number. The structural damping ratio (ζ) which is supposed to be the same irrespective of the model scale can not be fulfilled if a different material is selected for the model fabrication. However the other two new terms $\frac{\rho_s}{\rho}$ and $\frac{T}{H}\sqrt{\frac{E}{\rho}}$ can be used to formulate the necessary model laws required for the construction of the physical model.

Derivation of Model Laws for the Elastic Structure

The non-dimensional parameters obtained in Eqn. 4.7 can be used to construct the model laws required for the model design. Before constructing the model laws, let us first define certain terms used in the model to prototype scale relations. The length ratio of the model and prototype is defined as:

$$K_L = \frac{L_m}{L_p} \tag{4.8}$$

where the subscripts m and p refer to model and prototype, respectively. Secondly, the elastic moduli ratio of the model and prototype is defined as:

$$K_E = \frac{E_m}{E_p} \tag{4.9}$$

While considering the Froude scale similarity, the time ratio of model and prototype is defined as:

$$K_T = \sqrt{K_L} \tag{4.10}$$

It also can be proved that the geometric similarity in a Froude's law requires ideally (Sarpkaya and Isaacson, 1981):

$$K_E = K_L \tag{4.11}$$

However it is practically impossible to find a suitable material which satisfies the above requirement. Under this condition, a sectional distortion in the model structure is inevitably applied which leads to an additional geometric scale ratio defined as:

$$K_t = \frac{t_m}{t_p} \tag{4.12}$$

where t_m and t_p are the wall thickness of the tubular members of the model and prototype, respectively. Since the distortion of the external dimension of the tubular member affects the wave forces, the sectional distortion is given in terms of the wall thickness of the members.

Using K_t and K_L, the scale factor for the moment of inertia can be defined as:

$$K_I = K_L^3 K_t \tag{4.13}$$

When sectional distortion is applied to the model, as stated before, the following conditions should be fulfilled:

$$K_t = \frac{K_L^2}{K_E} \tag{4.14}$$

$$K_M = \frac{K_L}{K_E} \tag{4.15}$$

in which K_M is the submerged density ratio of the model and prototype material which is again defined as:

$$K_M = \frac{(\rho_s - \rho)_m}{(\rho_s - \rho)_p} \tag{4.16}$$

Eqn. 4.14 is used to find the member wall thickness of the model needed for a given geometric scale and for a selected model material. Additional mass which is distributed over the model structure in order to satisfy the similarity required by Eqn. 4.15 is calculated by using Eqn. 4.16. The scale factors for various desired physical quantities are set out in Table 4.1.

Table 4.1: Scaling relations for model study

Quantity	Prototype	Model
Length	L	$K_L\ L$
Tubular wall thickness	t	$K_t\ t$
Moment of inertia	I	$K_L^3\ K_t\ I$
Time	T	$K_L^{1/2}\ T$
Velocity	u	$K_L^{1/2}\ u$
Acceleration	a	a
Frequency	f	$K_L^{-1/2}\ f$
Mass	$\rho_s L^3$	$K_M\ K_L^3\ L^3$
Force	F	$K_L^3\ F$
Moment	M	$K_L^4\ M$
Pressure	P	$K_L\ P$
Stress	σ	$K_E\ \sigma$

4.3 Description of the Prototype Platform

Several deepwater concepts which possess large diameter circular cylinders were reviewed. Finally the Tripod Tower Platform (TTP) was chosen as the basic system. The general configuration of the TTP is shown in Fig. 2.2. The superstructure shown above the sea bed was selected as the prototype to serve as a guide in designing

the model structure for this study. The design of the model was aimed at a 1/50 reduction in the overall dimensions of the prototype and also in the outer diameter of its members. While designing the model, certain modifications were made. Before proceeding to the design details, a brief description of the prototype is presented herein.

The TTP essentially consists of a few large diameter heavy wall thickness steel tubular members connected together to form a deepwater structure. Its main central concentric vertical column is supported by three inclined legs, at a batter of 3:1. The basic geometric characteristics of the TTP is an original design, developed by Heerama Engineering Service, the Netherlands. The structure was proposed for two different water depths of 345 m and 315 m. The basic geometric characteristics of this platform are given in Table 4.2. Since the fatigue life of the TTP is directly related to its dynamic behaviour, a typical sea state table for the North Sea environment is also given in Table 4.3. (In Table 4.3, H_s = significant wave height and T_z = zero up-crossing period.)

Table 4.2: Summary of the prototype platform functional data

Sl. No.	Design Criteria	Values
(a)	Depth of water	315 m (or 345 m)
(b)	Deck weight	50,000 - 60,000 tonnes
(c)	Deck clearance	25 m above MSL
(d)	Total deck plan area	16 000 sq.m
(e)	Centre of gravity of topside	42.5 m above MSL
(f)	Outer diameter of main column	15 m
(g)	Wall thickness for column	0.125 m
(h)	Outer diameter of legs	8 m
(i)	Wall thickness for legs	0.165 m
(j)	First fundamental sway period	5-7 s
(k)	A 100-year design wave height	31 m
(l)	A 100-year design wave period	14 to 17 s

Table 4.3: A typical sea state table for fatigue analysis - North Sea design data (Michelsen and Meek, 1982)

Sea state	H_s (m)	T_z (s)	Probability of occurrence
1	1.10	5.50	0.1700
2	2.20	5.50	0.2010
3	2.20	6.50	0.1920
4	3.30	6.50	0.1620
5	3.30	7.50	0.0950
6	4.30	7.50	0.0830
7	4.30	8.50	0.0170
8	5.40	8.50	0.0570
9	6.80	10.00	0.0180
10	8.50	11.50	0.0043
11	10.30	12.50	0.0004
12	12.50	13.50	0.0002
13	15.00	14.50	0.0001

4.4 Design of the Model

Using acrylic tubes, the super-structure of the model was designed to meet the design objectives to the best possible extent. Acrylic material was selected because no other plastic tubes of large diametral sizes were readily available. Since the research investigation is interested in artificially introducing flow-separation at low KC numbers, large dimensions for the structural members are of paramount importance. Many difficulties were encountered in exactly keeping the prototype model guidelines. For example, scaling down the 60, 000 tonnes of the prototype deck weight is quite unsafe for the plastic structure at the model scale. However it is very essential to keep the fundamental natural frequency of the structure at a low level so that the commonly generated waves in the tank can cause the structure to resonate. Hence in the present model design a reduced deck weight was used and correspondingly the cantilever portion of the center column was increased to keep the structural

natural frequency close to the prototype situation as it vibrates in water. It should be emphasized here that it is not the purpose of this research to study the behaviour of any particular structure, rather to apply the concept of artificially inducing hydrodynamic damping to a resonating structure. However maximum effort was made to retain the originality of the design concept.

The wave tank facility available at the Institute for Marine Dynamics was utilized for the experiments. Due to certain practical problems, the water depth in the tank is always maintained at 7.0 m. Thus this physical restraint automatically set the water depth to 7 m for this model study which, in the prototype situation, corresponds to 350 m water depth.

The modulus of elasticity for the acrylic tube was 3.0 Gpa whereas for the steel (prototype) it was 210 Gpa. From Eqn. 4.9, the ratio of moduli of elasticity is obtained as 1/70. Knowing the K_E, the thickness ratio K_t also can be computed following Eqn. 4.12.

$$K_t = (\frac{1}{50})^2 \times 70 = 0.028$$

With the above scale ratio the geometric characteristics of the model can be fixed. The required sizes of the main column and inclined leg members for the model are given below:

Column diameter	= 0.30 m
Column wall thickness	= 3.51 mm
Leg diameter	= 0.16 m
Leg wall thickness	= 4.50 mm

Due to the availability of the material tubes in some standard sizes, the following dimensions were selected for the model structure:

Column diameter	= 0.30 m
Column wall thickness	= 3.00 mm
Leg diameter	= 0.15 m
Leg wall thickness	= 3.00 mm

In order to add the distributed extra masses over the length of the tubular members, the main column and the three supporting legs of the model were flooded with water.

4.5 Fabrication of the Model Platform

The structure was fabricated in three units: (a) the superstructure, (b) the deck and (c) the supporting base frame. The supporting base frame was made of heavy steel sections while the deck and the super-structure were fabricated using acrylic plates and tubes, respectively. Considerable care was given in the design phase of the model to avoid any damage that might occur during transportation and installation. The units were designed in such a way that they could be fabricated separately and transported to the test location in the wave tank and assembled in the water. The drawings produced for the fabrication of the model are shown in Figs. 4.1 to 4.6. Fig. 4.1 describes the key plan at the bottom elevation of the model. The tower portion of the model is detailed in Figs. 4.2 and 4.3. The horizontal bracing of the tower at the bottom elevation is shown in Fig. 4.4. Figs. 4.5 and 4.6 illustrate the deck details. To rigidly support the model structure at the base and also to anchor it at the bottom of the tank, a heavy steel frame was designed (see Fig. 4.7).

4.5.1 Fabrication of the Tower Portion

Acrylic tubes of 0.3 m diameter, 3 mm wall thickness and 1.8 m long were glued to construct the center column of the tower, since the overall length of the centre column was 7.9 m. At each connection, between tubes, the members were internally stiffened and glued by a circular sleeve of the same material. For the inclined supporting legs, 0.15 m diameter and 3 mm wall thickness tubes were used. Extensive effort and much time were spent for the fabrication of the major joint where the center column meets the three supporting legs. Quite a lot of microscopic cutting

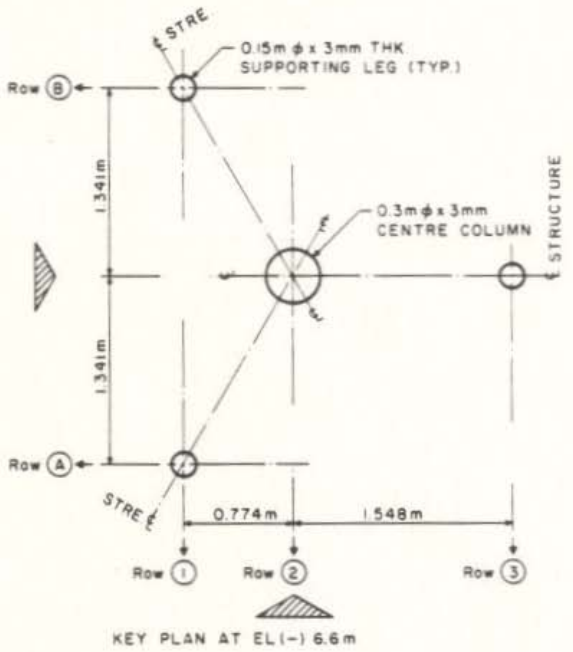

Figure 4.1: Key plan at EL(-) 6.6 m

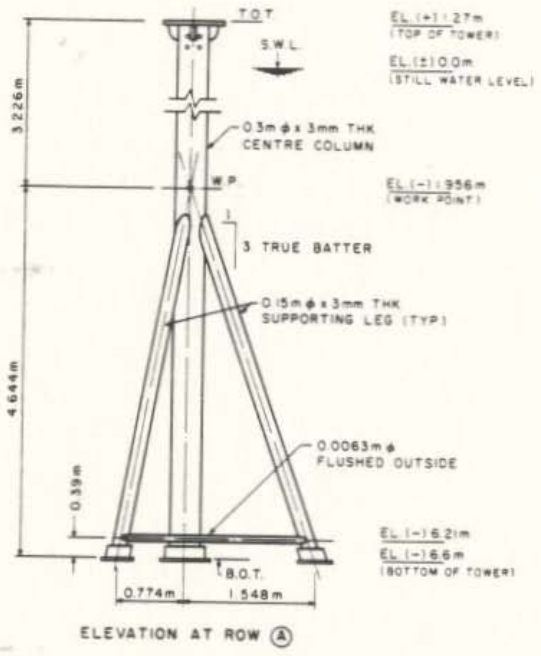

Figure 4.2: The fabrication drawing describing the front elevation of the tower

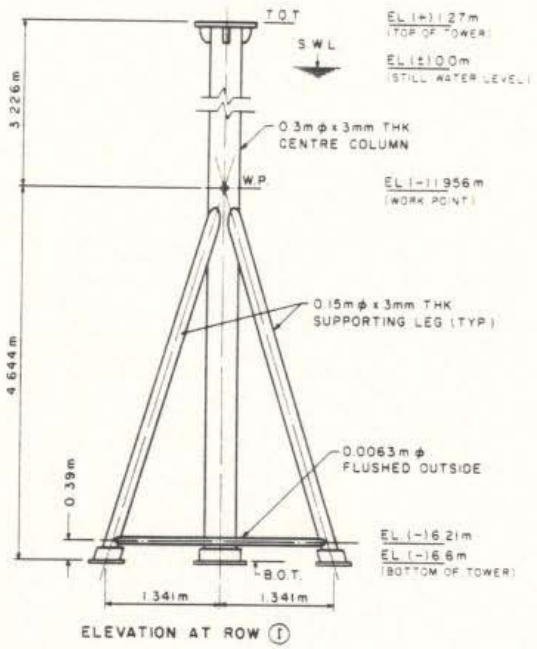

Figure 4.3: The fabrication drawing describing the side elevation of the tower

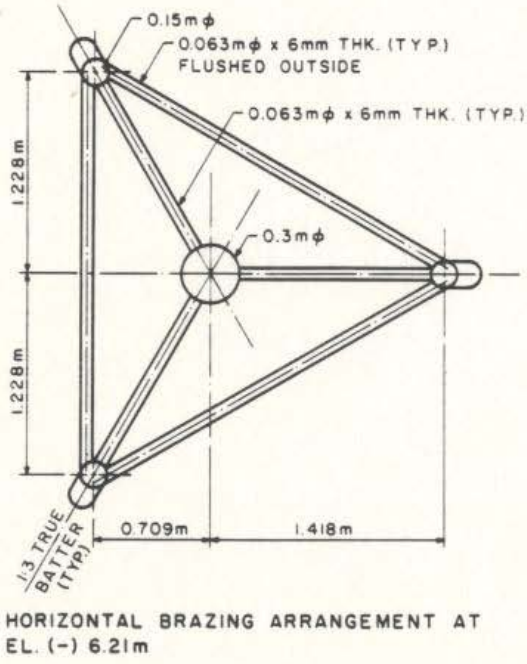

Figure 4.4: The fabrication drawing describing the horizontal bracing for the tower

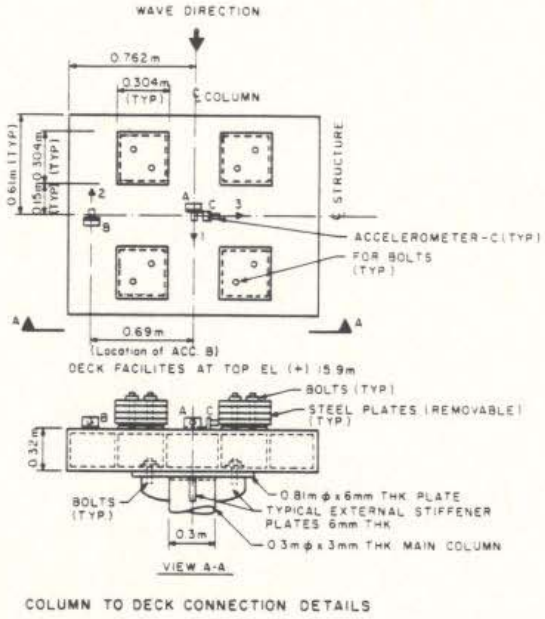

Figure 4.5: The fabrication drawing describing the deck configuration

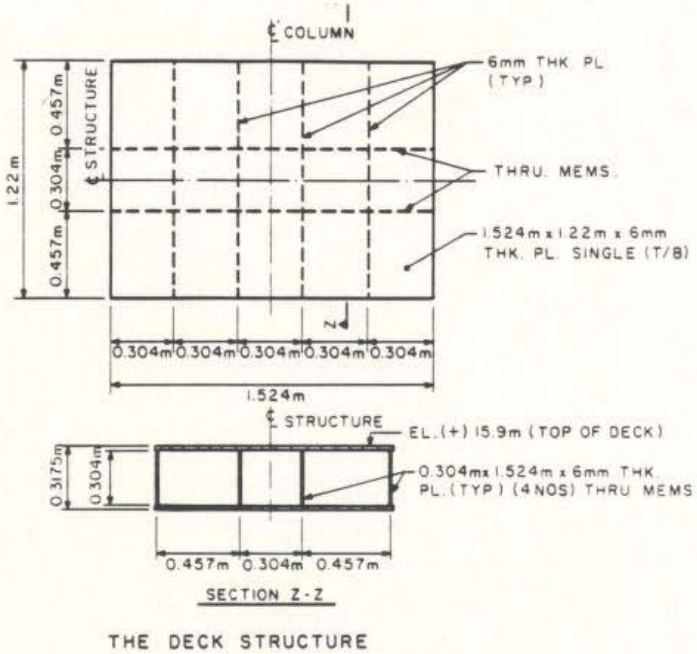

Figure 4.6: The fabrication drawing describing the deck structural details

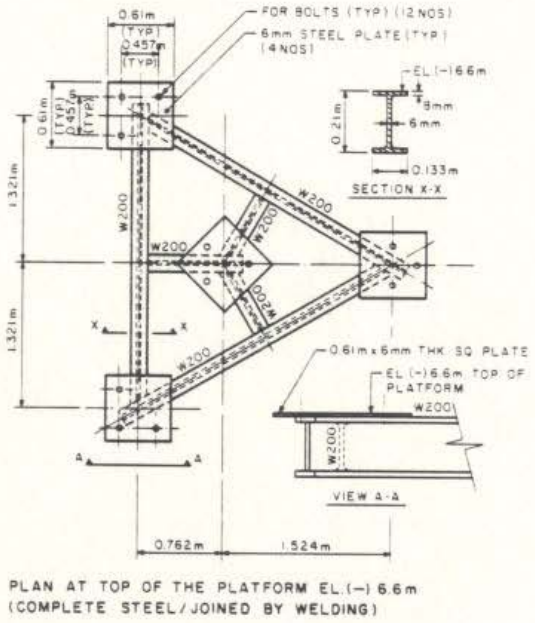

Figure 4.7: The fabrication drawing describing the structural details of the steel base frame

and machining was involved, in obtaining the profile, and in making the inclined legs to fit exactly into the central column at its designed angle of batter.

The legs were glued to the center column. The joint was also internally stiffened for adequate strength. Externally, flat acrylic plates were glued between the three inclined legs and the main column, to make the joint stiff. To enhance the integrity of the structure and to avoid any damage during transportation, a strong horizontal bracing was provided at the base of the structure. This, however, would not affect the flexural properties of the model tower. The connecting members between the center column and the legs at the horizontal bracing were 0.15 m diameter and 3 mm wall thickness tubes. The horizontal members connecting the legs were 0.063 m diameter and 6 mm wall thickness tubes. The whole structure was completely joined by strong gluing. Extra stiffeners were provided at major joints of the individual tubing to avoid any possible failure during testing. The gluing at each joint was

tested for its strength to ensure complete integrity of the structure. Fig. 4.8 shows a portion of the fabricated tower.

4.5.2 Fabrication of the Base Supporting System

To provide a rigid connection at the bottom supports of the tower a heavy steel base system (see Fig. 4.9) was fabricated. It consisted of 2.6 m long, W200 I-beam welded together to form a triangular shaped structure. Three 1 m long steel beams were welded perpendicular to each side to join at the centre of the triangle. This was designed to support the central column. Circular plates were welded on top of the base at its four supporting points. The three legs and the center column were attached to specially fabricated rigid circular connectors at their bases which were in turn bolted to the supporting base frame. In Fig. 4.10, the photograph shows the trial mounting of the tower supporting points over the steel base (in air). Levelling screws were also provided at the bottom of the steel base to take into account any imperfection at the tank bottom. Each corner of the triangular steel base was welded with a steel net for providing ballasting in the wave tank. Additional gravity weights were placed over the steel net to provide strong gravity type of fixity to the structure at the bottom of the tank.

4.5.3 Fabrication of the Deck Structure

The deck structure consisted of a plastic box reinforced with webs. Acrylic plastic plates, 6 mm thick, were glued together to form the deck. It was fabricated simply as a rigid structure with provisions to accommodate removable steel plates and three accelerometers. The design of the deck structure was similar to the modern production platform decks, where modular construction is used. The height of the deck was designed according to the height of the cellar deck of the prototype and the dimensions of the deck were fixed according to the prototype structure.

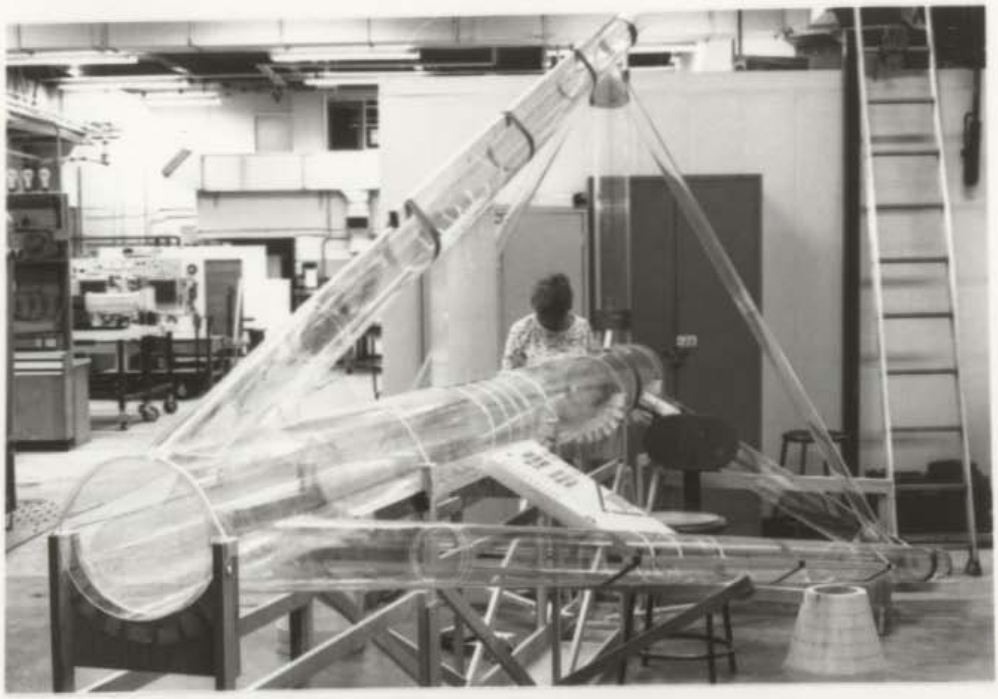

Figure 4.8: Photograph of the partly fabricated model tower

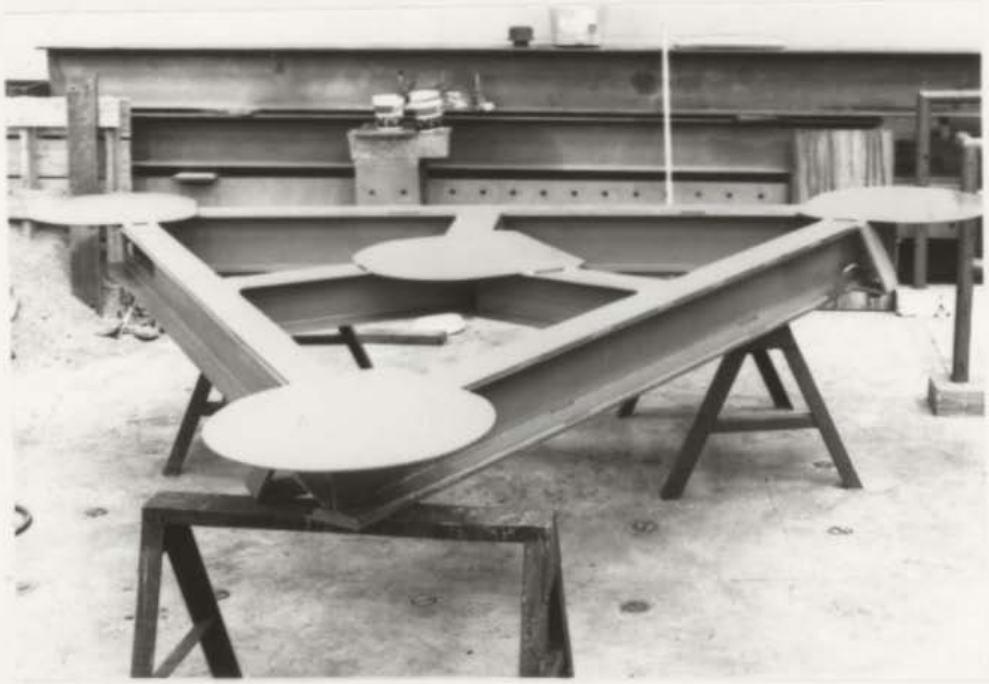

Figure 4.9: Photograph of the partly fabricated steel base system

For easy operation, the deck was fabricated as a separate integral unit which could be fixed to and removed from the superstructure at any time. Removable steel plates were utilized to simulate the maximum deck mass. The deck box was designed to act as a rigid unit during wave excited structural oscillations. The deck to main column connecting details are found in Fig. 4.5. Fig. 4.5 also shows the fixing arrangement of the steel plates and the accelerometers over the deck surface. The weight of the deck structure alone was 383 N. Steel plates, weighing 978 N, were added as additional deck weight. Thus the total deck weight used in the model was 1361 N. A separate launching truss, made of wood, was fabricated to hold the model in place during fabrication and transportation.

4.6 Transportation and Installation of the Model

Transportation of the model, without incurring any damage, was one of the major tasks faced in this project. The fabrication was carried out in the structures laboratory, Faculty of Engineering and Applied Science, Memorial University of Newfoundland, St. John's. Then the three components were carefully transported to the Institute for Marine Dynamics (National Research Council of Canada) building located next door, where the required wave tank facility is situated. Fig. 4.11 shows a view of the tank.

The 200 m long tank consists of a towing carriage which was often used for the installation purposes. The test was conducted almost at the middle of the tank which was 100 m away from the wave board. The steel base was first transported to the test location by a floating barge (see Fig. 4.12). The towing carriage was used to lift the steel base from the barge and gradually lower it into the water. After placing the steel base on the bottom of the wave tank, using divers, at 7 m water depth, heavy lead weights were placed over the steel wire mesh located at each corner of the triangular base.

Figure 4.10: Photograph showing the trial matching of the tower supports with the steel base

Figure 4.11: A view of the wave tank

The tower structure, without the deck portion, was slowly launched into the tank from the beach side. The wooden launch truss was used to gently the move structure into the tank. Fig. 4.13 shows the launching operation of the structure in the wave tank. The legs and the center column were flooded with water. Due to the support of the wooden launch truss the structure was floating in the water and then towed gently by the towing carriage. Two professional divers were used for the upending and installation procedures. Fig. 4.14 shows the upending procedure of the structure near the test location. The structure was slowly upended and placed over the steel base. The central column and the three inclined legs were positioned over their corresponding preset locations on the bottom supporting base. Then they were bolted together to have a rigid connection at the bottom supports. After that, the wooden launch truss was removed from the superstructure.

The carriage test frame was raised above the top of the installed tower and the center opening of the test frame was positioned to the center of the tower. The deck structure was placed above the central test area of the carriage and the test frame was lowered down. The deck structure was then mounted on top of the tower and fixed by bolting. The steel plates were added over the deck top surface and were bolted very tightly to the deck to prevent any sliding during vibration. Three accelerometers were mounted on the top of the deck. The deck, as installed on the structure in water, is shown in Fig. 4.15.

With the tower and deck joined together and the legs and center column fixed (at the bottom), the model possessed the important features common to typical deepwater tripod tower platforms.

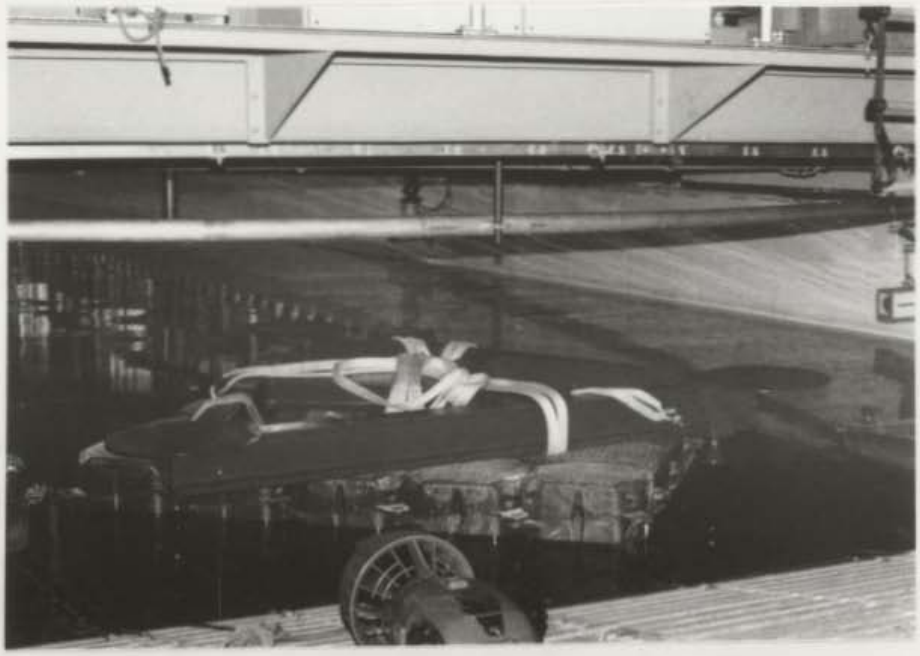

Figure 4.12: Photograph showing the transportation of the steel base system in the tank

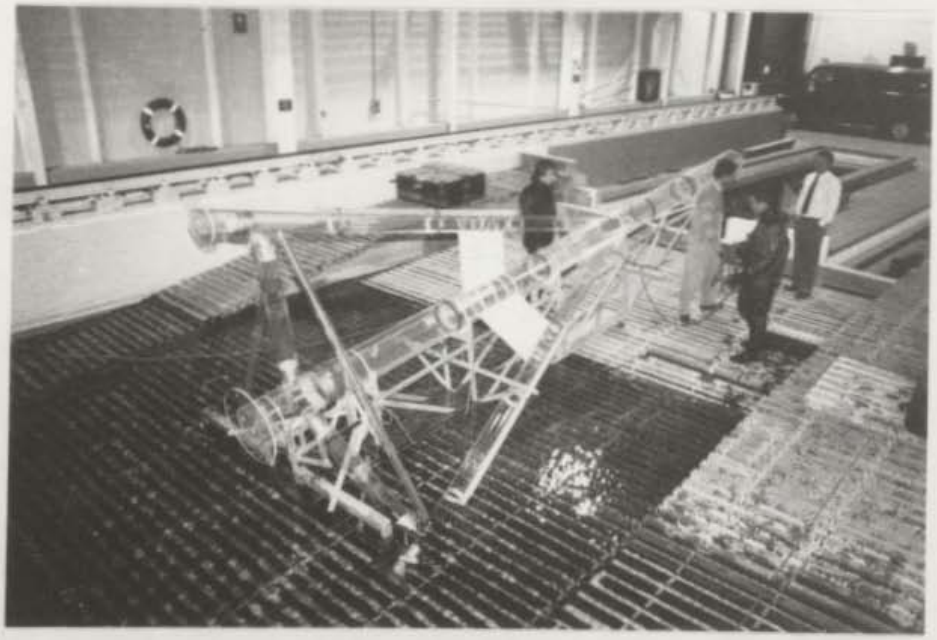

Figure 4.13: Photograph showing the launching of the tower into the tank

Figure 4.14: Photograph showing the up-ending of the tower in the water near the test location

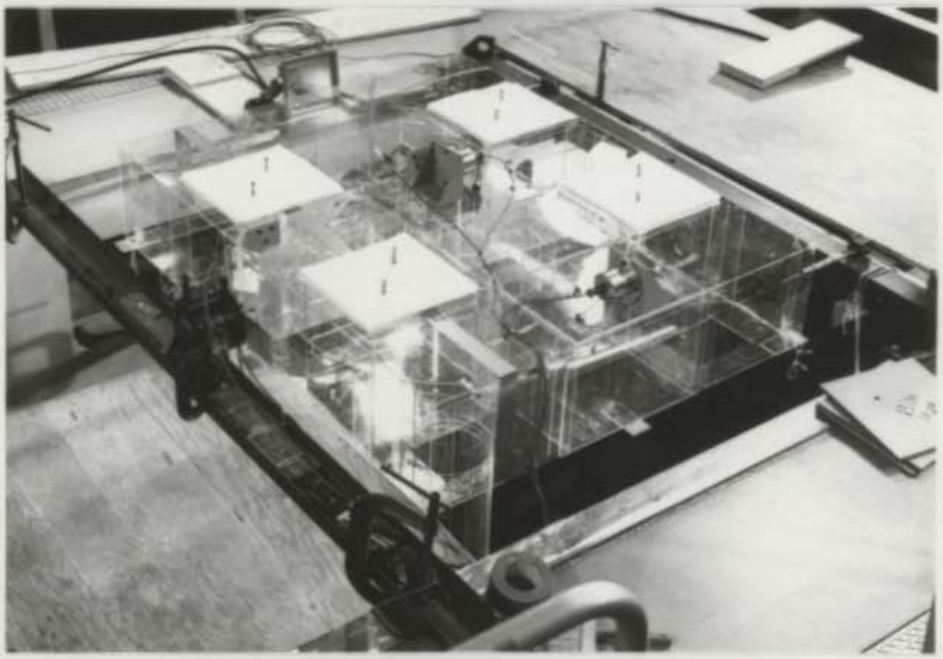

Figure 4.15: Photograph showing the instrumented deck structure mounted over the tower in the tank

Chapter 5

Estimation of Natural Frequencies and Damping Ratios for the Physical Model

When a structure is dynamically excited, acceleration and/or displacement/strain measurements can be recorded at appropriate locations in order to evaluate characteristics of the natural modes of vibration that are produced. The frequencies of these modes and the damping in these modes can be evaluated from the measurements, whether the excitation is unknown or is induced by means of measurable forces. In the prior case, signal analysis is customarily used and in the later case system analysis is generally followed. Signal analysis is the process of determining the characteristics of the response of the system, due to some generally unknown excitation. The dynamic assessments are made from the response of the structure. However the system analysis deals with techniques for determining the inherent properties of the structure. In this technique the structure is excited with measurable forces. Instead of analyzing the response, the technique examines the response/force ratio which is an independent, inherent property of the structure, irrespective of the type of excitation. A free vibration test is a typical example in which signal analysis is employed and modal testing is a typical example in which system analysis is followed.

In general, when dynamic testing is employed several test options are possible. Considering the information required, the prior knowledge of frequencies as well as damping values, and the relative convenience in employing the different test options, the appropriate dynamic test procedure can be selected to accomplish the objectives at hand.

Dynamic testing typically consists of applying an excitation to the structure and monitoring its response and operation. The vibration is induced in the structure by means of a controlled environment. A free vibration test (in which only an initial excitation or displacement is applied and removed so that the structure is allowed to vibrate freely) also comes under the general area of dynamic testing. However the system parameters can be estimated more precisely if a dynamic test is conducted for the known excitation force.

In this thesis, both free vibration and modal testing were applied to the model structure. These experiments were conducted in air. In water, only the free vibration test was employed. The main purposes of these tests are: (a) to obtain the prior knowledge of the resonant frequencies of the structure before proceeding to the main experiment in the wave tank; (b) to verify the natural frequencies obtained from the analytical model and (c) to estimate the level of damping in the physical model which is required to develop the damping matrix in the analytical model.

First the instrumentation of the model, the experimental set-up and the testing procedures used for the modal testing are described. Secondly the estimated modal parameters obtained from the modal test are compared with the results of free vibration test (conducted in air). Thirdly the results of free vibration analysis conducted in water are presented. In the final section, the structure was modelled using finite element technique and the eigenanalysis was carried out to extract the natural frequencies and their corresponding mode shapes.

5.1 Modal Testing in Air

Modal testing is a well-established experimental approach in which the dynamic behaviour of an elastic structure is characterized by its modes of vibration. Each mode has its own modal shape; the natural frequency and the damping value associated with each mode may be identified from measurements at different points on the structure. The main object of modal testing is to extract the modal parameters (such as mode shapes, natural frequencies and modal damping ratios), from the analysis of the measured responses of the structure for the known excitation. The modal testing and analysis were used here to determine the fundamental natural frequency and the corresponding modal damping ratio for the model structure.

5.1.1 Measurement System

The modal testing was conducted in air in the Structures Laboratory, Faculty of Engineering, Memorial University of Newfoundland, St. John's, Canada. Fig. 5.1 is a layout of the measurement system. The equipment used for this experiment is listed below:

1. One HP 5420B dual channel digital signal analyzer
2. One B & K type 4808 vibration exciter (permanent magnet type)
3. One B & K type 8318 accelerometer (piezo-electric type)
4. One B & K type 8001 force transducer
5. One B & K type 2706 power amplifier
6. One B & K type 2635 charge amplifier
7. One B & K type 2626 conditioning preamplifier
8. One HP 7550A pen plotter

9. One 32 channel Keithley System 500 ADC

10. One desk top computer with data acquisition software

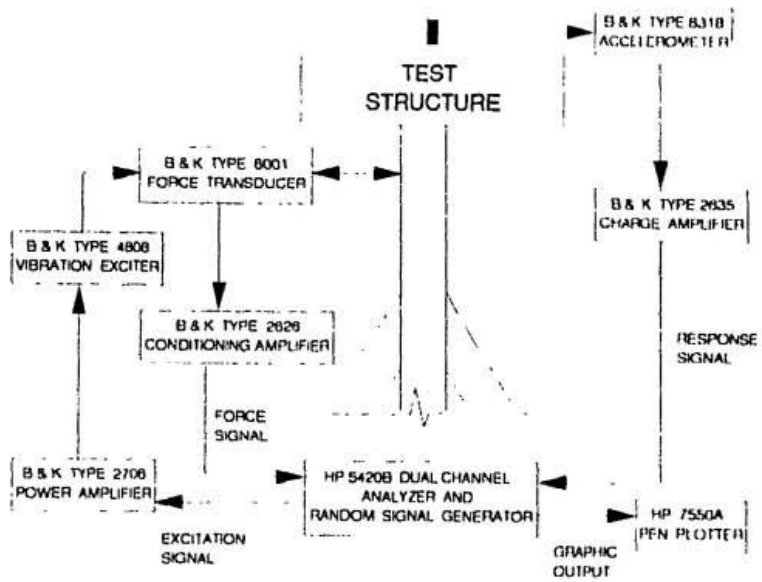

Figure 5.1: The test set-up in modal testing

The experimental model was fixed at the bottom by bolting onto the steel base, which was fabricated specially for this purpose. The deck structure (weighing 383 N) was mounted over the tower. Only the deck structural weight was considered for this experiment and no additional deck weight was added. In modal testing, the input force and the response signals must be measured simultaneously. To measure the structural responses an accelerometer was attached on top of the deck (pointing in the longitudinal direction). The accelerometer signal was passed through the charge amplifier and then fed to a HP 5420B Dual Channel Signal Analyzer. A permanent magnet type vibrator was used to excite the structure. The excitation force was applied on the central column at a distance of 0.83 m below the deck bottom. The exciter was instrumented with a force transducer which had one end attached to the

exciter and the other end attached to the structure. This arrangement measured the forces transmitted to the structure by the exciter. The random noise generation facility available in the analyzer was utilized to operate the exciter. The signal from the force transducer was passed through the preamplifier and then fed to the analyzer.

5.1.2 Frequency Response Function

The main function of modal testing is to extract the modal parameters from analysis of the measured frequency response function (FRF). The general scheme for measuring the FRF consists of measuring simultaneously the input and response signals, transforming these signals to the frequency domain, and estimating the FRF by dividing the transformed response by the transformed input. This can be explained mathematically as follows.

Consider that the signal measured from the force transducer, p(t), is the input to the system and the signal measured from the accelerometer, r(t), is the output from the system; then the FRF can be defined in the frequency domain as:

$$H(f) = \frac{R(f)}{P(f)} \tag{5.1}$$

where R(f) and P(f) are the Fourier transforms of the output r(t) and the input p(t), respectively. Eqn. 5.1 represents the complex ratio between the output and input, as a function of frequency f. The FRF obtained from the acceleration response output is called accelerance (or inertance).

If the input excitation is a random signal, the FRF can be determined as the ratio of the cross-spectral density $G_{PR}(f)$ of the input p(t) and the output r(t), and the power spectral density $G_{PP}(f)$ of the input, viz.,

$$H_1(f) = \frac{G_{PR}(f)}{G_{PP}(f)} \tag{5.2}$$

The above equation is one method of estimating the true FRF. This estimator is called the H_1 estimator. An alternate method for estimating the frequency response function, called H_2, is defined as:

$$H_2(f) = \frac{G_{RR}(f)}{G_{RP}(f)} \tag{5.3}$$

Coherence Function

In practice, measurement noise is always present at both the input and the output. (For example the measured output signal is contaminated by background noise in the laboratory.) It is important to estimate the effects of noise on the measurement. The coherence function provides a means for internally estimating the quality of an experimental determination of the FRF.

The coherence function defines the degree of linearity between the input and output signals which is given by the following equation:

$$\nu(f) = \frac{|G_{RP}(f)|^2}{G_{RR}(f)G_{PP}(f)} \tag{5.4}$$

where $0 \leq \nu(f) \leq 1$. The bounds for the coherence function are 1, for no noise in the measurements, and 0 for pure noise in the measurements. The interpretation of the coherence function is that for each frequency 'f' it shows the degree of linear relationship between the measured input and output signals.

Averaging

The H_1 and H_2 estimators defined in Eqns. 5.2 and 5.3 do not give the true value for the FRF. They are susceptible to the noises on the input and output signals. As stated earlier the noise in the signals, during measurement, are inevitable in an experiment. For this reason it is recommended to perform an averaging process, involving several individual time records, or samples, before a result is obtained which can be used with confidence. Averaging improves the statistical reliability

and removes the spurious random noise from the signals. (Obviously this method is time consuming.)

An important point about the H_1 estimator is that the random noise in the output is removed if averaging of the cross-spectrum is carried out. As the number of averages is increased, H_1 converges to the true FRF. Similarly by using H_2, the input noise is removed from the cross-spectrum if averaging is used. As the number of averages is increased, H_2 also converges to the true FRF. Considering H_1 as a lower bound and H_2 as an upper bound, the true frequency response function must lie somewhere in between. This suggests a third method of estimating FRF as the average of H_1 and H_2 as follows:

$$H_3(f) = \frac{H_1(f) + H_2(f)}{2} \tag{5.5}$$

The modal analysis theory defined in this subsection is sufficient for this thesis. However more details on the experimental modal analysis can be found in Ewins (1984).

5.1.3 Testing Procedure

Band limited signals (white noise) can be generated from the HP 5420B analyzer. Burst random signals were generated by setting the bandwidth to 4 Hz with the starting frequency as 0 Hz. In burst random noise generation, one can gate the noise signal off after a specified percentage of the analysis time. The result is a transient test signal. This improves the signal-to-noise ratio and thus the measurements are leakage-free. For this experiment, out of the total recording time, 81% of the time the noise generation was ON and rest of the time recording was done but for no noise generation. The generated signals were passed through a power amplifier where it was amplified to operate the exciter. Then the structure was excited for a time length of 64 s. It should be mentioned here that the vibration exciter which was available at the time of this experiment was not powerful enough to excite the higher

modes of the structure. Hence the experiment was aimed only to estimate the FRF near the first bending natural frequency of the structure.

The measured input force and the output acceleration response were fed simultaneously to the analyzer. The sampling frequency was set to 16 Hz. Figs. 5.2 and 5.3 show the typical time history of the recorded force and the acceleration signal. Note that the response just reaches zero by the end of the time record. (This should result in optimum signal-to-noise ratio.)

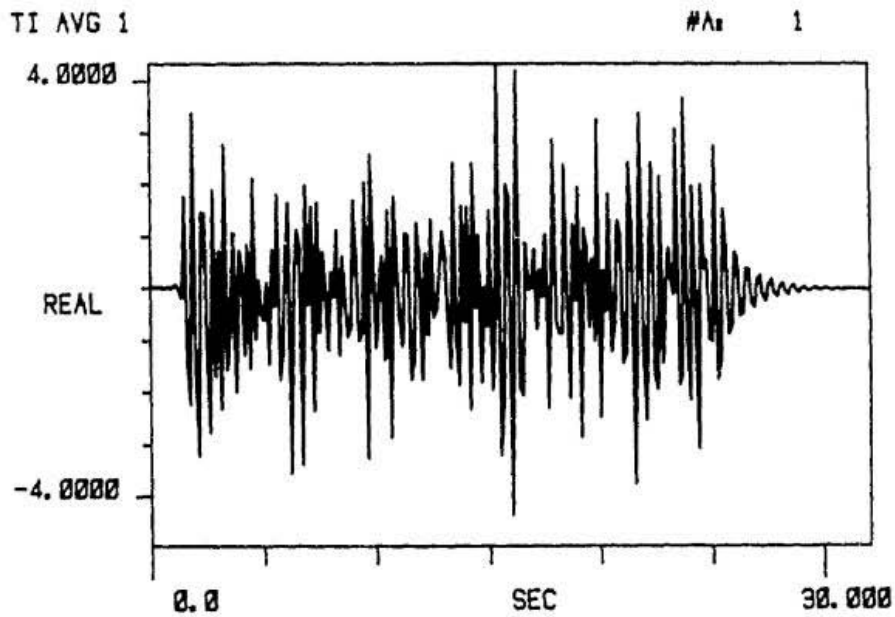

Figure 5.2: Typical time history of the recorded force signal

In order to improve the statistical reliability of the experiment and to obtain a smooth FRF curve, the test was repeated for 50 times and data recorded successively. Each time the frequency response function was computed in the machine and averaged automatically. The type of averaging used in the machine is called Power Spectrum Averaging in which the G_{PP}, G_{RR} and $|G_{RP}|$ were averaged and then the FRF and coherence function computed.

The results were then sent to the digital plotter. The magnitude of the frequency

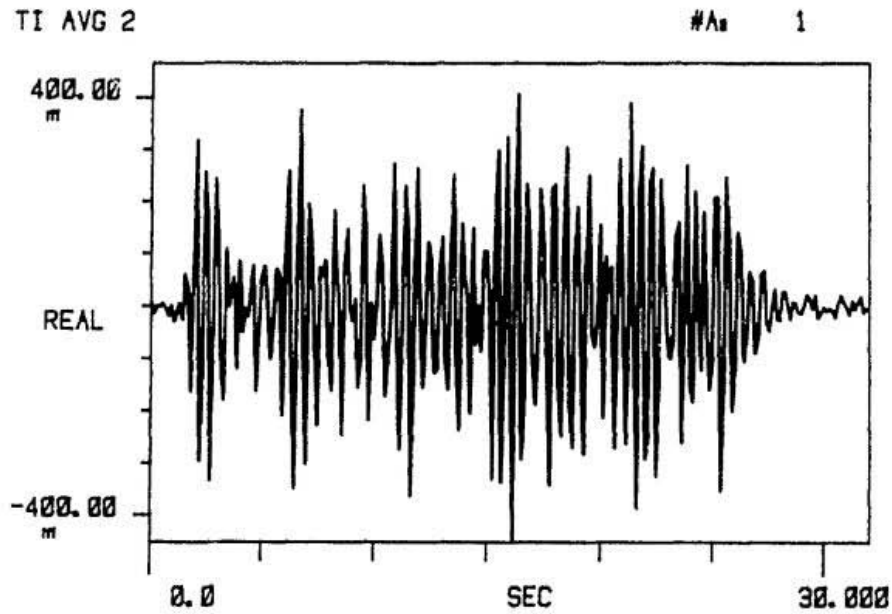

Figure 5.3: Typical time history of the recorded acceleration signal

response function obtained from this experiment is shown in Fig. 5.4. A fairly smooth curve is obtained due to the large number of samples and the averaging process. The function is plotted for the frequency range 0 to 4 Hz and its magnitude is presented in the log scale. The curve exhibits a single prominent peak which shows that the structure had experienced resonance at 1.615 Hz, the lowest bending mode of the structure. The single clear peak in the FRF curve shows that the response at resonance is not influenced by more than one mode. At frequencies higher than 1.615 Hz and lower than 4 Hz, no other peaks were identified in the curve. This shows that the higher modes were not excited by the exciter.

Since the frequency response function is a complex valued function, it may be appropriate here to display the function as a plot of the real vs the imaginary part, Nyquist plot. The Nyquist plot of the measured accelerance near the natural frequency (from 1.34 Hz to 1.78 Hz) is shown in Fig. 5.5. The FRF looks closer to a circle.

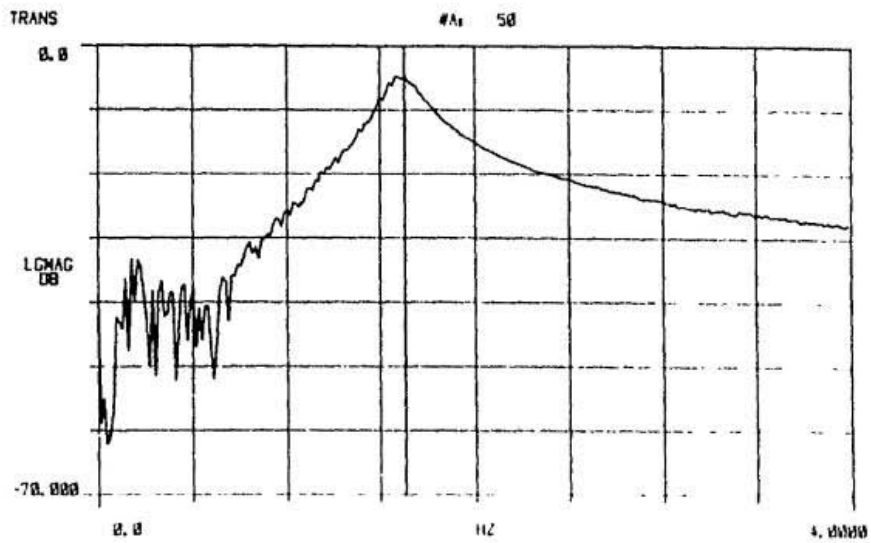

Figure 5.4: The measured frequency response function: a modulus plot of acceleration

Fig. 5.6 shows the plot of the coherence function for the measured signals. At a frequency of 1.2 Hz, and above, the value of the coherence function rises from 0.85 to 1. Even in the vicinity of resonance the value of coherence function is close to 1 indicating good measurement and exhibiting a linear relationship between the measured input and output signals. At higher frequencies (above 1.8 Hz) the value of coherence is 1. Only at very low frequency (less than 0.5 Hz) is a poor coherence seen. This shows that the force transmission between the exciter and the structure at very low frequency was not good in the experiment. However the good value of coherence obtained near the resonance frequency shows that the FRF curve is reliable for the subsequent analysis (damping estimation).

5.1.4 Parameter Estimation

The frequency response function contains all the information that is necessary to characterize the dynamic system. However in the present context only the natural

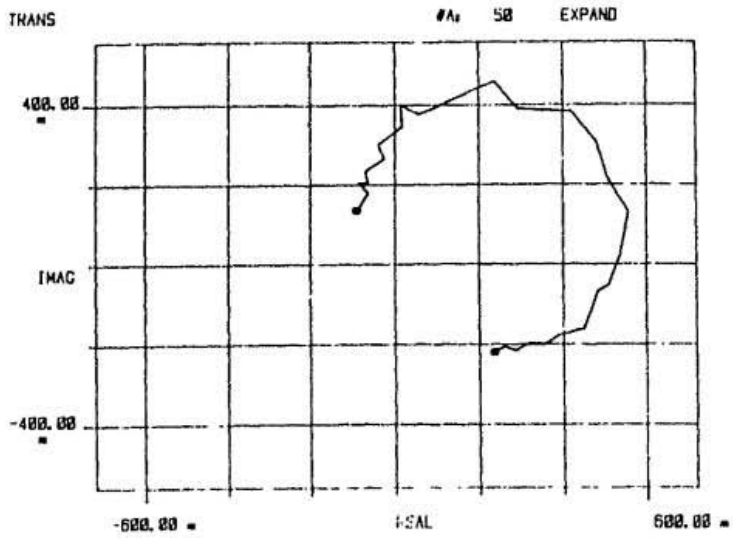

Figure 5.5: The measured frequency response function: a Nyquist plot of accelerance

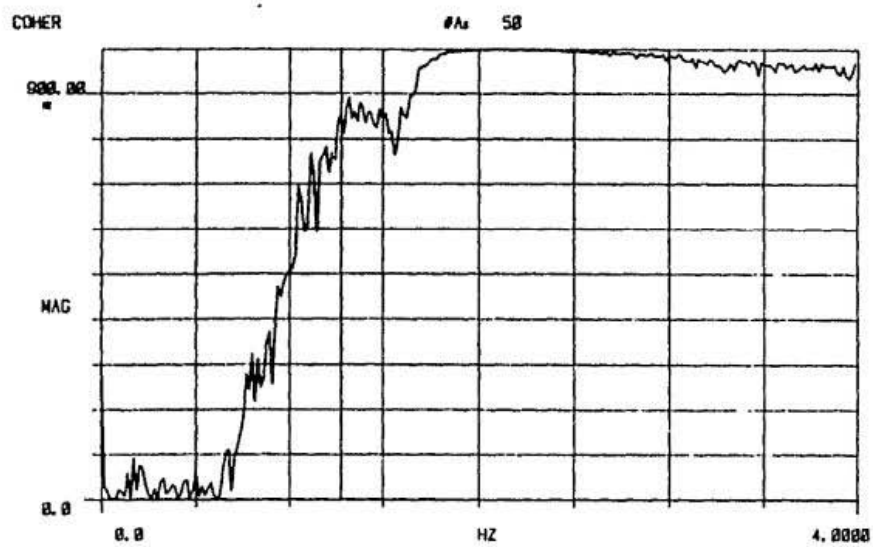

Figure 5.6: The measured coherence function

frequency and the damping ratio of the first bending mode are estimated. For the sake of simplicity a single-degree-of-freedom model is assumed. This is due to the fact that for structures with modes that are well separated, single-degree-of-freedom techniques result in very accurate answers. Secondly, in the damping calculation, a viscous damping model is assumed. It is also assumed that the damping ratio experienced by the structure during vibration is low.

Bandwidth Method

The natural frequency can be determined from the magnitude plot of the measured FRF (Fig. 5.4) where the magnitude is maximum. The damping factor also can be determined from Fig. 5.4 using a half-power point method (Ewins, 1984). By considering a single-degree-of-freedom oscillatory system with viscous damping, the magnitude of the frequency response function is (Clough and Penzien, 1975)

$$|H(f)| = \frac{f_n^2}{[(f_n^2 - f^2)^2 + 4\zeta^2 f_n^2 f^2]^{1/2}} \tag{5.6}$$

in which f_n the natural frequency and ζ the damping ratio. At $f = f_n$ the magnitude of the FRF function is maximum and is given by

$$Q = \frac{1}{2\zeta} \tag{5.7}$$

The frequency bandwidth (δf) of the FRF for a response level of $Q/\sqrt{2}$ is determined. The two corresponding points on either side of f_n are identified as f_1 and f_2 (thus $\delta f = f_1 - f_2$). By definition, f_1 and f_2 are the roots of the equation:

$$\frac{f_n^2}{[(f_n^2 - f^2)^2 + 4\zeta^2 f_n^2 f^2]^{1/2}} = \frac{1}{2\sqrt{2}\zeta} \tag{5.8}$$

Eqn. 5.8 can be expressed in the form

$$f^4 - 2(1 - 2\zeta^2) f_n^2 f^2 + (1 - 8\zeta^2) f_n^4 = 0 \tag{5.9}$$

This is a quadratic equation in f^2, having roots f_1^2 and f_2^2, which satisfy

$$(f^2 - f_1^2)(f^2 - f_2^2) = f^4 - (f_1^2 + f_2^2)f^2 + f_1^2 f_2^2 = 0 \tag{5.10}$$

Consequently,

$$f_1^2 + f_2^2 = 2f_n^2(1 - 2\zeta^2) \text{ and} \tag{5.11}$$

$$f_1^2 f_2^2 = f_n^4(1 - 8\zeta^2) \tag{5.12}$$

It follows that

$$\begin{aligned}(f_1 - f_2)^2 &= f_1^2 + f_2^2 - 2f_1 f_2 \\ &= 2f_n^2(1 - 2\zeta^2) - 2f_n^2\sqrt{(1 - 8\zeta^2)}\end{aligned} \tag{5.13}$$

Eqn. 5.13 can be solved for the damping ratio if the half power points and the natural frequency are precisely located on the FRF curve shown in Fig. 5.4. A good estimate of these points can be done by working with plots of the real part of FRF vs frequency and the imaginary part vs frequency which are shown in Figs. 5.7 and 5.8, respectively. The natural frequency f_n can be estimated as the the frequency at the maximum imaginary part of the measured FRF (see Fig. 5.8). The estimated natural frequency f_n found from this method is again 1.615 Hz. The real part of the FRF, shown in Fig. 5.7, can be used to find the half-power points. The curve has two peaks, one maximum at 1.547 Hz and the second one the minimum at 1.745 Hz. These two points are the best estimates of the half-power points, the f_1 and f_2, respectively (Ewins, 1984).

These three frequency values found from Figs. 5.7 and 5.8 can be substituted into Eqn. 5.13 and the damping ratio ζ can be computed. This can be done by bringing all the terms of the equation to the right-hand side and solving for the zero of the function with ζ as the only unknown variable. A subroutine (M-file) 'fzero' available in MATLAB (1989) was used. The computed damping ratio ζ was equal to 6.08% of critical damping, for the structure oscillating in air.

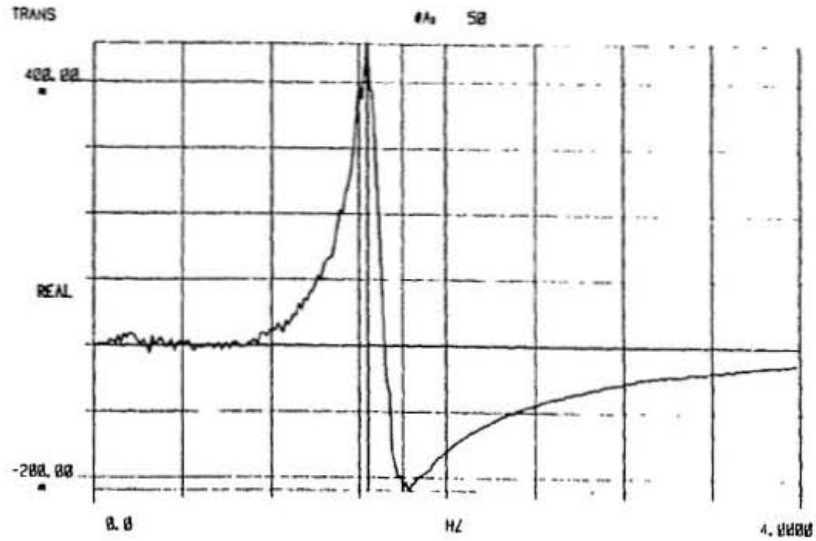

Figure 5.7: Real vs frequency plot of the measured FRF

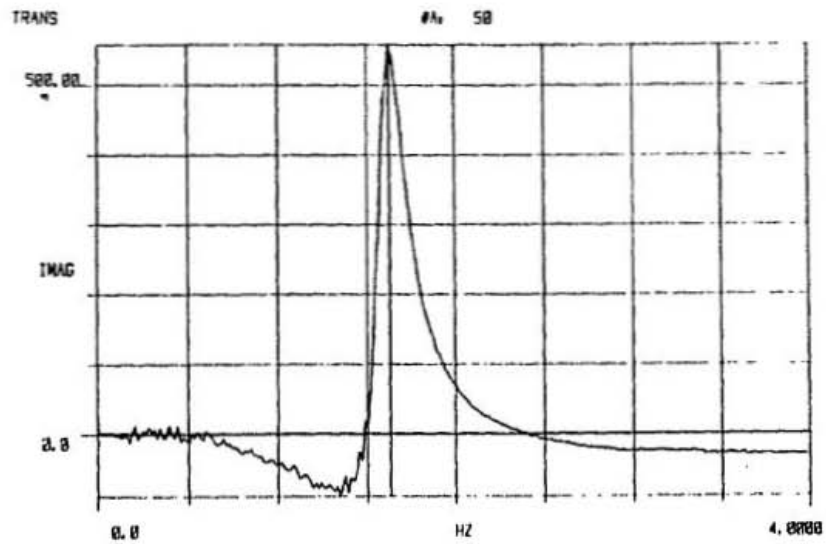

Figure 5.8: Imaginary vs frequency plot of the measured FRF

5.2 Pluck Tests

The natural frequency and the damping ratio were also estimated by using the simplest dynamic test. The pluck test is a common test in which one applies an initial displacement and then allows the structure to oscillate freely. In this case, the deck structure was displaced in the longitudinal direction from its equilibrium position, released and allowed to oscillate freely. The deck acceleration response was digitized in the Keithley System 500 ADC system and the data acquired by software in the desk-top computer. The amplitude decay curves were digitized at a sampling rate of 50 Hz. A digital filter was designed, as was done in the case of wave force experiment (see chapter 3), and the data files smoothed. Fig. 5.9 (dashed line) shows a typical experimental decay curve which was obtained, using this procedure, in air.

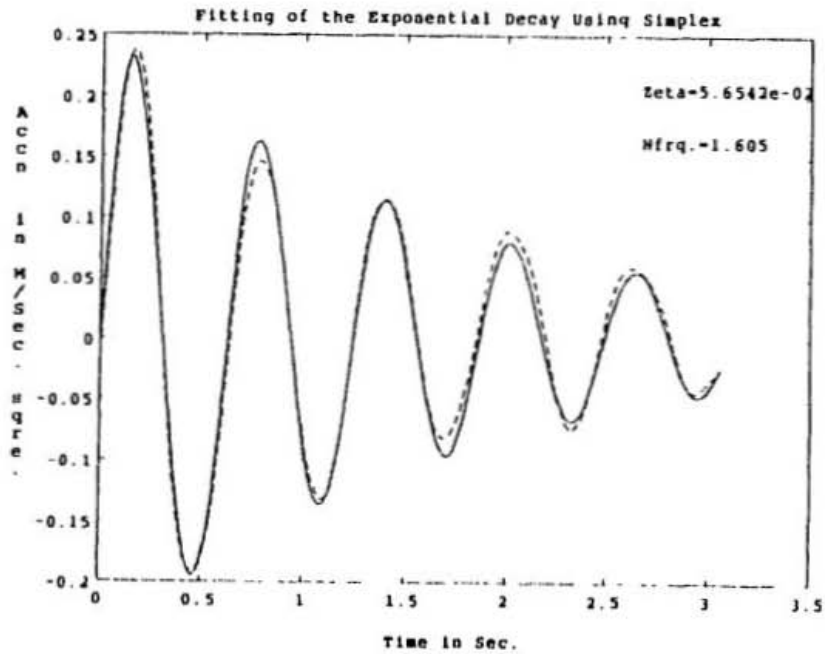

Figure 5.9: Free-vibration response of the structure in the air (note that '- -' for the Measured and '-' for the Fitted data)

Analysis of Decay Curve

The natural frequency f_n and the damping ratio ζ can be computed by analyzing the decay curve shown in Fig. 5.9. The logarithmic decrement method is conventionally used to estimate damping from the measured free decay curve. Otherwise the maximum and or minimum amplitude points are selected and the normal exponential envelope curve is fitted to determine the damping ratio. However in these techniques only a few data points are taken into consideration which result in a poor estimation of the damping ratio. An accurate estimation of the two parameters, natural frequency and the damping ratio, can be found if all the measured data points are utilized and the complete free decay curve is fitted.

Considering the single-degree-of-freedom oscillatory system with same viscous damping model, the time decaying acceleration response curve can be defined as (Clough and Penzien, 1975):

$$r(t) = r_0 exp(-\zeta 2\pi f_n t) sin(2\pi f_d) t \tag{5.14}$$

in which the damped natural frequency

$$f_d = f_n \sqrt{1 - \zeta^2} \tag{5.15}$$

In Eqn. 5.14, if the three unknowns r_0, f_n and ζ are determined, then the equation can be compared with the measured data. (In Eqn. 5.14, r_0 is the response at time $t = 0$.) First a function which is equal to ($r(t)$− Measured Data), can be defined for all the time points. Then the three unknowns can be solved for the minimum value of the function using the Nelder-Mead simplex algorithm. The algorithm is described in detail in Dennis and Woods (1987) and the subroutine (fmins) is given in MATLAB (1989). Excellent curve fitting was obtained by using this method and the natural frequency and the damping ratio were estimated. The solid line in the Fig. 5.9 shows the fitted curve, which is compared with the measured curve (dashed

line). The natural frequency and the damping ratio obtained from this method are 1.605 Hz and 5.65% of critical damping, respectively, in air. Note that they are in good agreement with the estimated values from the modal test.

Maximum Deck Mass Case

The pluck test was also carried out (in air) with maximum deck mass condition. Additional deck mass (101 Kg) was added by fixing the steel plates on top of the deck. Thus the total deck mass in this case was 140 Kg. The pluck test and the above described analysis procedure were repeated. Fig. 5.10 shows the fitting of the measured data by Eqn. 5.14. Again excellent agreement between the measured curve and the curve fitting is obtained. The estimated natural frequency and the damping ratio for this case are 0.77 Hz and 4.65%, respectively, in air.

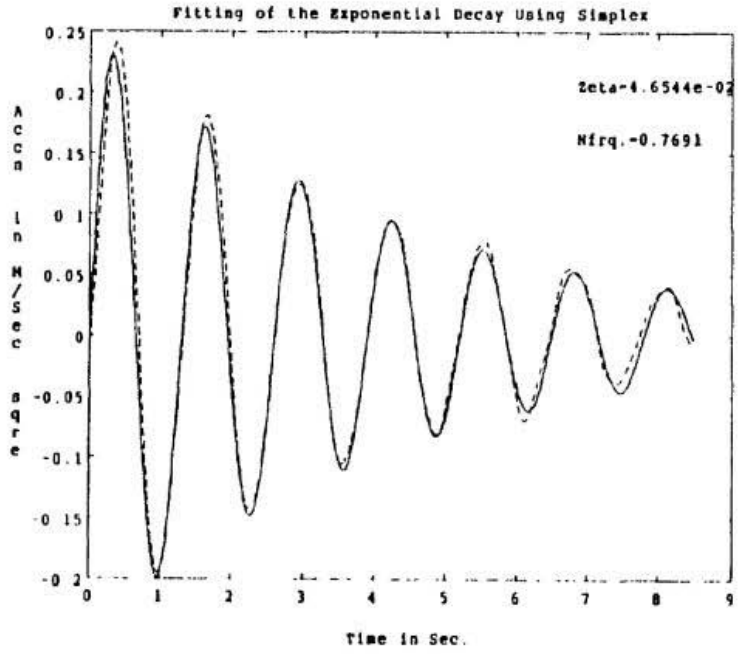

Figure 5.10: Free-vibration response of the structure in the air with additional deck mass (note that '- -' for the Measured and '-' for the Fitted data)

Pluck Test in the Water

After the structure had been installed in the wave tank, pluck tests were again carried out in the same manner as the in-air tests with the maximum deck mass case. A similar curve fitting was carried out and the comparison with the measured free-decay data is shown in Fig. 5.11. The computed natural frequency and the damping ratio are 0.74 Hz and 5.9% of critical damping, respectively. This test was

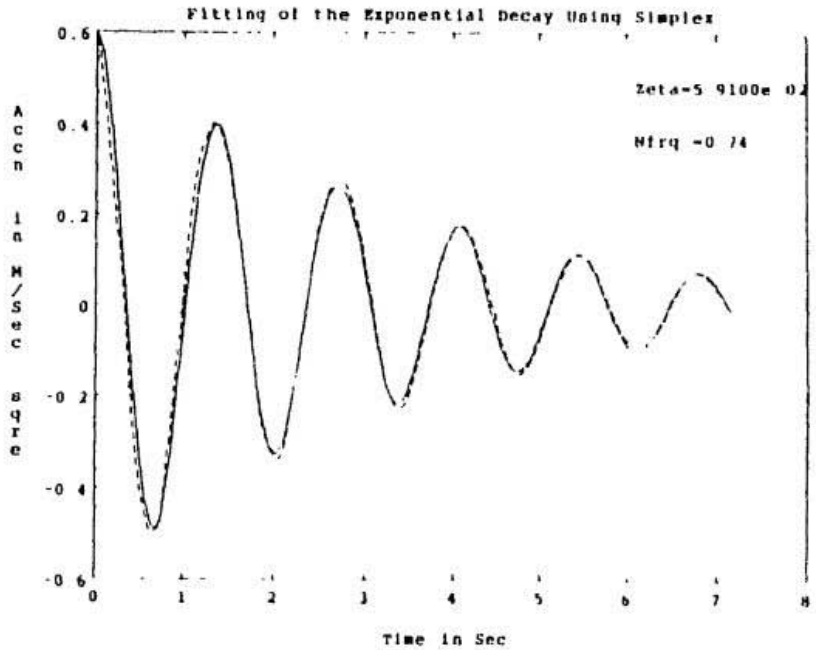

Figure 5.11: Free-vibration response of the structure in the water with additional deck mass (note that '- -' for the Measured and '-' for the Fitted data)

also repeated throughout the course of the experiment to ensure the integrity of the structure (with and without the device). For quick analysis and checking of the decay data, the HP dual channel data analyzer was utilized, and the natural frequency was calculated by obtaining the amplitude spectrum of the recorded data. Since such tests and analysis were carried out only for the purpose of checking the natural frequency of the structure, all the recorded data were not stored in the memory. In all the cases the natural frequency was found to remain almost the same (with a 2%

of error) indicating that the device had not changed the natural frequency of the structure. Due to the limited tank time available, elaborate testing and recording for the purpose of estimating the free-vibration damping of the structure with the device, was not carried out. However, the damping in still water with the device will not be significantly different from the damping of the simple structure in still water.

5.3 Discussion and Summary of the Dynamic Tests

Modal and pluck testing were conducted to experimentally determine the natural frequency and the damping ratio of the model structure. Due to the limited availability of the tank time, the time and effort given for the tests conducted in air were not given to the test conducted in water. However, good estimates of the modal parameters were obtained by carefully selecting the experimental and the analysis procedures. Since the thesis emphasizes the response of the structure near the primary resonance, at its first bending mode frequency, the estimation of parameters for the higher modes was not carried out. A good estimation of modal parameters requires large number of averages in the modal test which is definitely time consuming and also costly. Although the method gives the best estimate for the modal parameters, the estimated parameters obtained from the pluck test are observed to be equally good. The natural frequency obtained from the modal test in air is 1.615 Hz while the pluck test estimated it as 1.605 Hz with an error of 0.62%. Similarly, the damping ratio obtained from the modal testing in air is 6.08% whereas the one obtained from pluck test is 5.65% which shows a 7% error in the estimation. Unless an investigator is interested to obtain the parameters for the higher modes of vibration, modal testing is not highly demanded; the results of the pluck test are quite adequate for the subsequent analysis.

When the deck mass was increased from 39 Kg to 140 Kg, the natural frequency and the damping ratio in air were reduced from 1.605 Hz to 0.7691 Hz; and 5.65% to 4.65%, respectively. This shows that the model structure is very sensitive to the deck mass variation. However, the natural frequency of the structure in water is not very sensitive to the added mass due the surrounding fluid but the damping ratio is very sensitive to the water. This is evident by comparing the tests conducted in the air and water for the same deck mass condition. The natural frequency in the air was 0.77 Hz while in the water it decreased to 0.74 Hz. However, a significant increase in the damping ratio is seen due to the surrounding fluid (from 4.65% to 5.9%).

Lastly one more important comment must be made regarding the damping ratios obtained from these dynamic tests. The damping obtained from these tests is a large value which certainly does not represent the prototype situation. (The damping ratio in the prototype steel structure will be in the order of 2% of critical damping.) This is due to the fact that the acrylic plastic material used for this model fabrication has a larger structural damping than a steel material used for the prototype. The large damping ratio will limit the magnitude of the response in the vicinity of resonance which results in a lesser amplification factor than in the prototype. However this could not be avoided in the model design; but the model natural frequency is in a similitude scale relationship with the prototype. Hence the model structure can properly simulate the resonant condition similar to the prototype situation, but the magnitude of response will not be as severe as in the prototype. The second important question which might arise here is that if the damping ratio is large (6% of critical damping in the water), then does this violate the fundamental assumption made in the beginning that the damping is very small. This question can be answered by evaluating the Eqn. 5.15 and noting the difference between the damped natural frequency and the undamped natural frequency of the structure.

For $\zeta = 6$ %, the ratio of the undamped natural frequency to the damped natural frequency is $f_n/f_d = 1.002$, which can be considered as insignificant. Hence the assumption of small damping ratio is still well applicable to this present problem.

5.4 Finite Element Modelling and Eigenproblem Solution

Although the higher modes of vibration were not identified from the dynamic testing, a finite element model can be developed and used to evaluate the vibration frequencies and mode shapes of the model tower. ANSYS (1987), a general purpose computer program, was employed to model the structure mathematically. The model was prepared using three dimensional beam elements, interconnected at nodes. The mathematical model included the mass and stiffness properties and the submerged effect of the physical model. This was done using the immersed pipe element available in the element library of the ANSYS program. The immersed pipe element is a three dimensional pipe element with six degrees of freedom per node. One of its additional feature is that it takes in to account the effect of the fluid surrounded by the structure while constructing the element mass matrix. A consistent mass matrix was used in the procedure. For the mass matrix, the mass per unit length used for the axial motion is the pipe mass plus the mass of the fluid inside the tubular members. The mass of the fluid inside the members does not contribute to the rotational inertia of the member. The mass per unit length used for motion normal to the pipe is all of the above plus the added mass. (The added mass per unit length is defined as the mass of the fluid displaced by the cross section of the member.)

The deck member was idealized as a rigid unit which reflected the mass properties of the physical model. A pipe element (a three dimensional beam element whose cross section is a circular tube) was used to mathematically model the deck structure.

The three legs and the column supporting points were assumed to be fully fixed. The finite element model had a total of 87 nodes, and over 219 members. The mass density of the acrylic material used for constructing the structure was 1190 kg/m^3; while the modulus of elasticity was 3.0×10^9 N/m^2.

The vibration frequencies and mode shapes were evaluated using the full subspace iteration procedure, where no matrix reduction was done and, therefore no master degrees of freedom need to be defined. The computed vibration frequencies and their identified modes are summarized in Table 5.1. Figs. 5.12 through 5.18 illustrate the analytical mode shapes for the 1st bending mode in the longitudinal direction, the 1st bending mode in the transverse direction, the 1st torsional mode, the 2nd bending mode in the longitudinal direction, the 1st axial mode, the 3rd bending mode in the longitudinal direction, and the 4th bending mode in the longitudinal direction, respectively. It could be noted that in all these modes the deck structure behaved as a rigid frame. Also note that the 1st bending mode frequency in the transverse direction (0.732 Hz) is very close to the one in the longitudinal direction; not only that, but in higher modes they both are almost equal. The first bending mode frequency in the longitudinal direction was 0.73 Hz while the second bending mode frequency in the same direction was 2.784 Hz. So the modes are well separated in the structure. Lastly, the first bending mode frequency in the longitudinal direction, 0.73 Hz, obtained from the analytical model, when compared with the measured frequency in water of 0.74 Hz, shows that it is very close to the measured experimental value.

Table 5.1: Predicted vibration modes and their frequencies

Sl. No	Natural Frequency Hz	Natural Period s	Identified Mode of Vibration
1	0.730	1.370	1st longitudinal bending mode
2	0.732	1.367	1st transverse bending mode
3	2.395	0.418	1st torsional mode
4	2.784	0.360	2nd longitudinal bending mode
5	2.785	0.360	2nd transverse bending mode
6	3.625	0.276	2nd torsional mode
7	3.885	0.257	1st axial mode
8	3.947	0.253	2st axial mode
9	4.053	0.247	3rd longitudinal bending mode
10	4.081	0.245	3rd transverse bending mode
11	4.860	0.206	combined longitudinal bending & torsion
12	4.860	0.206	combined transverse bending & torsion
13	8.126	0.123	4th longitudinal bending mode
14	8.126	0.123	4th transverse bending mode

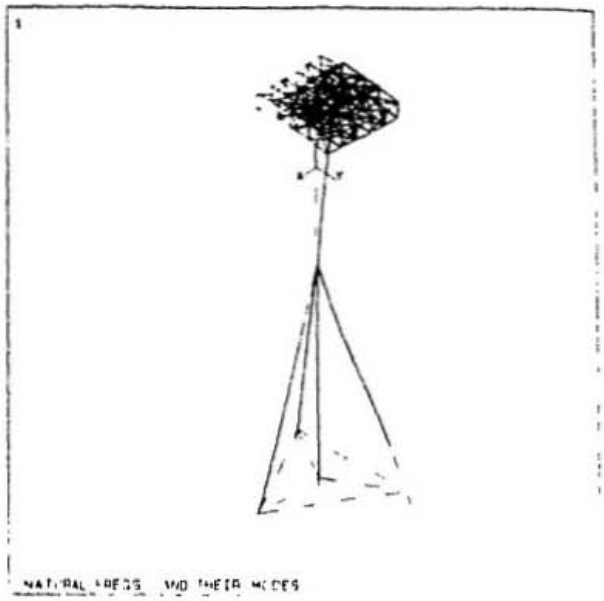

Figure 5.12: Analytical modal displacement for structure in the water: first bending mode oscillation in the longitudinal direction (Natural Frequency = 0.73 Hz)

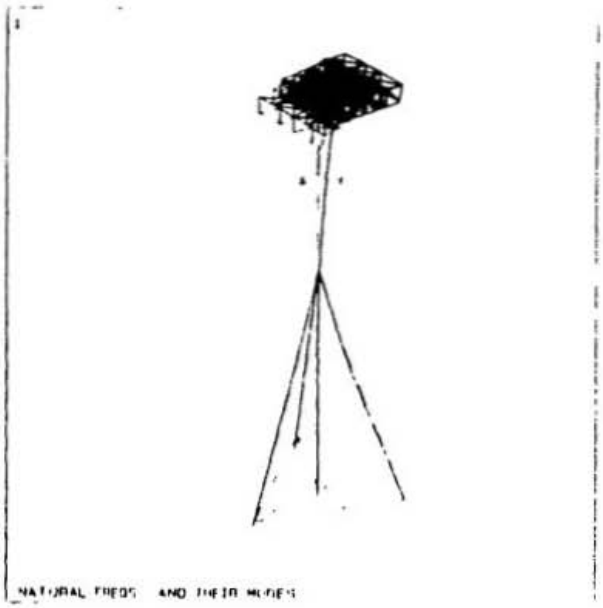

Figure 5.13: Analytical modal displacement for structure in the water: first bending mode oscillation in the transverse direction (Natural Frequency = 0.732 Hz)

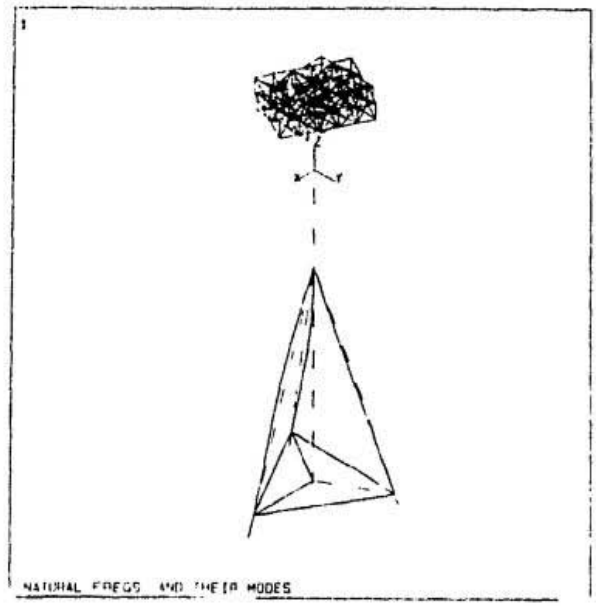

Figure 5.14: Analytical modal displacement for structure in the water: first torsional mode oscillation (Natural Frequency =2.4 Hz)

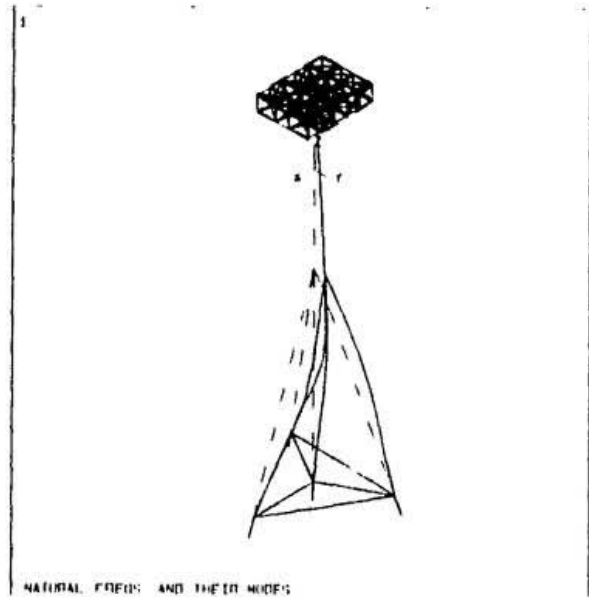

Figure 5.15: Analytical modal displacement for structure in the water: second bending mode oscillation in the longitudinal direction (Natural Frequency = 2.78 Hz)

Figure 5.16: Analytical modal displacement for structure in the water: first axial mode oscillation (Natural Frequency = 3.9 Hz)

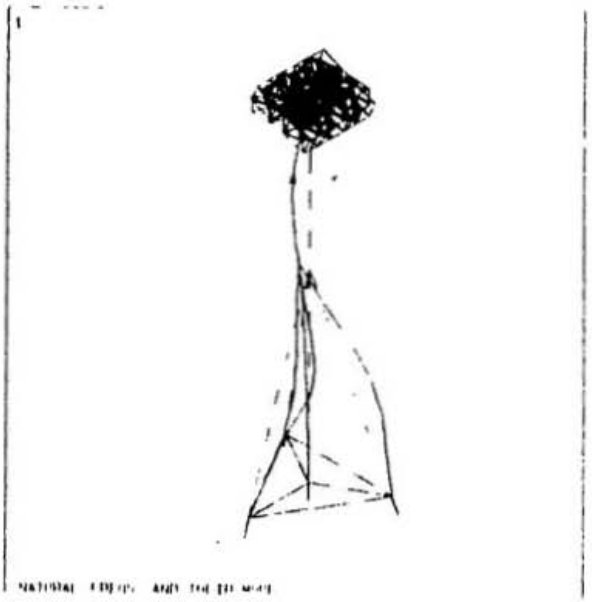

Figure 5.17: Analytical modal displacement for structure in the water: third bending mode oscillation in the longitudinal direction (Natural Frequency = 4.05 Hz)

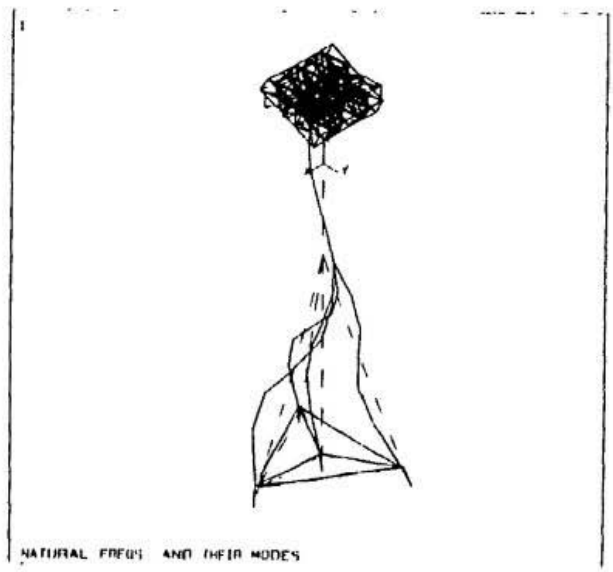

Figure 5.18: Analytical modal displacement for structure in the water: forth bending mode oscillation in the longitudinal direction (Natural Frequency = 8.13 Hz)

Chapter 6

Development of a Theoretical Model for Nonlinear Analysis

The dynamic analysis of any offshore structure is quite complicated since the wave exciting forces are nonlinear in terms of the structural response. The nonlinear forcing function in the governing differential equations may be considered by two different approaches, viz., the time domain and the frequency domain procedures. The main advantage of the time domain approach is the possibility of taking into account any kind of nonlinearity present in the mathematical model.

The frequency domain analysis generally requires a technique, to linearize the nonlinear forces, while determining the responses. However, such approximate techniques applied in the analytical model are not acceptable while seeking a solution at frequencies of oscillation near the region of resonant response. Particularly when the structural velocity response is large and comparable to the water particle velocity, it is very essential that the fluid-structure interaction effects be included in the theoretical model without making any equivalent linearization. As pointed out in the introduction chapter, it is one of the objectives of the thesis to investigate the effect of induced drag damping on the resonant response of the candidate structure. In order to include this effect accurately in the theoretical model, the time domain procedure will be used.

One of the advantages of the time domain method is that the theoretical results can be compared directly with the experimental measurements; as well, inferences can also be made in the frequency domain by obtaining the power spectral densities of the time domain results. The above considerations led to the development of a time domain approach for this specific problem.

The present chapter describes the theoretical model which was used to predict the dynamic response of the model structure to wave exciting forces. The computer program developed to solve the nonlinear differential equations is discussed. Of particular interest in the development of the mathematical model is the inclusion of the induced drag damping in the response analysis. Also the program must be capable of predicting the structural response in the time-domain for a given random wave elevation time series.

6.1 Modelling of Fluid-Structure Interaction

The mathematical model used here is the one developed by Morison et al. (1950) for the calculation of the force acting on a vertical cylinder, subjected to a sinusoidal wave, and modified later on for use on vibrating structures by Malhotra and Penzien (1970). When a rigid cylinder is free to move in waves the forces are written in terms of relative motion between the cylinder and the fluid particle. This model has been used extensively in the literature to evaluate the dynamic response of fixed offshore structures. Nevertheless, it is instructive to outline briefly the inherent drag damping included in the numerical model through a nonlinear fluid-structure coupling term.

For the sake of simplicity, let us first consider an inclined cylinder moving in an oscillatory flow as shown in Fig. 6.1. The hydrodynamic load intensity vector, the force per unit length, f(t), for the cylindrical member may be obtained by generalizing Morison's formula as (neglecting the tangential forces acting on the

cylinder):

$$f(t) = C_{ms} A_I \dot{u}_N - C_{as} A_I \ddot{x}_N + C_{ds} A_D |u_N - \dot{x}_N|(u_N - \dot{x}_N) \qquad (6.1)$$

in which

u_N = fluid velocity vector normal to the member axis

$\dot{u}_N$ = fluid acceleration vector normal to the member axis

$\dot{x}_N$ = member velocity vector normal to its axis

$\ddot{x}_N$ = member acceleration vector normal to its axis

C_{ms} = inertia coefficient for the section of the member

C_{as} = added mass coefficient for the section of the member

C_{ds} = drag coefficient for the section of the member

$A_I = \rho \frac{\pi}{4} D^2$

$A_D = \frac{1}{2} \rho D$

D = diameter of the member

ρ = mass density of water

The first term on the right-hand side of Eqn. 6.1 represents the wave inertia force on the cylinder and the second term represents the inertia force due to the added mass of the fluid based on acceleration of the cylinder. The third term is drag force which is quadratic in the relative velocity between the cylinder and the flow, with the direction of the force being that of the relative velocity. The fluid particle velocity and acceleration components u_N and $\dot{u}_N$, can be computed either through Airy's linear wave theory or by using a higher order Stokes' wave theory. For all practical purposes, C_{as} is assumed to be equal to 1. (The values of the coefficients C_{ms}, C_{as} and C_{ds} are generally determined from wave force measuring experiments.)

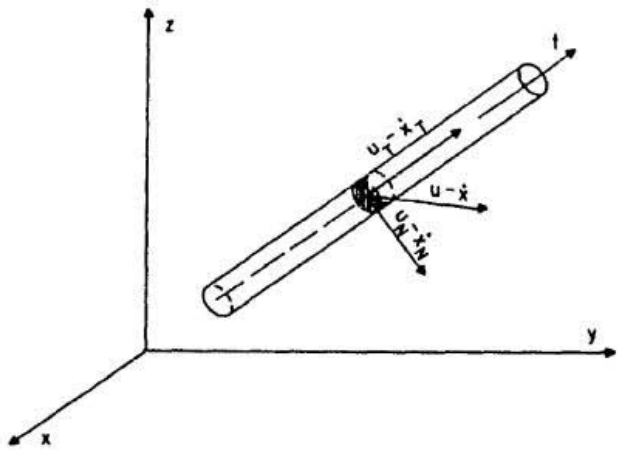

Figure 6.1: A moving cylinder in the oscillatory fluid

In case of the vertical cylinder, the horizontal fluid particle velocity and the acceleration vectors are normal to the cylinder axis and the suffix 'N' used for the velocity and acceleration of the fluid and cylinder can be removed from Eqn. 6.1 and rewritten as:

$$f(t) = C_{ms}A_I\dot{u} - C_{as}A_I\ddot{x} + C_{ds}A_D|u - \dot{x}|(u - \dot{x}) \tag{6.2}$$

In Eqn. 6.2, for convenience, the terms corresponding to the inertia coefficient and added mass coefficient have been separated. However, the coupling between the fluid and structure shown in the third term cannot be separated. When the velocity and acceleration of the moving cylinder are of the same order of magnitude as the particle velocity and acceleration, the fluid-structure interactions defined in Eqn. 6.2 must not be ignored. The motion of the structure relative to the fluid results in a damping effect which can be explained further by splitting the third term of Eqn.

6.2 in the following manner:

$$|u - \dot{x}|(u - \dot{x}) = |u - \dot{x}|u - |u - \dot{x}|\dot{x} \tag{6.3}$$

The first term on the right-hand side of Eqn. 6.3 can be treated as the forcing term, which may be set to $|u|u$. However when the cylinder velocity is comparable to the fluid particle velocity the above simplification introduces error in the forcing term. The second term on the right-hand side of Eqn. 6.3 can be treated as the fluid damping term. Taking $|u - \dot{x}|\dot{x} = |u|\dot{x}$ introduces a large error in the estimation of fluid damping when the cylinder motion is comparable to the fluid particle motions. At and close to resonance these simplifications significantly affect the response of the structure. Hence the nonlinearity in the third term of the Eqn. 6.2 must be retained in its original form.

The model defined in Eqn. 6.2 requires only two coefficients (assuming $C_{as} = 1$) and also has included the effect of fluid-structure interaction. However the procedure used for the choice of the values of the hydrodynamic coefficients, required for this model, has not been clearly defined in the literature. In order to find the appropriate values of the C_{ms} and C_{ds}, for the relative velocity model, wave force measurements for a cylinder oscillating in the fluid have to be carried out. Secondly, the fluid particle velocity and acceleration terms, in Eqn. 6.2, should also relate to the instantaneous position of the cylinder.

The last two considerations are very important to define the analytical model completely for the relative velocity formulation. However, incorporation of such complex analytical modelling is beyond the scope of this thesis. Hence the current model assumes that the hydrodynamic coefficients obtained from the fixed cylinder (given in chapter 3) are valid for the relative velocity model shown in Eqn. 6.2. For all practical purposes the fluid particle kinematics will be calculated at the equilibrium position of the structure not at the instantaneous position of the structure. (However the relative velocity formulation and the nonlinearity due to the square term in the

drag component of loading, defined in the right-hand side of Eqn. 6.2, will be retained in the analytical model developed for this study.)

The third term in Eqn. 6.2, representing the drag force, is nonlinear in terms of the cylinder motions. In order to apply spectral methods, the drag term is often modified with an equivalent linearized term. Since the procedure outlined in this chapter uses the time domain approach (which can accommodate the drag-term nonlinearity as it is) the discussions available on the linearization procedure are omitted here.

6.2 Modelling the Dynamic System

The fluid-structure interaction model discussed in the previous section can be applied to a fixed offshore structure and the dynamic analysis performed by assuming the structure to be a lumped mass system. The method assumes a discretized structure whose masses are lumped at its nodal points. The hydrodynamic load vectors are assumed to be concentrated at the nodes. Following Clough and Penzien (1975), the dynamic equations of motion for the discretized system can be written in a matrix form as:

$$[M]\{\ddot{x}\} + [C]\{\dot{x}\} + [K]\{x\} = \{F\} \tag{6.4}$$

in which

$[M]$ = mass matrix of the structure

$[C]$ = structural damping matrix

$[K]$ = structural stiffness matrix

$\{F\}$ = the nodal force vector

$\{x\}$ = the structural displacement vector

$\{\dot{x}\}$ = the structural velocity vector

$\{\ddot{x}\}$ = the structural acceleration vector

A finite element model can be developed and the spatial matrices defined for solving the above system of equations. However the degree of complexity which needs to be incorporated in the finite element model is based on the objectives of the theoretical study. Hence, before proceeding to the computer program development part, the main objectives required for this study are made clear herein. This will assist us in simplifying the analysis procedure and also in saving computer time. It should be pointed out here that such computer time savings are very essential while considering a time domain solution for a structure with a large number of nodes.

The main objectives of the program development required for this study are listed as follows:

1. The load vector should include the effect of fluid-structure interaction.

2. The mathematical model should adequately represent the inertial, stiffness and damping properties of the physical model.

3. Only the deck responses (displacement, velocity, acceleration) in the direction of waves need to be stored for comparison with the measured deck responses. (It is assumed that the wave loads exert no transverse forces on the structure.)

4. In the case of random waves, the program should have an option to find the responses for the measured wave elevations so that the computed random responses can be compared with the measured random responses.

5. The solution technique should follow a step-by-step numerical integration procedure and should include the effect of the nonlinear drag term without applying any linearization procedure.

6.2.1 Development of the Stiffness Matrix

The candidate structure was described as a space frame model with a list of nodes and their coordinates, a list of member incidences and a list of member properties.

The finite element model used a three-dimensional beam element to formulate the global stiffness matrix from the element stiffness matrix. The beam element has six degrees of freedom for each node, three translations and three rotations (the positive direction follows a right-hand screw rule). In the current finite element model, the details of the deck structure were ignored and it was considered as a lumped mass on top of the tower structure. The resulting model had a total of 38 joints with 45 member connectivities. The vertical distance between the nodes varied from 12.7 cm to 27.0 cm. At places close to the free surface, below the water level, smaller spacings were used so that the spatial variation of the wave forces can adequately be represented in the dynamic model. The structure was fixed at four points on the base. Hence, there were a total number of 204 active degrees of freedom in the structure. The schematic view of the finite element model developed for this study is shown in Fig. 6.2.

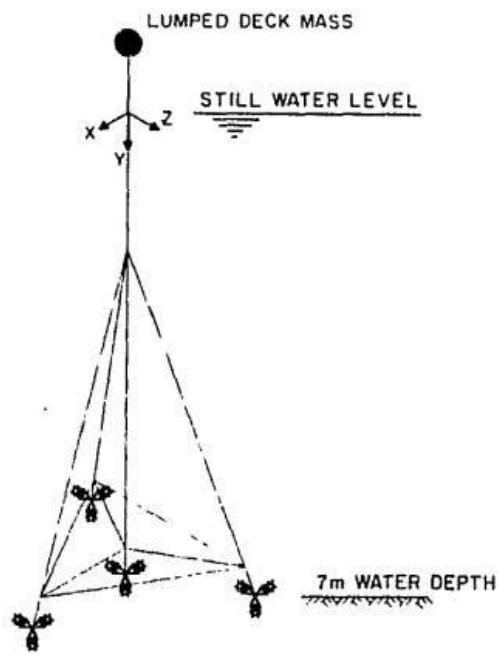

Figure 6.2: The finite element model of the structure

Unless the objective of the analysis is to evaluate the stresses in the structure,

a more refined model with the inclusion of all the 204 degrees of freedom is not essential for the present analysis. In fact, the inertial properties of the structure can be effectively modelled with fewer degrees of freedom. This is due the fact that, the inertial properties depend directly on the acceleration response of the structure and not all the degrees of freedom contribute actively to the inertial property of the structure. Hence it is seldom our interest to determine the displacements for all the 204 degrees of freedom.

Since the present model ignores the transverse forces on the structure and considers only the in-line wave forces, the displacements of the theoretical structure take place mainly in the plane of wave motion. However, it is in the interest of this study to keep the effect of the stiffness properties of the complete space structure in the theoretical model.

In order to include the effect of the stiffness properties of the complete model (shown in Fig. 6.2) and at the same time consider only the translational degrees of freedom along the wave direction, the reduced flexibility method defined in Clough and Penzien (1975) was used. The method eliminates the nonessential degrees of freedom from the dynamic model. In fact the static condensation procedure can also be applied for the same purpose. However (according to Clough and Penzien, 1975) the static condensation method is not an efficient procedure while dealing with a large structure. Hence the reduced flexibility matrix method was selected for the present purpose.

In this method, the structure is modelled as a space frame using 3-dimensional beam elements and by considering all the six degrees of freedom at each node. The desired degrees of freedom for the dynamic analysis are selected from the complete model. Then the reduced flexibility matrix is constructed by applying unit loads successively, corresponding to each of the essential degrees of freedom, and evaluating the displacements produced in each essential degree of freedom by each load.

The set of displacements for each loading condition is evaluated by a detailed static analysis *which includes the effects of all the degrees of freedom on the selected degree of freedom.* Consequently, the obtained results are almost representative of the complete structural stiffness property in a reduced form. Thus the results of a dynamic response analysis are not affected by the reduced degrees of freedom. Using this procedure the reduced flexibility matrix was assembled for the translational degrees of freedom. Once the reduced flexibility matrix was formed, the reduced stiffness matrix [K] was obtained by inverting the reduced flexibility matrix. The developed three-dimensional finite element model, shown in Fig. 6.2, was used to evaluate the reduced stiffness matrix.

6.2.2 Description of the Load Vector

The hydrodynamic load vectors were assumed to be concentrated at the nodes. The fluid-structure interaction model, defined in Eqn. 6.2, can be used in the place of the load vector $\{F\}$ of Eqn. 6.4.

In defining the concentrated load vectors, which basically act in the direction of the waves, it is convenient to apply the principle of projected area method (see Dawson, 1983). The method lumps the projected areas of the members and, the corresponding member volumes at the nodes of the finite element model. The horizontal wave forces can be calculated for these assumed concentrated bodies at the nodes. The advantage of this method is that the force matrix for the structure can be computed directly. The error involved in this method can be minimized by choosing the nodes adequately close to one other.

Let $A1$, $A2$, etc., be the concentrated joint areas and $B1$, $B2$, etc., the corresponding concentrated (or lumped) joint volumes. These concentrated areas and volumes are obtained for each node by summing the contributions of the members contained in the nodal tributary zone (the region halfway above and below each

node). These areas and volumes are calculated by considering the actual outside diameters of the members and their projected lengths normal to the direction of wave propagation. The computations are required only for the members beneath the still water level.

Based on Eqn. 6.2 and with the lumped description of areas and volumes, the wave force F_i acting on the ith joint for the global structure can be defined as:

$$F_i = \rho C_m(Bi)\dot{u}_i - \rho C_a(Bi)\ddot{x}_i + \frac{1}{2}\rho C_d(Ai)|u_i - \dot{x}_i|(u_i - \dot{x}_i) \qquad (6.5)$$

in which the $\dot{u}_i$ and u_i denote the horizontal water particle acceleration and velocity at joint i, respectively; $\ddot{x}_i$ and $\dot{x}_i$ denote the horizontal component of the joint velocity and acceleration response, respectively; and C_m, C_a and C_d are the inertia, added mass and the drag coefficients for member 'i', respectively.

The second term on the right-hand side of Eqn. 6.5, which accounts for the added mass, can be denoted as M_{a_i}, the added mass at joint i. The added mass M_{a_i}[1] may be computed as the equivalent mass of the water replaced by the volume of structure at joint i and can be taken to the left-hand side of Eqn. 6.4 and then added to the mass of the structure $[M]$.

Equation 6.4 and 6.5 may be combined with the foregoing treatment and the equation of motion can be written as:

$$[M_T]\{\ddot{x}\} + [C]\{\dot{x}\} + [K]\{x\} = [K_M]\{\dot{u}\} + [K_D]\{|u - \dot{x}|(u - \dot{x})\} \qquad (6.6)$$

in which

$$[M_T] = [\mathrm{M}]+[M_A]$$

$$[M_A] = \rho C_a[B] \text{ (the added mass matrix)}$$

$$[K_M] = \rho C_m[B]$$

[1]Note that it is customary in the offshore industry to compute the added mass in this form for the analysis and design of offshore structures

$$[K_D] = \frac{1}{2}\rho C_d[A]$$

$[B]$ = diagonal matrix indicating volume displaced by the structure

$[A]$ = diagonal matrix indicating area projected in the direction of the flow

While considering the waves of small amplitudes with periods, close to the natural period of the structure (1.35 s), not all the members below the water level are subjected to the wave forces. The wave lengths for the waves generated in the experimental program of this thesis were seldom greater than 3.2 m, whereas the water depth was set at 7m. Hence the submerged zone below one half of the wave length can be considered free from the wave forces. However the deeply submerged members in the silent zone contribute to the stiffness and the mass properties of the structure. In the candidate structure the inclined members are well below 2 m from the free surface. Hence the total wave forces act predominantly on the center vertical column of the structure above the major node and the forces on the inclined legs are negligibly small. Under this condition the projected area method considered in Eqn. 6.6 gives the same result as the normal component velocity method defined in Eq. 6.1. Hence the model developed for the dynamic analysis in Eqn. 6.6 has adequately defined the experimental conditions under which the structure was tested in the wave tank.

6.2.3 Development of the Mass Matrix

The mass matrix $[M]$ was modelled by taking the mass of each member and distributing it as lumped masses at the element nodes. The mass matrix included the physical mass of the structure, additional masses (like the added deck mass) and the mass of the water contained within the hollow members.

For example, considering the mass at the deck location, the deck structural mass of 37.4 kg (based on the actual weighing of the deck), the additional deck mass of 101.3 kg (which takes into consideration the deck appurtenances) and the mass of half the element length of the center column, connecting it to the deck, were added together and lumped at the top joint.

The lumped mass formulation gives a diagonal mass matrix having masses only at the translational degrees of freedom of each node. Because of the concentration of the masses at the nodal points, the terms corresponding to the rotational mass degrees of freedom automatically become zero.

The total lumped mass matrix $[M_T]$ was obtained as a sum of the structural mass matrix, $[M]$ and the hydrodynamic added mass matrix $[M_A]$.

6.2.4 Development of the Damping Matrix

In the present mathematical formulation, the damping matrix $[C]$ needs to quantify the structural damping together with the hydrodynamic damping. As mentioned earlier, the hydrodynamic damping has two physical sources: (i) the generation of surface waves radiating energy to infinity; and (ii) the drag effect. The modelling aspect of the drag damping has been discussed in detail in section 6.1.

The radiation damping is essentially associated with the presence of a free fluid surface and is linearly proportional to the local structural velocity. This process is present even in the case of an ideal fluid. It is commonly modelled as a 'viscous damping' which may be convenient to keep in the $[C]$ matrix of the Eqn. 6.6. The radiation damping experienced by fixed deepwater structures are relatively small compared to the case of floating structures.

Computation of the Radiation Damping

It is simpler and also adequate to compute the coefficient of the radiation damping by using the reciprocity relations developed by Newman (1962). The principle of reciprocity states that the wave radiation damping and the wave excitation forces are not independent quantities. The knowledge of one of them helps to evaluate the second one.

As a matter of fact, many researchers have used this principle to evaluate the radiation damping for fixed offshore structures. For brevity, the method defined in Vandiver (1980), was followed and the radiation damping ratio for the candidate structure was evaluated.

The modal wave radiation damping $B_{nn}(\omega)$ for incident waves of frequency ω, propagating in direction θ, may be expressed based on the Haskind/Newman relationship as:

$$B_{nn}(\omega) = \frac{\omega^3}{4\pi\rho g^3} \int_0^{2\pi} \frac{|F_n(\omega,\theta)|^2}{|A_n(\omega,\theta)|^2} d\theta \tag{6.7}$$

in which

$F_n(\omega,\theta)$ = modal wave exciting force for the nth mode.

$B_{nn}(\omega)$ = radiation damping coefficient for the nth mode of the structure.

$A_n(\omega,\theta)$ = amplitude of the wave approaching the structure at an angle θ.

g = acceleration due to gravity

ρ = fluid density

For the purpose of handling this term a transfer function can be defined as:

$$R_n(\omega,\theta) = \frac{F_n(\omega,\theta)}{A_n(\omega,\theta)} \tag{6.8}$$

where $R_n(\omega,\theta)$ is a measure of the nth modal force per unit wave amplitude. Its dependency on the incident angle can be removed by considering a mean square

value of R computed for the ov. rall angles of incidence.

$$< |R|^2 >_\theta = \frac{1}{2\pi} \int_0^{2\pi} \frac{|F_n(\omega, \theta)|^2}{|A_n(\omega, \theta)|^2} d\theta \tag{6.9}$$

Considering a directional sea and assuming that the modes of oscillation which are of interest are in-line with the direction of wave propagation, some simplifications in the evaluation of the damping coefficient can be made.

For such a special case the dependency of θ in Eqn. 6.9 may be dropped and $< |R|^2 >_\theta$ term may be replaced by $|R|^2$. Without loss laws of generality, Eqn. 6.8 may be extended for a spectral approach as:

$$S_{nf}(\omega) = S_\eta(\omega) |R(\omega)|^2 \tag{6.10}$$

where $S_{nf}(\omega)$ is the spectrum of a modal wave force, $S_\eta(\omega)$ is the spectrum of wave elevation.

From Eqn. 6.7 and Eqn. 6.9 it can be seen that:

$$B_n(\omega) = \frac{\omega^3}{4\pi\rho g^2} |R(\omega)|^2 \tag{6.11}$$

where the $B_n(\omega)$ is the coefficient of the radiation damping for the n th mode in case of the unidirectional sea.

Substitution of Eqn. 6.10 into Eqn. 6.11 results in:

$$B_n(\omega) = \frac{\omega^3}{4\pi\rho g^3} \frac{S_{nf}(\omega)}{S_\eta(\omega)} \tag{6.12}$$

Knowing the wave elevation spectrum $S_\eta(\omega)$ and then by computing the modal force spectrum for the 'n'th mode $S_{nf}(\omega)$, the radiation damping coefficient can be evaluated, using Eqn. 6.12, as a function of 'ω'. Since the in-line wave forces on the structure are dominated by the inertial forces, the drag force component can be neglected in the computation of $S_{nf}(\omega)$ for a given $S_\eta(\omega)$.

Modal Wave Force Spectral Matrix $[S_f(\omega)]$

The present objective is to calculate the spectral density function of the inertial component of the in-line wave forces on the structure having 'n' degrees of freedom.

The diagonal elements of the excitation spectral matrix of size n x n, associated with the inertial forces on each node, may be defined by extending the Morison formula using the methods of stochastic analysis:

$$S_F(\omega)_{ii} = \rho^2 C_m^2 (B_i)^2 S_{\dot{u}}(\omega)_i \tag{6.13}$$

where $S_{\dot{u}}(\omega)_i$ is the spectrum of horizontal fluid particle acceleration at node 'i' and B_i, the lumped joint volume defined at node i.

The non-diagonal elements of the excitation spectral matrix can also be defined as:

$$S_F(\omega)_{ij} = \rho^2 C_m^2 (B_i)(B_j) \sqrt{S_{\dot{u}}(\omega)_i \, S_{\dot{u}}(\omega)_j} \tag{6.14}$$

From linear wave theory the spectrum of fluid particle acceleration can be defined in terms of the spectrum of wave elevation:

$$S_{\dot{u}}(\omega)_i = \omega^4 (e^{-ky_i})^2 S_\eta(\omega) \tag{6.15}$$

in which y_i defines the vertical coordinate of the ith node located with the direction vector positive downward from the free surface. Assuming deepwater , the wave number 'k' is defined as:

$$k = \omega^2/g \tag{6.16}$$

Substituting Eqn. 6.15 into 6.13 and 6.14:

$$S_F(\omega)_{ii} = \rho^2 C_m^2 \omega^4 (e^{-ky_i} B_i)^2 S_\eta(\omega)_i \tag{6.17}$$

$$S_F(\omega)_{ij} = \rho^2 C_m^2 \omega^4 (e^{-k(y_i+y_j)} B_i \, B_j) S_\eta(\omega)_i \tag{6.18}$$

From Eqn. 6.17 and 6.18 the excitation spectral matrix $[S_F(\omega)]$ can be formed. Once this is done, then the modal wave force spectral matrix associated with the

generalized forces for each mode can be obtained as:

$$[S_f(\omega)] = [\Phi]\,[S_F(\omega)]\,[\Phi]^T \tag{6.19}$$

$[S_F(\omega)]$ is an n x n excitation matrix whose non-diagonal elements represent the cross-spectral density functions between the two modes. The term $[\Phi]$ used in Eqn. 6.19 is the n x n modal matrix which may be obtained by solving the linearized, homogeneous, and coupled equation of the motion, which will be defined later.

Since the effect of modal coupling are not relevant for this study, only the diagonal elements of the $[S_f(\omega)]$ will be considered. For an example, the first diagonal element of $[S_f(\omega)]$ corresponds to the nodal forces associated with the first fundamental mode of the structure. Using Eqn. 6.10, 6.11 and 6.18, the radiation damping coefficient can be evaluated as a function of frequency. Since we are interested only in the response of the structure in the primary resonant region, the radiation damping coefficient $B_n(\Omega)$ for the first natural frequency of the structure (Ω) was computed for the first three modes of the structure in the wave direction. Note that the radiation damping matrix constructed by $B_n(\Omega)$ is diagonal and is in the generalized coordinate form. The radiation damping matrix in the physical coordinate form can be obtained from the following transformation:

$$[C_{rad}] = [\Phi][B(\Omega)][\Phi]^T \tag{6.20}$$

Structural Damping Matrix

The precise form of the structural damping matrix is very difficult to quantify as in the case of the wave radiation damping. For the sake of simplicity, a commonly adopted approach in the offshore industry is followed here. The approach assumes that the damping matrix is proportional to the total mass $[M_T]$ or the structural

stiffness [K] or a linear combination of these two, i.e.:

$$[C_{str}] = \alpha[M_T] + \beta[K] \tag{6.21}$$

where α and β are factors to be evaluated. The above proportional damping formulation, called Raleigh damping, assures that the modal damping matrix is diagonal.

The structural damping, in the form of a percentage of the critical damping coefficient has already been obtained from the pluck test results conducted in air[2] (see chapter 5).

The approach whereby we express the structural damping coefficient as a percentage of the critical damping coefficient is based on the one-degree-of-freedom model. In other words a critical damping cannot be defined for a general N-degree-of-freedom system. But the fundamental mode of vibration may be assumed as the relevant one for reference to a one degree of freedom system. It is preferable to have different damping ratios for each independent mode of interest which needs to be included in the analysis. This may be achieved by a detailed modal testing and analysis technique. However due to the limitations of time, instrument, cost and so many other factors, such an experiment was not carried out. Moreover, the main interest of this thesis is only on the resonant vibration of the structure at its first fundamental natural frequency. Under this condition it can be assumed that the structural damping associated with the higher modes of vibration are less significant for the present model development. Thus the damping ratio corresponding to the first fundamental mode (obtained from pluck test) is used here.

Assuming $\beta = 0$ and $\alpha = 2\Omega\zeta$, the $[C_{str}]$ can be computed from Eqn. 6.21. Then the global damping matrix [C] of Eqn. 6.5 can be obtained by,

$$[C] = [C_{str}]_{air} + [C_{rod}] \tag{6.22}$$

[2]Note that the damping coefficient has to be corrected for the extra added mass of the wetted portion of structure in water. Also see Sec. 6.4 for discussion.

6.3 The Solution Technique

Several numerical methods are available to solve the formulated matrix equation defined in Eqn. 6.6. These methods are broadly classified as: (1) explicit methods and (2) implicit methods. In an explicit formulation, the response quantities are expressed in terms of previously determined values of displacement, velocity and acceleration. In an implicit formulation, the temporal difference equations are combined with the equations of motion, and displacements are calculated directly by solving these equations.

Some of the commonly used implicit methods, like the Newmark and Wilson-θ method, assume a constant or linear acceleration over an increment of time. The numerical damping involved in the implicit procedure may be diminished by selecting a very small time interval for the integration. However, it was felt that it would be more appropriate to use an explicit method for solving this problem. A most efficient and very accurate method was developed using the IMSL (1985) subroutines combined a with variable time-step algorithm.

For the sake of discussion, the Eqn. 6.6 is rewritten here:

$$[M_T]\{\ddot{x}\} + [C]\{\dot{x}\} + [K]\{x\} = [K_M]\{\dot{u}\} + [K_D]\{|u - \dot{x}|(u - \dot{x})\} \qquad (6.23)$$

It should be pointed out here that the nonlinearity in Eqn. 6.23 is only in the forcing term which would not affect the mass and stiffness properties of the structure, at any time step, in the step-by-step integration process. Under these conditions, the homogeneous equation on the left-hand side can be decoupled and only the first few important modes of vibration need be considered for the time step integration. Then a general normal mode superposition technique can be used to compute the response of the structure. However, at each time step, the response of the structure in the physical coordinate system must be computed and the response-dependent forcing term, on the right-hand side, has to be updated before proceeding to the next

time step. By following this procedure, the time and effort involved in solving the problem are drastically reduced. Note that, at the same time, the nonlinearity in the forcing term is also well maintained and not at all affected by this procedure. This method is applicable for lightly damped dynamic systems. However the accuracy of this method is not affected by the exclusion of the higher modes of vibration. This is due the fact that the modes higher than the first three modes of vibration are very difficult to excite by the wave forces.

In a normal mode solution the response of the structure is written as:

$$\{x\} = [\Phi]\{q\} \tag{6.24}$$

in which the modal matrix $[\Phi]$ is obtained from the solution of homogeneous undamped equation

$$[M_T]\{-\Omega^2 x\} + [K]\{x\} = 0 \tag{6.25}$$

in which Ω is the natural frequency of the structure.

Multiplying Eqn. 6.23 by the transpose of modal matrix, $[\Phi]^T$, the governing differential equation can be expressed in terms of the generalized coordinate $\{q\}$

$$[m]\{\ddot{q}\} + [c]\{\dot{q}\} + [k]\{q\} = [F_M]\{\dot{u}\} + [F_D]\{|u - [\Phi]\{\dot{q}\}|(u - [\Phi]\{\dot{q}\})\} \tag{6.26}$$

in which

$$\begin{aligned} [\mathrm{m}] &= [\Phi]^T[M_T][\Phi] \text{ is the generalized mass matrix} \\ [\mathrm{c}] &= [\Phi]^T[C][\Phi] \text{ is the generalized damping matrix} \\ [\mathrm{k}] &= [\Phi]^T[K][\Phi] \text{ is the generalized stiffness matrix} \end{aligned}$$

$[F_M] = [\Phi]^T[K_M]$ and $[F_D] = [\Phi]^T[K_D]$ are the coefficient matrices of the generalized fluid forces.

While solving for the generalized coordinate displacements q, the second order governing differential equation, Eqn. 6.26, defined in the normal coordinates, can

be reduced to a set of two first order equations. Then the system of first order differential equations, for the selected number of modes, can be solved explicitly using a predictor-corrector method. An IMSL (1985) subroutine 'DGEAR' which solves the system of first order differential equations was used. DGEAR is a stable predictor-corrector method with the least local error of the order '(h^6)' where h is the step size. To minimize the error the algorithm has been written for variable time step integration which allows the investigator to have his data stored in the time step of his convenience.

In order to include the nonlinearity in the forcing term the following procedure is applied at each time step of integration.

1. At time t the structural response, in the modal coordinates $(q, \dot{q} and \ddot{q})$, obtained from DGEAR was stored.

2. The response in the physical coordinates $(x, \dot{x} and \ddot{x})$ at time t was computed using Eqn. 6.24.

3. The computed structural velocity, at each submerged node, was then subtracted from the fluid particle velocity 'u' at time 't', and then the drag force matrix defined on the right-hand side of Eqn. 6.23 was evaluated.

4. The drag and inertial forces were transformed to the modal coordinates as defined in Eqn. 6.26.

5. Then Eqn. 6.26 was reduced to a system of first order differential equations, and solved by DGEAR

6. The above procedure was repeated till the results obtained from the successive iterations were identical.

7. Then the analysis was moved to the next integration time step $(t + \delta t)$ where δt is the time interval for the data storage.

In the above procedure the forcing function was up-dated with the current known structural response. The only difficulty with this method is that at each time step the transformation of the response from generalized coordinate to physical coordinate and vice versa has to be done. However a considerable saving in computer time was achieved by this method which enabled the author to compare a large number of experimental data with the theoretical predictions.

6.3.1 Particle Kinematics for the Measured Random Wave Elevations

Comparison of the theoretical response of the structure with the experimentally measured random wave response, in the time domain, is not a straightforward procedure as in the case of the regular waves. The procedure involves the computation of the particle kinematics for the measured wave elevations. Note that the generally followed Monte Carlo simulation technique from the wave spectrum cannot be used here. Based on linear wave theory a digital filter was designed; the wave elevations were passed through the filter and the particle kinematics was obtained for each water depth. The procedure used to design the linear filter is outlined below.

In a linear wave theory, the wave elevation spectrum, $S_\eta(\omega)$, and the particle velocity spectrum, $S_u(\omega)$, are related by:

$$S_u(\omega) = \omega^2 \, r(y)^2 \, S_\eta(\omega) \tag{6.27}$$

where r defines the variation with respect to depth 'y' (assuming deepwater) as:

$$r(y) = e^{-ky} \tag{6.28}$$

in which the k and ω are related by Eqn. 6.16. Since 'k' is a function of 'ω', r(y) is more properly written as $r(y, \omega)$ and in this form $r(y, \omega)$ can be interpreted as a frequency response function.

The impulse response function for the frequency response function, defined in Eqn. 6.28, may be written as:

$$h(t,y) = 2\int_{-\infty}^{\infty} \omega(e^{-ky})cos(\omega t)df \tag{6.29}$$

in which the df is the frequency increment and $\omega = 2\pi f$.

Once the impulse response functions at different depths are obtained, the particle velocity can be computed as:

$$u(t,y) = \int_{-\infty}^{\infty} h(\tau,y)\eta(t-\tau)d\tau \tag{6.30}$$

However in practice the integrations are performed by summation over finite increment in frequency 'df' as defined below:

$$h(jdt,y) = 2\sum_{i=1}^{N} \omega_i e^{-y\omega_i^2/g} cos(\omega_i\ jd\tau)df \tag{6.31}$$

$$u(kdt,y) = \delta\tau \sum_{j=-M}^{M} h(j\delta\tau,y)\eta(k\delta t - j\delta\tau) \tag{6.32}$$

The value of sampling interval used in the random wave response measurement was assigned here for $dt = \delta t = 0.03s$. The number of frequency points used was N = 128 and the frequency resolution chosen was df = 0.0163 Hz. The filter length was optimized to M = 100.

First the impulse response function, h, for each water depth of the structure was obtained using Eqn. 6.31. Then the measured wave elevation, η, was input to Eqn. 6.32 and the horizontal fluid particle velocity 'u' (in time series form) was obtained. Numerical differentiation of the particle velocity time series, with respect to dt, will give the particle acceleration time series $\dot{u}(kdt,y)$ at each depth 'y'. The depths 'y' at which the functions $u(kdt,y)$ and $\dot{u}(kdt,y)$ are evaluated correspond to the locations of the nodes of the structure.

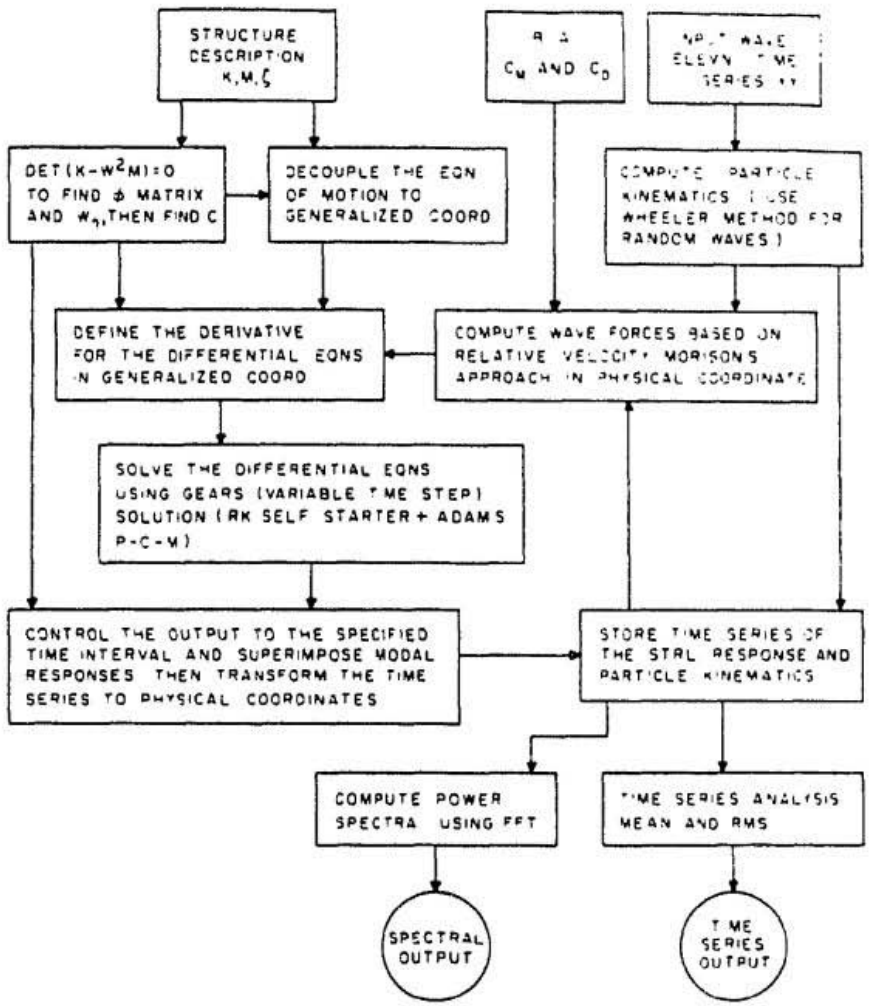

Figure 6.3: Flow-chart for the nonlinear time-domain analysis

6.3.2 Computer Implementation

A computer program was developed to numerically solve the nonlinear differential equation (6.23). The general flow of the computer program is shown in Fig. 6.3. The program consists of five major modules named as (1) INPUT, (2) LOAD, (3) MAIN, (4) DAMP and (5) EQN.

INPUT Module

The INPUT module has three subroutines called INPUT1, INPUT2 and INPUT3. The reduced flexibility matrix (SK) obtained from a set of static analyses, together with the lumped mass matrix (BM), are input to INPUT1. Other than these, INPUT1 also reads the vertical coordinate (YY) and the values of the lumped area and volume for each node. The still water level is selected as the origin for YY and its positive direction points towards the sea bed.

The hydrodynamic coefficients are input to the program interactively through INPUT2 and the analysis can be performed for different sets of C_m and C_d values for the same wave condition. INPUT3 reads the experimentally measured wave elevations.

LOAD Module

In this module the particle kinematics is computed for the measured wave elevations by the subroutine IRREG which uses the linear filter, defined in the previous subsection. However other options are also provided to find the particle velocity and acceleration time histories for the given wave parameters. In the case of regular waves, STOKES finds the particle kinematics using fifth order wave theory and in the case of random waves, the subroutine RAND simulates the particle kinematics, using the FFT.

The MAIN and DAMP Module

A part of the MAIN module computes the eigenvectors and eigenvalues for the structure using the reduced flexibility matrix and lumped mass matrix. The DAMP module first evaluates the radiation damping coefficient for the natural frequency of the structure. The global damping matrix is constructed by adding the radiation damping matrix to the structural damping matrix.

The EQN Module

This module forms the system of differential equations in modal coordinates. Subroutine DERY incorporates the fluid-structure interaction and defines the derivatives of the system of differential equations. These equations are solved by the IMSL subroutine DGEAR. The normal mode superposition technique is used to compute the structural response. The response, in the physical coordinate system, is stored in the computer.

General Comments

The analysis includes only the first three modes of oscillation of the structure in the direction of propagation of the waves. The program utilizes the subroutines available in the IMSL library and rest of the subroutines are provided with the main program. Certain input parameters like wave parameters and the hydrodynamic coefficients can be input to the program interactively. If required, the analysis can be repeated for another set of hydrodynamic coefficients with the same wave conditions. A random wave simulation program, using random number generation, provided in the program, allows one to conduct theoretical studies much like an experimental investigation.

6.4 Discussion on the Theoretical Results

The fundamental natural frequencies for the first three bending modes in the direction of waves for the space frame model obtained are 0.730 Hz, 2.784 Hz. and 4.053 Hz, respectively. The corresponding frequencies obtained from the reduced flexibility model are 0.728 Hz., 3.011 Hz. and 4.155 Hz, respectively. The first and the third mode frequencies of the reduced flexibility model agree well with the space frame results. Since our interest is on the response near the first natural frequency of the structure, the small discrepancy seen in the second mode will not affect the results of the reduced model. Moreover, the generated laboratory waves hardly have any energy to excite the structure at 3.0 Hz, the second fundamental mode frequency.

As stated before, the structural damping was incorporated in the Raleigh form, the damping ratio of 4.65% of the critical damping obtained from the free-decay test in the air, was used in the analysis. The values of the computed radiation damping ratio for the first three modes are 0.288%, 0.1312% and 0.0839% of critical damping, respectively. Note that, the obtained radiation damping is very small.

The impulse response functions for different water depths (0.0 m, 0.585 m, 1.041 m, 1.499 m and 1.956 m) computed by IRREG are shown in Fig. 6.4. These depths are arbitrarily selected for the purpose of illustration. However, it can be seen that the magnitude of the impulse response function rapidly decreases with the water depth and becomes insignificant for depth equal to 1.955 m. Hence it can be shown that the particle kinematics, and consequently the wave forces below 1.955 m will be negligibly small for the structure while considering waves of small amplitudes.

The validation of the reduced flexibility model was verified by comparing its result with the complete three dimensional model. Since the purpose of this comparison is to check the error involved in reducing the degrees of freedom, only a linear analysis was considered by keeping $C_m = 2.0$ and $C_d = 0.0$. The comparison

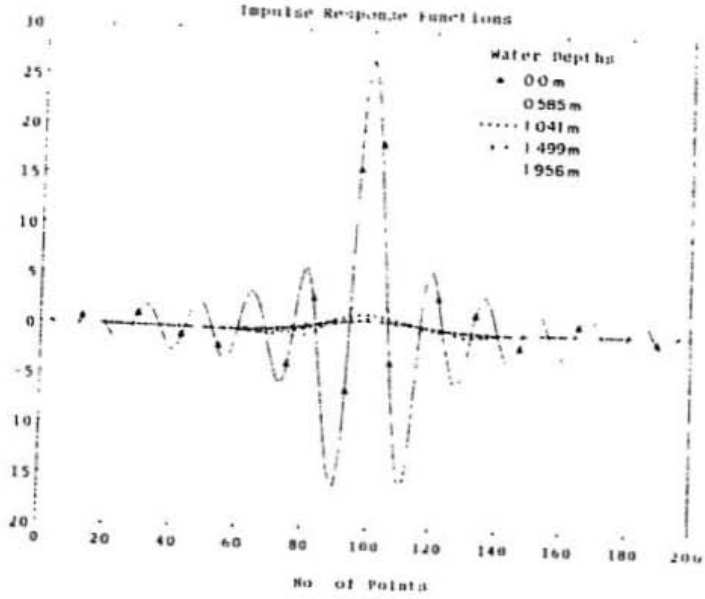

Figure 6.4: Impulse response functions for different water depths

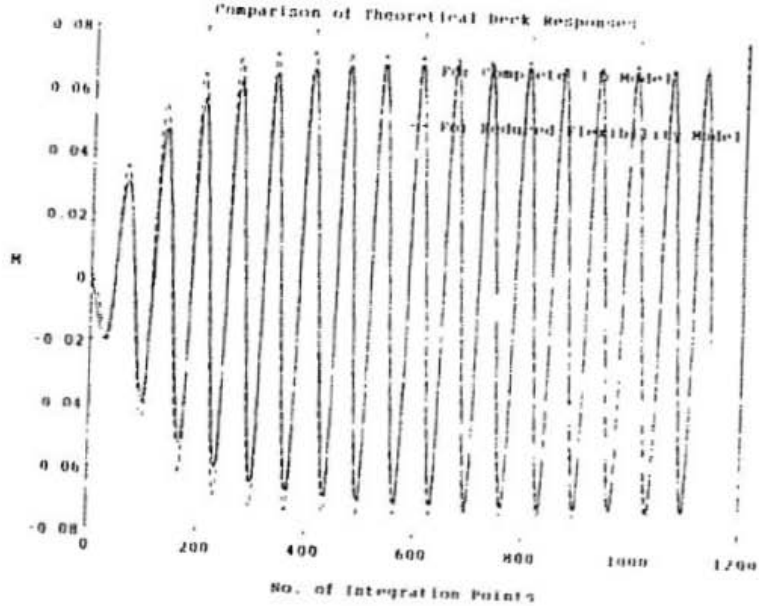

Figure 6.5. Comparison of the deck displacements: reduced flexibility model vs three-dimensional model

is shown in Fig. 6.5. The solid line shows the deck response for the three-dimensional model whereas the dashed line shows the results of the reduced model. The magnitude of the reduced flexibility model at steady state response is 2% greater than the complete model. However incredible computer time and memory were saved by using the reduced flexibility model. For example, the reduced flexibility model typically took 23 s of CPU time and 1000 blocks for storing data to integrate 2048 time points; the three-dimensional model took 36 minutes of CPU time and 27, 000 blocks to do the same length of analysis.

Before concluding this chapter, it would be appropriate to study the typical behaviour of the structure using the developed program. Random waves were simulated for three different sets of wave parameters. The JONSWAP spectrum was used and the peak frequency was varied as: 0.73 Hz, 0.54 Hz and 1.0 Hz. Note that the peak frequency for the first case is close to the resonant frequency (0.728 Hz), for the second case it is smaller than the resonant frequency and for the third case it is higher than the resonant frequency. The significant wave height H_s selected was 0.1016 m and the gamma value used was 3.0, in all three cases. The C_m and C_d values assumed are 2.0 and 1.0 respectively. These are arbitrary values selected for the purpose of this analysis. The numerical analysis began with the simulation of wave elevation in the Monte-Carlo sense. Fig. 6.6a shows the simulated wave elevation for the first set of wave parameters. The subsequent figures, Figs. 6.6b and 6.6c, show the corresponding particle velocity and acceleration time histories. The deck displacement time series, obtained from the above time-domain analysis, is shown in Fig. 6.6d.

Although the time domain analysis is important to the thesis, interpreting the results (for random waves) will be much easier if one transforms the response to the frequency domain. Hence the deck displacement spectrum of the computed time response was obtained using FFT technique. In Fig. 6.7 the power spectral

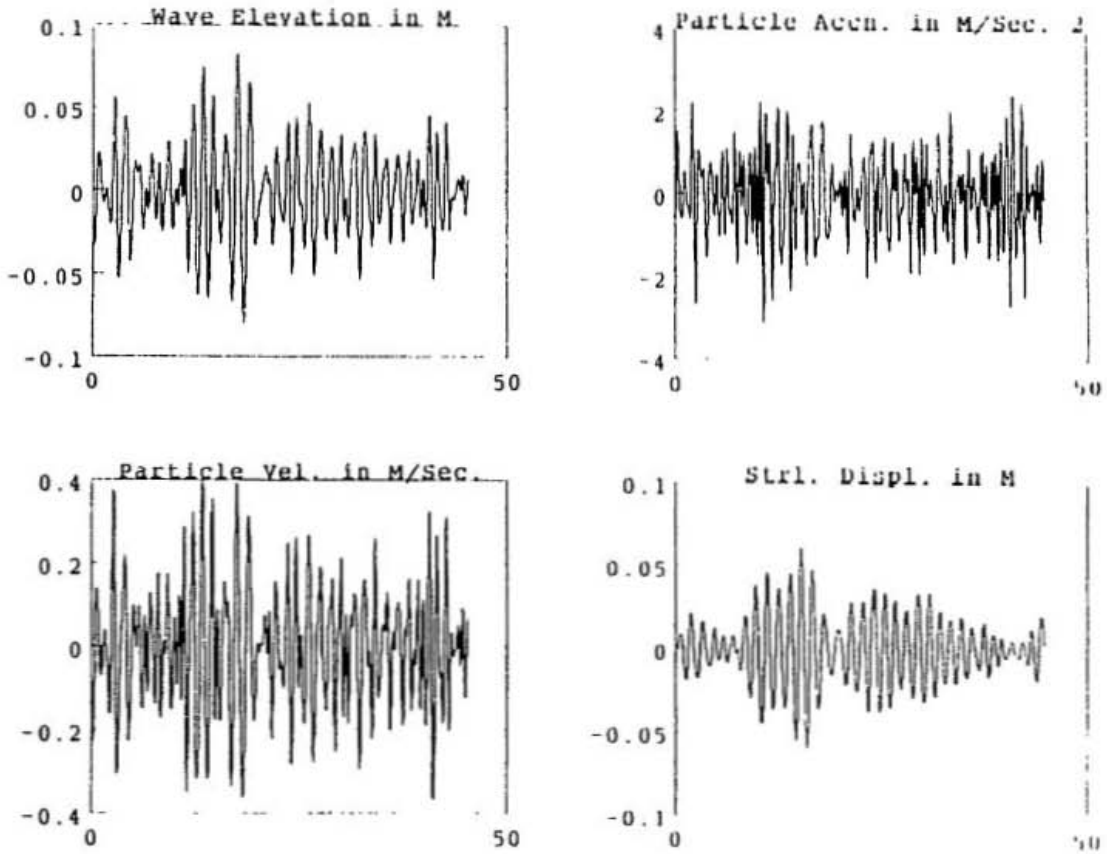

Figure 6.6: A typical result of the nonlinear analysis for simulated waves

densities of the deck displacements are shown. The dashed lines show the wave spectra and the solid lines show the response spectra. In Fig. 6.7a, where the wave peak frequency coincides with the structural natural frequency (0.728 Hz), a large single peak response is observed. In Fig. 6.7b two peaks in the response spectrum are seen; while one corresponds to the wave peak frequency the second one corresponds to the resonant frequency. However the amplitude of the spectral component at the wave peak frequency is 12% of that in Case 1, Fig. 6.7a. In the third case also, Fig. 6.7c, where the wave peak frequency is much higher than the natural frequency, the magnitudes of the spectral component at the wave peak frequency is 3% of that in case 1. However, the response in this case is a broad band spectrum.

For the overall behaviour, it is observed that the structural responses above 1.5 Hz are negligibly small and modes above this frequency are difficult to excite by the waves. This is because the stiffness is higher in the higher modes. Hence the first three modes used in the analysis are adequate for the response calculations. It is also observed that at resonance the magnitude of response is quite large and at excitations away from resonance the response is very small. In Fig. 5.11(d), the deck displacement spectra obtained for these three cases are compared separately. For the same significant wave height, the responses differ significantly with respect to the wave exciting frequencies.

It is once again emphasized here that the radiation damping in the structure (0.288% of critical) is negligibly small compared to the structural damping in air (4.65% of critical). In the case of the prototype situation, the structural damping also will be small. It can be shown that the structural damping obtained from the still water test (5.9% of critical) also includes the radiation damping. In that case 5.9% of critical damping can be used, directly, for the analysis. By this way, correcting the 4.65% of critical damping for the added mass of the wetted structure and the calculation of radiation damping can be avoided.

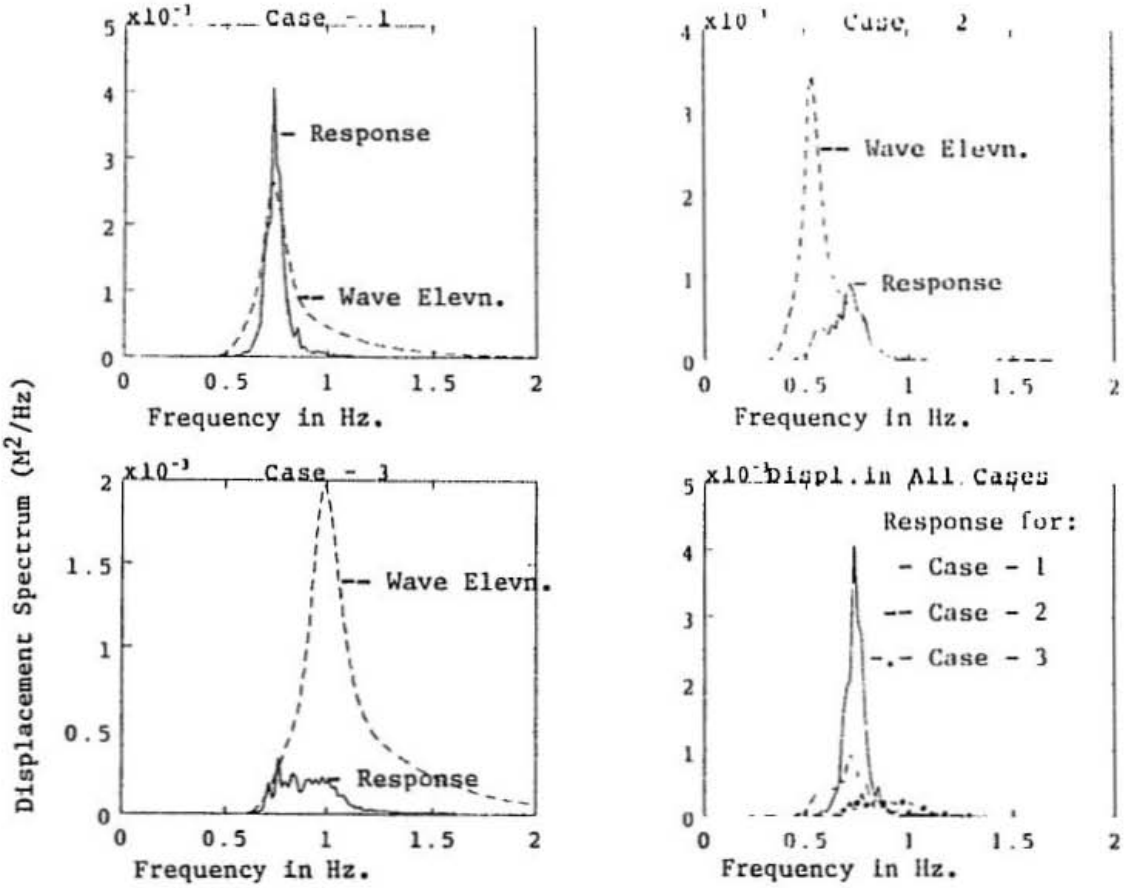

Figure 6.7: Comparisons of response spectrum with its corresponding wave spectrum

Chapter 7

The Near Resonant Response of the Model Structure to Regular and Random Wave Excitations

The dynamic analysis of a fixed deepwater structure is particularly important for waves of moderate height since they make the largest contribution to fatigue damage. The dynamic amplification of response is greatest when the sea state dominant frequency coincides with a structural natural frequency, and the response is predominantly under the control of the damping experienced by the structure. For this reason a detailed investigation of the response of the structure to waves, at and near resonance, has become an important aspect in the design of fixed deepwater platforms. The response near primary resonance is very sensitive to the input parameters of the structural properties.

Considerable amount of literature is available on the various methods used to solve the dynamic equations, and on the sophisticated mathematical models developed to describe the sea state and the fluid-structure interaction phenomenon. However, a detailed hydroelastic model study on the resonant response of a fixed deepwater structure, to laboratory generated waves, is rarely found in the literature. Hence one of the main objectives of this thesis is to examine how a physical structure behaves at resonance, to wave loading, and how precisely the response can be

predicted by the analytical approach.

This chapter consists of four parts: (i) The experimental set-up used for the wave response study; (ii) The analytical and experimental results for regular waves; (iii) Similar results and discussion for the case of random waves; and finally (iv) The summary of important findings obtained in this chapter.

7.1 Experimental Set-up

The hydroelastic behaviour of the tripod tower platform model to regular and random waves was investigated in the Clear Water Towing Tank (CWTT) situated in the Institute for Marine Dynamics (IMD), National Research Council Canada (NRCC), St. John's, Newfoundland Canada. The 200 m long, 12 m wide and 7 m deep tank has two main features, namely, its sophisticated towing carriage and a dual flap wave maker. The wave maker is hydraulically driven, and can generate regular and random waves. Regular waves, up to one metre in height, can be generated and wave lengths can vary between 0.5 m and 40 m. Random (irregular) waves can be generated with characteristic wave height of up to 0.7 m. The upper limit on waveboard frequency is about 1.8 Hz. The wave maker can be driven directly by analog control or by computer. The other end of the tank has a sloping parabolic slatted beach to prevent wave reflections. The schematic plan of the tank is shown in Fig. 7.1. (The photograph of the tank has already been shown in Fig. 4.11.) The experiments were performed at the middle of the tank, 100 m from the beach and 100 m from the wave maker. The towing carriage has a large opening at its center and it also carries a control room. The control room contains a computer and other sophisticated equipment systems that are required for acquisition, recording and analyzing of the measured data. As mentioned elsewhere in the thesis, the model was anchored to the bottom of the tank and positioned such that it extended through the carriage opening. All the data channels from the installed transducers were con-

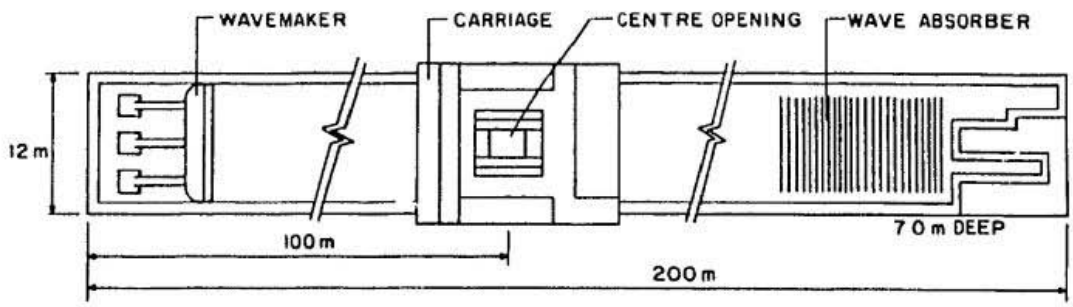

Figure 7.1: Plan of IMD deepwater wave/towing tank

nected to the data acquisition system. The measurement system monitored sensor for wave elevation and deck accelerations. Four capacitance-type wave probes were placed in the water in the CWTT. The first wave probe was placed 2.5 m upstream from the model, along the CWTT centreline and the second one was placed 2.5 m downstream on the CWTT centreline. The third and fourth wave probes were placed on both sides, port and starboard, of the model in line with the transverse centreline of the main column at a distance 2.3 m. The recorded data from the first two probes were used to judge the effect of any wave reflection from the beach on the measured wave elevation at the test location. Only the data recorded from the third probe, placed on the port side of the model, was used for all reference and analysis purposes. The fourth probe, placed on the starboard side of the model, served to check any cross tank oscillation during the recording of experimental measurements.

The deck acceleration data were acquired through three accelerometers fixed on the top surface of the model deck. The purpose of these three accelerometers was to measure the deck responses in the direction of the waves (longitudinal acceleration), in the direction perpendicular to the waves (transverse acceleration) and to assess the torsional oscillations in the structure. The first accelerometer was located at the

center of the deck facing the wave direction. The second one was 0.7 m from the center of the deck, on the port side of the platform, facing the opposite direction. The response measured from the first and the second accelerometers can be used to detect the the torsional oscillations in the structure. The third accelerometer, placed at the center of the deck facing the direction perpendicular to the wave action, was used to measure the transverse response of the structure.

The four wave probes and the three accelerometers were calibrated prior to the start of the experiments. The data acquisition software ACQUIRE, developed for the purpose of IMD tests, was used for this experiment. The equipment used for this experiment is listed as follows:

1. One 8 MB memory DEC MICRO VAX II computer (VAX/VMS system);
2. One NEFF system 620-100 with 64 channels of pre-amplifier, a single MUX and single 15-bit ADC;
3. One NEFF series 300 signal conditioner;
4. Programmable gain amplifier - can be controlled by software on a channel-by-channel basis with gains of 1, 2, 4, 8, 16 and 32;
5. Individual gain modules with gains of 1, 10, 100, or 1000 (hardware);
6. Individual anti-aliasing lowpass filter modules (hardware, 2 pole) 1, 10, 100, or 1000 Hz cutoff (-3db) frequencies;
7. One VT330 terminal and a LA75 dot matrix printer.

The data from all the seven channels were passed through individual analog filter modules (anti-aliasing) and the noise in the system, above 10 Hz, was filtered out of the analog voltages. Then the channels of analog input data were digitized using the 15 bit ADC. The acquisition software was used to sample the data through this

device. Preliminary data analysis and plotting of these data were performed on the Micro VAX. The data were then transferred to the main VAX/VMS computer system via the Ethernet network and then copied on to magnetic tape for permanent storage and subsequent analysis. The test programs were classified as: tests for regular waves and tests for random waves. In the case of the regular wave tests, a 50 Hz sampling rate was used but for the random waves the data were sampled at 33 Hz. Between each test run, sufficient time intervals were given for the tank to settle back to a calm condition.

7.2 Structural Response to Regular Waves

Regular waves of moderate amplitudes and periods, close to the first fundamental natural frequency of the structure, were generated in the wave tank and the deck response was measured. The wave height was varied from 0.071 to 0.159 m and the wave period was varied between 1.25 to 1.54 s. Fig. 7.2 shows a typical wave elevation and the corresponding deck acceleration response (longitudinal) for wave conditions, height H = 0.144 m and period T = 1.333 s. In the prototype situation these values correspond to H_p = 7.2 m and T_p = 9.42 s, respectively (note that the suffix 'p' indicates prototype). The wave period is very close to the fundamental natural period of the model (1.35 s). Fig. 7.2 shows that the response is at steady state, for the generated regular waves. The height and the period of the waves are uniform. Hence the recorded data must be free from the wave reflection effect of the beach. It can be noted that the phase angle between the deck acceleration response and the measured wave elevation time series is almost close to 90 degrees. This primarily indicates that the wave forces on the structure are inertia dominated. At resonance, it is seen from Fig. 7.2, that the magnitude of structural motions (accelerations) is very large and the response is under steady state, indicating a constant dissipation of energy through damping.

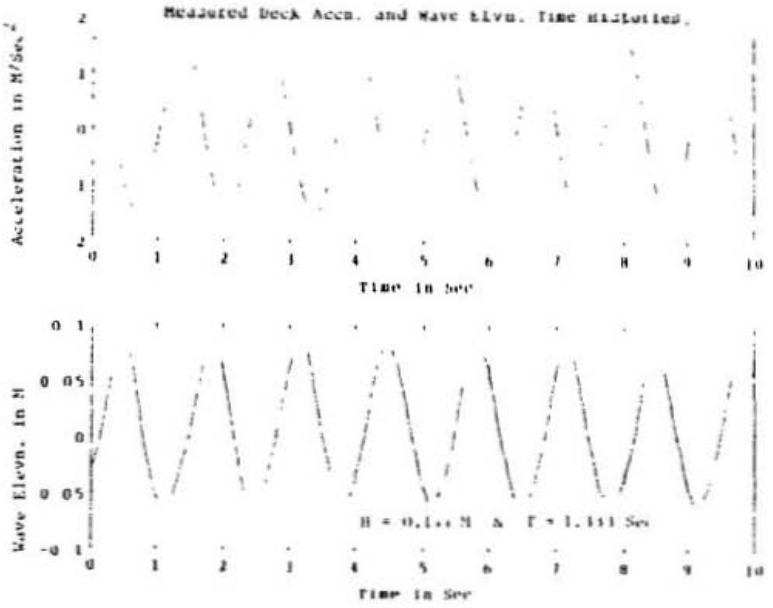

Figure 7.2: Measured wave elevation and longitudinal deck acceleration time series

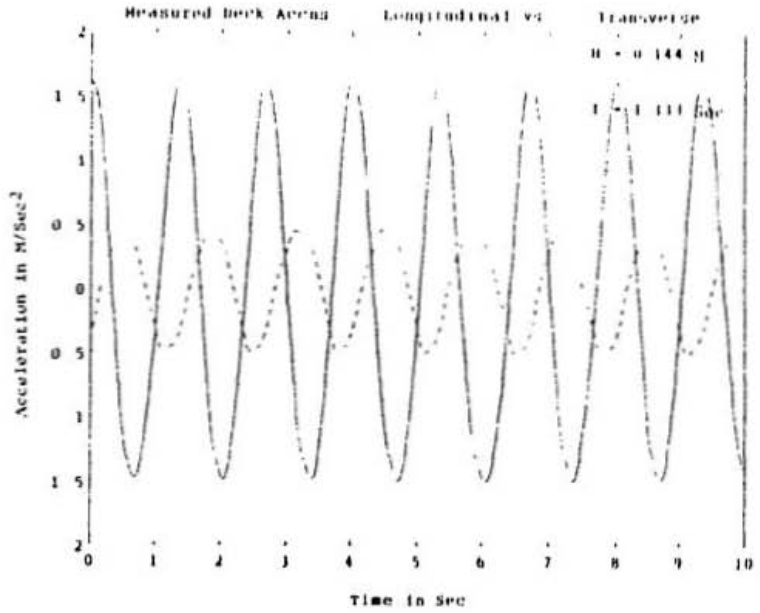

Figure 7.3: Comparison of deck accelerations at resonance: longitudinal vs transverse

The other important point that needs to be mentioned here is on the transverse response of the structure at resonance. Fig. 7.3 compares the transverse response of the structure with respect to the longitudinal response for the same wave data. A significant magnitude response is observed in the transverse direction. The dashed line in Fig. 7.3 shows the transverse response which is compared with its corresponding longitudinal response, given by the solid line. The magnitude of the transverse response is 27% of the longitudinal one. This is obviously a large value which suggests that a torsional mode of the structure may also have been excited when the structure undergoes a resonant excitation in the direction of waves. In order to investigate the presence of the torsional response in the structure for the same wave data, the deck acceleration responses from the center and port accelerometers are compared in Fig. 7.4. The longitudinal acceleration at the centre of the deck (dashed

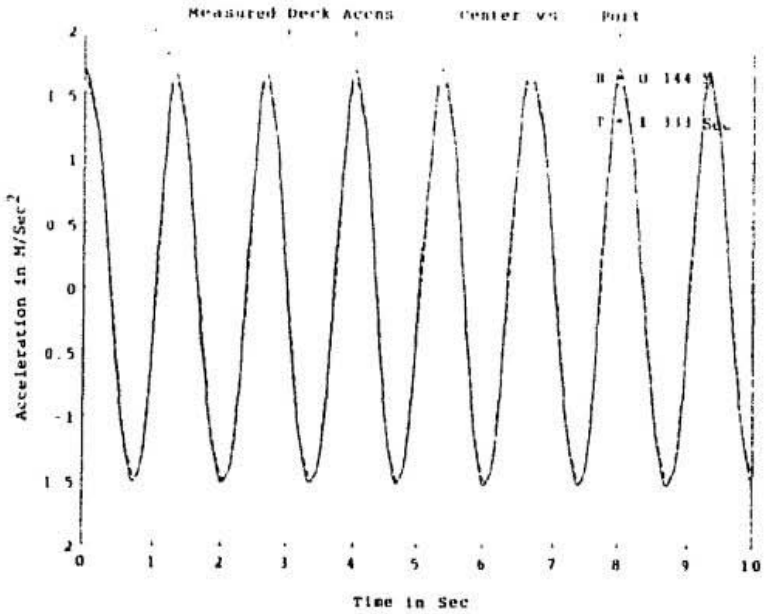

Figure 7.4: Comparison of deck accelerations at resonance: port vs. center

line) and at a distance of 0.7 m to port of the centreline (solid line) are in phase with one other and their amplitudes are also the same. This indicates that there

is no significant torsional response generated when the structure was subjected to resonant excitation in the wave direction. Hence the large transverse response observed in the experiment is not due to the torsional oscillations in the structure. However significant transverse forces, induced due to the resonant response in the longitudinal direction, have excited the structure in the transverse direction. It is interesting to examine whether such transverse vibrations are always present in the structure, irrespective of the wave exciting frequency.

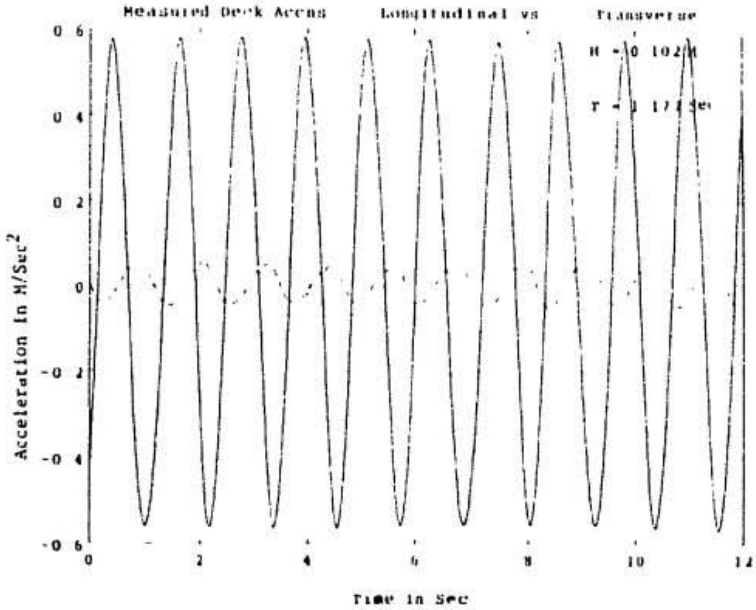

Figure 7.5: Comparison of deck accelerations at resonance: longitudinal vs. transverse

Fig. 7.5 presents another comparison in which the measured transverse deck acceleration is compared with the longitudinal deck acceleration, for a wave period (T = 1.17 s) lower than the natural period of the structure, 1.35 Hz. In this case, it can be seen that the magnitude of the transverse response is very small, being around 7% of the longitudinal value. Thus for wave exciting frequencies away from resonance, lower amplitudes of transverse vibration are observed whereas near res-

onance transverse vibrations are a large fraction of the amplitudes of longitudinal vibrations. The reason for such a behaviour can be explained by noting that the first natural frequency of the model structure in the transverse direction (0.732 Hz) is very close to the one in the longitudinal direction (0.73 Hz). The two possible explanations for this behaviour are: (a) due to the lift forces, even a small force magnitude is quite energetic to excite the structure around resonance in the transverse direction; and (b) due to the true orientation of the first bending mode which is different from the in-line and the transverse direction of the wave for 0.73 Hz and 0..732 Hz, respectively.

7.2.1 Comparison of Experimental Results with Theory

A typical behaviour of the physical structure at resonance has been examined in the foregoing discussion. However it would also be worthwhile to study the response of the structure to wave exciting forces using theoretical methods and then compare these with the experimental measurements. Such a study is divided into two groups for the purpose of discussion: (1) The structural response at resonance; and (2) Response to waves whose frequencies are away from the resonance.

Response at Resonant Excitation

To provide theoretical predictions, the computer program developed in chapter 6 was used with the input of the measured wave parameters and appropriate hydrodynamic coefficients given in chapter 3. For structural damping, the measured damping in air, 4.65% of critical damping, was incorporated (in Rayleigh form) in the analytical model. First the response of the structure to wave excitations near the resonant frequency is presented herein.

Fig. 7.6 compares the experimentally obtained longitudinal deck acceleration (solid line) with the predicted response (dashed line). The measured wave height

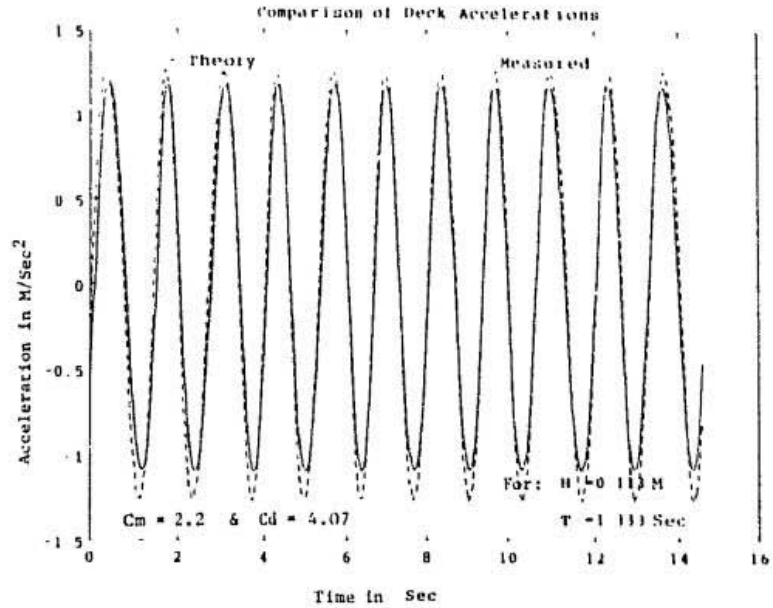

Figure 7.6: Comparison of deck longitudinal accelerations at resonance: measured vs theory

for this case is 0.113 m and the wave period is 1.333 s ($H_p = 5.65$ m and $T_p = 9.42$ s). The C_m and C_d values used to predict the response for this wave conditions are 2.2 and 4.07, respectively. A very good agreement can be seen between the prediction and measurement except at the peaks. The amplitude of predicted acceleration (1.24 m/s^2) is 7% grater than the measured value (1.16 m/s^2). This small discrepancy can be attributed to the greater damping experienced by the physical structure at resonance than that used in the mathematical model. Secondly, the effect of an increase of wave height for the resonant excitation in the wave tank was studied by increasing the H to 0.144 m ($H_p = 7.2$ m), for the same wave period. Similar comparison of results is presented in Fig. 7.7. The C_m and C_d values used are 2.15 and 3.87 respectively. Better overall agreement can be seen for this case. However, the magnitude of the predicted acceleration at the negative peak is slightly (6%) higher than the measured value.

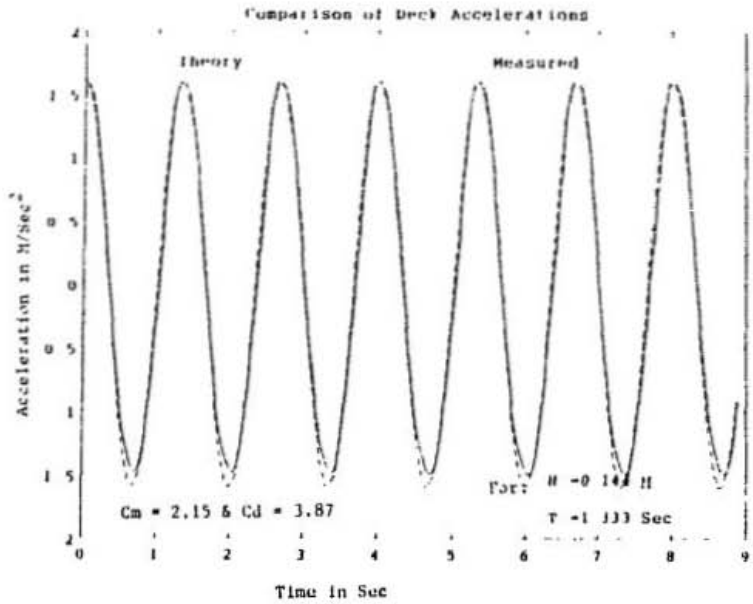

Figure 7.7: Comparison of deck longitudinal accelerations at resonance: measured vs theory

The magnitude of the peak acceleration (measured) for H = 0.144 m is 1.6 m/s^2 (Fig. 7.7), whereas for H = 0.113 m is 1.16 m/s^2 (Fig. 7.6). Thus the magnitude of the longitudinal acceleration increases with wave height. This behaviour can be seen, particularly in the oscillations of a structure where the inertial component of the wave force is much larger than the drag component. In a drag force dominated structure there is a possibility for the magnitude of the response to decrease as the wave height increases[1]. Since no flow-separation occurred due to the low KC number, the inertial force component of the wave dominated the situation and increased the magnitude of response for the increased wave height.

[1]Such a phenomena was observed and reported by Dunwoody and Vandiver (1987) for a drag force dominated structure

Excitations at Frequencies away from Resonance

The next series of experiments were conducted for a wave period of T = 1.43 s (T_p = 10.11 s). The wave heights selected are 0.135 m and 0.159 m (ie. H_p = 6.75 m & 7.95 m). The selected wave period is not completely different from the natural period of the structure (1.34 s). Hence the wave excitations may be considered to be still close to resonance. The C_m and C_d values for H = 0.135 m & T = 1.43 s were 2.03 and 2.05, respectively; and for H = 0.159 m & T = 1.43 s, they were 2.01 and 2.45, respectively. The comparisons between theory and prediction are shown in Figs. 7.8 and 7.9. Excellent agreement can be seen in the comparison shown in

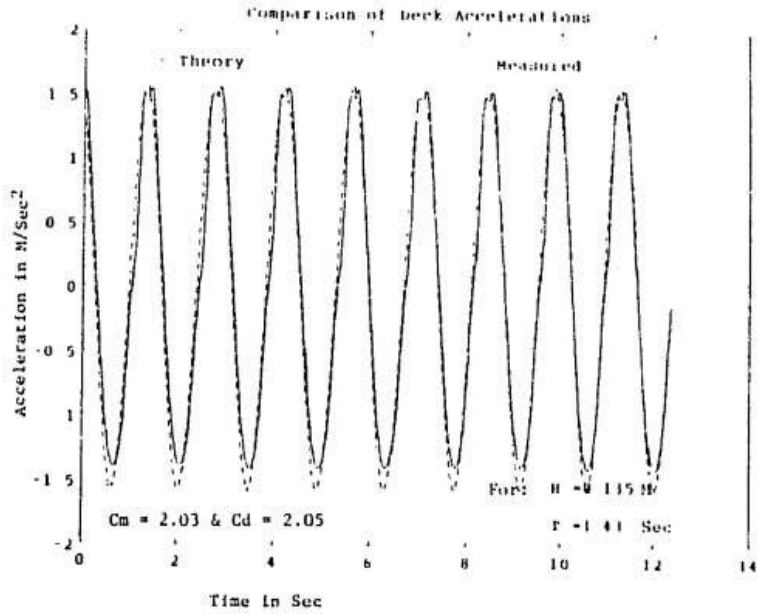

Figure 7.8: Comparison of deck longitudinal accelerations for a wave exciting frequency lower than resonance: measured vs theory

these two figures. Similar to the results, seen in the previous subsection, the theory again overpredicted (slightly) the measured longitudinal acceleration. This is due to the fact that the wave exciting frequency is very close to the natural frequency of the model; the results are still similar to the results of resonant excitations. However

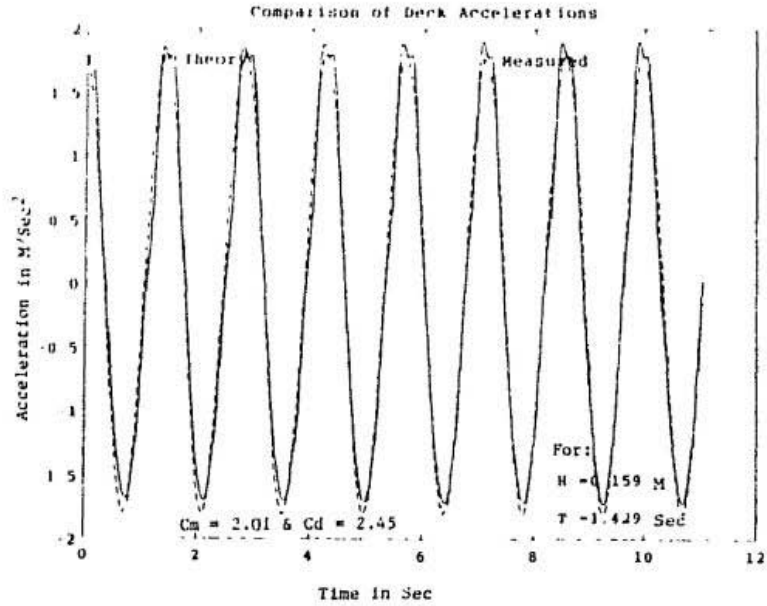

Figure 7.9: Comparison of deck longitudinal accelerations for a wave exciting frequency lower than resonance: measured vs theory

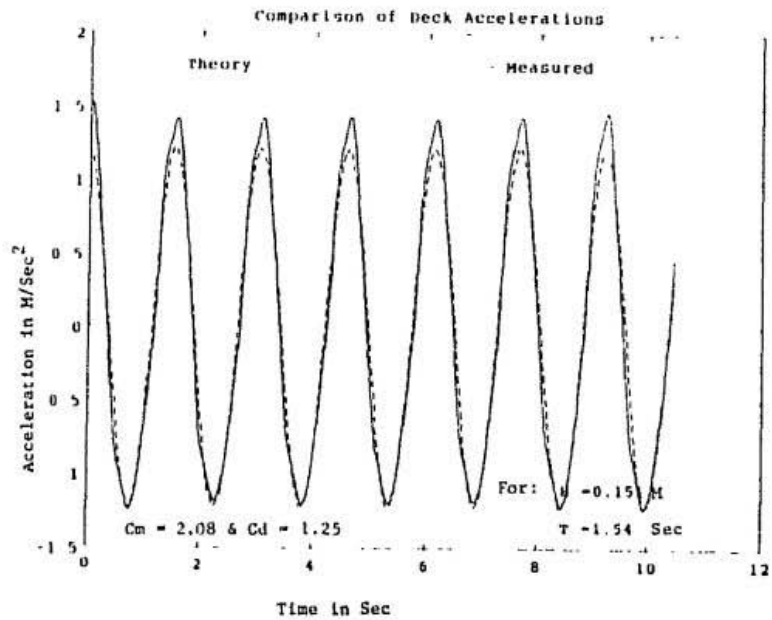

Figure 7.10: Comparison of deck longitudinal accelerations for a wave exciting frequency lower than resonance: measured vs theory

unlike in Figs. 7.6 and 7.7, the response at the peaks in Figs. 7.8 and 7.9 are double headed. This did not occur when wave exciting frequency was much lower than the natural frequency of the structure, even though the wave height was significantly large, see Fig. 7.10 (for H = 0.151 m & T = 1.54 s; C_m = 2.08 & C_d = 1.25).

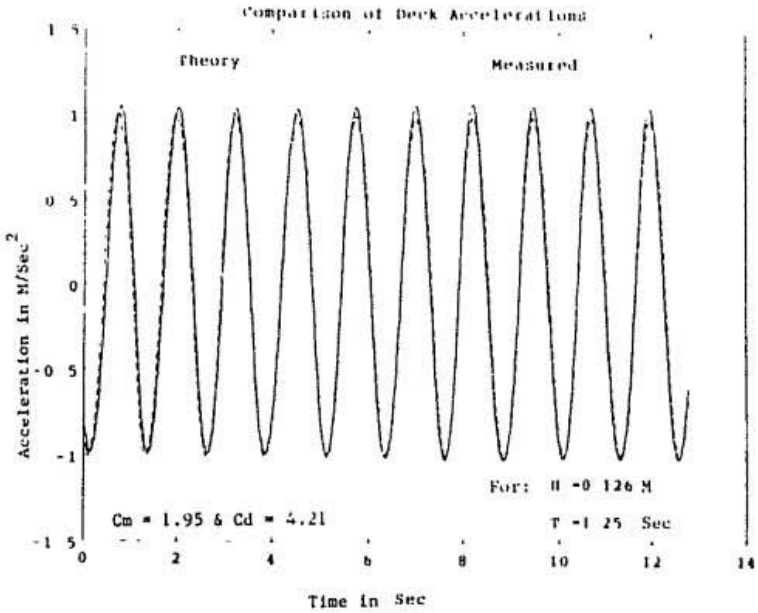

Figure 7.11: Comparison of deck longitudinal accelerations for a wave exciting frequency higher than resonance: measured vs theory

Comparing Figs. 7.9 and 7.10, almost for the same wave height, the magnitude of the peak response has reduced from 1.84 m/s^2 to 1.42 m/s^2 (ie., 23%) as the frequency decreases from 0.6998 to 0.65 Hz. Hence as the wave exciting frequency moves 7% away from resonance, the magnitude of response is reduced by 23%. Another important behaviour which should be noticed in Fig. 7.10 is that the magnitude of the theoretical response at the positive peaks is less than the measured response value. Hence for wave exciting frequencies, quite away from the resonant frequency the theory under-predicts the measured response; while at and near resonance, the theory over-predicts the measured response. This certainly shows that at

resonance the physical structure experiences some additional damping which results in a reduction in the longitudinal acceleration. However this physical phenomena cannot be accounted for by the theory.

Lastly, one more test was conducted for the completion of regular wave response study by generating waves of frequency higher than the resonant frequency. The wave parameters selected were H = 0.126 m & T = 1.25 s (H_p = 6.3 m & T_p = 8.84 s) and the C_m and C_d values used in this case are 1.95 and 4.21, respectively. Here the wave frequency was 0.8 Hz which is 8% above the lowest natural frequency of 0.74 Hz. Excellent agreement between prediction and measurement can be seen in Fig. 7.11. Again the theory (dashed line) under-predicted the measured (solid line) peak values which emphasizes the previous assessment made for Fig. 7.10. In conclusion, we observed that for wave exciting frequencies 7% below and 8% above the resonant frequency, the theory underpredicts the measured response by 23%. At and near resonance, the theory overpredicts the measured response. This also shows that at resonance the motion of the structure experiences some additional damping which results in a reduction of the magnitude of the longitudinal acceleration.

7.3 Structural Response to Random Waves

The response of the structure at and close to resonance has also been studied for the laboratory generated random waves. Different JONSWAP spectra (for the fully developed moderate sea) were selected, scaled down to the model tower, and then used to generate the random waves in the tank. Representative time signals of the spectra were simulated using an FFT technique. A cut-off-frequency of 2.0833 Hz was introduced in the spectra and 2048 wave elevation time points with 0.03 s time interval were simulated, in a Monte Carlo sense, using a digital computer. The simulated signals were used to control the wave board which generated random waves in the wave tank. For data acquisition, a 33.33 Hz sampling rate was selected

to increase the resolution in the Fourier transform analyses of the recorded wave elevation and deck acceleration data. Justifications can be made for the selection of a lower sampling rate (33.33 Hz) than the one selected for the regular wave cases (50 Hz) in the data acquisition.

In order to collect data at all the wave frequencies simulated from the target spectrum the same record length of 61.44 s should be used in the processing of the recorded data. For a 61.44 s record length, the resolution df would be 0.016276 Hz. The resolution df can be improved further by selecting a lower sampling rate. However, that would result in an increased time interval dt. The larger dt is not acceptable for the time domain analysis which had to be carried out in the correlation study of experimental data with theory. Hence the 33.33 Hz sampling rate was considered to be an ideal value for the random wave test.

One interesting feature of this section is that the measured random deck responses is compared with the predicted results in the time domain. Such comparisons are rare to find in the literature, and note that it is always customary to compare random response with theory in the frequency domain. In order to do the comparison in the time domain, the measured random wave elevations were input to the designed linear filter, discussed in chapter 6, and the time series for the particle kinematics for each water depth was computed. The rest of the procedures followed are the same as in the case of the regular wave response analysis. The hydrodynamic coefficients were input to the computer program, based on the corresponding random wave force analysis results obtained in chapter 3.

Fig. 7.12 compares the experimentally obtained longitudinal acceleration response of the structure (solid line) with that predicted response (dashed line) for the measured random wave elevation (also shown in the figure at the bottom half). The significant wave height H_s for the measured wave elevations is 0.1162 m, the zero up-crossing period T_z is 1.5663 s and the peakedness parameter γ is 2.3 ($H_{sp} = 5.81$

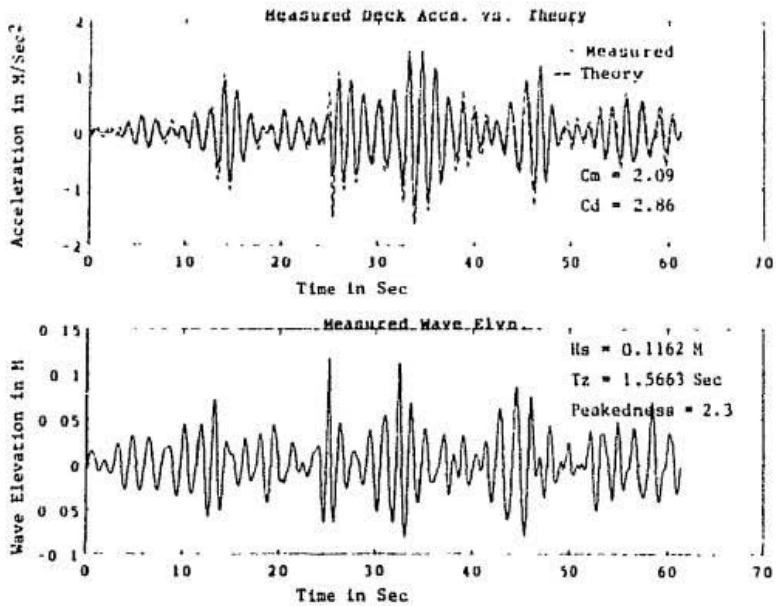

Figure 7.12: Comparison of deck longitudinal accelerations for random waves in the time-domain: measured vs theory

m & $T_{zp} = 11.07$ s). Note, that the zero up-crossing period of the wave elevations is close to the natural period of the structure (1.35 s). The C_m and C_d values used for this case are 2.09 and 2.86, respectively. Excellent agreement between measurement and prediction can be seen in this figure. The phase and the magnitude of both the results, experimental and theoretical, have matched well.

The rms value of the measured response of the structure is 0.41 m/s^2 and for the theory it is 0.46 m/s^2. A 10% error is observed in the present random wave response prediction. It can be noticed, in Fig. 7.12, that for certain peaks the magnitude of the predicted response exceeds the magnitude of the measured response. This small discrepancy can be explained by comparing the two responses in the frequency domain. The measured and the predicted time series of the responses were Fourier transformed to the frequency domain and then compared.

The power spectral densities for the measured response (solid line), for the pre-

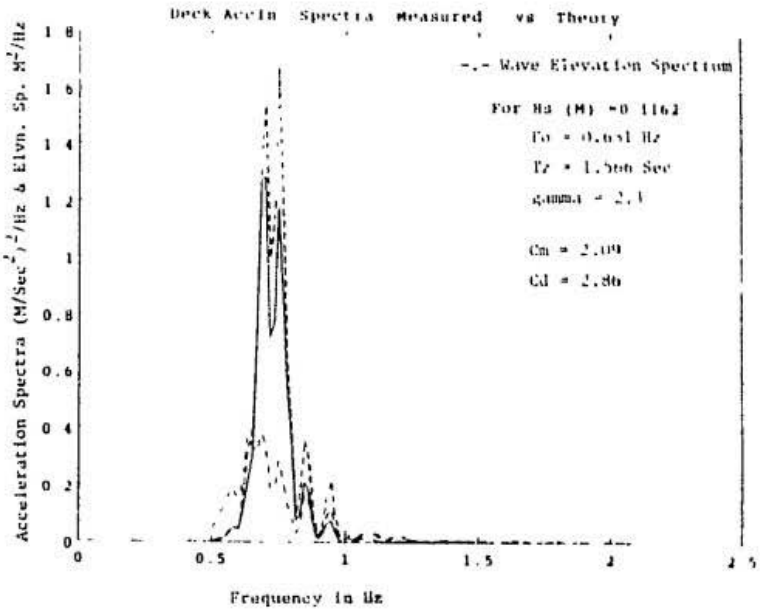

Figure 7.13: Comparison of deck longitudinal accelerations for random waves in the frequency-domain: measured vs theory

dicted response (dashed line) and for the measured wave elevations (dashed and dotted lines) are shown in Fig. 7.13. A very good agreement can be seen between the measured and predicted responses at all frequencies except at the resonant peak. Note that the wave elevation data has large power in the frequency range close to the fundamental natural frequency of the structure. Thus the structure was subjected to a resonant excitation during the measurement period. However, there are also excitations of significant wave power at frequencies away from resonance. The figure shows that though the wave elevation spectrum has a significant energy at 0.56 Hz, the magnitude of the response for that frequency is very low. At and near resonance the magnitude of the response is large. The response spectra, measured and theoretical, have two peaks, one at resonance ie., at 0.74 Hz, and the other at the peak of the wave elevation spectrum, ie., at 0.651 Hz (ie. close to resonance). At frequencies larger than 0.81 Hz the magnitudes of structural response are smaller.

It should be mentioned here that the measured wave elevation spectrum will not be as smooth as that of the desired target spectrum. Because the experiment was conducted in a large wave tank where reflections occur from the beach, the wave-board and the side walls, the measured spectrum has several small peaks along with the one at the peak frequency of the desired target spectrum. This has influenced the measured and predicted responses with multiple peaks in the spectra.

In Fig. 7.13, the solid line and the dashed line agree well with each other at frequencies away from resonance. However at the resonant peak, the magnitude of the measured response is found to be less than the magnitude of the predicted response. This again emphasizes the previous conclusion that the magnitude of the damping in the physical model is larger than that in the theoretical model, at or near resonance.

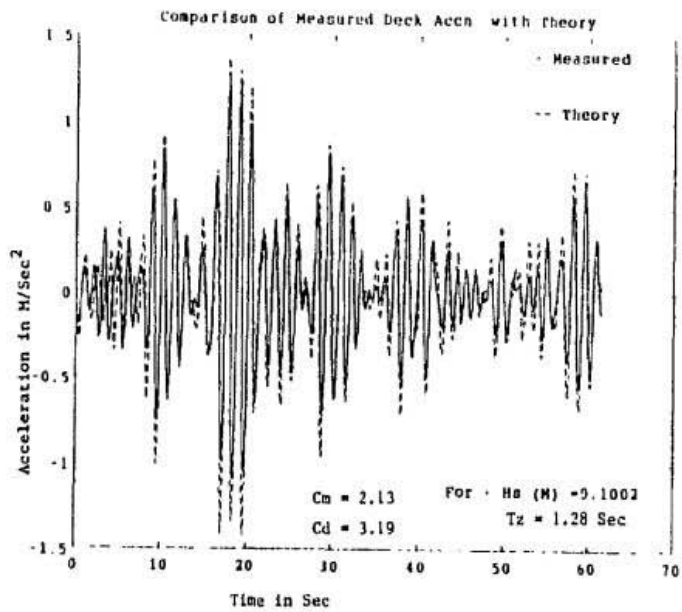

Figure 7.14: Comparison of deck longitudinal accelerations for random waves in the time-domain: measured vs theory

Three more random wave test results are presented in this section. Both the time

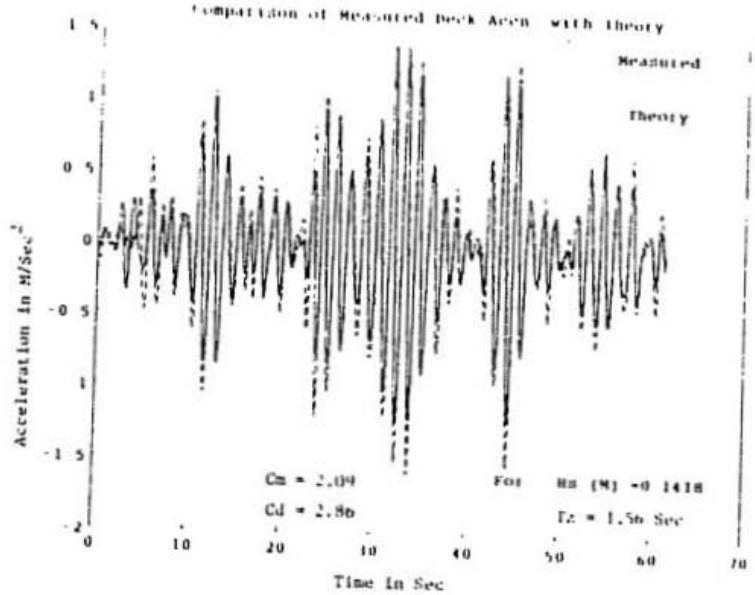

Figure 7.15: Comparison of deck longitudinal accelerations for random waves in the time-domain: measured vs theory

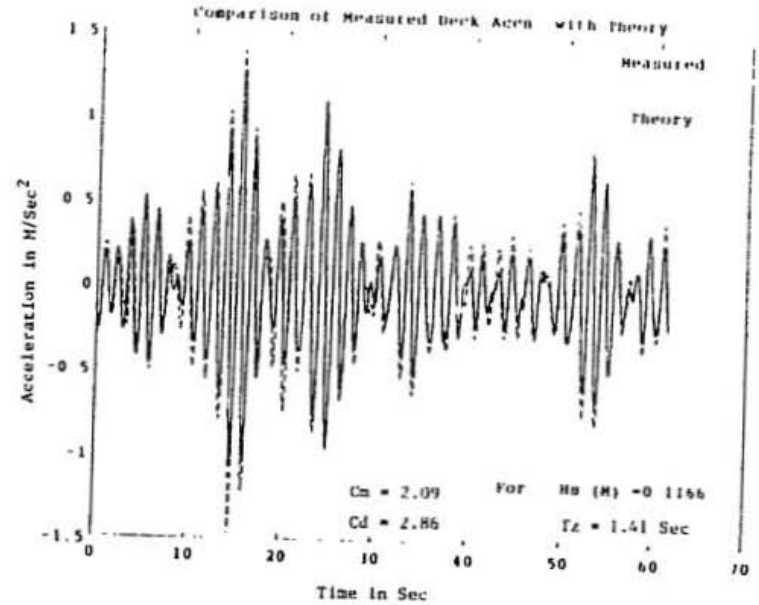

Figure 7.16: Comparison of deck longitudinal accelerations for random waves in the time-domain: measured vs theory

and frequency domain comparisons of responses between theory and measurements are made similar to the comparisons in Fig. 7.12 and Fig. 7.13. The wave simulation was carried out for the spectra typically used for fatigue analysis of a deepwater structure. They mostly represent a moderate wave environment which contribute predominantly to the fatigue damage of the structure.

Table 7.1: Wave parameters for random wave force simulation

IDENT	H_s m	T_z s	F_0 Hz	γ
Fig. 7.14	0.1002	1.28	0.667	2.3
Fig. 7.15	0.1418	1.56	0.635	2.3
Fig. 7.16	0.1166	1.41	0.623	2.9

The time domain comparison of results are presented in Figs. 7.14 to 7.16. The wave parameters obtained from these three tests are given in Table 7.1. The hydrodynamic coefficients used in the analyses and the rms values of the longitudinal acceleration of the deck obtained are summarized in Table 7.2.

Again excellent agreement between measurement and theory can be seen in Figs. 7.14 to 7.16. As could be observed from Tables 7.1 and 7.2, the rms value of the longitudinal acceleration of the deck increases for the spectra as H_s increases. The wave spectra of Fig. 7.12 and Fig. 7.16 have almost the same significant wave heights; however the rms displacement for Fig. 7.12 is 12.6% higher than the rms displacement for Fig. 7.16, though the peakedness for the latter one is higher (2.9 vs 2.3). This is due to the fact that the peak frequency of the wave spectrum for Fig. 7.16 is further away from resonant frequency of the structure (0.62 vs 0.64).

Table 7.2: Deck longitudinal accelerations to random wave excitation

IDENT	C_m	C_d	*rms value of deck response* m/s^2	
			Experiment	Theory
Fig. 7.14	2.13	3.19	0.34	0.38
Fig. 7.15	2.09	2.86	0.11	0.47
Fig. 7.16	2.09	2.86	0.33	0.37

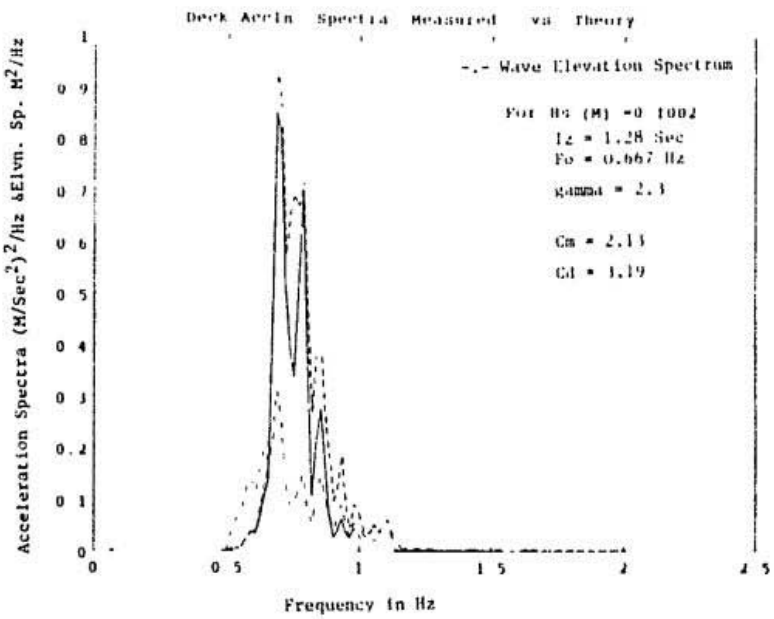

Figure 7.17: Comparison of deck longitudinal accelerations for random waves in the frequency-domain: measured vs theory

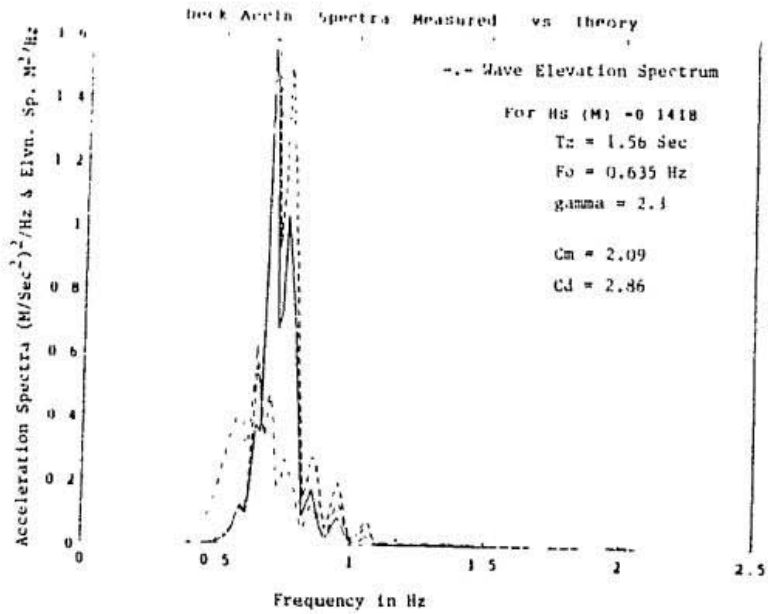

Figure 7.18: Comparison of deck longitudinal accelerations for random waves in the frequency-domain: measured vs theory

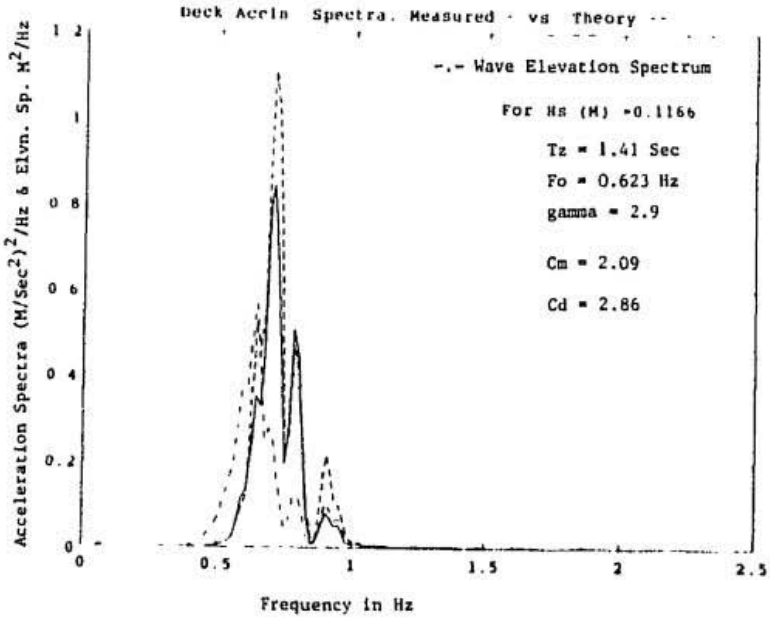

Figure 7.19: Comparison of deck longitudinal accelerations for random waves in the frequency-domain: measured vs theory

The corresponding frequency-domain comparison of results for the three above mentioned tests are shown in Figs. 7.17 to 7.19. For all the four spectra given in Figs. 7.17 to Fig. 7.19 and Fig. 7.13, a dominant peak occurs at 0.74 Hz which is the resonant frequency of the structure. Other peaks occur in the response depending on the wave loading energy content at those frequencies. In general, the magnitude of the response below 0.5 Hz and above 1.5 Hz is very low irrespective of the energy content of the wave exciting forces. It shows that the structure behaves in a quasi-static manner below 0.5 Hz and its higher modes above 1.5 Hz are hard to excite. However in the resonant region, the structure behaves in a compliant manner showing a large responses to wave exciting forces.

7.4 Summary

Before going on to the next chapter, a brief summary of the salient observations made in this chapter are presented. The resonant and near-resonant behaviours of the physical structure, for regular and random waves, were investigated in the laboratory wave tank. A comparison study with theory was also made using the developed time domain program. The hydrodynamic coefficients obtained from the first experiment were used for the theoretical predictions. In all cases good agreement between the theory and the experiment was observed.

Considering the regular wave response, the longitudinal response increases as the wave frequency approaches the natural frequency. A significant response in the transverse direction was also observed in the resonant region. The transverse response diminished for frequencies away from resonance. At resonance, the magnitude of the theoretical longitudinal acceleration of the deck at the peaks are 3 to 7% higher than the measured values. This is due to the fact that the physical model experienced larger damping and, consequently, the magnitude of response was observed smaller than the prediction. Such behaviour is seen only in the resonant

region; however for frequencies away from resonance excellent agreement between the theory and measurement is obtained. A similar behaviour is also observed in the case of random waves.

From the random wave tests the following additional points should be emphasized. Excellent agreement between theory and measurement is obtained in the time domain. The higher modes are very hard to be excited by the waves, because not much energy content is available at those frequencies. Although the wave energy at frequencies below 0.5 Hz was significant, the structure behaves in a quasi-static manner and the magnitude of response is found to be very small compared to the values near resonance. This indicates that the structure by nature is very stiff to wave forces. In spite of that the magnitudes of the structural response, in the resonant region, are observed to be very large. **At and close to resonance, thus the stiff structure behaves in a compliant manner to waves.**

Chapter 8

Effect of Induced Flow-Separation on the Near Resonant Response of the Model Structure

It must be appreciated at this stage that the presence of large structural motions, at and near resonance, due to wave excitations is the main reason why fixed structures are not suitable for deepwater offshore applications. The large amplitudes of response, to the most frequent moderate waves, limit the fatigue life of the structure. Hence it has become imperative that attention be focused on controlling this compliant response to resonant wave excitations either, by increasing the stiffness of the structure, or, by providing additional damping in the system. However it is economical to control the response in the resonant zone by increasing the damping rather than by increasing the stiffness. One such useful approach which introduces additional damping is described in this chapter.

In fluid-structure interaction, there are two fundamental phenomena which form the basis for the dissipation of energy in the fluid media. The first is the structural motion and the second is the flow-separation behaviour. They both act together and introduce a kind of hydrodynamic damping called separated-flow (or drag) damping. It has been established in the previous chapter that the structure undergoes large structural motions at and near resonance. We have also seen that the presence of

large structural motions at and near resonance increases the magnitude of damping in the structure. As a result of the above, the theoretical formulation underpredicts the responses in the resonant region. The additional damping experienced by the structure may be partly due to the structural and wave radiation sources, but the author believes that the major contribution must be from the flow-separation phenomena. Hence, at resonance, the structural motion interacts with the fluid and tries to introduce additional flow-separation in the water. It is the tendency of the structure to try its best to dissipate energy in the lowest possible mode. However the capacity, to introduce flow-separation, is very much limited because of another predominant factor called the KC number. Although the structure has the tendency to dissipate more energy when it undergoes resonant oscillation, the behaviour of the flow at low KC numbers limits the chances for the formation of flow-separation behind the circular cylinder by making frequent flow-reversals. Hence there is insufficient time, available within the half-period of oscillation, for stable flow-separation pattern to occur. This drastically reduces the possibilities for the structure to dissipate energy in the form of flow-separation. Hence, in spite of the large amplitude of structural response at resonance, the damping associated with the separated-flow drag forces are very small in the structure. This aspect of the study has already been discussed in chapter 3. In the same chapter we have also seen that, with the attachment of the designed device, the oscillatory wave flow behaves in an entirely different manner by inducing large flow-separation around the structure resulting in increased drag forces. It would be interesting to investigate the consequences of these induced drag forces, on the resonant response of the model structure.

In order to study these effects, the device shown in Fig. 3.4 was attached to the structure and the structural response measured for the laboratory generated waves. Wave heights which, in the prototype situation, represent moderate seas were applied. Before embarking on the discussion of the experimental results, the

theoretical results on the effect of induced drag forces are presented first. In the theoretical study the hydrodynamic coefficients obtained from the first wave tank experiments on a vertical cylinder with and without the attachment of the device, are used. The response of the structure for different wave parameters is predicted using the developed time-domain computer program. Lastly the important experimental and analytical results obtained in this part of the study are summarized.

8.1 Theoretical Study

It is well known that the inclusion of structural response velocities in the Morison wave force formula acts as a response reduction mechanism since the drag term which corresponds the structural response accounts for a kind of hydrodynamic damping in the fluid-structure system. An increase in the C_d value due to the attached device also increases the damping due to the drag forces in the structure. It would be most appropriate to examine first the effect of this damping on the structural response by analytical means before proceeding to the experimental investigation. The developed time-domain methodology, discussed in chapter 6, can be used to study the present problem. The effect of the physical device on the dynamic response can be simulated by using the corresponding hydrodynamic coefficients, for the cases with and without the device, which were determined earlier in chapter 3.

8.1.1 Response to Regular Waves

First the response of the structure to computer-simulated regular waves is analyzed. The wave height of 0.113 m (H) and the wave period of 1.333 s (T) are selected for the purpose of this study. (In the prototype situation these parameters are 5.65 m (Hp) and 9.41 s (T_p), respectively.) The selected wave period of 1.333 s is very close to the first fundamental natural period of the structure (1.37 s) and thus the structure is subjected to resonant excitation. The values of C_m and C_d coefficients

for the simple cylinder (for the selected wave parameters, from chapter 3) are 2.15 and 3.87, respectively. Using these values a dynamic analysis was carried out in the time-domain and the displacement responses obtained. With the device, for the same wave parameters, the values of C_m and C_d coefficients become 2.19 and 15.2, respectively. These new values of the coefficients were used for the portion of the

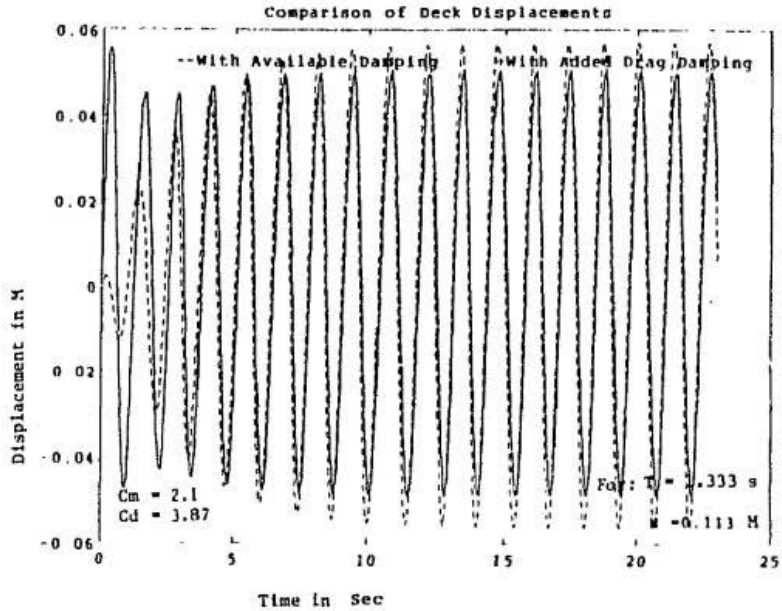

Figure 8.1: Comparison of theoretical deck longitudinal displacements for regular waves: with and without inducing drag damping (for ζ= 4.65%)

structure, where the device was attached, and the analysis was again carried out for the same wave parameters. The two deck longitudinal displacements corresponding to the two cases, with and without including the effect of the device, are compared in Fig. 8.1. The dashed line in the figure shows the response of the structure for the case without the device (hereafter called the simple structure), whereas the solid line shows the response of the structure with the attached device. Many interesting points could be observed from Fig. 8.1. For the simple structure the result shows that the structure behaves in the anticipated manner. The structure motion starts from

rest (deflection = 0 at time t = 0), and the motion gradually increases in amplitude until it attains its steady state. The maximum deck displacement obtained in this case was 0.057 m. For the case of the structure with the device, the amplitude of the response during the initial stage is large and later on, it reduces and then attains a steady state. At steady state, the maximum deck displacement was 0.048 m which is 16% less than the magnitude of displacement obtained in the previous case. In the transition zone the amplitude of response, with the device, is larger than that of the simple cylinder. However as time increases the amplitude of structural response, with the device, decreases and reaches its steady state level. The poossible reasons are as follows: (i) at the initial stage (when deflection = 0 at time t = 0), the drag force acts as a forcing mechanism; and thus a large transient response can be seen in the transition zone; (ii) as time increases, the large structural velocities increase the effect of the coupling between the fluid and structure; consequently the induced drag forces act as a response reduction mechanism, decreasing the structural response.

A 16% reduction in response, to the most probable moderate waves, is obviously a large value while considering the fatigue life of the structure. An important point which should be remembered here is that the structural damping incorporated in the present analysis (due to the acrylic model) is larger than what could be in the prototype situation. The acrylic plastic used in the model has larger structural damping (4.65% of critical damping) than the prototype material (steel). Hence the 16% reduction in resonant response, obtained for the model structure, would not represent the prototype value. In order to see the percentage reduction in the deck displacements for a lower structural damping, a similar analysis was carried out by incorporating a 2% structural damping into the numerical computations. The comparison of deck displacements for the same wave parameters, with and without the effect of the device, is presented in Fig. 8.2.

Only the steady state responses are shown in this figure. The dashed line indi-

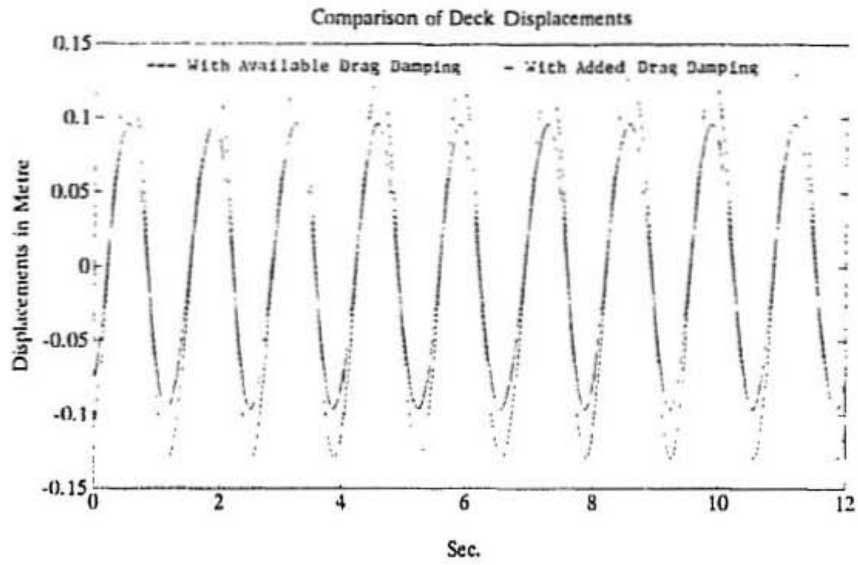

Figure 8.2: Comparison of theoretical deck longitudinal displacements for regular waves: with and without inducing drag damping (for $\zeta = 2.0\%$)

cates the response of the simple structure while the solid line shows the response of the structure with device. Due to the reduced structural damping used in the analysis, the amplitude of the deck displacement response is 0.13 m which is 56% larger than in the results shown previously in Fig. 8.1. In this case, the steady state response magnitude (maximum deck displacement is 0.095 m) has been reduced by 27% due to the inclusion of the effect of the device. This shows that the percentage reduction in response increases as the amplitude of the structural motion becomes larger. Thus the induced drag damping becomes more and more effective as the amplitude of the structural motion becomes larger and larger.

8.1.2 Response To Random Waves

It will be more interesting to see the effect of the induced drag damping for random wave excitations. Unlike the case of regular waves, the displacements are irregular.

Since the damping due to the drag effect is response-dependent, it is necessary to use the same wave elevation time history for both the cases, with and without the device. The wave elevation time histories are simulated in the Monte Carlo sense. In fact, the developed computer program has an option to simulate the water particle kinematics, directly, for a given set of JONSWAP or P-M spectral parameters. These simulated time series are stored in the computer and the analysis is carried out for different sets of hydrodynamic coefficients. This permits us to compare the responses of the structure, with and without including the device, for random wave excitations.

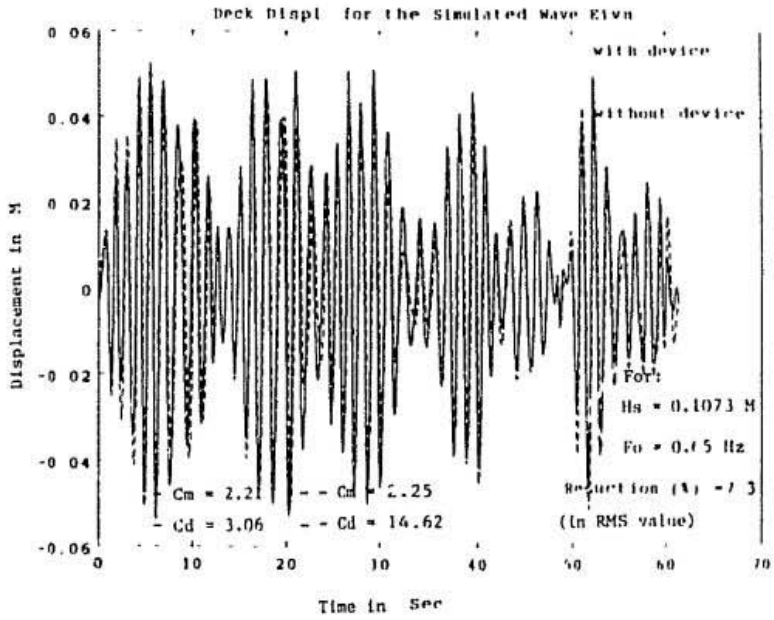

Figure 8.3: Comparison of theoretical deck longitudinal displacements for random waves: with and without inducing drag damping (for ζ= 4.65%)

One such comparison for a set of P-M spectral parameters, H_s = 0.1073 m (significant wave height) and F_o = 0.65 Hz (peak wave frequency), is presented in Fig. 8.3. These wave parameters correspond to H_{sp} = 5.4 m and F_{op} = 0.092 Hz, respectively in the prototype situation. Note that although the peak wave elevation

frequency (0.65 Hz) used here is slightly away from the natural frequency of the structure (0.73 Hz), resonant excitation occurs because of the relatively broader band (at low wave amplitudes) of the wave spectrum. The values of C_m and C_d used for the case of the simple structure, are 2.21 and 3.06, respectively; for the case of the structure with the device they are 2.25 and 14.62, respectively. The structural damping, 4.65% of critical damping, was incorporated in a Rayleigh form. The dashed line in Fig. 8.3 shows the deck displacement time series for the structure with the device, while, the solid line represents the simple structure. Both of them are, of course, in phase with one other because the same random wave elevation time history was input to the program. It is observed that the magnitudes of dashed lines are less than the solid lines, for most of the time. It should also be noticed here that the reduction in the response magnitude, due to the induced drag damping, is not uniform, unlike the case of regular wave response. Because both frequencies and magnitudes of structural response change, with respect to time, the magnitude of damping also changes. Hence the nonlinear effect of the drag damping which influences the structural response can be visualized in Fig. 8.3. The rms value of the longitudinal displacement of the simple structure, is 0.0233 m, and for the structure with device, it is 0.0216 m. Thus the rms value of structural displacement has been reduced by 7.3% due to the induced drag damping forces. This 7.3% will vary if the analysis is repeated for the same parameters, with different simulated random wave elevations. This is due to the response-dependent nature of the drag damping induced in the structure. For example, if larger structural displacements are simulated in the analytical model, then the percentage reduction increases.

The effect of induced drag damping for random wave excitations can be further illustrated by the power spectral densities of both the structural response time series (shown in Fig. 8.3) and comparing them in the frequency domain, as shown in Fig. 8.4. The Fast Fourier Transform was used to transform the longitudinal

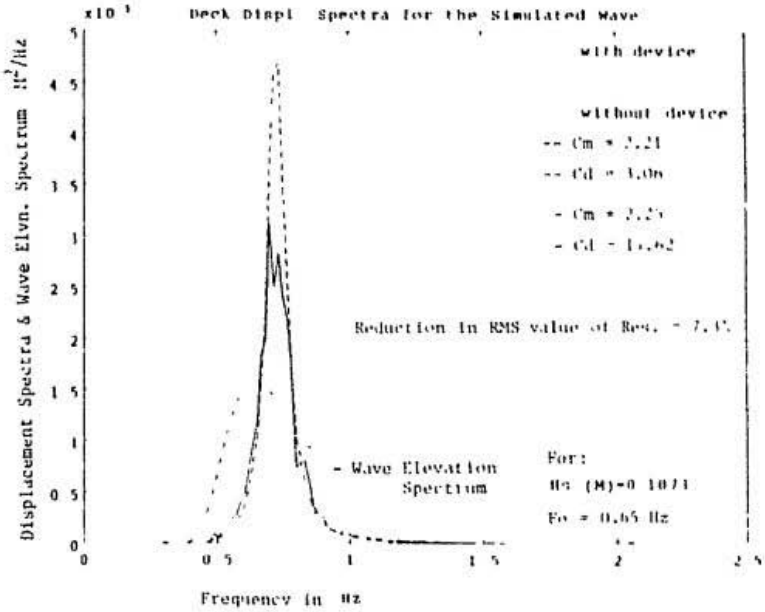

Figure 8.4: Comparison of theoretical deck longitudinal displacement spectra: with and without inducing drag damping (for $\zeta = 1.65\%$)

displacement (the time history) into a power spectra. The dashed line shows the power spectral density of the response for simple structure and the solid line indicates the same for the structure with the device. For better assessment, the wave elevation spectrum used for the simulation of particle kinematics is also presented in the same figure by the dashed and dotted line. The response of the simple structure, the dashed line, is almost smooth with a single peak at resonant frequency. Since the structure is inertia-dominated, the response vs frequency behaviour is mainly a linear transformation. The weak nonlinearity due to the poor drag damping, though included in the analysis, has not significantly affected the response. The response magnitude is large around resonance, with a narrow bandwidth. Though the energy in the waves is larger, at frequencies away from this band, the response is less significant at frequencies away from resonance. No significant response is found at higher bending modes, since the energy available in the wave spectra to tune

the second mode is much less than necessary. Furthermore, it may also be noticed that no nonlinear response is present due to any inertial nonlinearity in the forcing mechanism, such as those due to the sum and difference of wave frequencies.

The reduction due to the presence of the device as indicated by the solid lines, shows that the response has been reduced drastically in the resonant region. This reduction takes place predominantly within a frequency bandwidth of 0.10 Hz. in the resonant region, where the structure appears to be compliant to waves. This shows that the structure undergoes large motions only in the resonant region, and the induced drag damping is quite effective in reducing the response in that region. At frequencies away from the resonant frequency no significant difference occurs between the two responses, viz., those with and without the device. This clearly shows that no adverse effects are created due to the induced drag forces, at frequencies away from resonance.

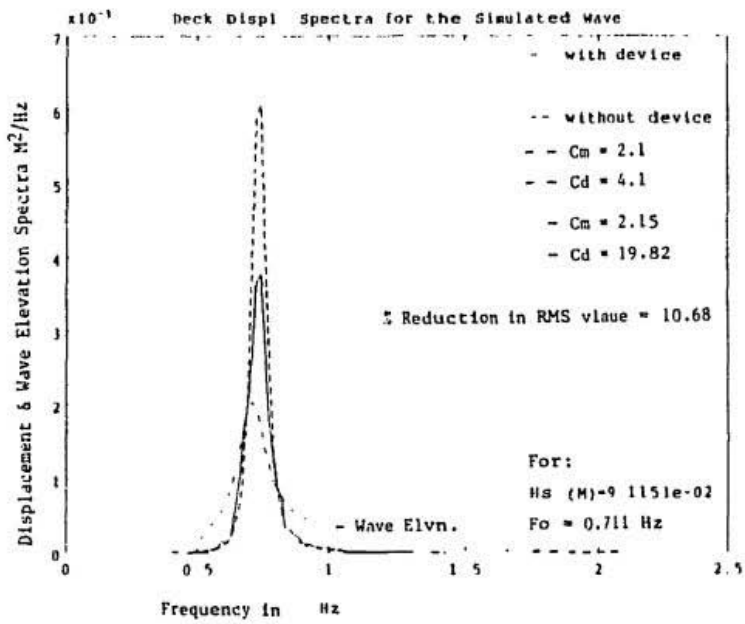

Figure 8.5: Comparison of theoretical deck longitudinal displacement spectra: with and without inducing drag damping (for ζ= 4.65%)

So far we have discussed a simulated response of the system to a broad band PM spectrum in which case the peak frequency was selected to be less that the natural frequency of the structure. It will be interesting to see an analogous study of a JONSWAP spectrum with its peak frequency very close to the resonant frequency of the structure. Fig. 8.5 shows such results obtained for H_s = 0.0912 m and F_o = 0.711 Hz and γ = 1.5 (H_{sp} = 4.56 m and F_{op} = 0.1 Hz). The C_m and C_d values used without the device are 2.1, and 4.1 respectively; the values are 2.15 and 19.8 respectively for the case with the device.

In this case one can very well see that the magnitude of the response is relatively very large compared to the previous case shown in Fig. 8.1. This is due to the fact that most of the wave energy is expended in exciting the structure in the resonant region, within a bandwidth of 0.1 Hz about the resonant frequency. There is a large reduction in response due to the induced damping. The rms value of response reduces by 10.7%, which is much greater than the previously obtained value of 7.3%. This shows that the percentage reduction in response increases as the magnitude of response increases; also the effect of the device is more pronounced in the resonant region.

Lastly one more simulation study is added to this section with regard to the question of what will happen if the peak frequency of the wave energy spectrum is larger than the natural frequency of the structure. A P-M spectrum with H_s = 0.091 m, F_o = 0.782 Hz (H_{sp} = 4.55 m and F_{op} = 0.11 Hz) is considered. The peak frequency of 0.782 Hz is greater than the natural frequency (0.73 Hz) of the structure. The deck response spectra for the cases, with and without the device, are shown in Fig. 8.6. The amplitude of the deck longitudinal displacement is smaller than in the case of Fig. 8.5 and thus the reduction in the rms value of the response is also small (6.1%). Here multiple peaks are observed due to drag nonlinearities. Also note that in Fig. 8.6, a larger portion of the wave energy is expended in exciting

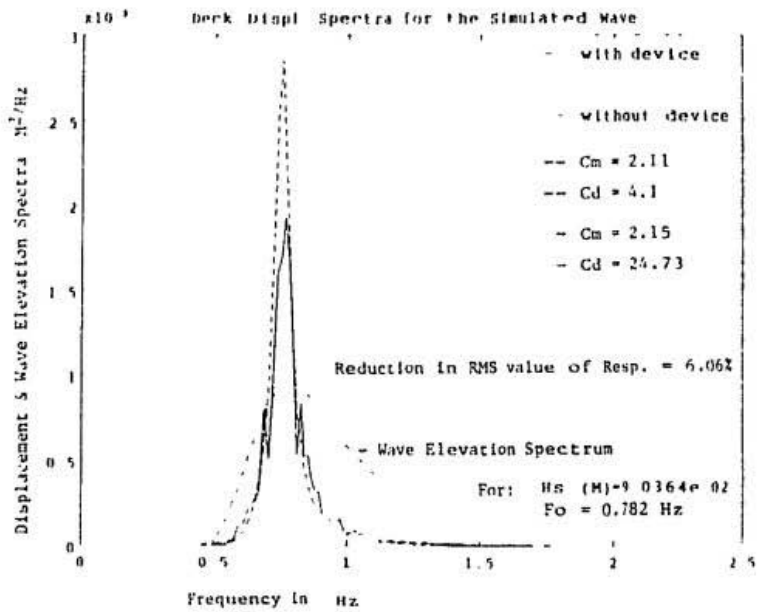

Figure 8.6: Comparison of theoretical deck longitudinal displacement spectra: with and without inducing drag damping (for $\zeta = 4.65\%$)

the structure at frequencies higher than the natural structural frequency, where the structure behaves more or less in a quasi-static manner.

From these studies three important points can be drawn which are stated as follows: (i) The induced drag damping is very effective at and near resonance in reducing the structural longitudinal displacements; (ii) The percentage of reduction depends on the magnitude of response in the resonant region; and (iii) At frequencies away from the resonant frequency the device becomes less effective and does not cause any adverse effects on the structure.

8.2 Experimental Investigation

All the foregoing discussions have been concerned with the analytical model and the consequent simulation study. Though the study clearly shows the effect of the induced flow-separation, experimental verification of this effect is of paramount

importance to this thesis. In the experimental evaluation, on the dominant effect of induced drag damping, only regular waves are considered. This is due to the fact that the damping is response-dependent and its effect in a random wave environment cannot be studied unless the same exact random wave time series can be generated from experiment to experiment.

Physical behaviour of the model structure is highly complicated and it is practically not possible to include all the effects in the computer model, although their sources are well known. In the previous chapter we have seen excellent agreement between theory and measurements. This is mainly due to the fact that the hydrodynamic coefficients were obtained for the same geometry and wave environment from a separate force measuring experiment and are then used in the computer model. In spite of that we also noticed a small disagreement between measurement and prediction at resonance. This is obviously due to the inherent increase of damping in the physical model structure. When the structure is without the device, the drag forces are very small and the behaviour of the structure is almost linear with wave height. The instant the device is introduced, into the system, there is a considerable increase in drag forces which causes the structure to behave in a nonlinear fashion. We have incorporated the effect of the device in the computer model by using appropriate hydrodynamic coefficients. The important factor which must be mentioned here is that such increased drag coefficients for the device, were obtained only for a fixed cylinder in the small wave tank. However at resonance, there is a large dynamic amplification of response which causes large motions in the model structure. Under these conditions the behaviour of fluid flow, due to the attached device, will be different from the fixed cylinder. In order to predict the exact effect of the device, by analytical means, the C_m and C_d values must be obtained for a cylinder (with the device) oscillating with large structural motions. Such an investigation, of course, is very important to this research, but was not carried out due to

the limitation of time and many other factors, involved in this research. Therefore the hydrodynamic coefficients obtained for the fixed cylinder, with the device, are used herein and the measured deck acceleration responses are compared with the theoretical results.

In this section, two types of comparisons are made. First, the measured deck accelerations are compared with the theoretical predictions for the structure with the device. Secondly, comparison is also made between the measured deck acceleration responses of the structure, with and without the device, for the same wave conditions.

8.2.1 Comparison of Results: Experiment vs Theory

From the data-reduction, available in the present study, three different experimental results are selected. Fig. 8.7 presents the measured deck acceleration response for a wave height of 0.1089 m and a wave period of 1.39 s ($H_p = 5.45$ m and $T_p = 9.83$ s). Note that the wave period 1.39 s is close to the fundamental natural period of the structure (1.35 s). With the values of C_m equal to 2.03 and C_d equal to 9.39, the time-domain response prediction was carried out for regular waves. The dashed line in Fig. 8.7 shows the predicted deck acceleration response, whereas the solid line shows the measured response of the structure with the device. Both the measured and predicted responses are in phase with one another. The magnitude of the measured response is much lower than the predicted one. Two obvious reasons may be presented here for this large reduction seen in Fig. 8.7. Firstly (as discussed in the previous chapter), even for the structure without the device, the theory slightly overpredicted the measured response, at frequencies around resonance. This is due to the tendency of the structure, to dissipate more energy at resonance, and thus the magnitude of damping in the physical structure increases considerably. In the computer model only a constant magnitude of damping is considered for all

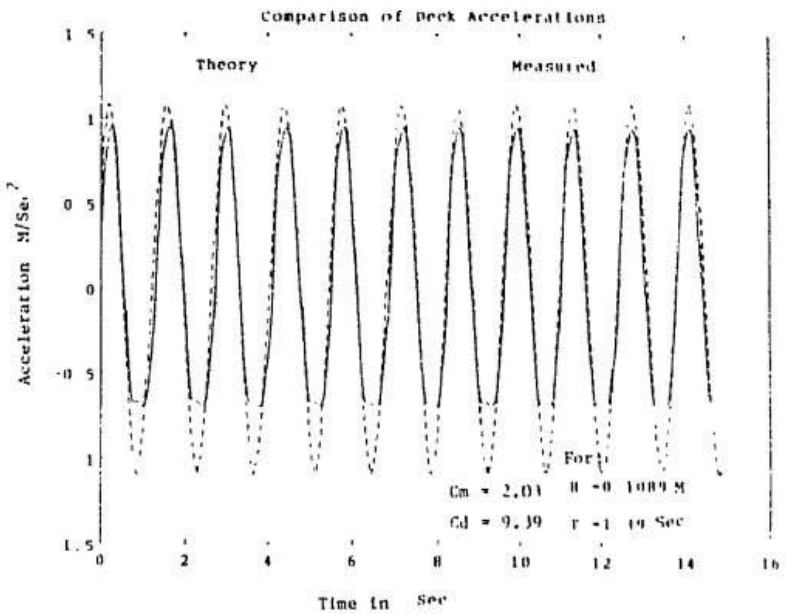

Figure 8.7: Comparison of deck longitudinal accelerations for regular waves (with device): experiment vs theory

motions and frequencies. Secondly, the hydrodynamic coefficients obtained from the first experiments are valid only for a fixed cylinder. However in the present set of experiment, the oscillating structure with the attached device, has much larger flow-separation than the fixed cylinder. Thus larger drag damping forces are experienced in the present experiment than what the theory has incorporated in the analysis.

In the second test the wave period T (1.39 s) was kept the same and the wave height H was increased to 0.122 m. Similar comparison between theoretical predictions and measurements are presented in Fig. 8.8. Again the magnitude of the measured response is much smaller than the predicted response. An interesting behaviour which can be observed, by comparing Figs. 8.7 and 8.8, is that for the same wave frequency the magnitude of the theoretical response has increased from 1.073 m/s^2 to 1.254 m/s^2 for an increase in wave height from 0.1089 m to 0.122 m. Thus a 16.8% increase is seen from the theoretical side. However if one compares the mea-

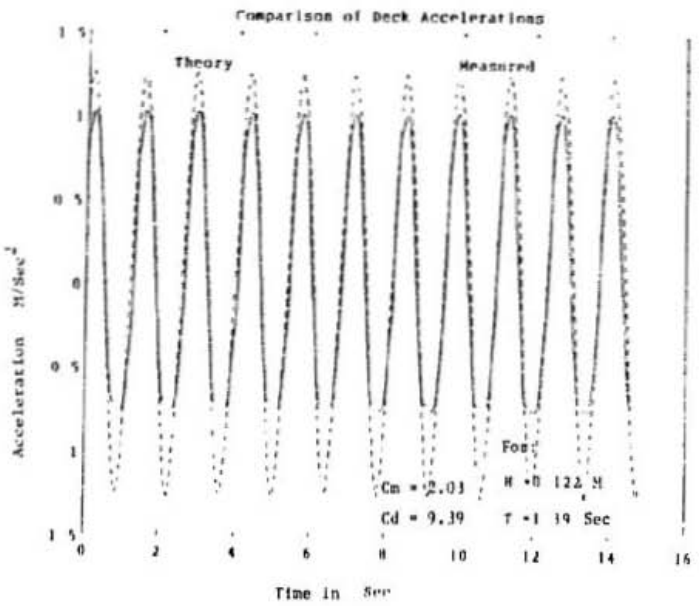

Figure 8.8: Comparison of deck longitudinal accelerations for regular waves (with device): experiment vs theory

sured response between Fig. 8.7 and Fig. 8.8, the magnitude of measured response has increased from 0.965 m/s^2 to 1.02 m/s^2 which gives only a 8.6% increase in the response which is only half the value of what was obtained by theoretical means. **This clearly shows that around resonance, as the wave height increases, the effectiveness of the device in increasing the drag damping forces also increases.** Thus the magnitude of induced damping forces increase not only with the magnitude of the structural response but also with the wave height.

In the third comparison, the frequency of the wave was increased from 0.72 Hz to 0.75 Hz, with a wave height of 0.111 m: the predicted and measured responses are presented in Fig. 8.9. In this case also, large deviations between the theory and measurements are obtained. From these results, it is clear that the magnitude of the induced damping experienced in the physical structure is much higher than the one incorporated in the computer model. The large motion of the structure increases

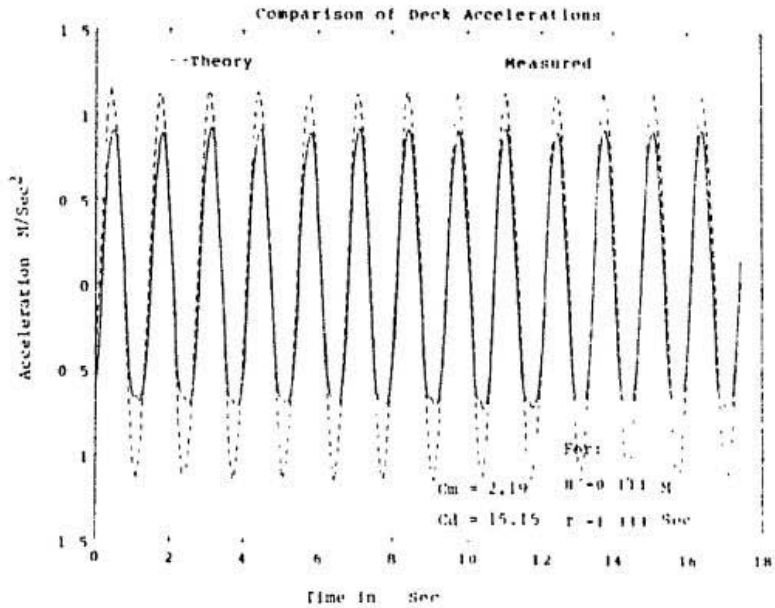

Figure 8.9: Comparison of deck longitudinal accelerations for regular waves (with device): experiment vs theory

the effectiveness of the device by inducing larger flow-separation than the case of the fixed cylinder. **Hence the theory underestimates the effectiveness of the induced drag damping, due to a lack of knowledge about the wave drag coefficient for the oscillating structure (with the attached device).**

8.2.2 Comparison Between the Measured Responses of the Structure: With and Without the Device

First we examined some of the characteristics of the induced drag damping based on the theoretical predictions. Secondly we noted the inability of the theory to include the complete effect of the induced damping. The only way in which we can examine the actual effect of the induced damping is by comparing the responses from two different tests, viz., one with the device and one without the device, for the same wave parameters. In Fig. 8.10, the two measured deck acceleration responses, with and without the device, are compared for the case of regular waves of height equal

to 0.113 m and period equal to 1.333 s. The dashed line indicates the response of

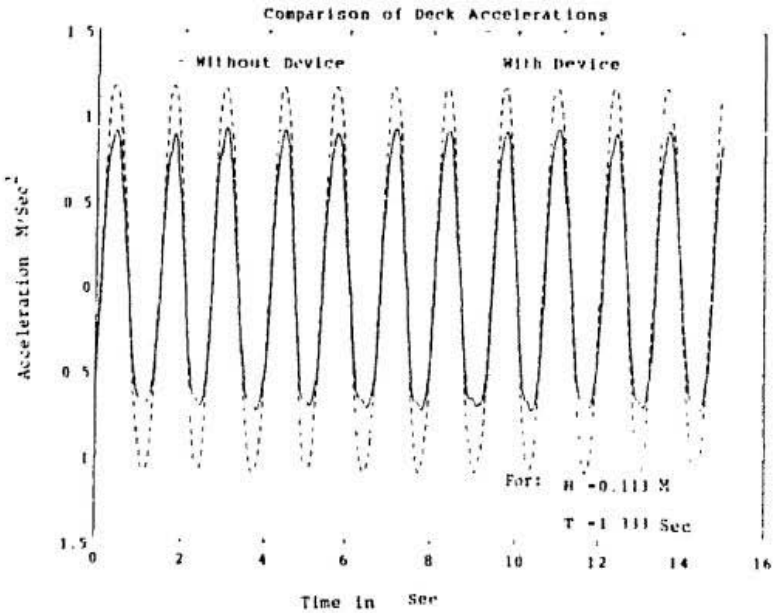

Figure 8.10: Comparison between the measured deck longitudinal accelerations for regular waves: with and without the device

the simple structure and the solid line indicates the structural response, with the device in place. They both are in phase with one another. The magnitude of the response with the device, has been drastically reduced due to the influence of the device. The peak longitudinal acceleration of the structure without the device is 1.164 m/s^2 and that with the device 0.909 m/s^2; a 21% reduction in response is observed due to the additional induced damping, while in the theoretical evaluation only a 16% reduction was obtained. This clearly shows that the physical damping induced by the device is much more than the one incorporated in the theory.

At this stage, it must be mentioned that the experimentation carried out in this investigation on the influence of induced drag damping has never been reported in the literature before; and the excellent results obtained from this study seem to indicate that this procedure could be beneficially used in the design of offshore

structures to increase fatigue resistance. Not many studies in the literature (except Dunwoody and Vandiver, 1987) have explicitly defined the effect of the drag damping on the dynamic response of an offshore structure. Mostly its effect was explained in the theory, only by considering the relative velocity formulation in the drag force term of Morison's wave force formula. From this one can understand only the source and the physics of the drag damping phenomena which exists in offshore structures. In the literature the presence of this type of damping has not been explained explicitly. By comparing the measured responses of two model offshore structures, one with induced flow-separation and one without flow-separation, we could see the effect of this damping. In this aspect this research is first of its kind which has demonstrated the existence of large response reduction due to drag damping in a fixed offshore structure.

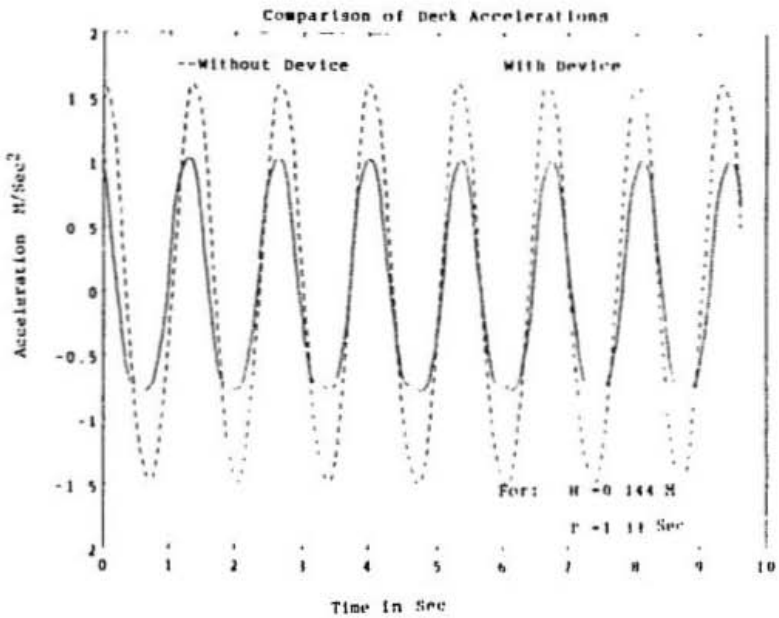

Figure 8.11: Comparison between the measured deck longitudinal accelerations for regular waves: with and without the device

In the previous subsection the effect of the device was found to increase with an

increase in the magnitude of response. Now it is interesting to see what will happen if the wave height is increased for the same wave period. One such test was carried out with a wave height H of 0.144 m (H_p = 7.2 m) and wave period T of 1.33 s (T_p = 9.4 s). The comparison of results between the measured responses, with or without the device, is given in Fig. 8.11. A large reduction in the response magnitude can be noted due to the device. In Fig. 8.11, the maximum deck longitudinal acceleration, with the device, is found to be 1.05 m/s^2 while for the structure without the device it is found to be 1.52 m/s^2. Hence for a larger wave height, the introduction of the device has resulted in a response reduction of 32%, which is quite large in comparison with the earlier 21% that has been obtained in Fig. 8.10.

The other noticeable effect which can be seen in the cases of the measured deck acceleration response (in Figs. 8.8 to 8.11) is that the troughs of the time traces are not regular when the device was attached. The reasons for this behaviour are: (a) the significant transverse response of the structure around in-line resonance; (b) the large induced drag damping which is nonlinear in terms of the response of the structure. It should be pointed out here that the large flow-separation induced by the device also generates significant transverse forces. The other possible reason is the turbulence effect of the flow field around the cylinder (when the device was attached). This was not noticed in the case of the simple structure because the magnitude of the drag forces were very small.

8.3 Summary

Before ending this chapter, it may be worthwhile to highlight some of the important conclusions derived from the numerical and experimental results presented in this chapter.

It has been established in the previous chapter that the structure behaves in a compliant manner to waves around resonance. Under such conditions, it is very

useful to use damping as an effective tool to control the response. The magnitude of the separated-flow drag force damping was found to be very small in the structure, due to the behaviour of the oscillatory flow at low KC numbers. With the help of the wave force measurement study given in chapter 3, a device was designed to introduce flow-separation for waves of moderate amplitudes in the laboratory environment. In this chapter the effect of this device in controlling the near resonant response has been investigated by theoretical and experimental means. From the theoretical and experimental investigations, the following salient conclusions are derived.

The presence of the device induces additional drag damping and reduces the magnitude of the deck longitudinal acceleration in the resonant region. This is shown to occur for both regular and random waves. It is found that the effect of the induced damping increases as the magnitude of structural response increases. Another important point is that the device is found to be ineffective for waves with frequencies away from the resonant frequency region. Hence, no adverse effect is seen to occur to the structure due to the presence of the device.

It was observed in the theoretical response study that the transient response of the structure was significantly larger with the device than the case of the simple structure. However its amplitude did not exceeded the amplitude of the study state response of the structure without the device (see Fig 8.1). Also the duration of the transient response was only 3 to 4 cycles and its effect in this region can be neglected while considering the large reduction in stress level in the steady state response which will be in the order of thousands of cycles in the real ocean. Thus the device is definitely very useful for the damping application to increase the fatigue life of the structure.

It is observed that at resonance the large motion of the structure increases the flow-separation due to the presence of the device. Thus the magnitude of damping, experienced in the physical structure, is much larger than the one incorporated in

the theory. **This is mainly due to the predicted theoretical results being based on the hydrodynamic coefficients obtained from a fixed cylinder in an oscillatory wave flow. Hence a larger reductions in the magnitude of response, than anticipated from theoretical evaluations, is obtained when the device is used in the experiments.** It is found that the magnitude of the induced damping not only increases with the magnitude of structural response but also with the wave height. In the final study which compared the deck longitudinal acceleration for the cases with and without the device, a large reduction in the magnitude of response, up to 32% was obtained. Thus it is clear that the damping induced by the flow-separation device is very effective in reducing the structural response at and near resonance.

The effect of the induced drag damping on the fatigue life of the structure is quite significant while considering the moderate waves and resonant excitation. Vandiver (1982) estimated (in the analysis of a fixed offshore structure for similar condition) that if the damping is underestimated by a factor of 2 it would corresponds to an overestimate of the fatigue life by a factor of 4.12. Considering this fact, one could easily visualize the significant effect of the damping on the fatigue life of the structure. Thus a 32% reduction in the response, and the consequent decrease in stress level, will increase the fatigue life of the structure by four to five times.

Chapter 9

Conclusions and Recommendations

This investigation has demonstrated the feasibility of controlling the near resonant response of a fixed deepwater platform by means of inducing flow-separation, on the central column near the free surface. The concept of inducing drag damping was restricted to a class of structures with large diameter circular members (around 15 m diameter), which are dynamically sensitive to moderate waves. Despite several physical possibilities which exist for dissipating energy through the surrounding media, unfortunately, the total damping in these structures is negligibly very small. In the light of low damping and resonant oscillation, this study has undertaken an innovative approach, a first of its kind, to increase the damping in the fluid-structure coupled system.

Two experimental investigations were carried out. In the first experimental study, the wave forces on a 0.3 m diameter vertical circular cylinder, which simulated the central column of the deepwater tripod tower platform, were measured. The study has developed a physical device to increase the drag forces by means of inducing flow-separation on a circular cylinder for an oscillatory flow at low Keulegan-Carpenter numbers. For the second experiment, a reduced scale (1:50) hydroelastic model of the tripod tower platform was fabricated and tested in lab-

oratory simulated waves. Apart from these experimental investigations, the study also carried out numerical computations to examine the dynamic behaviour of the model structure to modelled waves. A finite element method was used and the dynamic equations of motion formulated by defining the mass, damping and stiffness properties of the model structure. In order to incorporate the effect of the induced drag damping in the analytical model, a modified Morison's formula was used and the wave exciting forces were corrected for structural motions. Both hydroelastic model testing and analytical methods were used to investigate the effect of the device on the near resonant response of the model structure. In this chapter the important findings and conclusions of this study are summarized.

9.1 Conclusions

Effect of the Device on C_m and C_d

1. The method used for the wave force measurements, described in chapter 3, is a new technique and is very accurate if one is interested in measuring the total forces on a large diameter vertical cylinder.

2. The experimental study, undertaken for predicting the wave forces for regular and random waves, suggests that the behaviour of the vertical cylinder for an oscillatory wave flow at low KC numbers must be treated as a special problem and should not be misinterpreted based on the previous results obtained for a wide range of KC numbers. This means that if one is interested in the behaviour of a vertical cylinder at low KC numbers (≤ 4), then the experiment must be conducted only for that small range of KC number using large diameter circular cylinders (diameter ≥ 0.3 m). This conclusion is not only evident from the large value of C_d obtained for the circular cylinder in this treatise but also clear from the results given in the recent literature in related studies.

3. The general trend of increase in the C_d value with the decrease in KC , within a small range, (for example C_d for KC = 1.28 is 0.87 while for KC = 0.95 it is 4.1), shows that the C_d is sensitive to even a small change in the KC number at low KC numbers while the value of C_m is not.

4. The hydrodynamic coefficients did not exhibit any appreciable relationship with the R_e number within this small range.

5. The relationship between the mechanism of vortex formation and Keulegan-Carpenter number is very clear when the drag component of the wave force is compared with the inertial component of the wave force and the total wave force. (Although the C_d values obtained look larger, the total drag forces on the cylinder compared to the inertial forces were small.) The value of the maximum drag force was only 10 to 16% of the value of the maximum inertial forces while the inertial force were almost equal to the total forces exerted by the waves on the cylinder. The generation of vortices behind the cylinder is prevented in the oscillatory flow when the KC numbers for the flow is very small. Thus the drag forces on the cylinder are very small and the inertial forces dominate the total forces. This point was also physically observed from the flow pattern behind the circular cylinder in the wave tank (see Fig. 3.25).

6. The C_d value for the random waves is also very sensitive to the changes in the KC number while the value of C_m is not.

7. It is feasible to induce flow-separation on a circular cylinder at low KC numbers. If the flow-separation is induced artificially at low KC numbers, then the new system behaves contrary to a regular (or simple) circular cylinder. A drastic increase in the drag forces can be observed.

8. The designed flow-separation device is very efficient in inducing flow-separation

on a circular cylinder, at low KC numbers, without increasing the added mass of the cylinder. This means that the device is designed for adequate flow transparency and hence does not entrap any fluid mass in the bundle.

9. The device functions in two ways, first by generating local vortices behind the diamond tubes (due to large values of the local KC number ≥ 15), and second by initiating flow-separation on the main cylinder which induces global vortices behind the main cylinder. This can be seen from the photograph of the flow pattern behind the cylinder in the wave tank shown in Fig. 3.26. As a result of the generation of the vortices, both local and global, the width of the wake behind the main cylinder also increases.

10. At low KC numbers (≤ 2), the device increased the value of the drag coefficient (for regular waves) by a factor of 4, irrespective of the wave height and frequency. However the device did not significantly increase the value of the inertial coefficient of the main cylinder.

11. The C_d value for the cylinder, with the device, is also very sensitive to changes in the KC number and increases as KC number decreases, similar to the case of the simple cylinder, in regular waves.

12. Due to the attachment of the device, the maximum drag forces on the cylinder became 60% of the maximum wave force while without the device it was only around 15%. Thus the device can significantly increase the drag force on a large diameter circular cylinder at low KC numbers, without any noticeable increase in the inertial force in regular waves.

13. Out of the total increase in the drag forces, 81% of the increase was due to the induced separation effect on the cylinder by the device in regular waves. The device exerted, by itself, only 19% of the drag force in the total increase.

Hence it can be concluded that the flow-separation device is very effective in increasing the drag forces on an inertial force dominated cylinder, at low KC numbers.

14. The flow-separation device is equally effective in inducing drag forces for random waves. The device increased the drag forces by a factor of 5, while the inertial forces were not much affected by the device. In general, the increase in the value of the drag coefficient was found to be larger than the case of the regular waves where the value of C_d increased only by a factor of 4.

Hydroelastic Model

1. It is feasible to construct a hydroelastic model without violating the model laws provided the wave loading on the structure is dominated by the inertial component of the wave forces. Under such conditions, it can be demonstrated that the physics of the loading and the elastic properties are adequately represented in laboratory scale model of geometric scale 1:50. The experimental results are reliable because both the loading mechanism and the elastic behaviour are well represented in the fabricated model.

2. The size of the model (8.6 m high) and the water depth used (7.0 m deep) represent the situation of a large offshore structure, operating in a deepwater environment (350 m). Hence, an investigation of the dynamic response of the tower, to laboratory generated waves, is very useful considering the developments taking place in the deepwater offshore oil fields.

Dynamic Testing

1. Modal testing is a very accurate method that could be used to identify the modal parameters of the structure. However, in order to get a smooth fre-

quency response function, averaging of a large number of samples must be used. The averaging improves the statistical reliability of the estimation of the modal parameters determined from the frequency response functions.

2. Although the modal testing method gives the best estimate for the modal parameters, the estimated parameters obtained from the pluck test are also observed to be equally good. For the minimum deck mass case the natural frequency obtained from the modal test was 1.615 Hz while the pluck test estimated it to be 1.605 Hz, with an error of 0.62%. Similarly the damping ratio obtained from the modal testing was 6.08%, whereas the one obtained from the pluck test was 5.65% showing a 7% error in the estimation. Unless an investigator is interested in obtaining the parameters for the higher modes of vibration, modal testing is not highly essential; the results of the pluck test are quite adequate for the subsequent analysis.

3. The conventional logarithmic decrement method is not adequate for the analysis of the free decaying response. The Nelder-Mead simplex algorithm which takes into account all the data points in the time history of response is required to precisely estimate the natural frequency and the damping ratio.

4. The modal parameters are very sensitive to the deck mass variation. When the deck mass was increased from 39 kg to 140 kg (in air test), the natural frequency and the damping ratio were reduced from 1.605 Hz to 0.7691 Hz, and 5.65% to 4.65%, respectively.

5. The natural frequency of the structure is not very sensitive to the added mass of the fluid but the damping ratio is sensitive to the surrounding fluid. The natural frequency of the structure in the air test (with maximum deck mass condition) was 0.77 Hz, while in water it decreased to 0.74 Hz. However

significant increase in the damping ratio was seen due to the surrounding fluid (from 4.65% in air to 5.9% in water).

6. The damping ratio, obtained from the dynamic tests, is a relatively large value which certainly does not represent the prototype situation. This is due to the fact that the acrylic plastic material used for the construction of the model has larger structural damping than a steel material used for the prototype. Due to this, although the model structure can simulate the resonant condition similar to the prototype situation, the magnitude of responses will not be as severe as in the prototype.

Modal Extraction

1. The fundamental frequencies in the transverse directions were very close to the corresponding longitudinal values. The first bending mode frequency in the transverse direction was 0.732 Hz while the longitudinal one was 0.73 Hz.

2. The higher modes of oscillation in the longitudinal direction were well separated. The first bending mode frequency in the longitudinal frequency was 0.73 Hz while the second bending mode frequency in the same direction was 2.74 Hz.

Nonlinear Dynamic Model

1. The effect of fluid-structure interaction can be included in the mathematical model by considering the relative velocity formulation in the drag term of Morison's formula. Thus the motion of the structure relative to the fluid results in a damping effect in the mathematical model. When the velocity of the structure is comparable in order of magnitude to the fluid particle velocity, the fluid-structure interaction must not be ignored.

2. The analytical study also included the effect of radiation damping on the structure due to wave exciting forces. The radiation damping ratio for the first three modes were 0.29%, 0.13% and 0.08% of critical damping, respectively; while the free vibration damping in the water was 5.9%. Thus the radiation damping in the structure was very small.

3. From the response analysis study, the following conclusions can be derived. Waves at high frequency above 1.5 Hz (in the laboratory scale) were unable to excite the higher modes of oscillation of the structure. Only the first fundamental bending mode frequency (0.73 Hz) was excited by the random waves. Two peaks were identified in the response spectrum, one corresponding to the wave peak frequency and the second corresponding to the resonant frequency. When the wave frequency coincided with the natural frequency, a large single peak response, with a narrow band spectrum, was observed.

Response Near Resonance

1. A significant magnitude of response may appear in the transverse direction during resonant oscillation in the longitudinal direction if the two natural frequencies are very close. In regular wave tests, 27% of the magnitude of the longitudinal response was observed in the transverse direction. However the transverse response diminished to very small values for frequencies away from resonance. No significant torsional response was observed when the structure was subjected to resonant excitation in the wave direction.

2. At resonance in regular waves, the physical structure experiences higher damping than in the analytical model. In a comparison between the predicted acceleration with the measured acceleration, the magnitude of the predicted responses was 3 to 7% higher than the measured values. However in situations

away from resonance, the theory slightly over predicted due to the existence of greater damping in the physical model (at resonance) than that used in the mathematical model.

3. As the exciting frequency of the regular waves moves away from resonance the amplitude of response decreases sharply. In the regular wave experiments, when the wave exciting frequency moved 7% away from resonance, the amplitude of response reduced by 23%.

4. Again, for the case of random waves, the magnitude of the measured response at resonance was less than that of the prediction which emphasizes the previous conclusion that the magnitude of damping in the physical model is larger than that in the theoretical model, around resonance.

5. It is difficult to excite the higher modes with the waves, because not much energy content is available at those frequencies. In the experiment no significant peak in the random wave response was observed at frequencies above 1.5 Hz. Although the wave energy at frequencies below 0.5 Hz was significant, the structure behaved in a quasi-static manner and the magnitude of response was found to be very small compared to the values near resonance.

6. The above conclusions indicate that the structure behaved in a stiff manner to wave frequencies away from resonance. Conversely, it behaved in a compliant manner to waves, at resonance.

Effect of Induced Drag Damping

1. The induced drag damping is very effective at or near resonance in reducing the structural response. In the analytical study, the magnitude of the responses was observed to reduce from 7 to 11%, for the random wave conditions and 16% for regular wave conditions.

2. The percentage reduction in response depends on the magnitude of response in the resonant region. This is evident from the study in which the free vibration damping was assumed to be the same as the prototype situation (2% of critical damping). Here a greater reduction in the structural response, 27%, was observed due the effect of the flow-separation device. Thus the flow-separation device becomes more effective as the amplitude of the response becomes larger and larger.

3. At frequencies away from resonance the device becomes ineffective.

4. With the device in place the oscillating structure experienced larger drag forces and consequently larger damping in the physical model than the analytical one.

5. With the device in place, a large reduction of 21% in the measured longitudinal acceleration response was observed for a wave height of H = 0.113 m and period T = 1.33 s. This shows that the theory underestimated the effectiveness of the device. A correct estimation can be made only if the Cm and Cd values for an oscillating cylinder with the device are obtained from experiments.

6. As the wave height increases the effectiveness of the device also increases in the resonant region. In the experimental study, when the wave height was increased to 0.144 m and the wave period was set at 1.33 s, the magnitude of the measured response reduced by 32% due to the attachment of the device to the physical structure.

7. As an overall assessment, the study has demonstrated that the induced drag damping generated by the proposed device is very effective in reducing the resonant response of a deepwater structure whose main component is a vertical circular cylinder and the loading on the structure is dominated by the inertial component of the wave forces.

9.2 Contribution

This treatise has contributed to the field of offshore structures by carrying out an innovative method to control the resonant response of a deepwater platform. Many of the studies carried out in this thesis are new and they have not followed explicitly those already available in the literature. The aspects of the study which are considered to be new are listed below:

- A test was performed using an 8.6 m high hydroelastic model of a fixed offshore platform (tripod tower platform), one of the largest models fabricated in a university environment. Although the use of a hydroelastic model is not new in the literature, often only structures which were dominated by the drag forces were modelled in which case the physics of the loading were not according to the similitude relationships. However in this thesis, both the physics of loading and the elastic properties are in one-to-one correspondence to the prototype. The design, fabrication, transportation and installations were some of the major tasks of this thesis one could rarely imagine carrying out in a university environment.

- Modal testing of an offshore structural model was performed to estimate the modal parameters. Although modal testing is a powerful method for estimating the natural frequency and the damping ratios of a structure, obtaining a smooth frequency response function is a tough procedure and care must be exercised in the choice of the type of test that should be used for the particular structure and situation. A large number of spectral averages is required to improve the statistical reliability of estimation.

- One of the unique features of this treatise is that the hydrodynamic coefficients were determined experimentally, and were used in the structural response prediction analysis. Then the predicted response was compared with

the measured response of the model structure. Also note that the analytical model also incorporates the realistic damping obtained from measurement on the physical model. This type of realistic dynamic analysis has not been reported in the literature earlier.

- In the random response analysis the predicted structural response was compared with the measured random response in the time domain. Excellent agreement between, both the magnitude and phase, is observed. It should be noted that for the case of random waves it is always customary to compare results in the frequency domain with power spectral densities.

- Avoiding the occurrence of resonance for all operating conditions is uneconomical in the design of offshore structures for deepwater applications. Considering this situation numerous studies have focused on the phenomena of resonance using analytical approaches. However no detailed study has been reported on the physical behaviour of the structure under resonant excitation of waves. This thesis has investigated the resonant physical behaviour of an offshore platform model to laboratory generated waves.

- Finally the response near resonance was controlled by inducing drag forces on an inertial force dominated structure. This is an innovative technique which can be applied to many new structural concepts such as tension leg platforms, semisubmersibles and monotower platforms.

9.3 Recommendations

Occurrence of resonance is unavoidable under all operating conditions. When the wave forces on the structure are dominated by the inertial component of wave loading the hydrodynamic damping in the system is low. It is well known that the structural response reduces if energy can be dissipated through the fluid media in

the form of flow-separation. It can be stated here that the thesis has clearly demonstrated a feasible solution to the defined problem with elaborate experimental and analytical procedures. Despite such large efforts, undertaken in this study, some of the practical questions still remain unanswered. Although the concept of inducing flow-separation at low KC numbers has been successfully applied to a physical model, more understanding can be had if the experimental procedures are repeated for different situations and structures. The following suggestions are recommended for future studies on the related area:

- The wave force measuring experiment, carried out to investigate the effect of the device on the hydrodynamic coefficients, was only for a fixed cylinder. More interesting findings can be obtained if the experiment is repeated for an oscillating cylinder and the hydrodynamic coefficients determined. Also note that the C_m and C_d values were obtained for the complete 3-dimensional cylinder. The new experiment can attempt to find the C_m and C_d values for a 2-dimensional section by instrumenting at a localized part of the cylinder. Thirdly the experiment conducted in this treatise attached the device to the test cylinder. Hence it was not possible to directly assess the induced effect of the device. The future investigators can try to support the device separately and study the induced effect of the device on the hydrodynamic coefficients.

- The second important extension study, in connection with the C_m and C_d coefficients, is that the experiment should be carried out for a large number of wave conditions so that the investigator can try to obtain a smooth relationship between the hydrodynamic coefficients and the KC number. Such results are very useful for the design of the prototype structure, when the device is to be used. Limited tests were carried out in this thesis, since more attention was paid to the design and the selection of the appropriate device for the structure

by repeating the experiment for different types of device configuration. Although many previous studies have demonstrated that the effect of Reynolds number is insignificant at low KC number while considering a simple circular cylinder, a U-tube study is recommended to investigate the effect of Reynolds number on the circular cylinder with the device attached. Since the device induces large separation, Reynolds number may have some significant effect on the cylinder with the device.

- Modal testing techniques are a superior means of finding the modal parameters. However in this thesis no effort was made to identify the modal parameters for higher modes of vibration, using this technique. A more powerful excitor can be used and the higher modes excited; in addition if an array of accelerometers are installed along the height of the model structure, then the mode shapes also can be estimated from the measured frequency response function obtained for each location. These functions can be used, later on, to correct the model developed by analytical means. If the above investigations are performed one can be sure of obtaining an excellent agreement between the predicted and measured responses of the structure.

- Finally, some comments should be made here regarding the general applicability of the new technique developed for this research study. Many offshore structures possess large diameter circular members. They are also subjected to resonance oscillations due to environmental waves during the operational phase. For example, springing can seriously damage the tendons of a tension leg platform. Similarly, low frequency surge resonance has been proved to be present in both tension leg and semisubmersible platforms. The new generation concepts, yet to be published in the literature, may also have these similar problems. It would be interesting to investigate the feasibility of controlling

the response of these structures using similar concepts discussed in this thesis. The configuration of the device may be modified according to the type of structure and application. For example resonance in the vertical mode can be controlled by a simple ring type of device. There is certainly a need for potential research on this newly conceptualized innovation.

References

1. Andrier, B., et al., Roseau: a deep water platform. *Proceedings of the Offshore Technology Conference, Houston, Texas, 1986*, OTC 5256, pp. 299–307.

2. ANSYS, Engineering analysis system user's manual, *Swanson Analysis Systems, Inc., Houston, Texas, 1987*, pp. 4.59.1–4.59.14.

3. API-RP-2A, Recommended practice for planning, designing and constructing fixed offshore platforms, *American Petroleum Institute, Dallas, Texas, 1990.*

4. API-RP-2T, Recommended practice for planning, designing and constructing tension leg platforms, *American Petroleum Institute, Dallas, Texas, 1987.*

5. Basu, A. K., and Singh, R. P., Time-domain versus frequency-domain solution of steel jacket platform, *Proceedings of the First Indian Conference in Ocean Engineering, IIT, Madras, 1981*, vol. II, pp. 8–13.

6. Bathe, K. J., and Wilson, E. L., *Numerical Methods in Finite Element Analysis*, Prentice-Hall of India Pvt. Ltd., New Delhi, 1976, pp. 338–343.

7. Bearman, P. W., Wave loading experiments on circular cylinders at large scale, *Proceedings on Behavior of Offshore Structures, Trondheim, 1988*, Vol. 3, pp. 471–487.

8. Bearman, P. W., Downie, J. M. R., Graham, J. M. R., and Obasaju, E. D., Forces on cylinders in viscous oscillatory flow at low Keulegan-Carpenter

numbers, *Journal of Fluid Mechanics*, 1985, Vol. 154, pp. 337-356.

9. Berge, B., and Penzien, J., Three dimensional stochastic response of offshore towers to wave forces, *Proceedings of the Offshore Technology Conference, Houston, Texas, 1974*, OTC 2050, pp. 299-307.

10. Blevins, R. D., *Flow-Induced Vibrations*, Van Nostrand Reinhold Co., New York, 1977, pp. 119-145.

11. Borgman, L. E., Spectral analysis of ocean wave forces on piling, *Journal of the Waterway, Port, Coastal and Ocean Division*, ASCE, 1967, Vol. 93, No. WW2, pp. 129-156.

12. Borgman, L. E., Ocean wave simulation for engineering design, *Journal of the Waterway, Port, Coastal and Ocean Division*, ASCE, 1969, Vol. 95, No. WW4, pp. 557-583.

13. Borthwick, A. G. L., and Herbert, D. M., Resonant and non-resonant behaviour of a flexibly mounted cylinder in waves, *Journal of Fluid Mechanics*, 1990, Vol. 4, pp. 495-518.

14. Bostrom, T., and Overvik, T., Hydrodynamic force coefficients in random wave conditions, *The 5th International Conference on Offshore Mechanics and Arctic Engineering, Houston, Texas, 1986*, pp. 136-143.

15. Buslow, V. M., Deep water platform designs: an illustrated review, *Ocean Industry*, February, 1986, pp. 53-62.

16. Burke, B. G., and Tighe, J. T., A time series model for dynamic behaviour of offshore structures, *Society of Petroleum Engineers Journal*, 1972, Vol. 20, pp. 5-14.

17. Campbell, R. B., and Vandiver, J. K., The estimation of natural frequencies and damping ratios of offshore structures, *Proceedings of the Offshore Technology Conference, Houston, Texas, 1980*, OTC 3861, pp. 53-61

18. Chakrabarti, S. K., In-line forces on fixed vertical cylinder in waves, *Journal of the Waterway, Port, Coastal and Ocean Division*, ASCE, 1980, 102, No. WW2, Vol. 106, pp. 145-155.

19. Chakrabarti, S. K., Hydrodynamic coefficients for a vertical tube in a array, *Dynamic Analysis of Offshore Structures - Recent Developments*, (Editor: C. L. Kirk), Gulf Publishing Company, Houston, Texas, 1982, pp. 70-80.

20. Chakrabarti, S. K., *Hydrodynamics of Offshore Structures*, Computational Mechanics Publications, Springer-Verlag Berlin Heidelberg, New York, 1987, pp. 122-124.

21. Chakrabarti, S. K., Forces on vertical cylinder due to random waves, *Journal of the Waterway, Port, Coastal and Ocean Division*, ASCE, 1988, 102, WW2, Vol. 114, No. 3, pp. 267--280.

22. Chakrabarti, S. K., Hydrodynamic damping tests for vertical TLP leg model, *Marine Research Newsletter, CBI, Chicago, 1989*, Vol. 4, No. 2, pp. 1.

23. Chakrabarti, S. K., Added mass and damping of TLP column model, *Proceedings of the Offshore Technology Conference, Houston, Texas, 1990a*, Paper No. OTC 6406, pp. 559-571.

24. Chakrabarti, S. K., *Nonlinear Methods in Offshore Engineering*, Elsevier, New York, 1990b, pp. 110-169.

25. Clough, R. W., and Penzien, J., *Dynamics of Structures*, McGraw-Hill, New York, 1975, pp. 191-207.

26. Cook, M. F., and Vandiver, J. K., Measured and predicted dynamic response of a single pile platform to random wave excitation, *Proceedings of the Offshore Technology Conference, Houston, Texas, 1982*, OTC 4285, pp. 637–646.

27. Craig, Jr., R. R., *Structural Dynamics: An Introduction to Computer Methods*, John Wiley & Sons, New York, 1981, pp. 49–77.

28. Davies, P. G., *Wave Loading on Vertical and Inclined Cylinders*, M.Eng. Thesis, University of Liverpool, UK, 1976, pp. 32–41.

29. Dawson, T. H., *Offshore Structural Engineering*, Prentice-Hall, New Jersey, 1983, pp. 287–290.

30. Delacour, J., *Oil & Enterprise*, No. 21, April 1985, pp. 65–73.

31. Dennis, Jr., J. E., and Woods, D. J., New computing environments: Microcomputers in large-scale computing, (Editor:Wouk), *SIAM*, 1987, pp. 116–122.

32. Duncan, D. A., Vander, H., The first tripod tower platform (TTP): design, installation, operation and economic viability, *Proceedings of the Offshore Technology Conference, Houston, Texas, 1987*, OTC 5542, pp. 501–512.

33. Dunsire, R., and Oven, D. G., Model tests of TLP systems, *3rd Offshore Mechanics and Arctic Engineering Symposium, 1984*, Vol. 1, pp. 20–31.

34. Dunwoody, A. B., and Vandiver, J. K., The influence of separated-flow drag on the dynamic response of offshore structure to random waves, *International Symposium on Hydrodynamics in Ocean Engineering, The Norwegian Institute of Technology, Trondheim, 1981*, Vol. 1., pp. 263–285.

35. Dunwoody, A. B., and Vandiver, J. K., Wave-induced damping of offshore structures, *Proceedings of the Offshore Technology Conference, Houston, 1987*, OTC 5412, pp. 453–459.

36. Earl, C., and Silva, T. M., Deep water fixed steel platforms, *Offshore Engineering Group International Symposium on Developments in Deep Waters, The Royal Institution of Naval Architects, London, October, 1986*, Vol. 1.

37. Ewins, D. J., *Modal Testing: Theory and Practice*, Research studies press ltd., Letchworth, Hertfordshire, England, 1986, pp. 158-195.

38. Freire, A. C. G., Roitman, N., and Ronaldo, C. B., An experimental model study for deep water TLP platform, *Proceedings of the 6th International Symposium on Offshore Engineering, COPPE*, Pentech Press, London, 1987, pp. 762-777.

39. Graham, J. M. R., Forces on cylindrical bodies in oscillatory flow at low K_c numbers, *Proceedings of Symposium on Mechanics of Wave Induced Forces on Cylinders, IAHR, Bristol, England, 1978*, pp. 461-474.

40. Graham, J. M. R., The forces on a sharp edged cylinder in oscillatory flow at low K_c numbers, *Journal of Fluid Mechanics*, 1980, Vol. 97, pp. 331-346.

41. Graham, J. M. R., Calculation of hydrodynamic damping of offshore structures, *Proceedings on Behavior of Offshore Structures, NIT, Trondheim, 1988*, Vol. 2, pp. 579-589.

42. Gray, R. M., Berge, B., and Koehler, A. M., Dynamic analysis of the North Sea forties platform, *Proceedings of the Offshore Technology Conference, Houston, Texas, 1975*, OTC 2258, pp. 819-830.

43. Gundy, W., and Scharton, T. D., Damping measurements on an offshore platform, *Proceedings of the Offshore Technology Conference, Houston, Texas, 1980*, OTC 3863, pp. 77-92.

44. Hamel-Derouich, Wave forces on rectangular cylinders at low K_c Numbers, *Proceedings of the Offshore Technology Conference, Houston, Texas, 1991*, OTC 6520, pp. 207-216.

45. Holmes, P., Fundamental aspects of wave loading and modelling, *Proceedings of a Conference on the Use of Physical Models in their Design, The Construction Press, 1981*, pp. 179-197.

46. Hunter, A. F., et al., Designing the TLWP, *Proceedings of the Offshore Technology Conference, Houston, Texas, 1990*, OTC 6360, pp. 147-158.

47. Huse, E., Resonant heave damping of tension leg platform, *Proceedings of the Offshore Technology Conference, Houston, 1990*, OTC 6317, pp. 431-436.

48. IMSL-library, FORTRAN subroutines for mathematics and statistics, *IMSL Problem-Solving Software Systems, IMSL Inc., Houston, Texas, 1985*.

49. Isaacson, M., Wave forces on rectangular caissons, *Proceedings of the Civil Engineering in the Oceans IV, San Francisco, ASCE, 1979*, pp. 161-171.

50. Isaacson, M., and Nwogu, O., Short-Crested wave forces on a vertical pile, *The 7th International Conference on Offshore Mechanics and Arctic Engineering, Houston, Texas, 1988*, pp. 47-54.

51. Justesen, P., Hydrodynamic forces on large cylinders in oscillatory flow, *Journal of Waterway, Port, Coastal and Ocean Engineering*, ASCE, July, 1989, Paper no. 23677, Vol. 115, No. 4, pp. 497-514.

52. Keulegan, G. H., and Carpenter, L. H., Forces on cylinders and plates in an oscillating fluid, *Journal of Research of the National Bureau of Standards*, May 1958, Vol. 60, pp. 423-440.

53. Kint, T. E., and Morrison, D. G., Dynamic design and analysis methodology for deep water bottom founded structures, *Proceedings of the Offshore Technology Conference, Houston, Texas, 1990*, OTC 6343, pp. 607–614.

54. Klopman, G., and Kostense, J. K., *The Loading on a Vertical Cylinder in Random Waves at High Reynold's Numbers*, October, 1989, Delft Hydraulics Publications, No. 426.

55. Langewis, C., The Gulf of Mexico: newest proving ground for deep water technology, *Ocean Industry*, May, 1987a, pp. 37–39.

56. Langewis, C., Jolliet field development in green canyon, *Deep Offshore Technology Conference, Monaco, 1987b*, Paper No. G5.

57. Lian, W., A numerical study of the two dimensional separated flow past bluff bodies at moderate K_c numbers, *Ph.D. Thesis*, Division of Marine Hydrodynamics, The Norwegian Institute of Technology, The University of Trondheim, Norway, 1986.

58. Malhotra, A. K., and Penzien, J., Nondeterministic analysis of offshore structures, *Journal of Engineering Mechanics Division*, ASCE, 1970, Vol. 96, No. EM6, pp. 985–1003.

59. Marchand, E. LE., et. al., Low frequency heave damping of semi-submersible platforms: some experimental results, *Proceedings on Behavior of Offshore Structures, Trondheim, Norway, 1988*, Vol. 2, pp. 591-604.

60. Marthinsen, T., Hydrodynamics in TLP design, *The 8th International Conference on Offshore Mechanics and Arctic Engineering, 1989*, pp. 127–133.

61. Matlab for VAX/VMS computers: user's guide, *The Math Works, Inc., South Natick, Ma 01760, June, 1989*, pp. 3.77–3.79.

62. McCormick, M. E., Analysis of offshore structure dynamics with nonproportional damping, *Journal of Waterways, Port, Coastal and Ocean Engineering*, November, 1989, Vol. 115, No. 6, Paper no. 24074, pp. 775-791.

63. Mercier, J. A., Evolution of tension leg platform technology, *Proceedings on Behavior of Offshore Structures, MIT, Cambridge, 1982*, Vol. 1, pp. 19-49.

64. Michelsen, F. C., and Meek, J., Development of the tripod tower platform design, *Proceedings on Behavior of Offshore Structures, MIT, Cambridge, 1982*, Vol. 2, pp. 847-863.

65. Morison, J. R., O'Brien, M. P., Johnson, J. W., and Schaf, S. A., The force exerted by surface waves on piles, *Petroleum Transactions AIME*, 1950, Vol. 189, pp. 149-157.

66. Nielsen, F. G., and Herfjord, K., The importance of nonlinear wave forces to fatigue of deep water structures, *Proceedings of the Offshore Technology Conference, Houston, Texas, 1985*, OTC 4952, pp. 493-501.

67. Newman, J. N., The exciting forces on fixed bodies in waves, *Journal of Ship Research*, SNAME, December, 1962, Vol. 6, No. 3, pp. 10-17.

68. Patel, M. H., Dynamics of Offshore Structures, Butterworths, London, 1989, pp. 215-249.

69. Penzien, J., Structural dynamics of fixed offshore structures, *Proceedings on Behavior of Offshore Structures, Trondhiem, 1976*, Vol. 1, pp. 581-592.

70. Pierson, W. J., and Moskowitz, L., A Proposed spectral form for fully developed wind seas based on the similarity theory of S. A. Kitaigorodskii, *Journal of Geophysics*, 1964, Res. Vol. 69, pp. 5181-5190.

71. Qi, X. Y., Feng, Y., and Zhang, J. L., Low frequency surge motion of TLP in survival sea state, *The 6th International Conference on Offshore Mechanics and Arctic Engineering, Tokyo, Japan, 1984*, pp 120-125.

72. Rajabi, F., and Mangiavacchi, A., Model test of a pile founded guyed tower, *Proceedings of the Offshore Technology Conference, Houston, Texas, 1988*, OTC 5675, pp. 493-501.

73. Roitman, N., Batista, B. C., and Carniro, F. L. L. B., Reduced model of fixed platform for investigation of fluid structure interaction, *International Symposium on Offshore Engineering, Rio De Janeiro, Brazil, 1985*.

74. Sami, K., and Vandiver, J. K., A numerically efficient technique for the simulation of random wave forces on offshore structures, *Proceedings of the Offshore Technology Conference, Houston, Texas, 1984*, OTC 4811, pp. 301-308.

75. Sarpkaya, T., Hydrodynamic forces on various multiple tube riser configurations, *Proceedings of the Offshore Technology Conference, Houston, Texas, 1985*, OTC 3539, pp. 1603-1606.

76. Sarpkaya, T., Forces on a circular cylinder in viscous oscillatory flow at low Keulegan-Carpenter numbers, *Journal of Fluid Mechanics*, 1986, Vol. 165, pp. 61-71.

77. Sarpkaya, T., Collins, N. J. and Evans, S. R., Wave forces on rough walled cylinders at high Reynold's numbers, *Proceedings of Ninth Offshore Technology Conference, Houston, Texas, May, 1977*, OTC 2901, pp. 175-184.

78. Sarpkaya, T., and Isaacson, M., *Mechanics of Wave Forces on Offshore Structures*, Van Nostrand Reinhold, New York, 1981, pp. 473-570.

79. Sawaragi, T., Dynamic behaviour of a circular pile due to eddy shedding in waves, *Coastal Engineering in Japan*, 1977, Vol. 1, pp. 114–120.

80. Selna, L. and Cho, D., Design of offshore structures against resonance, *Proceedings of Civil Engineering in the Oceans II, ASCE, Florida, 1969*, pp. 78–91.

81. Shaw, T. L., *Mechanics of Wave Induced Forces on Cylinders*, Pitman Publishing Ltd., London, U. K., 1979.

82. Shinozuka, M., Yun, C., and Vaicaitis, R., Dynamic analysis of fixed offshore structures subjected to wind generated waves, *Journal of Struct. Mech.*, 1977, Vol. 5(2), pp. 135–146.

83. Skjelbreia, L., and Hendricksen, J. A., Fifth-order gravity wave theory, *Proceedings of Seventh Conference on Coastal Engineering, 1961*, pp. 184–196.

84. Spidsoe, N., and Langen, I., Damping of fixed offshore platforms, *Proceedings on Behavior of Offshore Structures, Delft, The Netherlands, 1985*, P18, pp. 915–925.

85. Srinivasan, N., and Swamidas, A. S. J., Hydroelastic modelling of tripod tower platform, *Proceedings of OCEANS Conference, Halifax, 1987*, Vol. 3, pp. 530–536.

86. Srinivasan, N., and Swamidas, A. S. J., Damping-controlled response of a deep water tripod tower platform, to moderate waves, *Proceedings of the 2nd International Conference on Computer Aided Design, Manufacture and Operation in the Marine and Offshore Industries, CADMO, Southampton, U. K., 1988*, pp. 729–744.

87. Srinivasan, N., Swamidas, A. S. J., and Pawlowski, J. S., Experimental study of In-line forces on a large diameter fixed vertical cylinder to random waves,

The 9th International Conference on Offshore Mechanics and Arctic Engineering, Houston, 1990a, Vol. 1, Part-A, pp. 63-71.

88. Srinivasan, N., Swamidas, A. S. J., and Pawlowski, J. S., A Wave-tank study on the investigation of induced flow-separation for a large diameter fixed vertical cylinder at low Keulegan-Carpenter numbers, *The Proceedings of the First European Offshore Mechanics Symposium, ISOPE, Trondheim, Norway, 1990b*, pp. 68-76.

89. Srinivasan, N., Swamidas, A. S. J., and Pawlowski, J. S., Effect of induced drag damping on the near resonant responses of a deep water tripod tower platform *Proceedings of Offshore Technology Conference, Houston, Texas, May, 1991a*, OTC 6606, pp. 175-184.

90. Srinivasan, N., Swamidas, A. S. J. Pawlowski, J. S., and Williams, C., 1991b. Hydroelastic Model Study of a Deep water Tripod Tower Platform: Response to Regular and Random waves, *The 10th International Conference on Offshore Mechanics and Arctic Engineering, Stavanger, Norway, 1991b*, Vol.1B, pp. 465-474.

91. Stansby, P. K., and Isaacson, M., *Recent Developments in Offshore Hydrodynamics*, Workshop Report, Siman Engineering Laboratories, University of Manchester, Manchester-M13 9PL, 1986, pp. 15-33.

92. Stokes, G. G., On the effect of the internal friction of fluids on the motion of pendulums, *Trans. Cambridge Phil. Soc.*, 1851, Vol 9, pp. 8-106.

93. Taylor, R. E., and Rajagopalan, A., Superharmonic resonance effects in drag dominated structures, *Integrity of Offshore Structures*, (Editor: D. Faulkner et al.), Proceedings of the Symposium, Applied Science Publishers, Glasgow, July, 1981, pp. 85-104.

94. Vandiver, J. K., The use of finite element models in dynamic analysis of offshore structures, *Design Engineering Technology Conference, Chicago, Ill., ASME, New York, September, 1977*, pp. 1–18.

95. Vandiver, J. K., Prediction of the damping-controlled response of offshore structures to random wave excitation, *Society of Petroleum Engineers Journal*, 1980, Vol. 20, pp. 5–14.

96. Vandiver, J. K., The sensitivity of fatigue life estimates to variations of structural natural periods, modal damping ratios and directional spreading of the sea, *Ocean Science and Structures*, 1982, Vol. 7(3), pp. 279–289.

97. Verley, R. L. P and Moe, G., The effect of cylinder vibration on the drag force and the resultant hydrodynamic damping, *Mechanics of Wave Induced Forces*, (Editor: T. F. Shaw), Pitman, London, U. K., 1979, pp. 521–531.

98. Vugts, J. H., and Hayes, D. J., Dynamic analysis of fixed offshore structures: a review of some basic aspects of the problem, *Engineering Structure*, April, 1979, vol. 1, pp. 114–120.

99. Will, S. A., Critical parameters in the design and construction of large single segment fixed platform jacket, *Proceedings of Deep Offshore Technology, Monaco, 1983*, Vol. 3., pp. 239–253.

Appendix - A

Computer program for C_m and C_d analysis - Regular waves.

The appendix gives the computer coding for the C_m and C_d analysis. The program is written using MATLAB, a computer software package. The measured regular wave elevation and the wave force time histories are the input quantities to the program and the value of C_m and C_d coefficients are determined. The variables used in the program are described at the beginning of the listing. The program is a set of subroutines, called as m-files in the MATLAB package. To run this program, the MATLAB environment has to be invoked and the m-files have to be executed in the given sequence. Result and Plot files will be written by the program automatically while running the m-files.

```
%************** Description of Variable ********************
%
% Ld        -  the deepwater wave length
% L         -  wave length based on 5th order theory
% C         -  wave celeritry
% H         -  wave height
% T         -  wave period
% h         -  water depth
% K         -  2*pi/L
% w         -  2*pi/T
% g         -  acceleration due to gravity
% rho       -  density of water
% dia       -  diameter of cylinder
% lenth     -  total no. of pts. considered
% fs        -  sampling frequency
% A*,B*,C*  -  coefficients reqd. for fifth order theory
% a*        -  coefficients for fifth order profile
% a         -  lamda, the real root of the fifth order eqn.
% G(*)      -  Stokes fifth order wave - velocity parameters
% count     -  no. iterations reqd. to solve stokes therory
% count1    -  no. iterations reqd. for linear theory
% wp2       -  results of wave probe
% f         -  frequency scale (hz.)
% t         -  time scale (secs.)
% dt        -  time interval
% F         -  predicted total force
% flb       -  measured total force
% H/L       -  Wave Steepness
% pi*D/L    -  Diffraction Parameter
% H/D       -  Froudian Scaling Parameter
% Re        -  Reynolds Number
% Kc        -  Keulegan Carpender Number
% Cm        -  Inertial Coefficient
% Cd        -  Drag Coefficient
% Fmx       -  Maximum Predicted Force
% Flb       -  Maximum Measured Force
% stderr    -  Standared Error in the Correlation
% covCm     -  Coefficient of variation or Cm
% covCd     -  Coefficient of variation or Cd
```

```
%
%****************** end of Description of Variable **********
%
%************************************************************
% routine name : LCS
%************************************************************
% This routine computes the wave force
% time series from the load cell output
%------------------------------------------------------------
echo on
% 'fs' - sampling frquency
fs=43.520836;
dt=1/fs;
offset=0.0;
slope=0.4535535*0.248;
lc=s(:,12);
flb=(((((lc)-2048)/409.6)-offset)/slope)*1.0;
%to convert them in to Newton SI-Units
flb=flb*4.448222;
lenth=length(lc);
t=0:1:(lenth-1);
t=t*dt;
clear slope offset lc fact
%************************************************************
% routine name : WPS
%************************************************************
% This routine computes the wave elevation time series
% measured from probe # 2
%------------------------------------------------------------
slope2=0.021173;
offset2=2.687833;
wp2=s(:,2);
wp2=(((((wp2)-2048)/409.6)-offset2)/slope2)*1.0;
wp2=wp2/100.0;
clear slope2 offset2
%************************************************************
% routine name : FINE
%************************************************************
% Fine filters the high frequency signal noises
```

```
% in the measured time series
%-------------------------------------------------------
coeff;
[yy,zz]=filter(Bh,Ah,wp2(1)*ones(1,1000));
yy=filter(Bh,Ah,wp2,zz);
wp2=yy;
clear yy zz
[yy,zz]=filter(Bh,Ah,flb(1)*ones(1,1000));
yy=filter(Bh,Ah,flb,zz);
flb=yy;
clear yy zz Ah Bh
%*******************************************************
% routine name : VINDOW
%*******************************************************
%  The purpose of this routine is to select the constant
%  portion of wave elevn. time series. The profile is
%  viewed and the cut-off points are then entered.
%-------------------------------------------------------
lenth=length(flb);
mn=1:lenth;
pause % choose a point at the leading edge to cut-off
clc
plot(mn,wp2),grid,..
xlabel('No. of Pts.'),ylabel('Wave Elvn. in M.'),..
title('Vindowing of Measured Wave Elevn. Time Series '),..
pause % strike return
ncutf=input('enter cutoff pt. at the leading edge')
wp2=wp2(ncutf:lenth);
flb=flb(ncutf:lenth);
lenth=length(flb);
t=0:1:(lenth-1);
t=t*dt;
mn=1:lenth;
pause % choose a point at trailing edge to cut-off
clc
plot(mn,wp2),grid,..
xlabel('No. of Pts.'),ylabel('Wave Elvn. in M.'),..
title('Vindowing of Measured Wave Elevn. Time Series '),..
pause %strike return
```

```
ncutb=input('enter cutoff pt. at the trailing edge')
wp2=wp2(1:ncutb);
flb=flb(1:ncutb);
t=t(1:ncutb);
lenth=length(flb);
mn=1:lenth;
%*************************************************************
% routine name : PREFLB
%*************************************************************
% This routine does the necessary pre-processing for the
% wave force data. The zero-crossing periods are
% calculated based on that the wave period will be fixed.
%-------------------------------------------------------------
lenth=length(flb);
j=1;
for i = 1:(lenth-1)
if sign(flb(i))<=0&sign(flb(i+1))>0
n(j) = i;
j = j+1;
end
end
xx=diff(n);
Tflb=xx*dt;
for j= 1:(length(n)-1)
ii = find(flb==max(flb(n(j):n(j+1))));
jj = find(flb==min(flb(n(j):n(j+1))));
end
Tflb,
T=input('enter wave period T in sec. =');
pause % strike to see flb
clc
plot(flb),title('Wave Load - flb'),..
xlabel('No. of Pts. '),ylabel('Wave force. in N.'),..
grid, pause
pause % strike to see wp2
clc
plot(wp2),title('Wave Elvn.'),..
xlabel('No. of Pts.'), ylabel('Wave Ht. in M.'),grid,pause
ncut1=input('input, ncut1, in npts. based on flb crest');
```

```
nwave=input('no of wave to be taken (5) = ');
ncut2=ncut1+nwave*(fs/fcr);
if lenth<=ncut2
ncut2=lenth;
end
wp2=wp2(ncut1:ncut2);
flb=flb(ncut1:ncut2);
lenth=length(flb);
t=t(1:lenth);
ncut=find(wp2(1:(fix(fs/fcr)))==max(wp2(1:(fix(fs/fcr)))));
ncut=ncut-2;
wp2=wp2(ncut:lenth);
flb=flb(ncut:lenth);
lenth=length(flb);
t=t(1:lenth);
plot(wp2),grid,..
pause
pause %strike return to quit PREFLB
wp2=wp2*100.0/2.54;
H=max(wp2(60:210))-min(wp2(60:210))
clear ncut ncut1 ncut2 nwave Tflb xx i j ii jj n
%*************************************************************
% routine name : SOLVE5
%*************************************************************
% This routiune solves the constants required for the
% stokes fifth order wave theory for a given wave ht. and
% wave period.The constants are used by the routine STOKES
%-------------------------------------------------------------
h=57.6
count=0;
g=386.1;
w=2*pi/T;
K=(w^2/g);
dk=1;
kh=K*h;
for ii=1:23;
if dk<=0.0000000000001,break,end
k1=kh;
K=kh/h;
```

```
CH=cosh(kh);
SH=sinh(kh);
B33=3*(8*CH^6+1)/(64*SH^6);
B35=(88128*CH^14-208224*CH^12+..
70848*CH^10+54000*CH^8-21816*CH^6);
B35=(B35+6264*CH^4-54*CH^2-81)/..
(12288*SH^12*(6*CH^2-1));
B55=(192000*CH^16-262720*..
CH^14+83680*CH^12+20160*CH^10-7280*CH^8);
B55=B55+(7160*CH^6-1800*CH^4-1050*CH^2+225);
B55=B55/(12288*SH^10*(6*CH^2-1)*(8*CH^4-11*CH^2+3));
rt(1)=(B35+B55);
rt(2)=0.0;
rt(3)=B33;
rt(4)=0.0;
rt(5)=1.0;
rt(6)=-(K*H/2);
count=count+1;
aa=roots(rt);
a=aa(5);
C1=(8*CH^4-8*CH^2+9)/(8*SH^4);
C4=(12*CH^8+36*CH^6-162*CH^4+141*CH^2-27)/(192*CH*SH^9);
kh=(h*w^2)/(g*(1+C1*a^2+C4*a^4)*tanh(kh));
dk=abs(k1-kh);
end
CH=cosh(kh);
SH=sinh(kh);
A11=1/SH;
A13=-CH^2*(5*CH^2+1)/(8*SH^5);
A15=-(1184*CH^10-1440*CH^8-..
1992*CH^6+2641*CH^4-249*CH^2+18)/(1536*SH^11);
A22=3/(8*SH^4);
A24=(192*CH^8-424*CH^6-312*CH^4+480*CH^2-17)/(768*SH^10);
A33=(13-4*CH^2)/(64*SH^7);
A35=(512*CH^12-4224*CH^10-..
6800*CH^8-12808*CH^6+16704*CH^4-3154*CH^2+107);
A35=A35/(4096*SH^13*(6*CH^2-1));
A44=(80*CH^6-816*CH^4+1338*CH^2-197)/(1536*SH^10*(6*CH^2-1));
A55=-(2880*CH^10-72480*CH^8+324000*CH^6-432000*CH^4-16245);
```

```
A55=(A55+163470*CH^2)/(61440*SH^11*(6*CH^2-1)*..
(8*CH^4-11*CH^2+3));
B22=CH*(2*CH^2+1)/(4*SH^3);
B24=CH*(272*CH^8-504*CH^6-192*CH^4+322*CH^2+21)/(384*SH^9);
B33=3*(8*CH^6+1)/(64*SH^6);
B35=(88128*CH^14-208224*CH^12+70848*CH^10+54000*CH^8-21816*CH^6);
B35=(B35+6264*CH^4-54*CH^2-81)/(12288*SH^12*(6*CH^2-1));
B44=CH*(768*CH^10-448*CH^8-48*CH^6+48*CH^4+106*CH^2-21);
B44=B44/(384*SH^9*(6*CH^2-1));
B55=(192000*CH^16-262720*CH^14+..
83680*CH^12+20160*CH^10-7280*CH^8);
B55=B55+(7160*CH^6-1800*CH^4-1050*CH^2+225);
B55=B55/(12288*SH^10*(6*CH^2-1)*(8*CH^4-11*CH^2+3));
C1=(8*CH^4-8*CH^2+9)/(8*SH^4);
C2=(3840*CH^12-4096*CH^10+2592*CH^8-..
1008*CH^6+5944*CH^4-1830*CH^2+147);
C2=C2/(512*SH^10*(6*CH^2-1));
C3=-1/(4*SH*CH);
C4=(12*CH^8+36*CH^6-162*CH^4+141*CH^2-27)/(192*CH*SH^9);
G(1) = (A11*a+A13*a^3 + A15*a^5);
G(2) = 2.0*(A22*a^2 + A24*a^4);
G(3) = 3.0*(A33*a^3 + A35*a^5);
G(4) = 4.0*(A44*a^4);
G(5) = 5.0*(A55*a^5);
K=kh/h;
a1=a/K;
a2=(B22*a^2+B24*a^4)/K;
a3=(B33*a^3+B35*a^5)/K;
a4=(B44*a^4)/K;
a5=(B55*a^5)/K;
C=g*tanh(kh)*(1+C1*a^2+C2*a^4)/K;
C=sqrt(C);
H=2*(a+B33*a^3+(B35+B55)*a^5)/K;
w=(K*(g*(1+C1*a^2+C4*a^4)*tanh(kh)));
w=sqrt(w);
T=2*pi/w;
L=C*T;
% This part calculates the contants reqd.
% for Morison's approach of wave loading on
```

```
% a vertical cylinder. Using 5th order thoery it also
% finds the Re & Kc numbers at still water level
dia=12.0;
rho=0.934e-4;
nu=.0015192;
vel=G(1)*cosh(kh)+G(2)*cosh(2*kh)+G(3)*cosh(3*kh);
vel=vel+G(4)*cosh(4*kh)+G(5)*cosh(5*kh);
vel=C*vel;
Re=vel*dia/nu;
Kc=vel*T/dia;
constd=rho*dia*w^2/(2.0*K^3);
consti=-(rho*pi*dia^2*w^2/(4.0*K^2));
Ld=(g*T^2)/(2*pi);
clear dk k1 ch sh rt aa ii ystok
end
% to computes the Stokes fifth order profile.
w=2*pi/T;
lenth=length(flb);
t=t(1:lenth);
for i=1:lenth
ystok(i)=a1*cos(w*t(i))+..
a2*cos(w*t(i)*2.0)+a3*cos(w*t(i)*3.0);
ystok(i)=ystok(i)+a4*cos(w*t(i)*4.0)+a5*cos(w*t(i)*5.0);
end
%************************************************************
% routine name : it2
%************************************************************
% This routine compares the Stokes fifth order
% profile with the experimental, wp2, profile.
% It also adjust them to be in phase with each other.
%------------------------------------------------------------
lenth=length(flb);
npt2=input('enter npt2 (1) = ')
npt2=fix(npt2);
y3=wp2((npt2+1):lenth)*2.54/100;
y5=wp21((npt2+1):lenth);
lc=flb((npt2+1):lenth);
y2=ystok(1:(lenth-npt2))*2.54/100.0;
time=t(1:(lenth-npt2));
```

```
pause %return to compare 5th order profile vs. airys
clc
plot(time,y2,'-',time,y3,'--'),grid,..
xlabel('Time in Sec.'),ylabel('Wave Elvn. in M.'),..
title('Comparison of Measured Profile with Fifth Order'),..
text(0.75,.9,'-  Predicted','sc'),..
text(0.75,.81,'-- Measured','sc'),..
pause
key=input('enter key = 3 to finalize');
if key ~= 3,break,end
if key==3
t=time;
ystok=y2*100/2.54;
flb=lc;
wp2=y5;
end
meta
clear key y2 y3 y5 time lc
%************************************************************
% routine name : STOKES
%************************************************************
% This routine computes the wave forces on the vertical
% pile using fifth order theory Inertial & Drag forces
% are found for unit hydrodynamic coefficients
%------------------------------------------------------------
Fd=zeros(flb);
Fm=zeros(flb);
lenth=length(flb);
t=0:1:(lenth-1);
t=t*dt;
ystok=wp2(1:lenth);
wp2a=wp2*2.54;
w=2*pi/T;
for i=1:lenth
y=(ystok(i)+h);
% Drag Part of the Wave Loading
F1=(exp(5*K*y)/5+exp(3*K*y)/3-exp(-3*K*y)/3-exp(-5*K*y)/5);
F2=(exp(5*K*y)/5+exp(K*y)-exp(-K*y)-exp(-5*K*y)/5);
F3=(exp(4*K*y)/4+exp(2*K*y)/2-exp(-2*K*y)/2-exp(-4*K*y)/4);
```

```
F4=(exp(4*K*y)/4-exp(-4*K*y)/4+2*y);
F5=(exp(3*K*y)/3+exp(K*y)-exp(-K*y)-exp(-3*K*y)/3);
F6=(exp(2*K*y)/2-exp(-2*K*y)/2+2*y);
Fd1=F1*G(1)*G(4)*cos(t(i)*w)*abs(cos(4*t(i)*w));
Fd2=F1*G(1)*G(4)*cos(4*t(i)*w)*abs(cos(t(i)*w));
Fd3=F2*G(2)*G(3)*cos(2*t(i)*w)*abs(cos(3*t(i)*w));
Fd4=F2*G(2)*G(3)*cos(3*t(i)*w)*abs(cos(2*t(i)*w));
Fd5=F3*G(1)*G(3)*cos(t(i)*w)*abs(cos(3*t(i)*w));
Fd6=F3*G(1)*G(3)*cos(3*t(i)*w)*abs(cos(t(i)*w));
Fd7=F4*(G(2)^2)*cos(2*t(i)*w)*abs(cos(2*t(i)*w));
Fd8=F5*G(1)*G(2)*cos(t(i)*w)*abs(cos(2*t(i)*w));
Fd9=F5*G(1)*G(2)*cos(2*t(i)*w)*abs(cos(t(i)*w));
Fd10=F6*(G(1)^2)*cos(t(i)*w)*abs(cos(t(i)*w));
Fd(i)=(Fd1+Fd2+Fd3+Fd4+Fd5+Fd6+Fd7+Fd8+Fd9+Fd10)/4.0;
Fd(i)=constd*Fd(i);
% Inertial Part of the Wave Loading
Fm(i)=G(5)*sin(5*t(i)*w)*sinh(5*K*y);
Fm(i)=Fm(i)+G(4)*sin(4*t(i)*w)*sinh(4*K*y);
Fm(i)=Fm(i)+G(3)*sin(3*t(i)*w)*sinh(3*K*y);
Fm(i)=Fm(i)+G(2)*sin(2*t(i)*w)*sinh(2*K*y);
Fm(i)=Fm(i)+G(1)*sin(t(i)*w)*sinh(K*y);
Fm(i)=consti*Fm(i);
end
Fm=Fm*4.448222;
Fd=Fd*4.448222;
Fdl=zeros(Fd);
Fml=zeros(Fm);
y=11.0;
for i=1:lenth
% Drag Part of the Wave Loading
F1=(exp(5*K*y)/5+exp(3*K*y)/3-exp(-3*K*y)/3-exp(-5*K*y)/5);
F2=(exp(5*K*y)/5+exp(K*y)-exp(-K*y)-exp(-5*K*y)/5);
F3=(exp(4*K*y)/4+exp(2*K*y)/2-exp(-2*K*y)/2-exp(-4*K*y)/4);
F4=(exp(4*K*y)/4-exp(-4*K*y)/4+2*y);
F5=(exp(3*K*y)/3+exp(K*y)-exp(-K*y)-exp(-3*K*y)/3);
F6=(exp(2*K*y)/2-exp(-2*K*y)/2+2*y);
Fd1=F1*G(1)*G(4)*cos(t(i)*w)*abs(cos(4*t(i)*w));
Fd2=F1*G(1)*G(4)*cos(4*t(i)*w)*abs(cos(t(i)*w));
Fd3=F2*G(2)*G(3)*cos(2*t(i)*w)*abs(cos(3*t(i)*w));
```

```
Fd4=F2*G(2)*G(3)*cos(3*t(i)*w)*abs(cos(2*t(i)*w));
Fd5=F3*G(1)*G(3)*cos(t(i)*w)*abs(cos(3*t(i)*w));
Fd6=F3*G(1)*G(3)*cos(3*t(i)*w)*abs(cos(t(i)*w));
Fd7=F4*(G(2)^2)*cos(2*t(i)*w)*abs(cos(2*t(i)*w));
Fd8=F5*G(1)*G(2)*cos(t(i)*w)*abs(cos(2*t(i)*w));
Fd9=F5*G(1)*G(2)*cos(2*t(i)*w)*abs(cos(t(i)*w));
Fd10=F6*(G(1)^2)*cos(t(i)*w)*abs(cos(t(i)*w));
Fdl(i)=(Fd1+Fd2+Fd3+Fd4+Fd5+Fd6+Fd7+Fd8+Fd9+Fd10)/4.0;
Fdl(i)=constd*Fdl(i);
% Inertial Part of the Wave Loading
Fml(i)=G(5)*sin(5*t(i)*w)*sinh(5*K*y);
Fml(i)=Fml(i)+G(4)*sin(4*t(i)*w)*sinh(4*K*y);
Fml(i)=Fml(i)+G(3)*sin(3*t(i)*w)*sinh(3*K*y);
Fml(i)=Fml(i)+G(2)*sin(2*t(i)*w)*sinh(2*K*y);
Fml(i)=Fml(i)+G(1)*sin(t(i)*w)*sinh(K*y);
Fml(i)=consti*Fml(i);
end
Fml=Fml*4.448222;
Fdl=Fdl*4.448222;
clc
Fd=Fd-Fdl;
Fm=Fm-Fml;
clear Fdl Fml F1 F2 F3 F4 F5 F6 Fd1 Fd2 Fd3 Fd4
clear Fd5 Fd6 Fd7 Fd8 Fd9 Fd10
pause % strike return to plot net forces
clc
plot(t,wp2a,'-.',t,Fm,'-',t,Fd,'--'),grid,..
xlabel('Time in Sec.'), ylabel('M*10e-2. & N.'),..
title('Results of the Stokes Fifth Order Theory'),..
text(.72,.7,' -  Inertia','sc'),..
text(.72,.75,' -- Drag ','sc'),..
text(.72,.81,' -. Prfl.','sc'),pause
pause  % strike return to leave FORCE
meta
%*************************************************************
% routine name : CMCD
%*************************************************************
% This routine computes the hydrodynamic
% coefficients based on least-square fit
```

```
%-------------------------------------------------------
alfa  = sum(flb.*Fm);
beta  = sum(Fd.*Fd);
gama  = sum(flb.*Fd);
eta   = sum(Fd.*Fm);
theta = sum(Fm.*Fm);
Cm = ((alfa*beta-gama*eta)/(theta*beta-eta^2));
Cd = ((gama*theta-alfa*eta)/(theta*beta-eta^2));
clear alfa beta gama eta theta
Cm,Cd
%*******************************************************
% routine name : PL3
%*******************************************************
% From this subroutine some of the post plots are created
% and the statistical computations are obtained.
%-------------------------------------------------------
F=Cm*Fm+Cd*Fd;
pause % strike return to compare predict vs. measured
plot(t,F,'-',t,flb,'--'),grid,..
title('Comparison:-Predicted vs.--Measured Wave Forces'),..
ylabel('Force in N'), xlabel('Time in Sec.'),..
text(.75,.81,['Cm = ',num2str(Cm)],'sc'),..
text(.75,.75,['Cd = ',num2str(Cd)],'sc'),..
pause
meta
Fm=Cm*Fm;
Fd=Cd*Fd;
pause % strike return to plot inertial & drag forces
plot(t,Fm,'--',t,Fd,'-.',t,F,'-'),grid,..
xlabel('Time in Sec.'), ylabel('N.'),..
title('Inertial, Drag & Total Forces on the Cylinder'),..
text(.75, .9, '-- Inertial','sc'),..
text(.75,.84,'-. Drag','sc'),..
text(.75, .77, '- Total','sc'),..
pause
pause %strike return to quit
meta
Fmx = max(F);
flbmx = max(flb);
```

```
deav = (flb-F);
stderr=std(deav);
statm(:,1)=Fm;
statm(:,2)=Fd;
stat=cov(statm);
s11=stat(1,1);
s12=stat(1,2);
s22=stat(2,2);
covCm=s22/(s11*s22-s12^2);
covCd=s11/(s11*s22-s12^2);
covCm=sqrt(covCm)*stderr/Cm;
covCd=sqrt(covCd)*stderr/Cd;
clear deav statm stat s11 s12 s22
%*************************************************************
```

Appendix - B

Computer program for C_m and C_d analysis - Random waves.

The appendix gives the computer coding for the C_m and C_d analysis. The program is written using MATLAB, a computer software package. The measured random wave elevation and the wave force time histories are the input quantities to the program and the value of C_m and C_d coefficients are determined. The variables used in the program are described at the beginning of the listing. The program is a set of subroutines, called as m-files in the MATLAB package. To run this program, the MATLAB environment has to be invoked and the m-files have to be executed in the given sequence. Result and Plot files will be written by the program automatically while running the m-files.

```
%****************** Description of Variable ********************
% fs        -  sampling frequency Hz. (36.4)
% N         -  no. of points in time series (2048)
% dt        -  time increment  in time series (1/fs=0.0275)
% T         -  record length (56.264secs.)
% df        -  freq. increment in frq. domain Hz. (1/T=0.01777)
% dw        -  freq. increment in frq. domain rad/sec.
% fu        -  cut of frq. in Hz. (2.275 Hz.)
% wu        -  cut of frq. in rad./sec. (2*pi*fu=14.294)
% nf        -  no. of points considered in frq. domain (128)
% ff        -  frq. scale in Hz.
% ww        -  frq. scale in rad/sec
% fmax      -  Nyquist frq.in hz (fs/2=18.2)
% wp2       -  wave elvn. time series
% flb       -  wave force time series
% Tz        -  mean zero crossing period in sec.
% Tc        -  mean crest period in sec.
% W0        -  peak freq. in rad./sec.
% Hs        -  significant wave height inch. (4*std(wp2))
% Tm        -  mean period used in ISSC spectrum (sec.)
% f0        -  peak freq. used in JONSWAP spctrum (Hz.)
% gamma     -  peakness factor used in JONSWAP spctrum
% Sp        -  torget spectrum-power spctral density
% h         -  water depth
% g         -  acceleration due to gravity
% rho       -  density of water
% dia       -  diameter of cylinder
% Cm        -  Inertial Coefficient (least square fit)
% Cd        -  Drag Coefficient (least square fit)
% Cm1       -  Inertial Coefficient (cross spectral method)
% Cd1       -  Drag Coefficient (cross spectral method)
% Spwp2     -  measured wave elvn. power spectrum
% Spflb     -  measured wave force power spectrum
% Raoi      -  inertia RAO
% Raod      -  drag force RAO
% Spi       -  predicted inertial spectrum
% Spd       -  predicted drag spectrum
% Sptf      -  predicted total spectrum
%******************* end of Description of Variable **********
```

```
%*****************************************************************
% routine name : LCS
% This routine computes the wave force time series.
%*****************************************************************
echo on
% 'fs' - sampling frquency
fs=36.4;
dt=1/fs;
offset=0.0;
slope=0.4535535*0.248;
lc=s(:,12);
flb=(((((lc)-2048)/409.6)-offset)/slope)*1.0;
lenth=length(lc);
t=0:1:(lenth-1);
t=t*dt;
%*****************************************************************
% routine name : WPS
% This routine computes the wave elevation time series.
%*****************************************************************
slope2=0.021053;
offset2=2.690133;
wp2=s(:,2);
wp2=(((((wp2)-2048)/409.6)-offset2)/slope2)*1.0;
wp2=wp2./2.54;
%*****************************************************************
% routine name : FINE
% Fine filters the high frequency signal noises.
%*****************************************************************
coeff;
[yy,zz]=filter(Bh,Ah,wp2(1)*ones(1,1000));
yy=filter(Bh,Ah,wp2,zz);
wp2=yy;
clear yy zz
[yy,zz]=filter(Bh,Ah,flb(1)*ones(1,1000));
yy=filter(Bh,Ah,flb,zz);
flb=yy;
clear yy zz Ah Bh
wp=detrend(wp2);
%*****************************************************************
```

```
% routine name : PRE
% This routine does the pre-processing for the wave data.
% The zero up/down - crossing periods will be calculated.
%*************************************************************
lenth=length(wp2);
j=1;
for i = 1:(lenth-1)
if sign(wp2(i))<=0&sign(wp2(i+1))>0
n(j) = i;
j = j+1;
end
end
xx=diff(n);
xx=xx*dt;
Tzup=mean(xx);
clear xx
j=1;
for i = 1:(lenth-1)
if sign(wp2(i))>=0&sign(wp2(i+1))<0
nn(j) = i;
j = j+1;
end
end
xx=diff(nn);
xx=xx*dt;
Tzdn=mean(xx);
clear xx i j n nn
% To find certain statistics of wp2
Tz=(Tzup+Tzdn)/2;
Hs=4*std(wp2);
Wz=2*pi/Tz;
fz=1/Tz;
%*************************************************************
% routine name : POWER
% Given a wave elvn. time series this
% m - file computes the power Spectrum
%*************************************************************
fs=36.4;
T=56.264;
```

```
nf=128;
fu=2.275;
wu=2*pi*fu;
dt=1/fs;
df=1/T;
N=T/dt;
N=fix(N);
dw=df*2*pi;
ww=1:nf;
ww=ww*dw;
ff=ww/(2*pi);
xx=fft(wp2);
yy=xx.*conj(xx);
yy(1)=0.0;
yy(2)=0.0;
yy(3)=0.0;
yy(4)=0.0;
yy(5)=0.0;
yy=yy(1:nf);
yy=yy*2;
yy=yy*(T/(N^2));
yy=yy/(2*pi);
Spwp2=yy';
pause %strike return to do smoothing
ma
Spwp=mav;
clear xx zz yy mav
%*************************************************************
% routine name : JN
% This m - file computes and plot JONSWAP - Spectrum
%*************************************************************
W0=find(Spwp == max(Spwp));
W0=W0*dw;
f0=W0/(2*pi);
T0=1/f0;
c(1)=-0.00065;
c(2)=0.01581;
c(3)=((0.11661)-((Hs/12)/T0^2));
gamma=roots(c);
```

```
gamma=gamma(2)
gamma=input('enter -gamma- facter for JONSWAP (2.2) =');
clear c NDIM Y Z H
f0two=f0^2;
f0four=f0two^2;
A=(5.0*(Hs^2)*f0four);
A=A/(16.0*(gamma^(1./3.)));
B=5.0*f0four/4.0;
for i=1:128,
f=ff(i);
if f<=f0,
sigma=0.07;
sigma2= sigma^2;
ffour=f^4;
smalla=((f-f0)^2)/(2.0*sigma2*f0two);
smalla=exp(-smalla);
Sp(i)=(A/(f*ffour));
Sp(i)=Sp(i).*(exp(-B/ffour));
Sp(i)=Sp(i).*(gamma^smalla);
end
if f>f0,
sigma=0.09;
sigma2= sigma^2;
ffour=f^4;
smalla=((f-f0)^2)/(2.0*sigma2*f0two);
smalla=exp(-smalla);
Sp(i)=(A/(f*ffour));
Sp(i)=Sp(i).*(exp(-B/ffour));
Sp(i)=Sp(i).*(gamma^smalla);
end
end
Sp=Sp/(2.*pi);
Y=Sp.*ww;
NDIM=nf;
H=dw;
intgrn;
M1=Z(nf);
M0=(Hs^2)/16;
Wm=M1/M0;
```

```
fm=Wm/(2*pi);
Tm=1/fm;
clear NDIM H M1 M0 f0two f0four ffour
clear smalla sigma sigma2 A B fact
spectype='JONSWAP'
Hs=Hs*(2.54/100.0);
Spwp=Spwp*((2.54/100.0)^2);
Sp=Sp*((2.54/100.0)^2);
pause %strike return to compare measured vs. JONSWAP
plot(ww,Spwp,'-',ww,Sp,'--'),grid,..
title('Wave Elvn. Power Spectrum '),..
xlabel('Rad./Sec., -- JONSWAP vs. - Measured'),..
ylabel('M.**2.Sec./Rad.'),..
text(.68,.81,['Hs (M.)=',num2str(Hs)],'sc'),..
text(.68,.75,['W0 (Rad./Sec.)=',num2str(W0)],'sc'),..
pause
Hs=Hs*(100.0/2.54);
Spwp=Spwp*((100.0/2.54)^2);
Sp=Sp*((100.0/2.54)^2);
meta
%*************************************************************
% routine name : POWERF
% Given a wave force time series this m - file
% computes the power Spectrum.
%*************************************************************
xx=fft(flb);
yy=xx.*conj(xx);
yy(1)=0.0;
yy(2)=0.0;
yy(3)=0.0;
yy(5)=0.0;
yy(5)=0.0;
yy=yy(1:nf);
yy=yy*2;
yy=yy*(T/(N^2));
yy=yy/(2*pi);
Spflb=yy';
pause %strike return to do smoothing
ma
```

```
Spflb1=mav;
mav=mav*(4.44822^2);
pause %strike return to plot spectrum
plot(ww,mav),..
title('Power Spectrum - From Wave Force Time Series'),grid,..
xlabel('Frqncy. Rad./Sec.'), ylabel(' N.sqre.Sec./Rad.'),..
pause
meta
clear xx zz yy mav
%*************************************************************
% routine name : SOLVE
% This routiune solves the transcendental equation
% to obtain wave number for each frequency in
% random wave using first order theory
%*************************************************************
h=56.7;
h1=11.0;
g=386.1;
dia=12.0;
rho=0.934e-4;
nu=.0015192;
pause %strike return to get K's for WW's
load kdat
pause %strike return to find Lm
Ti=2*pi/(Wm);
La=(g*Ti^2)/(2*pi);
dk=1;
for ii=1:32;
if dk<=0.000001,break,end
kha=2*pi*h/La;
La1=La;
La=((g*Ti^2)/(2*pi))*tanh(kha);
dk=abs(La1-La);
end
Lm=La;
pause %strike return to find Lz
Ti=2*pi/(Wz);
La=(g*Ti^2)/(2*pi);
dk=1;
```

```
for ii=1:32;
if dk<=0.000001,break,end
kha=2*pi*h/La;
La1=La;
La=((g*Ti^2)/(2*pi))*tanh(kha);
dk=abs(La1-La);
end
Lz=La;
pause %strike return to find L0
Ti=2*pi/(W0);
La=(g*Ti^2)/(2*pi);
dk=1;
for ii=1:32;
if dk<=0.000001,break,end
kha=2*pi*h/La;
La1=La;
La=((g*Ti^2)/(2*pi))*tanh(kha);
dk=abs(La1-La);
end
L0=La;
clear count Ti dk kha count La1 La ii
%*************************************************************
% routine name : RAO
% This routine computes 'RAO' for the Inertial & Drag parts
% of random wave loading and find the predicted spectrum
% for Inertia, and Drag wave forces
%*************************************************************
% Constant terms for drag & inertial force spectrum
Ai=1.0;
Ad=(sqrt(8.0/pi));
y=h1:1.5:h;
nnn=length(y);
% RAO for Ineratial part of wave force spctrum
for i=1:nf
Raoi(i)=(ww(i)^2)/(k(i)*sinh(k(i)*h));
Raoi(i)=Raoi(i)*(sinh(k(i)*h)-sinh(k(i)*h1));
end
% RAO for Drag part of wave force spctrum
Raod=zeros(1,nf);
```

```
for j=1:(nnn-1)
for i=1:nf
Su(i)=(ww(i)*cosh(k(i)*y(j+1))/(sinh(k(i)*h));
end
Y=Su.*Su;
Y=Y.*Sp;
NDIM=nf;
H=abs(ww(6)-ww(5));
intgrn;
stdu=Z(nf);
stdu=sqrt(stdu);
clear Y Z
for i=1:nf
Raodd(i)=(Ad*ww(i))/(k(i)*sinh(k(i)*h));
Raodd(i)=Raodd(i)*(sinh(k(i)*y(j+1))-sinh(k(i)*y(j)));
Raodd(i)=Raodd(i)*stdu;
Raod(i)=Raod(i)+Raodd(i);
end
end
clear A B H nnn Su Y NDIM Z Raodd temp stdumx
% Inertial part of wave force spctrum
Raoii=Raoi*(rho*pi*dia^2/4);
Raodd=Raod*(rho*dia/2);
Raoii=Raoii*(4.44822/0.0254);
Raodd=Raodd*(4.44822/0.0254);
pause %strike retn to plot RAO for Inertia
plot(ww(20:nf),Raoii(20:nf)),..
title('Inertia Force RAO'),..
xlabel('Frqncy. Rad./Sec.'), ylabel('N./M. '),grid,pause
% To plot the RAO for Drag Force.
pause %enter retn
clc
plot(ww(20:nf),Raodd(20:nf)),..
title('Linearized Drag Force RAO'),..
xlabel('Frqncy. Rad./Sec.'), ylabel('N./M. '),grid,..
pause
clear Raoii Raodd
%************************************************************
% routine name : CMCD
```

```
% this ruotine finds the Cm & Cd coefficients using
% least-square fitting method.
%*************************************************************
Spi=Raoi.*Raoi;
Spi=Spi.*Spwp;
Spd=Raod.*Raod;
Spd=Spd.*Spwp;
Spu=Spi./ww;
Spu=Spu./ww;
Spflbr=Spflb1;
f1=sum(Spflbr.*Spu);
f2=sum(Spd.*Spu);
f3=sum(Spi.*Spu);
f4=sum(Spflbr.*Spi);
f5=sum(Spd.*Spi);
f6=sum(Spi.*Spi);
Kd=((f3*f4-f1*f6)/(f3*f5-f2*f6));
Km=((f1*f5-f2*f4)/(f3*f5-f2*f6));
constm=rho*pi*dia^2/4.0;
constd=rho*dia/2;
if Kd<0
Km,Kd
pause %note Km & Kd
rand(1);
rand('seed');
Kd=(constd^2);
Kd=Kd*1.8;
Kd=Kd*rand(1);
end
Cm=sqrt(Km)/constm;
Cd=sqrt(Kd)/constd;
Cm,Cd
%*************************************************************
% routine name : SPEC
% this ruotine computes the Cm & Cd coefficients using
% cross-spectral method.
%*************************************************************
X=fft(wp2);
Y=fft(flb);
```

```
Pxy=Y.*conj(X);
Qnf=imag(Pxy);
Cnf=real(Pxy);
band=input('pl. give band 2.4 for jn, 3.2 for issc=')
Wa=W0-(band/2.0);
Wb=W0+(band/2.0);
Wa=Wa/(df*2*pi);
Wb=Wb/(df*2*pi);
Wa1=fix(Wa);
Wb1=fix(Wb);
Qnf=Qnf(Wa:Wb);
Cnf=Cnf(Wa:Wb);
constm=rho*pi*dia^2/4.0;
constd=rho*dia/2;
Qnf=(2*T/((2*pi)*N^2))*Qnf;
Cnf=(2*T/((2*pi)*N^2))*Cnf;
Kmw=Raoi.*Spwp2;
Kdw=Raod.*Spwp2;
Kmw=Kmw(Wa:Wb);
Kdw=Kdw(Wa:Wb);
Qnf=Qnf';
Cnf=Cnf';
Cmw=Qnf./Kmw;
Cdw=Cnf./Kdw;
Cmw=Cmw/constm;
Cdw=Cdw/constd;
Cm1=mean(Cmw);
Cd1=mean(Cdw);
Wb1=Wb-(Wa-Wa1);
ww1=ww(Wa1:Wb1);
pause %strike return to sea frq. dependent coefficients
subplot(211),..
plot(ww1,Cmw),grid,..
title('Frqncy. Dependent Morison Coefficients'),..
ylabel('Inertia'),..
xlabel(['Cm (mean)= ',num2str(Cm1)]),..
subplot(212),..
plot(ww1,Cdw),grid,..
ylabel('Drag'),..
```

```
xlabel([' Rad./Sec.,      Cd (mean)= ',num2str(Cd1)]),..
pause
meta
subplot
%************************************************************
% routine name : PLT
% From this subroutine some of the post plots are created
% and the statistical computations are obtained.
%************************************************************
Spi=Raoi.*Spwp;
Spi=Spi.*Raoi;
Spd=Raod.*Spwp;
Spd=Spd.*Raod;
Spflb=Spflb1;
Km=Cm*constm;
Km=Km^2;
Kd=Cd*constd;
Kd=Kd^2;
Spit=Spi*Km;
Spdt=Spd*Kd;
Sptf=Spit+Spdt;
Km1=Cm1*constm;
Km1=Km1^2;
Kd1=Cd1*constd;
Kd1=Kd1^2;
Spit1=Spi*Km1;
Spdt1=Spd*Kd1;
Spcrs=Spit1+Spdt1;
pause %strike retn to plot Inertia & Drag Forces Spectrum
plot(ww,Spit,'-',ww,Spdt,'--'),..
title('Power Spectrum for Inertia & Drag Forces'),..
xlabel('Frqncy. rad/sec, Cm & Cd from least sqre. fit'),..
ylabel('lb.sqre.sec./rad.'),grid,..
text(.68,.81,' - Inertia','sc'),..
text(.68,.75,' -- Drag','sc'),..
pause
meta
Sflb=Spflb*4.44822^2;
Stf=Sptf*4.44822^2;
```

```
Scrs=Spcrs*4.44822^2;
pause %strike retn to compare predicted vs. measured Sp.
plot(ww,Sflb,'-',ww,Stf,'--'),grid,..
title('Wave Force Power Spectrum '),..
xlabel('Rad./Sec., -- Least Sqre. vs.- Measured'),..
ylabel('N. sqre.Sec./Rad.'),..
text(.68,.81,['Cm = ',num2str(Cm)],'sc'),..
text(.68,.75,['Cd = ',num2str(Cd)],'sc'),..
pause
meta
plot(ww,Sflb,'-',ww,Scrs,'--'),grid,..
title('Wave Force Power Spectrum '),..
xlabel('Rad./Sec., -- Cross Spec. vs.- Measured'),..
ylabel('N.sqre.Sec./Rad.'),..
text(.68,.81,['Cm =',num2str(Cm1)],'sc'),..
text(.68,.75,['Cd =',num2str(Cd1)],'sc'),..
pause
meta
Sptfmx = max(Sptf);
Spflbmx = max(Spflb);
deav = (Spflb-Sptf);
stderr=std(deav);
for i=1:nf
statm(i,1)=Spi(i)*constm^2;
statm(i,2)=Spd(i)*constd^2;
end
stat=cov(statm);
s11=stat(1,1);
s12=stat(1,2);
s22=stat(2,2);
covCm=s22/(s11*s22-s12^2);
covCd=s11/(s11*s22-s12^2);
covCm=sqrt(covCm)*stderr/(Cm^2);
covCd=sqrt(covCd)*stderr/(Cd^2);
covCm=sqrt(covCm);
covCd=sqrt(covCd);
clear deav statm stat s11 s12 s22
%*****************************************************************
```